Disposable Microbial And Animal Cell Bioreactors For Use In A Disposable Biopharmaceutical Manufacturing Process

By

Alison Baker (M.Sc.)

Thesis submitted for the degree of
Doctor of Philosophy
in
Biochemical Engineering

The Advanced Centre of Biochemical Engineering
Department of Biochemical Engineering
University College London
Torrington Place
London
WC1E 7JE

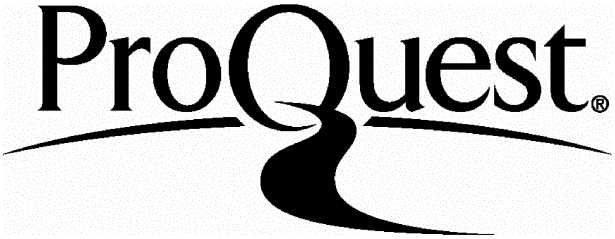

Acknowledgements

I would like to thank my supervisors Prof. Michael Hoare and previously Dr. Andrew Ison for their help with this thesis. In the pilot plant Billy Doyle and Ian Buchanan were of great help in getting the practical aspects of this thesis to work. For this work I was part of the Disposable team and thus I would like to thank Nick Murrell, Natialie Boldering and Jonna Novais. This work was performed in conjunction with Lonza Biologics at Slough and Hyclone Europe at Newcastle. I would particularly like to thank Jez Wayte and Jon Reid for their valuable contributions. Finally most people at UCL ACBE helped me in one way or another through the course of this thesis but there are too many names to mention.

Abstract

This thesis concerns the concept of disposables for use in the manufacture of biopharmaceuticals. A disposable process is where all the equipment in contact with the process is disposable. Specifically disposable bioreactors for microbial fermentation and animal cell culture were investigated.

For the disposable microbial bioreactor, the plunging jet reactor was proposed as the best option where the thesis details the design and manufacture for a disposable plunging jet bioreactor for use in a microbial fermentation. The 14 L disposable plunging jet bioreactor was compared with a 5 L stirred tank bioreactor. The comparison was made on both the physical performance of the bioreactors and the resultant performance of the fermentation.

The maximum k_La in the plunging jet bioreactor was 0.13 to 0.15 s^{-1}, which was comparable to k_La of 0.12 s^{-1} in the stirred tank bioreactor. This oxygen transfer was achieved with the stirred tank operating at a maximum power per unit volume of 11.2 to 12.7 kW m^{-3} whilst the plunging jet bioreactor operated at a lower maximum power per unit volume of 1.4 kW m^{-3}. The plunging jet bioreactor incurred a higher maximum shear rate of 85000 s^{-1}, compared to the stirred tank bioreactor with a maximum shear rate of 13000 to 135000 s^{-1}. The mode of operation to maintain the DOT above 10 to 20 % for the two bioreactors was different. For the plunging jet bioreactor the k_La increases with the OUR so that bioreactor was operated with a fixed power per unit volume. Operating the stirred tank bioreactor at a fixed power per unit volume results in a k_La that is fixed whilst the OUR increases. Thus for the stirred tank the power per unit volume was periodically increased resulting in an instantaneous increase in the k_La. For the plunging jet bioreactor the k_La was affected by the position of nozzle with respect to the outlet. For the plunging jet bioreactor operating at a power per unit volume of 1.4 kW m^{-3}, with the Fab fermentation at an OUR of 5 mol L^{-1} hr^{-1}; the k_La increased from

0.005 s^{-1} to 0.045 s^{-1} as a result of moving the nozzle angle from vertical (0°) to 5° away from the outlet (i.e. to an of angle of -5°).

For both the Wild Type and Fab fermentation there were distinct differences between the resultant performance of the fermenations in the stirred tank bioreactor and the plunging jet bioreactor. For the Wild Type fermentation in the plunging jet bioreactor, lysis occurred within the first 140 minutes of growth, whilst in the stirred tank bioreactor the fermentation was grown as per the protocol. Unlike with the Wild Type fermentation, the Fab fermentation was grown in both the bioreactors without lysis, where the growth in the plunging jet bioreactor was attributed to the greater strength of Fab microbial cells compared to the Wild Type microbial cells. Despite the growth of the Fab fermentation in both bioreactors, there were distinct differences in the resultant performance of the fermentation. In the plunging jet bioreactor the Fab fermentation had both a lower maximum OUR and a lower final dry weight. In addition the RQ varied between 0.5 to 1.0, where addition of glycerol resulted in an increase in the RQ. In the stirred tank bioreactor the final concentration of the Fab product was 75 mg L^{-1} in the solid fraction and 14 to 22 mg L^{-1} in the supernatant. In the plunging jet bioreactor, the final concentration of the Fab product was 0.005 mg L^{-1} in the supernant and zero concentration in the solid fraction. This difference in the Fab concentration between the two bioreactors was attributed to shear in the plunging jet bioreactor stripping away the outer polysaccharide layer, so that the Fab product was released and subsequently degraded in the fermentation broth.

The thesis suggests that these differences in the resultant performance of the Wild Type and Fab fermentation are attributed to the higher shear rate in the plunging jet bioreactor. Further work must be performed to determine whether reducing the shear rate of the nozzle whilst maintaining the mass transfer and mixing will result in a bioreactor whose resultant performance of the fermentation is comparable with the stirred tank bioreactor. The high turbulence nozzle, developed by Kenyres has been suggested as a potential method of reducing the shear rate in the bioreactor.

The plunging jet reactor, bubble column reactor and the airlift reactor were all evaluated as potential disposable animal cell bioreactors. The comparison was made on the basis of measuring the k_La, CO_2 stripping and mixing versus the power per unit volume for the three reactors. The targets for the k_La, CO_2 stripping and mixing were measured in the airlift at a superficial velocity of 0.01 and 0.015 ms^{-1} which is the typical maximum superficial velocity range that a large scale industrial airlift operates during a biopharmaceutical process.

The thesis concludes that the plunging jet reactor is not suitable as a disposable animal cell bioreactor. A 6 L plunging jet reactor was operating with a maximum power per unit volume of 0.01 kW m^{-3} which corresponded to a shear rate and stress of 15000 s^{-1} and 15 N m^{-2} respectively. Whilst the upper k_La and mixing targets of 8.9 hr^{-1} and 13 seconds respectively were achieved below this maximum power per unit volume, operating at the maximum power per unit volume resulted in CO_2 stripping of 0.030 hr^{-1}, which was just within the range of the lower target. Whilst the 6 L plunging jet reactor performance was limited by its CO_2 stripping, the principle reason for rejecting the reactor was that there were perceived to be problems in scaling up the reactor. Increasing the scale of the reactor would probably require an increase in the nozzle diameter and the use of multiple nozzles in order to maintain a low shear rate and prevent a 'foam' in the upper part of the bioreactor.

Measuring the k_La, mixing and CO_2 stripping for an airlift and bubble column both of 26 L scale, showed that at small scale the two reactors had comparable performance. In terms of construction the only difference between the bubble column reactor and the airlift reactor is the presence of a divider in the latter. The proposed design for the disposable airlift shown in section 7.3 has a square cross section so that the divider is diagonal. This insures that the divider is taut and is welded along the main seams of the disposable bag. Thus the airlift's construction is not sufficiently more complex than the bubble column and thus is the preferred option for a disposable animal cell bioreactor. This is because at large scale, published work has shown that the airlift has better mixing and aeration than the bubble column so that the airlift is more scaleable. Further work is

required to determine whether the proposed design will result in a 7 day animal cell culture that is comparable with the same animal culture performed in a conventional airlift or stirred tank bioreactor.

Contents

Figures

Tables

1. Introduction

This thesis concerns the design and operation of disposable bioreactors for use with microbial fermentations and animal cell culture.

The introduction discusses the definition and benefits of a disposable process and how disposables are currently used in biopharmaceutical manufacture. For both the microbial and animal cell culture, the requirements and possible reactors for use as disposable bioreactors are discussed. The rationale for selecting specific reactors as potential microbial and animal cell bioreactors is then presented, followed by the scope of the work and aims of the thesis.

1.1 Disposables in Bioprocessing

1.1.1 Definition of a disposable process

A disposable bioprocess is a process where all the equipment that is in contact with the process stream is disposable, and is sterilized and validated by the equipment supplier. The unit operations require virtually no maintenance and incur minimal cleaning costs. All the WFI water, media and buffers are supplied in sterile disposable bags by an external supplier. The equipment and storage bags are connected by a disposable pipe work, which consists of flexible tubing and pinch valves. The equipment supplier sterilizes the equipment by sealing and then gamma irradiating it, so that it is delivered to the user as a sterile closed system. The user must then maintain the integrity of the sterile equipment and pipe work. This requires pipe work to be connected using a sterile welder. The instrumentation can be non-invasive or invasive but disposable. The invasive disposable instrumentation can either be present in the equipment at the time of gamma irradiation or connected to the equipment at the time of use as a sterile loop. All the unit operations must be disposable, which includes non-invasive pumping by peristaltic

pumps and use of a disposable heat exchanger. For the fermentation process a stirred tank reactor must be replaced by reactor that uses non-mechanical agitation and aeration. For most processes, the downstream process must be changed so that centrifugation is exchanged for filtration and alterations are made to the process, so that both the total membrane area and amount of chromatography media is reduced. The only exception is high resolution purification requiring column chromatography where the media is too expensive for economic disposable.

As with conventional processing, both the plant layout and the air handling system must comply with the European Union and US Federal Regulations for bulk biopharmaceutical operation to the clinical trial and production level chosen. Since the equipment is disposable different unit operations could be performed sequentially in the same rooms provided the air handling regulations are met.

1.1.2 Using disposables for biopharmaceutical manufacture

1.1.2.1 Advantages of a disposable process

The three most critical factors for biopharmaceutical drug development are time to market, cost effectiveness and flexibility (Novais et al, 2001). Cost effectiveness is important because the industry is operating under increasing government and market enforced price controls (Gamerman and Mackler, 1994). Developing biopharmaceutical drugs is an expensive and drawn out process; it takes over seven years to bring a drug to market and costs between 125 to 250 million US dollars to develop (Bullock et all, 1995; Gosse et al, 1996). In addition there are significant risks since 85% of drugs in development fail at a regulatory stage, often after going into clinical trials (Struck, 1994). Since these products have a fixed time in which they are highly profitable, which is governed by their patent, time to market is a crucial factor in a drug's profitability. According to Davidson, (1998) it has been estimated that between 0.2 to 1 million US dollars is lost in sales for each day lost before market authorisation. This requires all procedures that are on the critical path to drug development to be reduced to the shortest possible time. This includes the manufacture of clinical trial material. Both biopharmaceutical development and manufacture must have considerable flexibility to

allow for constant priority changes occurring as a result of safety and clinical data in the development phase, and the need to allow for future expansion (Basu et al, 1998). Often multiproduct processing is used to cope with these priority changes (Harmers, 1993). A conventional manufacturing facility must be constructed, commissioned and validated before the commencement of a clinical trial 3 phase, with a scale that will meet market demand after market authorization. In addition once a manufacturing plant is conceived the opportunity for process changes are small and can only occur in a short time frame. (Karri et al, 2000). This is because the quality of the biopharmaceutical product is determined by the manufacturing process, where small changes to the process can affect the product's quality (Knaack et al, 1998; CPMP, 1999). Thus a conventional manufacturing facility based on stainless unit operations must be well defined from the beginning taking into consideration any future and potential evolution of the plant. As a result the investment in the process is directly linked to the accuracy of the forecasts. In addition there is considerable financial risk since it is expensive to transform an existing suite. (Novais et al, 2001). The decision of when to build and at what scale is made harder because of the uncertainty of product demand and the risk of clinical failure (Struck, 1994). Building a plant early in development will ensure that its construction is not on the critical path, but this decision is associated with higher risks since there is less confidence in the likelihood of success of the product. (Novais et al, 2001).

Considering the above requirements disposable manufacture has several advantages over conventional processing. There is an increased flexibility from the concept of 'pay as you need' where the capital costs are transferred to running costs so that there is less financial damage if a product fails in clinical trials. Disposable equipment allows for a quicker changeover between products, which typically occurs in multiproduct plants that are used for clinical trials production. As explained below a disposable process also has shorter construction, commission and validation times, which allows for a shorter time to market and gives more time for process optimisation before moving to construction. (Novais et al, 2001). In addition to the production of clinical trial material, a disposable plant may be useful for the manufacture of small volumes of biopharmaceutical products

such as orphan drugs and 'personalised' products (Marshall, 1997a and 1997b). For these products it may be uneconomical to use a dedicated plant.

1.1.2.2 How the use of disposables reduces validation and commissioning

The time taken to construct, commission and validate a new bioprocessing plant is significantly reduced with disposables. Construction of the plant is reduced to a minimum because all the process equipment is supplied as bags that are connected together quickly using a sterile welder.

Validation is documentation that proves to the regulatory authorities that the manufacturing process produces a safe product, without harm to the environment and personnel working in the facility (Hill and Beatrice, 1989). It consists of four parts that are carried out in the following order: installation qualification (IQ), operational qualification (OQ), performance qualification (PQ) and process validation. With a few possible exceptions, all the equipment and systems are validated. This includes the control systems, the utilities and the HVAC systems (Hill and Beatrice, 1989). For a disposable process, with the exception of the sterile welds, the IQ and the OQ for all the unit operations will be performed by the individual disposable equipment manufacturers. The IQ is documentation to prove that the equipment and systems are constructed and installed to the critical design specifications set (Huges, 1998). The OQ proves that the equipment and systems can operate within their critical design parameters (Hill and Beatrice, 1989; Huges, 1998). The critical design parameters are those that could affect product quality, where each parameter has a defined range at which product quality can be assured. Although this validation is transferred to the equipment manufacturer, the end user must evaluate the raw data rather than just accepting the certificate of acceptance. Also the equipment manufacturer's validation procedure must be in the end user's standard operating procedure (SOP), which forms part of the validation documentation (Hill and Beatrice, 1989).

Both the performance qualification (PQ) and process validation is still performed by the end user. PQ is documentation to prove that during an actual production the equipment

and systems will perform reliably and consistently where the critical process functions are within their proven acceptable ranges (Hill and Beatrice, 1989; Huges, 1998). The proven acceptable ranges must be well within the safe operating range where product quality can be assured (Medical Control Agency, 1998). The final documentation is process validation, where the process must be run at least three times, where all the critical process functions are within their proven acceptable ranges to prove that product quality can be assured (Huges, 1998). The use of disposables removes the requirement for cleaning, sterilisation, production of WFI water and the associated utilities and thus the associated IQ, PQ and process validation associated with these procedures. The validation for both steam and WFI water is extensive because these are critical utilities to the overall product quality assurance. Cleaning validation is documentation to prove that the cleaning procedure will consistently reduce the product residuals and cleaning agents to predetermined acceptable levels (van Holden, 1998). It is an important factor in the quality assurance because of the requirement for the final product to have a high degree of purity.

1.1.2.3 Process economics of conventional and disposable processing

Novais et al, (2001) have conducted an economic evaluation of disposable based bioprocessing. This paper evaluated the disposable based running costs as being 70% higher than the conventional system and the NPV (net present value) at 25% less than the conventional system. In addition the paper performed a sensitivity analysis that showed if the disposable process could lead to a nine month reduction in time to market compared to the conventional process, then the NPV would be the same for both processes. The paper examined the effect of the bioreactors yield on the NPV and found that a 25% reduction in the yield due to lower biomass resulted in a 9% drop in the NPV, whilst a 25% lower expression level resulted in a 18% drop. Although the disposable process leads to a fall in the NPV, these figures were based on the cost of materials as sold for multiuse conventional plants. The author considered the effect of a 50% reduction in materials costs due to disposable equipment producers responding to higher production

scales with lower prices. This resulted in an NPV of 112% for yield loss due to biomass and 96% for yield loss due to lower expression level.

1.1.3 Current use of disposables in biopharmaceutical manufacture

1.1.3.1 Disposable bioreactors

Four disposable bioreactors have been developed for animal cell culture, all of which are formed from two sheets that are welded along their respective edges to form a pillow shaped bag.

A disposable internal split cylinder airlift, European patent publication number EP 0343 885, has an internal divider that is welded along the sides, where its width is such that when the bag is inflated the divider is taut. A sparger with an attached magnet is suspended from the top. Another magnet is positioned on the outside of the bag at a desired location so that the sparger is held in place. From the picture the sparger appeared to be a circular with a few holes mounted in the top. The bag can be suspended at the top and thus can be immersed in a liquid cooling bath so that the temperature can be maintained.

World patent international publication number WO 98/13469 describes a disposable animal cell culture bioreactor where bubbles are produced at the bottom and thus the bioreactor resembles a bubble column. The bioreactor allows for a portion of the medium containing cells to be harvested, so that the remaining culture can be used for a consecutive culture. According to the patent a battery of these bioreactors can be interconnected so that the scale of production can be adjusted.

World patent international publication number WO 96/12715 describes a disposable bioreactor for recombinant T-lymphocycte cell culture for use in gene therapy. The cells are held within a relatively small compartment down one side of the bag, that is separated

from a larger volume compartment holding the culture medium by a semipermeable membrane. The outer volume compartment has a gas permeable outer wall that allows oxygen in and diffusing carbon dioxide out.

A British patent no. 215370/20 describes a vessel that is externally agitated, so that it resembles a large rocker. The externally agitated vessel has been developed by Vijay Singh and subsequently commercialized by Panacea Solutions, Inc., Bedminster, New Jersey, USA as a rocking platform system, WaveBioreactor™ and cell culture bags, Cell-bag™. In this system a rectangular disposable plastic bag, which is gamma irradiated, is half filled with media with the remaining volume acting as a headspace, which is inflated by air pumped across it. The media and cells are transferred into the bag by a sterile connection. The air is pumped into the headspace via an integral sterile inlet filter and out via a sterilizing filter and a backpressure control valve. The control valve function is to ensure that the headspace is fully inflated at any airflow rate but not over inflated so that the bag ruptures.

The bag is mounted on top of a platform, which rotates in one axis by 5 to 10° at a rate of 5 to 40 rpm. This 'rocking motion' produces waves at the liquid air interface that are claimed to increase the oxygen transfer significantly, promote bulk mixing and off the bottom suspension of cells. The airflow provides the oxygenation and allows gas exchange so that the pH is controlled and CO_2 stripping can occur. Both the temperature and the pH are controlled by putting the entire unit in a conventional cell culture CO_2 incubator. Alternatively temperature control can be achieved by heating the underside of the bag. Both the dissolved oxygen and carbon dioxide concentration can only be measured off line. The dissolved carbon dioxide concentration is controlled by adjusting the carbon dioxide concentration of the inlet air so that CO_2 stripping is controlled. The DOT is controlled by periodically measuring the cell density off line and by using the knowledge of the oxygen transfer rate for different rocking speeds, adjusting the aeration rate. Additions and sampling can be performed without a laminar flow hood, by use of special ports that allow sterile additions and removals.

This system has a maximum oxygen transfer rate measured as a k_La of 4 hr^{-1}. The mixing times defined as the time to achieve complete homogeneity were 5 seconds to 10 seconds for a 10 L working volume and 60 seconds for a 100 L working volume. For cells with an oxygen demand of 0.1 $mMO_2/10^6$ cells hr^{-1}, 7×10^6 cells mL^{-1} can be grown where the DOT is maintained above 10%. A NSO cell line expressing a humanized monoclonal antibody was grown to a cell density greater than 5×10^6 cells mL^{-1}, where the DOT was maintained above 50% (Singh, 1999).

This system has been used for suspension and microcarrier culture for a wide variety of cells including insect, plant, animal and virus cultures. Further adaptations have allowed perfusion culture where a filter floats on the liquid surface. A flat cell retension membrane is located on the underneath of the filter so that cell free filtrate can be drawn through the filter and out of the bag without removal of the cells. The filter moves across the surface with the rocking motion of the bag so that the cells are oxygenated and rapid mixing occurs. This tangential motion also keeps the filter surface from clogging. (Ohashi et al, 2001).

Hollow fiber bioreactors are often used to culture anchorage dependent cells and are typically disposed at the end of the culture (Knight, 1989). These bioreactors consist of bundles of tubes called capillaries, each with a diameter of 300 to 400 μm which have either a micro or ultra filtration membrane. The cells are immobilized at high density in the spaces between the tubes called the extracapillary spaces. The media containing the dissolved oxygen and the nutrients is circulated through the tubes. (Knight, 1989) Due to the complexity of the bioreactor with so many capillary tubes it is difficult to clean and sterilize by a validated method. Compared to all the other conventional animal cell bioreactors, hollow fiber bioreactors require smaller amounts of serum and other macromolecular media supplements and require a simpler downstream process (Butler 1986). The culture can be run for about 30 days after which the productivity reduces (Corrigan-Handa et al, 1995).

1.1.3.2 Other uses of disposables in biopharmaceutical manufacturing

Disposable bags can replace storage tanks for fermentation and animal cell culture media, WFI water and chromatography and filtration buffers. Often the production of media, buffers and WFI water is contracted out to an external supplier who supplies these products in bags. The use of disposable bags as storage vessels removes the requirement for cleaning, maintenance and associated validation of storage tanks so that time and hence costs are reduced. (Joly, 1998) The practice of disposing rather than cleaning membrane filters and chromatography media after a process run already occurs in industry. Millipore has developed a disposable heat exchanger, US Patent, publication number 6131649. This practice is particularly common in multiproduct plants where cleaning validation requirements are more stringent (Hill and Beatrice, 1989).

1.2 Disposable bioreactor design

1.2.1 Overview of disposable bioreactor design

A disposable bioreactor must deliver the specific requirements of either the microbial fermentation or the animal cell culture. A clear distinction between disposable and conventional bioreactors, is that a disposable process requires construction of a new bioreactor for each process run. These bioreactors must all perform in an identical manner and thus the design must allow reproducible construction. Thus the bioreactors must have a simple construction with non mechanical aeration and agitation. For greater flexibility it should be possible to transfer a process from disposable unit operations to conventional hard piped equipment. This essentially requires the productivity of the fermentation or cell culture to be equivalent in both the disposable and hard piped bioreactor. This is because fermentation and animal cell culture protocols and media are set according to the bioreactor reaching specific biomass concentrations. Thus a disposable bioreactor that produces a lower yield than a conventional bioreactor will require significant alterations to the fermentation or animal cell culture reducing its flexibility. The disposable bioreactors should be designed to operate as part of a

disposable biopharmaceutical manufacturing process and thus must operate at a scale of at least 100 L. Furthermore since in conventional biopharmaceutical processing bioreactor volumes often exceed 100 L, disposable bioreactors that can operate at a scale of greater than 100 L would be of greater use. A disposable bioreactor also requires changes to the monitoring and control system where the monitoring equipment must either be disposable or non-invasive.

There is no disposable fermentation equipment for microbial fermentations. Such a disposable vessel would require a non mechanically agitated vessel that can meet the high oxygen demand as well as provide good heat transfer.

Of the disposable animal cell culture vessels currently in use or proposed, they each have significant problems. The rocker system is limited in productivity since the maximum k_La that can be achieved is 4 hr^{-1}, which does not compare favourably with an airlift where a k_La of 10 hr^{-1} is readily achievable. In addition although the bag can be scaled up to 200 L and even possibly 500 L, there are potential problems with such a large bag on the rocker system. The disposable internal spilt cylinder, European patent publication number 0343 885 is the best proposed system for an alternative to a stainless airlift. With this proposed design the sparger is not fixed and it is thought unlikely that a magnet would hold the sparger in place. Erratic movement of the sparger would present a major problem since the air flow would not be delivered in a reproducible manner and could for example be channelled down the side of the vessel. Thus these designs need to be reviewed and alternatives proposed. Any disposable animal cell culture vessel must provide good mixing and mass transfer of both oxygen and carbon dioxide so that a homogenous environment is provided.

1.3.1 Microbial

1.3.1.1 Requirements

Microbial fermentations require a bioreactor design that allows aspectic operation, ease of scale up, and ease of process control and automation. For optimum growth and productivity of microbial fermentations both the temperature and pH must be maintained within a range. Unlike with animal cells however, if a fermentation is controlled outside these parameters the cells are unlikely to die. The DOT must be maintained above the critical level of 1% so that cell lysis, which results in cell death, does not occur (Chen et al, 1985). Since microbial fermentations have a high oxygen demand, which must be maintained, they are typically supported in a stirred tank bioreactor. In addition to providing the high oxygen demand, the bioreactor is also capable of controlling the temperature and providing the mass transfer demanded by the fermentation.

With these fermentations, the productivity is typically linked to the oxygen transfer rate that can be supported by a bioreactor. Thus the disposable bioreactor should be compared against the oxygen transfer rate of a conventional stirred tank system. According to Hatch, (1975) the oxygen transfer rate for a 100 L bioreactor is between 100 to 223 mmol L^{-1} hr^{-1}. This corresponds to a k_La of 0.12 s^{-1} to 0.27 s^{-1} assuming this OUR range was supported at a DOT of 10%. According to Prave et al (1987) a stirred tank reactor operating at a power per unit volume of 8 kW m^{-3}, has a oxygen transfer rate of 4 g L^{-1} hr^{-1}. The corresponds to an OUR is 125 mmol L^{-1} hr^{-1} and a k_La of 0.15 s^{-1}, again assuming that this OUR is supported at a DOT of 10%. According to Atkinson and Mauituna (1991) a stirred tank operating at a power per unit volume of 1 kW m^{-3} has a k_La between 0.045 to 0.08 s^{-1}.

Compared to animal cells, bacteria cells are smaller in size with a typical diameter of 1 to 10 μm and have a rigid cell wall, comprising of a cross-linked peptidoglycan moiety. The bacterial cells typically respond to shear forces by increasing in cell volume and performing asymetric rather than sysmetric cell divison (Joshi, et al, 1996; Edwards et al, 1989). These differences result in greater shear sensitivity for animal cells so that shear

is not a significant problem for microbial fermentations. Thus compared to animal cell culture, shear is not a significant problem.

1.3.1.2 Possible reactors as a disposable microbial bioreactor

This section outlines the possible reactors that could be used as a disposable microbial bioreactor. These reactors are shown in figure 1 and for each reactor the k_La versus power per unit volume is shown in figure 2.

1.3.1.2.1 Nozzle reactors

Nozzle reactors are reactors that use either a two-phase nozzle or a one-phase nozzle as the aerator. Thus they are suitable as a disposable because mixing and aeration is achieved without complex invasive equipment. In the two-phase nozzle, gas is dispersed by a high velocity jet, which is immersed in the liquid pool. A one-phase nozzle, which is used in a plunging jet reactor, uses a liquid jet to hit the liquid pool surface, so that air is entrained into the pool. (Schugerl, 1985). These nozzle reactors are discussed in more detail below.

Two-phase

There are several types of two-phase nozzles according to the mechanism for gas dispersion; which are the ejector, the injector and the radial type. These are discussed in Schugerl (1985). Both ejectors and injectors are used in bubble column reactors, jet loop reactors and airlifts. Ejector nozzles are more widely used and there are several reported investigations of using ejector nozzle in bioreactors in scales of up to 125 m^3 (Prokop et al, 1983; Orfaniotis et al, 1996; Laari et al, 1997; Kundu et al, 1994; Havelka et al, 1997 and Dutta and Raghavan, 1987). The energy efficiency of ejector loop reactors improves with scale. This is because with increasing scale the bubble size remains the same but the volume increases so that the contact time of the bubbles increases (Schugerl, 1985).

One-phase

A plunging jet reactor aerates its liquid by using a liquid jet to entrain air. The liquid jet is produced by circulating part of the liquid through an external loop. The liquid is withdrawn from the vessel via an outlet at the bottom and re enters the vessel via a nozzle, which produces the jet. The jet then travels through the headspace before entraining air as it hits the liquid. Typically the nozzle is simply a long tube although novel more complex nozzles have been designed which increase air entrainment. (Schugerl, 1985)

In terms of the k_La versus the power per unit volume there are three types of plunging jet reactor, these are the basic plunging jet, the down flow bubble column and the high turbulence plunging jet reactor. The basic plunging jet reactor has the lowest k_La per power per unit volume and is the simplest construction with a nozzle above a vessel, which is typically 1:1 aspect ratio. The oxygen transfer performance of the basic plunging jet reactor can be increased by insertion of a downcomer in the region where the jet hits the pool of liquid. This concept is developed further in a down flow bubble column where the jet is directed into a column which connects to the rest of the bioreactor at the bottom of the column. Examples of downflow bubble column can be found in Evans and Jameson (1995); Fujie et al (1980) and Dutta and Raghavan (1987). The high turbulence plunging jet reactor uses a specially designed nozzle where air is channelled through the nozzle so that it hits the jet at an angle and thus roughens the jet. Such a device increases the oxygen transfer efficiency by 30 % to 60 %. Typical k_La versus power per unit volumes for these three types of reactors are shown in figure 2, which is taken from Bin (1993).

1.3.1.2.2 Bubble column reactors

A bubble column is aerated by a sparger located at the bottom of the reactor that produces bubbles. Due to the buoyancy force of the bubbles produced, they rise upwards through the liquid. The liquid flows upwards so that the gas liquid flow is concurrent (Merchuk et al, 1994). Potential disposable spargers are a perforated plate or ring, an orifice, a rubber

membrane sparger or the injector and ejector nozzles (Heijenen and Riet, 1984; Hebrard et al, 1996 and Poulsen and Iversen, 1998). Although the oxygen transfer rate of a bubble column increases with the gas flow rate, it is ultimately limited by a condition called blow out. Blow out occurs when the fluid in the bubble column can't hold any more gas, so that the gas is blown out of the column. (Merchuk et al, 1994).

Figure 1 – The reactor options for the disposable microbial bioreactor

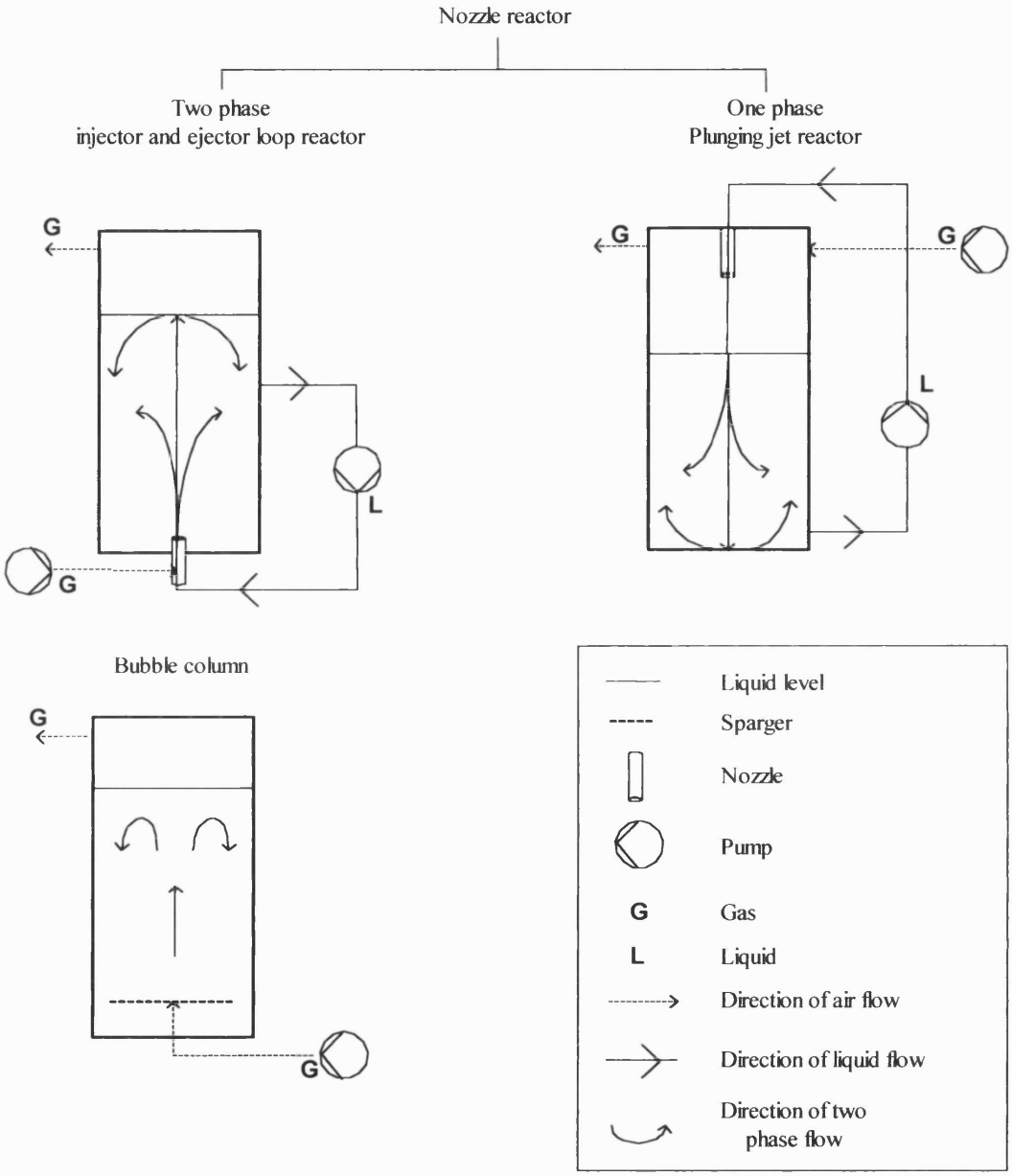

Figure 1
The figure shows the three different reactors, which could potentially be used, as a disposable microbial bioreactor. There are two nozzle reactors, the one phase plunging jet reactor and the two phase injector or ejector loop reactor. The bubble column is the third potential reactor, which is not a nozzle reactor.
The diagrams show the direction of the liquid, 'L' and the gas, 'G' flows for each reactor.

Figure 2 - Comparison between the plunging jet reactor, bubble column, jet loop reactor, stirred tank and down flow bubble columns.

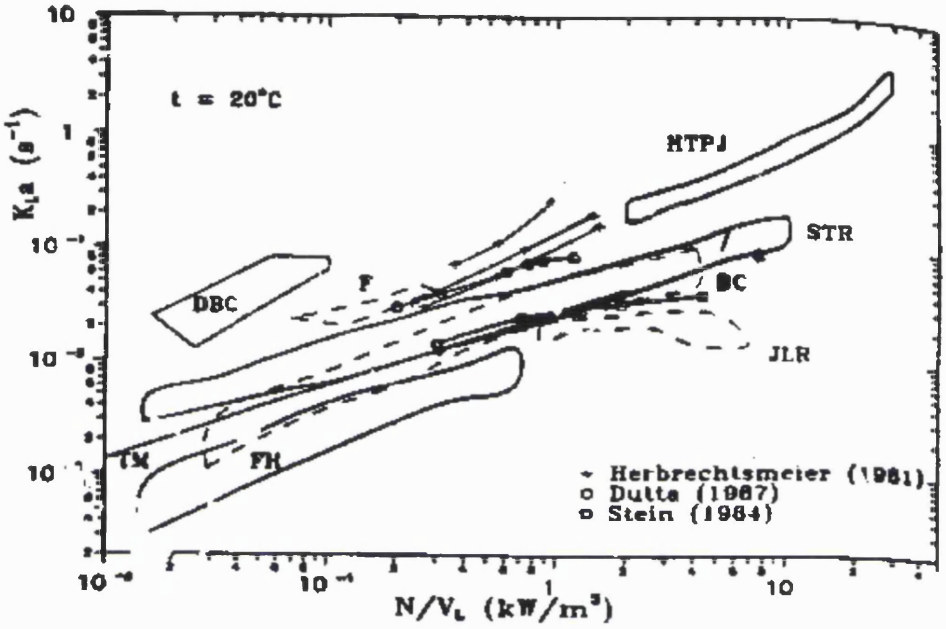

The mass transfer coefficient, k_La (s^{-1}) at 20 °C for different operating power per unit volumes ($kW\ m^{-3}$) for various reactors as follows.

'TM' plunging jet reactor, (Tojo and Miyanami, 1982)

'FH' plunging jet reactor, (Funatsu et al 1988b)

'DBC' down flow bubble column, (Ohkawa et al,1985a, 1985b)

'F' down flow bubble column, (Fujie et al, 1980)

'Dutta' down flow bubble column, (Dutta and Raghavan, *1987)*

'Herbrechstmeier' down flow bubble column, (Herbrechtsmeier, 1981)

'HTPJ' high turbulence plunging jet reactor (Kenyeres, 1991)

'STR' stirred tank reactor, (Linek et al, 1989)

'JLR' jet loop reactor, (Wachsmann et al, 1985)

'BC' bubble column, (Ohkawa et al, 1985a, 1985b)

1.3.1.3 Productivity comparison

As discussed in the microbial requirements section 1.3.1.1 the productivity of the microbial fermentation is linked to the oxygen transfer rate that can be supported by the bioreactor. Thus for each of the reactor options, the oxygen transfer efficiency should be considered. There are several references that compare the performance of the disposable options, which are the bubble column, plunging jet and ejector loop reactor with the conventional stirred tank reactor (Schugerl, 1985; Prave et al 1987).

The best comparison is shown in figure 2, which is from Bin (1993). This figure shows the performance in terms of the power per unit volume required to achieve a given k_La. The figure shows that the performance of the basic plunging jet, marked 'TM' is comparable to the bubble column marked 'BC'. When the plunging jet is operated at its maximum power per unit volume its performance is better than the jet loop reactor marked 'JLR' and is comparable with the lowest range for the stirred tank reactor marked 'STR'. Both the performance of the plunging jet downflow bubble columns marked 'DBC', 'F', 'Dutta' and 'Herbrechstmeir' and the high turbulence plunging jet reactor marked 'HTPJ' are greater than the basic plunging jet reactor, the bubble column, the stirred tank reactor and the jet loop reactor.

1.3.1.4 Rationale for selecting th e plunging jet reactor

The conventional method for an *E. coli* fermentation is a stirred tank bioreactor that has a sparger at the bottom, baffles as the sides and a drive shaft with attached Rushton turbines to break up the air bubbles and aid mixing. This type of reactor can not be used as a disposable reactor because it is unlikely that these complex internals can be made to be disposable. Even the Rushton turbines can not be replaced by a simplified plastic mixer connected to a motor via a magnetic drive because the disposable bag lacks rigidity.

As discussed above the bubble column oxygen transfer efficiency is equivalent to the stirred tank reactor. This equivalence in oxygen transfer efficiency requires a bubble column with a high aspect ratio, which at a significant scale would require a purpose built

room to house the bioreactor. A disposable bubble column would require insertion of a disposable sparger in a reproducible manner across the bottom of vessel, which is more complex in construction than the jet reactors. In addition unlike both the plunging jet reactor and an ejector loop reactor, the bubble column lacks an external loop in which a heat exchanger and monitoring and control systems can be located.

The ejector loop reactor has a similar performance to the basic plunging jet. The ejector loop reactors performance is highly dependent on the exact design of the nozzle, where the reproducible construction of this nozzle is more complex than the nozzle used for the plunging jet reactor. Also according to Havelka et al (1997) the efficient operation of an ejector loop reactor occurs over a much narrower scale than in a bubble column and stirred tank reactor. Thus an ejector loop reactor may not be able to efficiently match the range in oxygen demand required by a microbial fermentation.

The oxygen transfer efficiency of both the high turbulence plunging jet reactor and the down flow bubble column is greater than the stirred tank reactor and the basic plunging jet reactor. The down flow bubble column has an internal draft tube which makes it highly unsuitable as a disposable bioreactor. This is because it would be difficult to ensure that the tube was fixed in an identical position for each disposable bag and thus the disposable bags may not have reproducible performance. The high turbulence plunging jet uses a specially designed nozzle where air is channeled through the nozzle so that it hits the jet at an angle. Whilst this nozzle has a higher oxygen transfer efficiency than the basic nozzle, its complex construction makes is less suitable. Thus the basic plunging jet reactor has been selected with a nozzle constructed of a straight tube of a specified length and diameter. If this bioreactor does not provide sufficient oxygen transfer then the high turbulence plunging jet should be considered.

1.3.1.5 Microbial fermentations used as basis for design of disposable microbial bioreactor

1.3.1.5.1 Overview

The experimental approach was divided into two distinct phases, which were to establish the design and operation for the disposable plunging jet and then to compare the bioreactor with the conventional system.

The plunging jet bioreactor was be designed using a combination of experimental data and information on plunging jets obtained from engineering journals which is presented in Chapter 2. A comparison between the disposable plunging jet bioreactor and the conventional stirred tank bioreactor was made by performing two different fermentations in each bioreactor, which were of a similar scale. The two microbial fermentations are a fragmented antibody fermentation, called the Fab fermentation and a Wild Type fermentation which are both discussed below.

1.3.1.5.2 The Wild Type Fermentation

The Wild Type fermentation is a K12 strain that differs from the Fab W3110 since it has a higher intrinsic growth rate and has no product. The fermentation is useful to test the oxygen transfer capacity of the bioreactor since the oxygen uptake rate, OUR, increases in proportion to the dry cell weight. The fermentation is operated as a batch fed process where additions of glucose, which is the primary carbon source, is fed on demand.

1.3.1.5.3 The Fab Fermentation

The Fab fermentation is an industrial strain, which produces a fragmented antibody and is typical of the microbial fermentations that would be supported in a disposable plunging jet reactor. The fermentation is Bacteria *E. coli* W3110 containing a plasmid, which incorporates ompA, and the tac promoter, which allows IPTG/lactose induction of a humanized Fab antibody fragment. This antibody fragment is produced inside the cell and is then exported to the periplasmic space where chain assembly and disulfide bond formation occurs. Downstream processing is then used to disrupt the microbial cells, so

that the Fab product is released and then with further processing the product is isolated. (Bowering, 2000) (Pluckthun, 1991 and Carter et al 1992).

The typical dry cell weight titre for a batch Fab fermentation in a stirred tank is 45 g L^{-1} which produces a Fab titre of 100 mg L^{-1} and requires a maximum oxygen demand of approximately 200 mmol L^{-1} hr^{-1} (Bowering, 2000). This fermentation has a very high oxygen demand and thus is run in a stirred tank bioreactor, which requires the use oxygen and an increased headpressure to increase the bioreactors oxygen transfer rate during the fermentations peak oxygen demand. In addition the Fab fermentation requires a drop in temperature of 3°C at the peak of cell growth when the fermentation is producing its maximum heat and thus the bioreactor must have an efficient heat transfer system.

The Fab fermentation is a two stage fermentation where for the purposes of maximum Fab yield, production of the cell mass and product occur sequentially. This requires expression of the Fab protein to be controlled, so that it is switched off during cell production and switched on for Fab production. The Fab protein is under the control of the Lac promoter, where lactose is used as the inducer, switching on the Fab expression and hence Fab production (Donovan et al 1996). The maximum specific growth rate is 37 °C to 39 °C, whilst the Fab production is greater at a temperature between 20 °C to 30 °C compared to a temperature of 37 °C. For this process the cells are grown at a temperature of 30 °C and then the temperature is reduced to 27 °C. The lower temperature enhances the proper export, folding and assembly of the functional Fab fragments (Cabilly et al, 1989). The lower temperature also probably reduces the rate of Fab secretion by reducing the rate of leakage from the outer membrane, cell lysis and death. Thus the two stage fermentation allows both the production of cell mass and Fab fragments at their optimum temperatures. The Fab product is produced in the periplasmic space, therefore during product production the strength of the outer wall must be maintained to prevent leakage. The outer wall is strengthened a few hours prior to initiation of product formation by addition of both calcium chloride and magnesium sulphate. The overall Fab yield is dependent on the cell yield and the protein yield per cell (expression rate). There is a correlation between the volumetric productivity and copy number defined as the number of plasmids per cell which breaks down at high copy

numbers (Zabriskie et al, 1986). The presence of the plasmid in the cells is maintained by the plasmid conferring resistance to an antibiotic, which in this case is chloramphenicol.

1.3.2 Animal cell

1.3.2.1 Requirements

The essential requirements for animal cell culture are aseptic operation, ease of scale up and ease of process control and automation. Other requirements include mixing, which allows the cells to remain in suspension, sufficient mass transfer of oxygen, carbon dioxide, waste and nutrient products and minimization of pH gradients (Varley and Birch, 1999). Animal cells have a very low oxygen requirement, where the oxygen demand, qO_2 is typically 20 to 200 mg L^{-1} hr^{-1} for a biomass of less than 10^7 cells ml^{-1} (Drapeau, 1990). Thus an animal cell culture requires a bioreactor which has a k_La, (a measure of the oxygen transfer rate) between 4 hr^{-1} to 10 hr^{-1}. The concentration of CO_2 affects both the concentration of H_2CO_3 and the pH. Since the ratio of CO_2 and HCO_3^- is critical over a narrow range and dissolved CO_2 is toxic to cells at a partial pressure above 120 mm Hg (Aunins et al, 1991; Drapeau, 1990; Varley and Birch, 1999) its mass transfer must be carefully controlled. At the start of the culture CO_2 is often used to control the pH (Varley and Birch, 1999). As the culture progresses, the carbon dioxide evolution rate, (typically 1×10^{-8} mg hr^{-1} per cell), increases as the cells start producing lactic acid so that stripping of CO_2 is required, to prevent the dissolved CO_2 reaching toxic levels (Aunins and Henzler, 1991; Varley and Birch, 1999). This stripping of CO_2 requires bubbles with a relatively large diameter of about 2 mm to 3 mm rather than micro-bubbles with a diameter of about 1mm or less (Gray et al, 1996).

Cell damage in suspension culture is almost entirely due to bubble aeration since in the absence of bubbles extreme agitation is required to induce cell damage (Oh et al, 1989; Kunas and Papoutsakis, 1990). Wood and Thompson (1986) found that there is a wide range in the maximum shear stress that animal cells can tolerate, from less than 0.05

N m^{-2} to 500 N m^{-2}. Another study by Bliem and Katinger (1988) measured a wide range of industrially relevant cell lines and found them to be relatively insensitive to shear. Thus the study by McQueen and Bailey (1989) which found that the turbulent shear stresses required to produce significant cell death for hybridomas, to be greater than 15 N m^{-2} is a useful target. It had been observed in certain medium compositions that cell damage occurs by cells being loosely absorbed to gas-liquid interfaces so that they are exposed to damage as a result of fluid shear (Handa et al, 1987, 1987a; Chalmers and Bavarian, 1991; Bavarian et al, 1991; Orton and Wang, 1990). Although cells are damaged as bubbles form, burst and coalesce, bubble break-up is the main cause of cell damage (Hua et al, 1993; Cherry and Hulle, 1992, Tramper et al, 1991 and Handa-Corrigan, 1989). Cell damage from rising bubbles is thought to be insignificant (Tramper et al, 1987; Glasgow et al, 1989 and 1992).

The extent of cell damage as a result of bubble breakage partly depends on the bubble diameter. Several authors have developed the concept of a killing volume associated with a bursting bubble. This killing volume involves the lamella above a bubble and the jet produced upon bursting and lamella contraction. It has been shown that the cell death rate decreases as the diameter of the bubble increases towards 6 mm (Aunins, and Henzler 1991; Tramper et al, 1986; Chalmers and Bavarian, 1991; Bavarian et al, 1991; Orton and Wang, 1990; Newitt et al, 1954; Garner et al, 1954; Gardner et al, 1990; Murhammer and Goochee, 1988; Garcia-Briones et al, 1994; Boulton-Stone and Blake, 1993). The aeration efficiency (the k_La divided by the power per unit volume) increases as the diameter of the bubble decreases. This means that for bubbles with a diameter of 1mm and below, cell damage is minimized because a significantly lower sparging gas flow rate is required (Aunins and Henzler, 1991). This theory fits with observations made by Wu and Goosen, 1995 that for bubble diameter between 2 mm to 6 mm, the cell death was found to decrease with increasing the bubble diameter and decreasing the gas flow rate. Thus taking into account the requirement for CO_2 stripping, the ideal bubble size is 4 mm to 6 mm in diameter.

The use of surfactants such as Pluronic F68 minimizes damage due to bubble breakage by preventing the cells from adhering to the bubble surface (Chattopadhyay et al, 1995;

Michaels et al, 1995). This surfactant was found to have a concentration dependent effect so that under identical conditions the cell death rate decreases as the concentration of Pluronic increases (Handa-Corrigan et al, 1989).

1.3.2.2 Possible reactors as a disposable animal cell bioreactor

This section outlines the possible reactors that could be used as a disposable animal cell bioreactor. These reactors are also shown in figure 3.

1.3.2.2.1 Airlifts

Airlifts are widely used for animal cell culture. The airlift is a variation on the basic bubble column design. The airlift is split into two or more vertical sections, which are the riser(s) and downcomer(s). These vertical sections are connected together at the top and the bottom to form a loop. There are several different variants of the airlift, depending on how the airlift is vertically spilt. Internal loop airlifts have an internal partition, which is either a baffle as in the spilt cylinder airlift or a draft tube as in the concentric draught tube airlift. External airlifts consist of a riser and a downcomer that are separate and distinct conduits, which are joined together at the top and the bottom by two horizontal conduits to form a loop. (Chisti and Moo-Young, 1987).

For all these variants mixing and aeration is achieved by sparging air into the bottom of the riser(s). This sparged air travels up the riser to the gas disengagement zone, which is the top horizontal section. At the gas disengagement zone, some of the air leaves the fluid so that fluid density increases. As a result of sparging air in the riser, the riser's fluid density is lower than in the downcomer. This difference in the mean density of the fluid between the downcomer and the riser is the driving force for recirculation, so that mixing occurs as a result of liquid recirculation superimposed by mixing due to dispersion (Chisti and Moo-Young, 1987). For an airlift mixing and mass transfer are coupled since both are determined by the gas flow rate. Since animal cells have a very low oxygen demand, the gas flow rate required to drive reactor mixing is often in excess of what is required for oxygenation. Thus both the dissolved oxygen concentration and

carbon dioxide concentration are controlled by altering the partial pressures of these gases and of the nitrogen in the sparged air. This method of control also allows mixing and mass transfer to be uncoupled, so that the flow rate can be increased with extra nitrogen, resulting in a decrease in the mixing time but no change in the transfer of oxygen. Airlifts used for animal cell culture are operated at a very low superficial gas velocity, so that the bubbles are typically in the separate bubble region although at high gas flow rates the chain bubbling regime can occur. This low superficial velocity means that the vast majority of the bubbles entering the riser leave at the gas disengagement zone, so that very few bubbles enter the downcomer. (Varley and Birch, 1999)

The geometry of an airlift has an important effect on its hydrodynamics and therefore on its performance. Increasing the ratio of the riser to downcomer has several effects, including decreasing the overall mixing time (Gavrilescu and Tudose, 1996). The mixing time is also affected by the liquid height above baffle. It has been observed in airlifts, that increasing the liquid height above the baffle beyond a critical height results in two zones being formed. The bottom zone mixes with the rest of the airlift whilst the top zone remains relatively stagnant so that there is little mixing with the rest of the airlift (Russell et al, 1994; Chisti, 1989; Siegel et al Schugerl, 1986). The baffle clearance at the bottom is another critical parameter, where its height should not exceed 1·65 times the area of the downcomer (Russel et al, 1994). The sparger must be located above the bottom of the baffle, so that recirculating fluid flowing from the downcomer does not cause the gas emerging from the sparger to be distributed over to the far wall of the riser (Chisti and Moo-Young, 1987). The sparger design is important since it affects the size of bubbles produced and thus is discussed in section 9.1.

1.3.2.2.2 Bubble column reactors

Bubble column bioreactors have been used to culture insect cells, CHO cells and hybridoma cells (Tramper et al, 1996; Tramper et al; 1988; Lu et al, 1995). The operation of a bubble column for animal cell culture is similar to an airlift. Both the dissolved oxygen concentration and carbon dioxide concentration are controlled by

altering the partial pressures of these gases and of the nitrogen in the sparged air. This results in mixing and mass transfer being uncoupled, so that the flow rate can be increased with extra nitrogen, resulting in a decrease in the mixing time but no change in the transfer of oxygen. As with bubble columns for microbial fermentations, the disposable sparger could either be a perforated plate or ring, an orifice, a rubber membrane sparger or the injector and ejector nozzles (Heijenen and Riet, 1984; Hebrard et al, 1996; Poulsen and Iversen, 1998). The sparger design affects the size of the bubbles produced and thus the sparger design is discussed in section 9.1.

Using the hypothetical killing volume model an equation for designing a bubble column for animal cell culture was developed. The results from this equation showed that increasing the aspect ratio reduced the cell death rate (Tramper et al, 1996; Tramper et al, 1988). In order to prevent excessive cell damage as a result of bursting bubbles, a bubble column should be operated with a superficial gas velocity in the separate bubble regime so that coalescence and dispersion, both producing altered bubble size are minimized (Aunins and Henzler, 1991). Inclining a bubble column at an angle of between 30° to 45° allows good liquid circulation whilst exposure of cells to bursting bubbles is minimized. It has been shown that moving a column from vertical to an angle of 30° results in almost a doubling of the product antibody titre (Lu et al, 1995).

1.3.2.2.3 Plunging jet reactor

A plunging jet reactor has not been used for animal cell culture and thus is an experimental option. It is likely that there will be several differences between the plunging jet reactor used for microbial fermentation and the plunging jet reactor for animal cell culture. Animal cells have a vastly lower oxygen demand and greater shear sensitivity so that the operating power of the plunging jet would need to be much lower. This will result in changes in the nozzle diameter and possibly aspect ratio since the bubble penetration depth will be significantly less. The lower shear sensitivity could result in an animal cell plunging jet reactor having more nozzles per unit volume. It is not known whether the dissolved oxygen and carbon dioxide tension would be controlled

by altering the partial pressures of these gases and the nitrogen in the headspace air or by increasing the pump flow rate.

1.3.2.2.4 Rocker

A vessel can be externally agitated by putting the vessel on a rocker. A disposable plastic bag, which is gamma irradiated, is half filled with media with the remaining volume acting as a headspace, which is inflated with air pumped across it. The bag is mounted on top of a platform that rotates in one axis so that this 'rocking motion' produces waves at the liquid air interface, which results in oxygen transfer, bulk mixing and suspension of cells. The airflow provides the oxygenation and allows gas exchange so that the pH is controlled and CO_2 stripping can occur. As with the airlift the dissolved carbon dioxide concentration is controlled by adjusting the carbon dioxide concentration of the inlet air so that CO_2 stripping is controlled. According to Singh, 1999 the DOT is controlled by adjusting the rocking speed. This idea has been patented by British patent no. 215370/20 and subsequently developed by Vijay Singh whose design has now been commercialized by Panacea Solutions, Inc., Bedminster, New Jersey, USA, as a rocking platform system, WaveBioreactor™ and as a cell culture chambers, Cell-bag™. This system is discussed in more detail in section 1.1.3.1.

Figure 3 - The reactor options for the disposable animal cell bioreactor

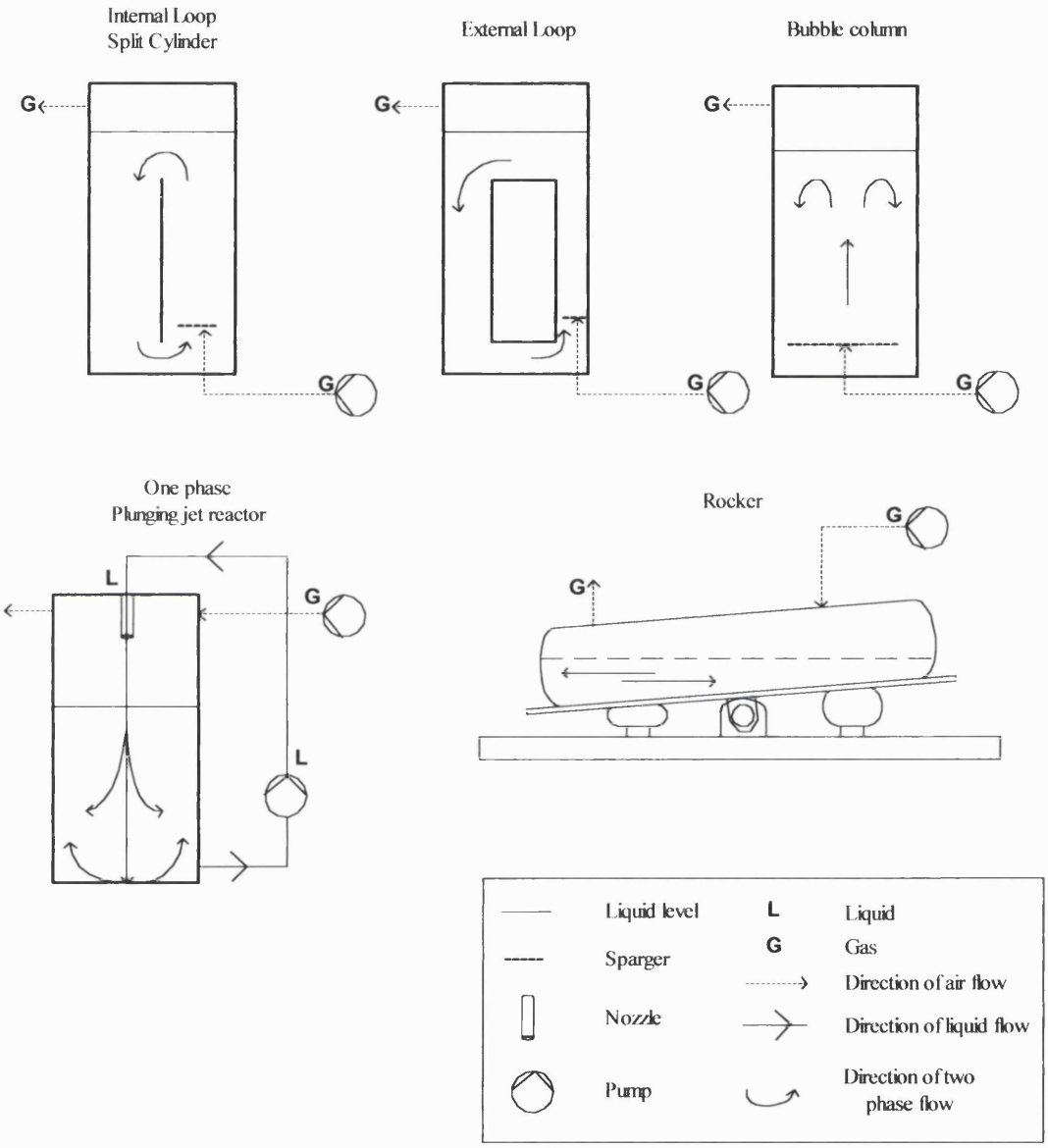

Figure 3
The figure shows the four different reactors, which could potentially be used, as a disposable animal cell bioreactor. There are two airlift reactors, internal loop spilt cylinder and the external loop. There is one nozzle reactor the one phase plunging jet reactor. The other two reactors are the bubble column and the rocker.
The diagrams show the direction of the liquid, 'L' and the gas, 'G' flows for each reactor.

1.3.2.3 Productivity comparison

The productivity of an animal cell bioreactor is an important consideration of a disposable bioreactor and thus is discussed for each of the reactor options.

The maximum k_La at which cell culture can be performed for the rocker is 4 hr^{-1}, whereas in an airlift 10 hr^{-1} is readily achieved. The mixing times in the rocker are 10 seconds and 60 seconds at respective volumes of 10 L and 100 L which is comparable to airlifts (Varley and Birch, 1999) (Singh, 1999).

The plunging jet system has not been used for cell culture and thus it is not known whether cell culture can be supported by such a bioreactor. In addition no work had been performed to determine the power per unit volume required to meet the requirements for animal cell culture

Bubble columns are not used for larger scale production involving animal cells because the reactor has poorer mixing compared to airlifts (Varley and Birch, 1999). Several authors have stated that at comparable power per unit volumes, airlifts have better mixing and therefore lower mixing times. Verlaan et al (1988) stated that unlike the bubble column, the airlift has a circulation of liquid down the downcomer, which provides efficient mixing. Varley and Birch (1999) stated that bubble columns have a compartmentalized flow so that in general this leads to poorer mixing in bubble columns compared to airlifts. Wu and Jong (1994) measured the dispersion coefficients, which are a measure of the degree of mixing in an internal draught tube airlift, and reported these coefficients to be higher than in a corresponding bubble column. Choi et al (1996) also found that the bubble column had poorer mixing than the concentric airlift. Bello et al (1984) stated that the mixing efficiency of the concentric tube airlift is intermediate between a bubble column and a stirred tank reactor.

According to several authors (Margaritits and Sheppard,1981; Orazem and Erickson, 1979; Hatch, 1975; Siegel and Merchuk, 1988), airlifts particularly of the vessel type

(cylinder or rectangular) have higher aeration efficiencies compared to conventional aeration tanks and bubble columns. The aeration efficiencies were the k_La compared on a power per unit volume basis. Both Henzler and Kauling (1993) and Choi et al (1996) found that in a concentric airlift the mass transfer is lower in the airlift than in the bubble column.

The animal cell titre achieved in the rocker was 7×10^6 cells mL^{-1} whilst in the airlift a typical animal cell titre is 5×10^7 cells mL^{-1} (Hu and Aunis, 1997). In a bubble column a cell titre of 1×10^6 cells mL^{-1} has been achieved (Lu et al, 1995). It should be noted that a direct comparison could not be made between these titres.

1.3.2.4 Rationale for selecting th e plunging jet reactor and comparison with an airlift and bubble column

The conventional systems for large-scale suspension culture are airlifts and stirred tank reactors with marine impellers operating at a low agitation speed. As with the microbial fermentations the stirred tank reactor's internals are too complex to be used as a disposable vessel. The most suitable disposable airlift is either the external loop or the spilt cylinder airlift. The draft tube airlift is unsuitable as a disposable because it has an internal tube. As with the down flow bubble column, it would be difficult to ensure that the tube was fixed in an identical position for each disposable bag and thus the disposable bags may not have reproducible performance. The external loop airlift and the spilt cylinder airlift both have internals, which must be located in a reproducible manner as their position affects the performance of the airlift. Both airlifts have a sparger positioned at the bottom of the riser and the spilt cylinder airlift additionally has a baffle, which cuts across the center of the bag.

Whilst bubble columns have been used for animal cell culture, at large scale the reactor has poorer mixing than the airlift and thus is of limited use. In addition as with the

airlifts the bubble column has a sparger, which must be located at the bottom of the reactor in a reproducible manner.

The rocker, which is discussed in section 1.1.3.1, has been well characterized where it has an upper limit on both the k_La and the scale. The rocker has an upper k_La limit of 4 hr^{-1}, which is significantly below the airlifts upper limit of 8 hr^{-1} to 10 hr^{-1} and thus compared to the airlift the rocker has a lower maximum productivity. Although the rocker has a proposed scale of up to 500 L, (Singh, 1999) there are potential problems with operating a rocker at a scale of 200 L or more. This is because the system requires the bag to be attached to a platform, which then moves 10° in one plane at a rate of 40 rpm. The rocker has no external loop so addition of monitoring instrumentation is difficult without the use of a laminar flow hood. Thus although this system is a potential option its scale and k_La constraints mean that alternatives should be investigated.

The plunging jet reactor has no complex internals and unlike all the other potential disposable bioreactors, it has a loop in which a heat exchanger and monitoring instrumentation can be located. Thus in terms of complexity of construction and operation, the plunging jet reactor is the most suitable disposable reactor. Unlike the other potential disposable bioreactors, there is no published work using a plunging jet reactor for animal cell culture. Although the plunging jet reactor has the simplest construction, there is concern that the plunging jet's shear associated with the nozzle, pump and most significantly the bubbles within the plume, will be too high for animal cell culture.

Unlike with the disposable microbial bioreactor, the plunging jet reactor is not the clear experimental choice for the disposable animal cell bioreactor. This is because animal cells are more sensitive to shear and thus are more likely to be damaged by the shear associated with the nozzle, pump and bubbles within the plume. The plunging jet reactors potential as a disposable animal cell bioreactor should be investigated by

measuring the power per unit volume and shear rate incurred for the reactor to match the k_La, CO_2 stripping and mixing in the conventional airlift.

The other options are the airlift, bubble column and rocker. The rocker is limited both by scale and by the k_La so that it is not considered to be a large scale production vessel. As discussed in section in 1.3.2.2.5 at a large scale the airlift has better mixing and aeration than the bubble column operating at the same power per unit volume. Thus an appraisal on converting the airlift to a disposable bioreactor should be performed to consider how complex the construction is in comparison to the bubble column.

Whilst at large scale the airlifts mixing and aeration outperforms the bubble column, at a smaller scale the bubble column may be comparable to the airlift. Thus a comparison between the airlift and bubble columns performance should be performed.

1.3.2.5 Animal cell culture used as basis for design of disposable animal cell bioreactor

1.3.2.5.1 Overview

The experimental approach was divided into three distinct phases, which were to conclude on the best experimental option for the disposable animal cell bioreactor and then to establish the design and operation for this disposable bioreactor. A comparison between the disposable and the conventional bioreactor should then be performed.

1.3.2.5.2 Animal cell culture

Animal cell culture is divided into two principle categories: anchorage dependent, cells that require a surface for attachment, and suspension culture, cells that grow free in suspension. This research concerns suspension culture since this is the preferred system. This is because the scale up is more straightforward and relatively homogenous conditions occur so that the culture can be maintained at key process parameters by an efficient monitoring and control system. Cell suspension can be performed by three modes of reactor operation: batch, fed batch and a continuous perfusion system. Fed batch is commonly used in industry where by small volumes of selected nutrients are fed

into the culture so that productivity is greater than in a batch process. (Flickinger and Drew, 1999). An example of a fed batch process is described by Xie and Wang (1997) that resulted in a cell and monoclonal antibody titre of 1.7×10^{7} cells mL^{-1} and 2.4 g L^{-1} respectively.

1.3.3 Overall scope of work

This work on the design and operation of disposable bioreactors concerns meeting the requirements for both animal cell culture and microbial fermentation and principally considers providing sufficient mixing and aeration. The designs were given to Hyclone Europe who were tasked with producing the disposable bags for experimentation. At the time of doing this experimental work, Hyclone Europe were one of the main suppliers of sterile bags as discussed in section 1.1.3 and thus had considerable experience in the use of materials in disposable equipment for biopharmaceutical manufacture. Thus the scope of this thesis does not include evaluating the materials.

A disposable bioreactor requires changes to the monitoring and control system where the monitoring equipment must either be disposable or non-invasive. Thus consideration should be given to the monitoring and control of these bioreactors. Since evaluating the monitoring and control system for disposable bioreactors could be covered in another thesis, the scope of this work is limited to a review of the possible different monitoring and control methods.

1.4 Aims

1.4.1 Aims for microbial disposable bioreactor

1) To design and determine the operation a disposable plunging jet reactor for microbial fermentation.

2) To make a comparison between the disposable plunging jet reactor and the conventional stirred tank reactor based on the Fab fermentation and the Wild Type fermentation.

The comparison is based on:

i) The physical performance of the bioreactor, which is the operating variables (airflow rate, stirrer speed and pump flow rate), power per unit volume, shear rate incurred and oxygen transfer rate.

ii) The resultant performance of the fermentation, which is the cell growth rate, the RQ, the OUR, the percentage of protein released and for the Fab fermentation the concentration of the Fab product.

3) To review the methods of monitoring and control for a disposable microbial bioreactor.

1.4.2 Aims for the animal cell bioreactor

1) To evaluate how the bubble column and the conventional airlift compare at a relatively small scale.

2) To measure the power per unit volume and shear rate incurred for the plunging jet reactor to match the k_La, mixing and CO_2 stripping of the conventional airlift.

3) To design a disposable airlift bioreactor in order to evaluate it's potential as a disposable bioreactor.

4) To conclude on the best experimental option for a disposable bioreactor and to evaluate the design and operation of this bioreactor.

5) To perform a comparison between a conventional animal cell reactor and the disposable animal cell reactor. The comparison should be based on both the physical performance of the bioreactor and the resultant performance of the animal cell culture.

6) To review the methods of monitoring and control for a disposable animal cell bioreactor.

2. *The Theory of Plunging Jet Reactor*

2.1 Overview

The plunging jet reactor was selected as the proposed disposable bioreactor for microbial fermentation. The experimental approach was to establish the design and operation of the plunging jet bioreactor and then compare this with the conventional stirred tank bioreactor. The experimental approach included evaluating the plunging jet reactor as a potential disposable animal cell culture bioreactor. Thus the plunging jet reactor is included in both the microbial and animal cell culture investigations.

There has been little published work on using the plunging jet reactor for either microbial or animal cell culture. Thus a literature survey was conducted to determine the factors that would affect the design and operation of the plunging jet reactor both as a microbial bioreactor and an animal cell culture bioreactor.

Figure 4 - Diagram of the parameters concerning the plunging jet reactor

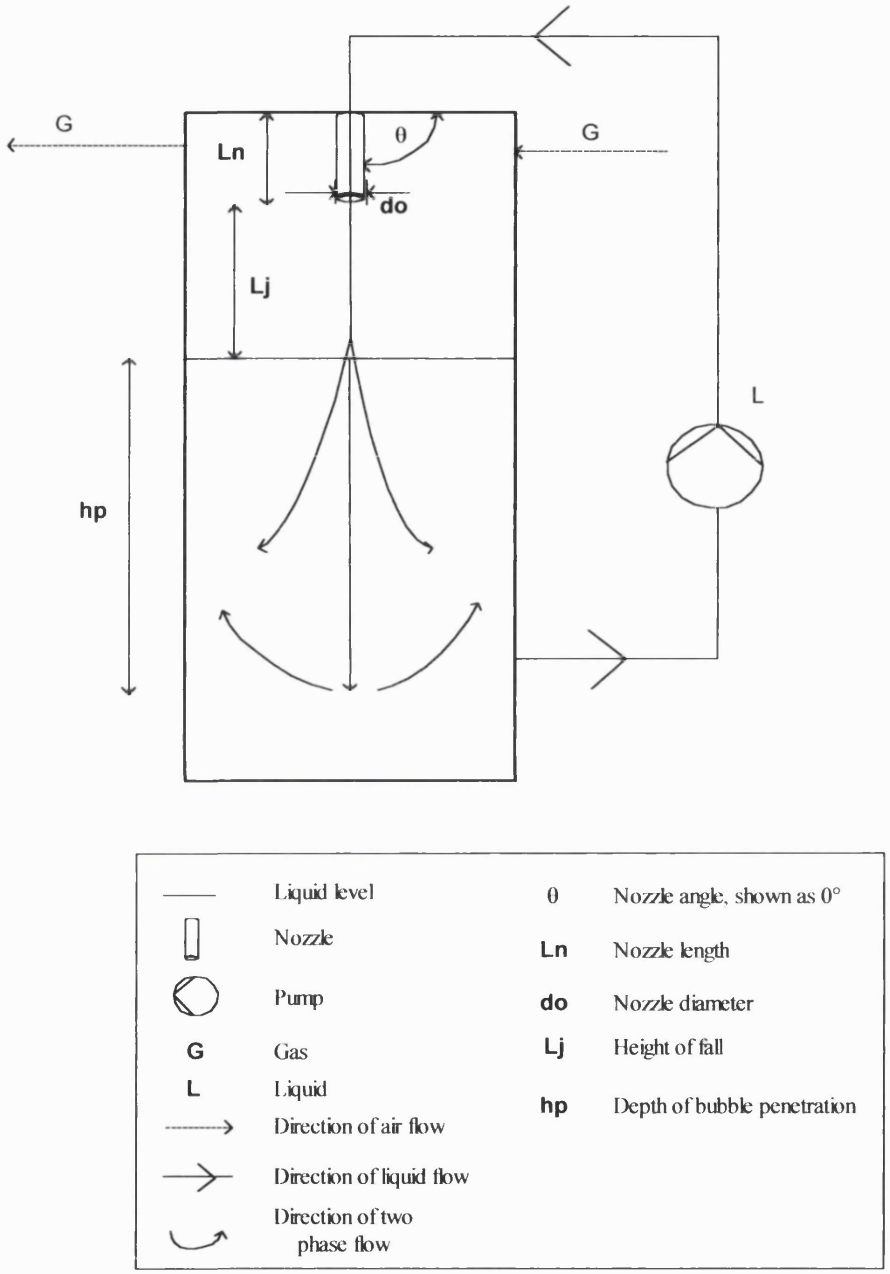

Figure 4
The figure shows the parameters that concern the plunging jet reactor which are discussed in this chapter. These are the nozzle angle, length of the nozzle (nozzle length), diameter of the nozzle (nozzle diameter), distance with the end of the nozzle and the liquid pool which is the height of fall and the vertical length of the entrained bubbles in the liquid pool which is the depth of bubble penetration. The direction of the liquid flow, 'L' and gas or air flow, 'G' are both shown.

2.2 Mass transfer in a plunging jet system

This section discusses the factors that effect the overall oxygen transfer rate of the plunging jet reactor. These factors are the nozzle configuration and operating power, constituents in the liquid pool, mixing times and nozzle design. In this section the overall oxygen transfer rate is measured as the mass transfer factor. This overall oxygen transfer rate or mass transfer factor is a combination of the rate of air entrainment by the jet and the rate of oxygen transfer from the entrained air bubbles to the liquid. Both the rate of air entrainment and the rate of oxygen transfer from the bubbles to the liquid are discussed in subsequent sections.

There are three locations within the jet where mass transfer occurs. Both the mass transfer to the turbulent free liquid jet as it passes through the gaseous atmosphere and the mass transfer to the free liquid surface of the pool is negligible. The third location, which has the most significance, is mass transfer between the bubble dispersion and the pool of liquid. (Bin and Smith, 1982)

The mass transfer factor measures the amount of oxygen that is transferred from the gaseous atmosphere to the liquid pool and is measured as the volumetric rate, with the units $m^3\ s^{-1}$. This is different from the mass transfer coefficient, k_La, which also measures the rate of oxygen transfer from the gaseous atmosphere to the liquid pool but is measured as a rate with the unit s^{-1}. Although in the literature the mass transfer factor is referred to as the K_LA, to avoid confusion in this thesis it has the nomenclature, Q_{KLA}.

The mass transfer is a combination of two processes that can be measured separately. The first stage of the process is the entrainment of air into the liquid pool by the jet. This can be measured as the rate of entrainment or the gas hold up. The second stage is the transfer of the oxygen from these bubbles to the pool of liquid. This stage depends on many factors including the residence time of the bubbles in the liquid, and the extent to which the bubbles' energy is dissipated. The residence time of the bubbles moving

downwards is determined by the momentum of the submerged jet and is measured as the depth of bubble penetration. The residence time of the bubbles moving upwards is determined by their buoyancy force and thus the size of these bubbles. Since the size of these bubbles is independent of the jet velocity and nozzle diameter, the residence time is determined by the momentum of the submerged jet and is measured as the depth of bubble penetration. As discussed in Bin (1993) 'the entrainment efficiency does not necessary go hand in hand with the mass transfer efficiency'. This is because increasing the roughness of a jet so that it is more dispersed will result in a greater volume of gas being entrained, but the depth of bubble penetration will be lower. The energy in the biphasic region is dissipated more diffusely so that the initial bubble size distribution and the liquid phase mass transfer coefficient are likely to be less favorable than the more coherent plunging jet (McKeogh and Ervine, 1981). Thus the rate of air entrainment and the bubble penetration depth can not be analyzed separately. The mass transfer factor, Q_{KLA}, which measures the combination of the rate of air entrainment and the residence time of the bubbles, provides the best guide to assessing the plunging jet's performance. This is discussed first and then a review of the factors affecting the rate of air entrainment and dispersion of the bubbles follows.

2.2.1 Effect of nozzle configuration and operating power

According to Bin and Smith (1982), the mass transfer factor is proportional to the power of the jet. The power of jet is defined by equation 2.0

$$Po = 1/2\rho Q Vo^2 \qquad \text{(Equ. 2.0)}$$

(Bin, 1993)

$$Q_{KLA^\circ} = 9\times10^{-5} Po \qquad \text{(Equ. 2.1)}$$

which is valid for Po, 0.02 to 750 W

(Bin and Smith, 1982)

The equations from Zlokarnik, (1980) show that the mass transfer factor is proportional to the velocity of the jet, the nozzle diameter and the height of fall of the jet. For small diameter nozzles with a diameter between 3 mm to 20 mm and a height of fall between 0·03 m to 0·8 m the following equation 2.2 applies.

$$Q_{KLA20°} = 2{\cdot}68\times10^{-2}Vo^{1{\cdot}634}do^{1{\cdot}383}Lj^{0{\cdot}2} \qquad \text{(Equ. 2.2)}$$

For larger diameter nozzle the following equation 2.3 applies

$$Q_{KLA20°} = 0{\cdot}13Vo^{1{\cdot}7}do^{1{\cdot}65}Lj^{0{\cdot}5} \qquad \text{(Equ. 2.3)}$$

(Zlokarnik, 1980)

Bin (1993) obtained the following equation for long cylindrical nozzle of a small diameter between 3 mm to 20 mm.

$$Q_{KLA20°} = 4{\cdot}28\times10^{-4}Po^{0{\cdot}71}do^{0{\cdot}2}Lj^{0{\cdot}2} \qquad \text{(Equ. 2.4)}$$

which is valid for Po from 0·2 to 100 W

Lj from 0·025 to 0·8 m

Equation 2.4 was compared to data from Funatsu et al (1988b) where the nozzles were shorter. The actual Q_{KLA} was below that of the predicted Q_{KLA}, so it was concluded that for shorter nozzles the mass transfer factor was lower for a given power of the jet, Po.

Notation for the above equations are:

$Q_{KLA20°}$ = Mass transfer factor at 20°m ($m^3\ s^{-1}$)

ρ = density ($kg\ m^3$)

Po = Power of the jet (W)

Vo = Velocity of the jet ($m\ s^{-1}$)

do = Diameter of the jet (m)

Lj = Height of fall, length of jet (m)

Q = volumetric flow rate (m^3 s^{-1})

There is some controversy concerning the effect of the angle of jet inclination (jet angle) on the mass transfer factor, Q_{KLA}. Ahmed (1974), van de Donk (1981) and Van de Sande (1974) all reported that the highest mass transfer factors were obtained for vertical jets. The mass transfer factor was reduced by 10 % to 20 % by changing the jet angle from vertical to 45 °and 60 ° respectively. This was contradicted by Tojo et al (1982) who found that by moving the jet angle from vertical to 60 °, the mass transfer factor increased by a factor of 2.3 for the low power jets and 1.7 for the high power jets. Onkawa et al (1986a) found no significant effect of the jet angle of 45 °and 60 ° on the mass transfer factor, Q_{KLA}.

Two authors have compared the performance of a two jet system with single jet system operating at the same power as the two jets combined. Van de Donk (1981) found that the mass transfer factor, Q_{KLA} decreased slightly as the distance between the two jets increased. Both van de Donk (1981) and Tojo et al (1982) found that the mass transfer factor, Q_{KLA} of the two jet system was lower than the one jet system operating at the same power as the two jets combined. Tojo et al (1982) also found that the single jet system had a shorter mixing time than the two jet system.

2.2.2 Effect of other constituents in addition to water

All the above work was performed in an oxygen water system. The effect of other constituents on the mass transfer rate is complex. Since the plunging jet is a coalescing system, a constituent that hinders the coalescing process will increase the interfacial area of the bubble and thus increase the mass transfer factor. This is shown by Van de Donk et al (1979) and Van de Donk, (1981) where the mass transfer factor was increased due to the presence of salts. Contaminants also reduce the mass transfer factor by 'hindering the

free liquid surface movement' and thus hindering the liquid around the bubbles Bin, (1993). The plunging jet is also effected by changes in the viscosity. At a viscosity of above 6·5 mPa s 'the shear between the pool liquid and the jet controls the entrainment'. Below 6·5 mPa s the roughness of the jet and the air boundary layer affect the entrainment (Bin, 1993).

2.2.3 Mixing

According to Bin, (1993) mixing times in a plunging jet are generally much less than the residence time of the liquid pool and vary from 1 to 150 seconds depending on the pool size, jet velocity and jet angle. According to Bin and Smith, (1982) a plunging jet reactor with a volume of up to $30\times(Hp)^3$, where Hp is the bubble penetration depth can be 'regarded as well mixed'. The most complete mixing occurs when the center line liquid velocity is sufficiently large enough that the bubbles are pushed to the bottom of the vessel and are then deflected upwards. In other words the bubble penetration depth is greater than the liquid height. Tojo et al, (1982) investigated the effect of the jet angle and found that the lowest mixing times were achieved with the jet angle at 60 °.

2.2.4 Effect of nozzle design

Van de Donk (1981) investigated the effect of nozzle design on the mass transfer factor and concluded that the more disturbed jets entrained more air into the pool and produced a higher mass transfer factor. With longer jets the difference in the mass transfer factor, Q_{KLA} between different types of nozzle diminished so that the height of fall had a greater influence on the mass transfer for smooth jets than disturbed jets.

According to Bin (1993) although artificially induced turbulence increases the rate of air entrainment the dispersed jet has a lower depth of bubble penetration. Thus increasing the roughness entrains a greater volume of gas but the energy is dissipated in the biphasic region more diffusely. The US patent, Kenyeres et al., no. 4,840,751 states that the efficiency is determined both by the surface roughness and the coherency of the jet. The more coherent the jet, the 'finer the gas dispersion' and the greater the depth of bubble

penetration. Thus more coherent jets have a longer residence time and hence a greater intensity of contacting. The patent states that increasing the surface roughness by increasing the velocity, height of fall or level turbulence results in a lower energy efficiency of contacting. This is because these methods are associated with significant hydraulic losses and a decrease in the coherency of the jet. The patent claims to increase the surface roughness whilst maintaining the coherency of the jet by blowing a liquid or gas directly onto the jet. This is performed by a specially designed nozzle, which increases the energy efficiency by 30 % to 60 %. As discussed in section 1.3.1.3, Figure 2 which is taken from Bin (1993) shows that the nozzle results in a sufficiently higher k_La than for the basic plunging jet reactor.

It is recommended to use a gas for closed reactors where the gas is under pressure and a liquid for open reactors where the gas to be contacted is the atmosphere itself. A mixture of a gas and liquid is recommended when the pressure or amount of gas is not sufficient to produce the surface roughness required (Kenyeres et al, 1989). The US patent number 4,840,751 gives several comparisons between nozzles that have been roughened and the conventional counterpart, which is operated at the same volumetric flow rate and has the same reactor volume but is not roughened by the nozzle. The comparison is made on the basis of the oxygen transfer rate, measured as the rate of oxygen transfer per unit volume and on the basis of the oxygen transfer efficiency, which is the rate of oxygen transfer per unit power. This information is shown in table 1.

Table 1 - The oxygen transfer rate, k_La for the high turbulence nozzle

Type	How jet is roughened	Liquid volume (m^3)	Liquid flow rate (m^3hr^{-1})	Air flow rate (Nm^3hr^{-1})	OTR ($mmolL^{-1}hr^{-1}$)	OTR efficiency ($kgkW^{-1}hr^{-1}$)
HTPJ	Liquid	0.3	20.4	0	850	8.97
Conv. PJ		0.3	20.4		525	5.54
HTPJ	Gas - circle	0.3	18.9	4.5	680	7.82
Conv. PJ		0.3	18.9		380	4.92
HTPJ	Gas – slots	0.1	6.84	16	1290	5.57
Conv. PJ		0.1	6.84		905	3.92
HTPJ	Gas + Liquid	0.3	20.4	4.5	970	9.18
Conv. PJ		0.3	20.4		525	5.54

Table 1

The table shows the four comparisons between a high turbulence plunging jet labeled 'HTPJ' and a basic plunging jet labeled 'Conv. PJ'. For each of the comparisons the two different plunging jet reactors are operated by identical conditions with the exception of the nozzle. For the high turbulence plunging jet reactor, the jet is roughened either by liquid, gas or gas and liquid, which are all fired on to the jet by the nozzle. This is distinguished in the column 'how the jet is roughened'. The oxygen efficiency is measured as the rate of oxygen transfer per unit volume, OTR and the oxygen transfer rate efficiency, which is the rate of oxygen transfer per unit power.

'Liquid' is where 4% of the liquid flow rate specified is fired at the jet through six holes which are positioned into groups on either side of the jet.

'Gas – Slots' is where gas at the air flow rate specified enters through six slots that are at an equal distance around the jet.

'Gas - circle ' is where gas at the air flow rate specified enters through a slit either side so that it surrounds the jet.

'Gas + Liquid' is where 4% of the liquid flow rate specified enters through six holes positioned either side of the jet and the gas at the air flow rate specified enters through six slots that are at an equal distance around the jet. The ring through which air is directed is below the ring through which liquid is directed.

For the basic plunging jet reactor the jet is not roughened by the nozzle.

The nozzle patented by Kenyeres that uses gas to roughen the jet was used by Zaidi et al (1991) for a Xanthan fermentation. The flow rate supplied by SP 50 Bredel (Delden, Netherlands) peristaltic pump varied between 3.0 to 4.8 m^3 hr^{-1} and the liquid volume was 0.1 m^3. At the end of the fermentation when the Xanthan concentration was 19 kg m^{-3}, the k_La was measured for a series of power per unit volumes. The power per unit volume was increased from 0.07 kW m^{-3} to 0.5 kW m^{-3} resulting in an increase in the k_La from 0.01 s^{-1} to 0.02 s^{-1}. The oxygen transfer rate, k_La versus the power per unit volume was compared with Tojo and Miyanami (1982). The Xanthan fermentation had a better performance than the air water system and this was attributed to the nozzle design patented by Kenyeres et al (1989). The paper states that the maximum power input was limited by the heat transfer rate to the cooling water in the jacket of the reactor.

Another type of plunging jet nozzle, is the falling tube where water runs freely down the wall of the tube. At the bottom the tube narrows so that the jet reforms. The energy usage was 2.5 to 5.0 kg of O_2/kWhr (Jagusch and Puschel, 1968; Jagusch and Schonherr, 1972), which was at the lower limit of the high turbulence plunging jet reactor whose energy usage was 5.6 to 9.2 kg of O_2/kWhr (Kenyeres et al, 1989).

2.3 Mechanisms of air entrainment

The proposed mechanisms for air entrainment, which is how the jet entrains the air bubbles into the liquid pool, are briefly discussed.

There are four mechanisms, all of which are dependent on the velocity and turbulent intensity of the liquid jet. At low velocities the air entrainment is intermittent and pulsating. At high velocities the air entrainment is continuous. At intermediate velocities, there is a transitional mechanism. The jet velocity at which the air entrainment becomes continuous is inversely proportional to the turbulence of the liquid jet. Thus larger velocities are required for initiation of the continuous mechanism for smooth jets compared to rough jets. According to one paper, continuous entrainment is initiated at

velocities of greater than 5 to 8 ms^{-1}. The fourth mechanism is when the liquid jet breaks up into drops before it hits the pool. In this region the rate of entrainment is proportional to the kinetic energy of the jet. (McKeogh and Ervine, 1981 and Bin, 1993)

2.4 Rate of air entrainment

As discussed in section 2.2 the oxygen transfer rate is divided into the rate of air entrainment and the rate of oxygen transfer from the entrained air bubbles to the liquid pool. The rate of air entrainment, which is the rate at which the jet entrains air bubbles, is discussed in this section. The rate of air entrainment is divided into three regions and thus is discussed for each of these regions.

Figure 5 from Bin (1993) shows the log of jet velocity versus log of amount of gas entrainment. This graph shows that the rate of entrainment increases with jet velocity and can be divided into three regions, which are:-

1. Initial or low jet velocity region
2. Transitional region
3. High jet velocity region

Van de Sande and Smith (1974, 1976) concluded that the low velocity region extended to a jet velocity of 5 m s^{-1}. Van de Sande and Smith (1973, 1974) stated that the high jet velocity region was at a Weber number of greater than 10. This Weber number is determined by the following equation.

$$We_A = Vo^2 dj \rho_G / \sigma \qquad \text{(Equ. 2.5)}$$

Figure 5 - Log of the rate of air entrainment versus the log of the jet velocity

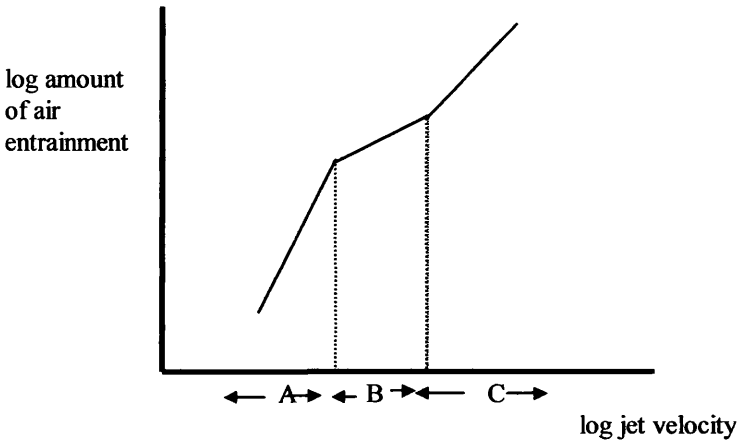

Figure 5
The figure shows how the log of the amount of air entrainment is affected by the log of the jet velocity (taken from Bin, 1993). The graph is divided into three regions, which are labelled as follows.
'A' Intermittent air entrainment
'B' Transitional air entrainment
'C' Continuous air entrainment

Low velocity region

Van de Sande (1974), Van de Sande and Smith (1976), suggested the Y parameter for determining the rate of air entrainment is given by the following equation.

$$Y = do^2 Vj^3 Lj^{0.5} (\sin\alpha)^{-0.5}$$

(Equ. 2.6)

The following equation relates the Y parameter to the rate of entrainment, Qa.

$$Qa = 0{\cdot}015 Y^{0.75}$$

(Equ. 2.7)

This equation is valid for the following conditions

nozzle diameter, do from 2.85×10^{-3} m to 0·10 m

nozzle length to nozzle diameter ratio, Ln:do of 50

jet angle, α between 20 ° to 60 °

height of fall, Lj of up to 4.7 m

Jet velocity, Vj of between 2 m s^{-1} to 5 m s^{-1}

According to Bin (1993) several authors have produced data that show for jets produced from nozzles with a nozzle length to diameter ratio of less than 10, will entrain less air for the same value of Y (Bin, 1988; Funatsu et al, 1988a, Kusabiraki.et al 1990a; Ohkawa et al, 1986, 1986a, 1987).

There is some controversy with the jet angle. According to the equation 2.8 angled jets entrain more air than vertical jets since the rate of entrainment, Qa is affected by the jet angle as follows.

$Qa \alpha (\text{Sin } \alpha)^x$, where $x = -1{\cdot}125$

(Equ. 2.8)

This differs from work by other authors who give different values for the power exponent, x. According to Kumagai and Endoh, (1982) the exponent, x is –0·27 whilst Kumagai and Imai, (1982) gives the exponent, x as +0·21.

<u>High velocity region</u>

High velocity jets entrain air that is captured by the jet roughness and air that is dragged as a laminar boundary layer. The following equations shows how these factors contribute to the rate of air entrainment, Qa (Bin, 1993).

Rate of air entrainment by the jet roughness, Qa_1

$$Qa_1 = \pi Vo/4 (dj^2 - do^2)$$

(Equ. 2.9)

Rate of air entrainment as the laminar boundary layer, Qa_2

$$Qa_2 = \int_{dj/2}^{\alpha} Va \; 2\pi r \partial r$$

(Equ. 2.10)

Total rate of air entrainment, Qa

$Qa = Qa_1 + Qa_2$

(Equ. 2.11)

According to Bin, (1993) the contribution of the boundary layer, Qa_2 to the total amount of air entrained is typically between 20 % to 70 %.

The roughness of the jet can be measured by changes in the mean value between L_l and L_r, which is respectively the surface length of the left and right side of the jet from nozzle exit to the pool surface. The greater the change in the shape of the jet before plunging, the greater the amount of air entrained. It has been shown that increasing the nozzle length to nozzle diameter ratio, Ln/do, the height of fall to nozzle diameter ratio, Lj/do and the Froude number, Fr produces a very similar increase in both the air entrainment and roughness. Thus it is thought that these parameters increase the roughness, which in turn produces a corresponding increase in air entrainment (Kusabiraki, et al 1992).

The Froude number is defined as follows:-

$$Fr = \frac{Vo^2}{(gdo)}$$

(Equ. 2.12)

As with the low jet velocity there is not agreement between authors for the effect of the jet angle. (Van de Sande, 1974, Kumagai and Endoh, 1982, Kumagai and Imai 1982, Ohkawa et al 1986a and Kusabiraki et al 1990).

The above equations for the low and high velocity region have the following notation:

We_A = Weber number

Vo = velocity at the nozzle, (m s^{-1})

dj = jet diameter, (m)

ρ_G = density of gas, (kg m^{-3})

σ = surface tension, N m^{-1}

α = angle of jet inclination, jet angle, °

Qa = total rate of the air entrained, (m^3 s^{-1})

Qa_1 = rate of air entrained by the jet roughness, (m^3 s^{-1})

Qa_2 = rate of air entrained as a laminar boundary layer, (m^3 s^{-1})

Va = local velocity of boundary layer air at a given radius measured from the jet axis, (m s^{-1})

r = jet radius (m)

g = acceration due to gravity, (m s^{-1})

Fr = Froude number

Vj = velocity of the jet, (m s^{-1})

The velocity of the jet, Vj can be calculated using the following equation:

$$Vj = (Vo^2 + 2gLj)^{1/2} \qquad \text{(Equ. 2.13)}$$

2.5 Characteristics of bubble dispersion

This section discusses the characteristics of the bubble dispersion, which is how the air entrained by the jet is distributed in the liquid pool. This is important because the transfer of oxygen from the entrained air bubbles to the liquid pool is affected by the extent to which the bubble's energy is dissipated and the residence time of the bubbles. The characteristics of the bubble dispersion also have relevance when considering the plunging jet reactor as a potential bioreactor, particularly for animal cell culture.

The characteristics of the bubble dispersion are discussed for the different zones of the liquid pool in the plunging jet reactor as show in Figure 6 over the page.

Figure 6 - The different zones of the liquid pool in the plunging jet reactor

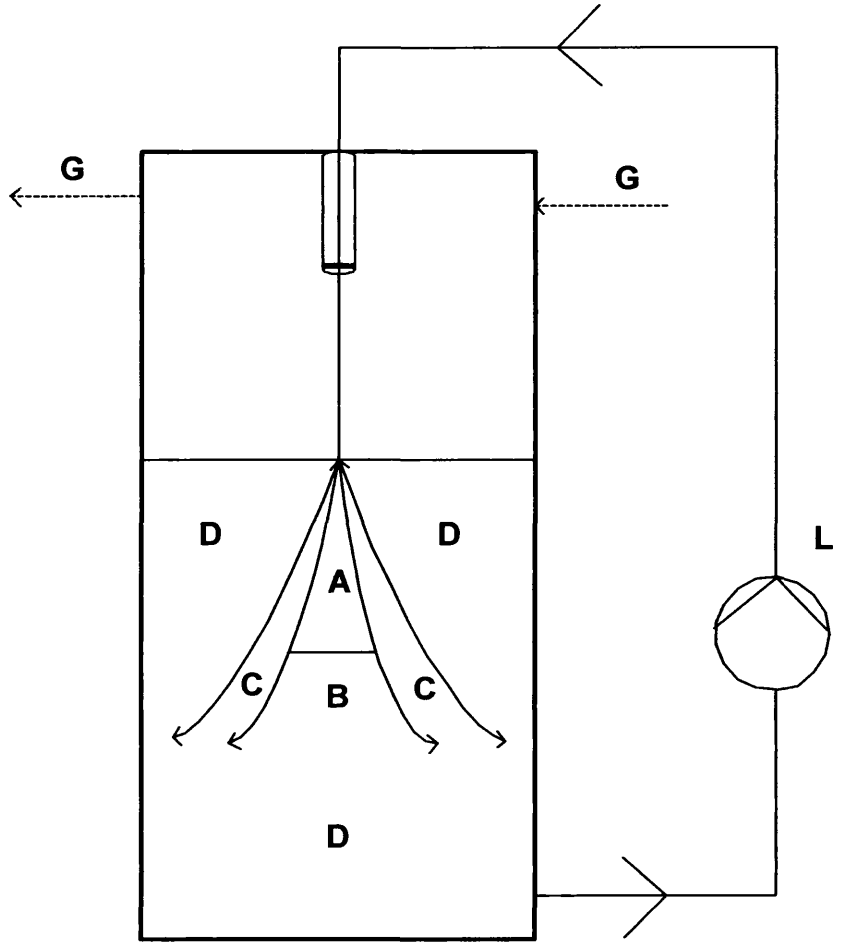

Figure 6

The figure shows diagrammatically the four regions of the plunging jet plume, which are labeled as described below.

'A' Mixing Zone, upper part of biphasic core
'B' The rest of the core, the lower part of the biphasic core
'C' Region surrounding the core where the secondary bubbles are located
'D' The rest of the pool
'L' and 'G' are liquid and gas respectively

2.5.1 Description of the bubble dispersion

Figure 6 shows the different zones of the bubble dispersion in the liquid pool of the plunging jet reactor. The biphasic core consists of the upper part, the mixing zone (region A) and the lower part, the rest of the core (region B). The mixing zone is where the fine primary bubbles with diameters of less than 1mm are located (van de Sande, 1974, Suciu and Smigelschi 1976, Hara et al 1977). These small bubbles in the core are the result of high turbulence intensity and shear stresses (created by the bubbles) which break up the entrained air into the bubbles. Larger bubbles are in the rest of the core and the region that surrounds the core (region C). These secondary bubbles have a sauter mean diameter of 3 to 4 mm which is practically independent of the jet velocity and nozzle diameter (Bonetto and Lahey, 1993, Bin and Smith, 1982).

The bubbles produced in the core as a result of the jet, move down until they either reach the bottom or move sideways, in both cases the momentum of the submerged jet is counteracted by the buoyancy force. The bubbles escape both at the bottom and side because the liquid velocity decreases in both the vertical and radial directions. Coalescence of these primary bubbles also occurs so that they become larger with a greater buoyancy force. This leads to a biphasic core in which the primary bubbles of less than 1 mm are moving down and out and a surrounding 'bubble column' in which secondary bubbles are moving up (Bin, 1993).

The roughness of the liquid jet also affects the biphasic core. The size of the bubbles in the biphasic core is proportional to the roughness. In one experiment a turbulent intensity of 0.8% produced bubbles with diameters in the range of 15 to 300 μm, whilst at a turbulent intensity of 3% the range was 1 to 3 mm. The size of a bubble is also proportional to its buoyancy force, so that the larger bubbles produced by the rough jet have a lower slip velocity (Bonetto and Lahey, 1993; McKeogh and Ervine (1981)

In the mixing core the primary bubbles have a log normal size distribution skewed towards the smaller size range and a bimodal distribution superimposed upon it. This distribution is due to the initial distribution of small bubbles generated by the jet and a

subsequent distribution due to the gradual break-up of the larger bubbles which recirulate in the mixing zone (Evans, 1990, Evans et al, 1992). The secondary bubbles have a normal distribution (Bin, 1993; Bonetto and Lahey, 1993; McKeogh and Ervine, 1981).

As a result of this distribution of bubbles in the pool, the gas fraction also has an uneven distribution in the pool. At the specified depth of zero (at the pool surface), the gas faction increases in a radial direction from zero at the jet axis to a maximum near the original liquid jet radius. Due to dispersion as the depth is increased, the volume of the gas phase increases so that with increasing depth, the maximum gas fraction value decreases. With increasing depth this maximum gas fraction value occurs at progressively shorter radial distances from the jet axis, until at a specific depth the maximum is at the jet axis (McKeogh and Ervine, 1981, Van de Donk, 1981).

2.5.2 Depth of bubble penetration

As described above the bubbles entrained by the jet penetrate the liquid to a depth, which is determined by the momentum of the submerged jet and the buoyancy force of the bubbles. This depth is continually fluctuating so the depth of bubble penetration is measured as a time average and can be estimated by the following equation.

$$hp = C_{54} Vo^{n} do^{p}$$

(Equ. 2.14)

For Vodo ≥ 0.01 $m^2 s^{-1}$, n = p = 0.66, $C_{54} = 2.4$

Vodo < 0.01 $m^2 s^{-1}$, n = p = 1.36, $C_{54} = 61$

(Bin (1983), Bonsignore et al (1985), McKeogh and Ervine (1981), van de Donk (1981), van de Sande and Smith (1974))

Vo = jet velocity at nozzle (m s^{-1})
do = diameter of nozzle (m)

hp = depth of bubble penetration (m)

According to Ohkawa et al (1987) the depth of penetration is dependent on the nozzle geometry and ratio of nozzle length to nozzle diameter. These effects disappear for a nozzle length to diameter ratio of greater than 15 and a height of fall to nozzle diameter greater than 20.

According to Suciu and Smigelschi (1976) the volume of the biphasic cone is determined by the velocity and diameter of the jet. This is in agreement with Tojo and Miyanami, (1982) where the volume of the biphasic cone is proportional to the power of the jet.

Roughness of the jet is inversely proportional to the penetration depth so rough jets produce more compact biphasic cores. This is because jets with a high roughness produce larger bubbles, which have a greater buoyancy force and thus a lower slip velocity (Bonetto and Lahey, 1993).

3. *Monitoring and Control*

3.1 An Overview

A bioprocess that is both validated and running at its optimum requires monitoring and control of its critical parameters. Conventional and disposable bioprocessing differ both in terms of the design and the operation of all the unit operations, including the monitoring and control associated with them. Any monitoring and control system must deliver the accuracy, speed of response and precision that each parameter requires in order to remain within their optimal limits. The aim of this chapter is to review the different methods of monitoring and control and for each parameter consider why the parameter should be controlled and a rough estimate of the extent of control required. *E. coli* fermentations are used for the basis of the microbial fermentation discussion whilst CHO and hybridoma cell lines are used for the basis of the animal cell culture discussion.

3.2 Disposable monitoring and control methods

The following methods can be used to monitor the bioreactor.

i) Off line sampling

ii) On line sampling

iii) At line sampling

Off line sampling

In conventional bacterial fermentations and animal cell cultures, off line sampling is used to measure parameters such as the biomass and the substrate and product concentrations.

In a disposable system samples can be taken to measure parameters that would conventionally be measured by an invasive probe such as pH.

On line sampling

On line sampling can be performed with either

i) disposable invasive probes

ii) non invasive monitoring

iii) conventional invasive probes

Disposable invasive

An invasive disposable probe can be used to monitor the process variables where either a process or an indirect variable is measured. Calibration is performed using standards although some indirect variables require process data. The calibration can be performed by the equipment manufacturer provided that the calibration holds through both time and gamma irradiation. If the end user calibrates the probe, sterility must be retained. Thus for end user calibrations the probe could either be calibrated in the bioreactor or within a separate loop, which is subsequently connected to the bioreactor by a sterile weld. This method also requires calibrating fluids that are sterile and compatible with the process.

Non invasive

Process variables can be monitored non-invasively by measuring either the process variable or an indirect variable. Calibration is performed either with standards or during a process run. Examples of non-invasive monitoring are off gas mass spectrometry, NAD(P)H fluorescence and near infra red spectrometry.

Conventional probes in a loop

A conventional probe can be autoclaved and then calibrated in a sealed loop. This external loop could then be attached to the bioreactor via a sterile weld. Alternatively the probe could be inserted into the disposable bioreactor under a laminar flow hood so that sterility is retained.

At line sampling

The bioreactor can be monitored at line by circulating samples through an external loop with an automated sampling device that contains the measuring instrument. The sampling device is connected to the bioreactor by sterile welds. Cleaning, sterilization and calibration would all be performed by automated procedures.

3.3 The Control Parameters

3.3.1 pH

Requirements

E. Coli

Why control: Maximum growth and possibly product production occurs at an optimum pH (Norris and Ribbons, 1970)

Range – The optimum pH is fermentation specific but typically around pH 7·0 (Norris and Ribbons, 1970)

Precision - ± 0·2

Frequency - The pH is continually changing and therefore requires continuous monitoring.

Animal cell

Why control: Both the product productivity and cell growth rate are very sensitive to the pH (Wayte et al 1997). pH can affect the glycosylation pattern of the product (Borys et al 1993).

Range – The optimum pH is cell line specific but typically within 7·0 to 7·5 (Birch, 1999)

Precision - ± 0·02 units Differences in pH as little as 0·1 units can profoundly affect the cell growth and the productivity of the hybridomas and the myeloma cell lines significantly (Wayte et al 1997).

Frequency - The pH continually changes and thus requires continuous monitoring.

Methods

Conventional on line measurement

The pH is usually measured with a combined glass reference electrode, which has a measuring, and a reference electrode. The potential difference between these two electrodes is calibrated to the pH by the Nernst equation. (Schugerl, 1991)

Disposable methods

The pH can be measured optically with certain pH sensitive indicators, where changes in the optical properties can be calibrated to the pH. The indicator is immersed into the media, so that the hydrogen ions interact with it altering the emission, absorption or transmission spectra. Changes in the spectra can either be measured in the media or non-invasively. The transmission spectrum is measured by a photodiode. The absorption spectra can be measured either by attaching the immobilised polymer on the end of an optical fiber or non-invasively using a photodiode. Typically the light source is either a LED or a xenon arc lamp. The indicator must be immobilised onto a polymer so that is stable and does not leach into the media. (Reardon and Scheper, 1991) Optical probes where an indicator is attached to the end of the probe have been used in fermentations (Agayn and Walt, 1993) (Ferguson et al 1997). In these examples the calibration was not altered by the standard sterilization procedure. For disposables the indicator would have to be measured non-invasively using a photodiode. It is not know whether gamma irradiation would alter the calibration of such an indicator.

At line methods

The pH can be measured at line by a sampling device, which removes a cell free sample. Cleaning, sterilization and calibration can all be performed by automated procedures. In an instrument designed by Joanneum Research (Institute for Chemical and Optical Sensors, Austria), the pH is measured optically with a pH sensitive indicator. This indicator is recalibrated every hour by an automated procedure. The instrument uses a self cleaning membrane to remove the cell free samples.

3.3.2 Dissolved oxygen tension (dO_2)

Requirements

E. Coli

Why Control: E. coli growth requires the DOT to be above 0% (Chen et al, 1985).

Range: > 5 %

Precision - ± 4 %

Frequency - The DOT must be kept above 0% by controlling the power of the aeration system.

Animal cell

Why control: To insure that the DOT is not outside its cell line specific limits.

Range – Optimum DOT varies between cell lines, although most grow over a wide range. Growth rate for a hybridoma cell line was not influenced at a DOT range of 20% to 80% although the specific death rate were lowest at 20 % to 50 % (Ozturk and Palsson, 1991).

Precision - ± 2 %

Frequency - The DOT changes relatively frequently and is conventionally monitored continuously. In the rocker system the DOT is mointored off line (Singh, 1999)

Methods

Conventional on line measurement

The conventional method of measuring the DOT is with a polarographic electrode. The probe consists of two electrodes and an electrolyte which are separated from the measuring liquid by a membrane. The dissolved oxygen diffuses through the membrane and is reduced at the measuring electrode. Thus the dissolved oxygen tension can be calibrated to the potential difference between the reference electrode, the anode and the measuring electrode, the cathode. (Schugerl, 1991)

Disposable methods

As with pH, the dissolved oxygen tension can be measured optically using oxygen sensitive indicators, whose optical properties are calibrated to the oxygen tension. Although absorbance can be the measured optical property, fluorescence is used because it gives a better selectivity and sensitivity. Measuring the oxygen tension by fluorescence requires a chemical indicator whose fluorescence is quenched by oxygen molecules. As with optical pH measurement, the oxygen indicators are immobilized, in for example a silicone rubber membrane. The fluorescence can be measured as its intensity or as its lifetime. The latter is preferred as the selectivity and sensitivity is greater and an LED or ELL can be used as the excitation light source. The fluorescence lifetime is measured by Phase modulation fluorometery rather than the time domain as the instrumentation required is cheaper. (Reardon and Scheper, 1991; Joanneum Research Institute, Institute for Chemical and Optical Sensors ,Austria; Bambot et al, 1994).

An optical sensor has been designed for a bioreactor where a bifurcated fiber optic bundle is directed through a glass window to a silicone membrane with an embedded flurophore. One arm of the fiber optic carries the excitation light whilst the other feeds back the intensity modulated phase shifted fluorescence (Bambot et al, 1994). This method could be used in disposables where the silicone membrane could be attached to the side of the bag and the fiber optic bundle is directed to a clear window in the bag. As with optical pH probes, the optical oxygen probes have been used in fermentations where their

calibration is not altered by the sterilization; however it is not know whether gamma irradiation alters the calibration (Bambot et al, 1994).

Non invasive

E. coli fermentations require process data, which indicates when the aeration rate of the bioreactor must be increased in order to maintain the DOT above 0 % rather than a precise measurement of the DOT. Thus the bioreactor could be controlled by measuring other variables and relating these measurements to the DOT using previous process data. These methods are based on the assumption that for a given reproducible fermentation, all the disposable bioreactors have the same k_La at a specific power per unit volume. Suitable variables are the OUR and CER measured by mass spectrometry and the biomass measured by NAD(P)H dependent fluorescence and near infra red spectroscopy (Heinzle and Dunn, 1991). Other potential variables are substrate and product concentration measured by NAD(P)H dependent fluorescence and near infra red spectroscopy. NAD(P)H dependent fluorescence has been used to estimate the biomass concentration using the tryptophan and riboflavin fluorescence and the 'dynamics of dissolved oxygen concentration' using the pyridoxine fluorescence. These fluorescence measurements can be extended from initial runs to future runs because batch fermentations are repeated routinely using the same cultures and substrates. (Tartakovsky et al, 1996) Near infra red spectroscopy is discussed in later parameter sections.

Animal cells have a very low oxygen demand, so the DOT is maintained within its broad band by controlling the percentage of oxygen in the air, in addition to controlling the gas flow rate. For a reproducible culture, the DOT could be kept within its broad band by fixing the gas flow rate and percentage of oxygen with the time of the culture. As with *E. coli* fermentations an indirect variable such as the OUR could be used to predict the DOT.

At line methods

The oxygen tension can be measured at line by a sampling device, which removes a cell free sample. Joanneum Research (Institute for Chemical and Optical Sensors, Austria)

has designed an optical oxygen sensor, which is similar to their pH sensor described in section 1.5.3.1. In this sensor, the dissolved oxygen tension is calibrated to the fluorescence of a porphyrin dye.

3.3.3 Carbon dioxide (dCO_2)

Requirements

E. Coli

No control required

Animal cells

Why control:. To prevent the CO_2 partial pressure reaching its toxic concentration and to keep it below its cell line specific partial pressure range. Dissolved CO_2 has been shown to influence glycolyation of recombinant proteins (Kimura and Miller 1997).

Range – Dissolved CO_2 is toxic at partial pressures above 120 mm Hg (Aunins et al, 1991). For CHO cells productivity of recomibant product was at a maximum between 30 to 76 mm Hg and inhibited above 105 mm Hg (Gray et al, 1996)

Precision - ± 10 mm Hg

Frequency - The partial pressure is typically mointored once a day.

Methods

Conventional on line measurement

Samples are removed from the bioreactor and the dissolved carbon dioxide is measured using a BGA monitor (Radiometer Copenhagen, Radiometer AS, Copenhagen, Denmark).

Disposable methods

Chang et al (1998) developed an autoclavable sensing film based on fluorescence resonance energy transfer (FRET). As with the dissolved oxygen sensors fluorescence lifetime was measured by Phase modulation fluorometery using a light emitting diode (LED) as the excitation light source. This particular sensing film used the ion pair indicator technique, (Mills et al 1992, Mills and Chang 1993, Mills and Chang 1994a, Mills and Chang 1994b, Weigl and Wolfbets 1995 and Siphior et al 1996) to prepare a near solid-state sensing film which was insensitive to changes in the osmotic pressure. This meant that the film did not require preconditioning by storage or repeated autoclaving in the fermentation media. This ion pair indicator technique would be useful for sensors in disposables.

3.3.4 Temperature

Requirements

E. Coli

Why control: To ensure maximum growth of *E. coli* cells. The productivity of a product can be effected by temperature.

Range – The optimum temperature for growth is between 30 to 37 °C, where the maximum growth rate is typically at 37°C (Farrel and Rose, 1967; Ingraham, 1958). Optimum range for product productivity can differ from the optimum growth. For example the concentration of a fully functional Fab fragment was greater at a temperature of 21°C or 30°C than at 37°C (Cabilly, 1989).

Precision - ± 0·5 °C

Frequency - The temperature continuously changes and therefore requires continous monitoring.

Animal cells

Why control: Animal cells have an optimum temperature range (Birch, 1999)

Range – 37 °C (Birch, 1999). Bloemkolk et al (1992) found for a hybridoma cell line the optimum temperature for growth and antibody production was 37 °C whilst growth was completely inhibited at 39 °C. For some cell lines the optimum temperature for product accumulation is below 37 °C (Mather and Tsao 1990).

Precision - ± 0·1 °C

Frequency – Continuous monitoring

Methods

Conventional on line measurement

The conventional method of measuring the temperature is with electrical resistance thermometers and thermistors, which both have an element whose resistance is calibrated to the temperature. In thermometers the resistance element is a metal wire mounted in a mica or ceramic framework whilst for thermistors it is a semiconductor made from mixtures comprising of oxides of iron, nickel, cobalt, manganese, magnesium and other metals. (Schugerl, 1991)

Non invasive method

The temperature could be measured outside the plastic bag by a resistance thermistor or thermometer. The response time depends on the conductivity between the thermistor or thermometer and the measuring liquid. Although this conductivity partly depends on the plastic bag conductivity; it can be increased by putting the measuring element in a sealed pocket filled with a highly conductive medium.

3.3.5 Biomass

Requirements

E. Coli

Why control: To check that there are no problems with the cells and that the times for feeding and induction are correct.
Frequency -Off line, every time the biomass doubles which varies from about 1 to 3 hours.

Animal cells

Why control: To check that there are no problems with the cells and that the times for feeding and induction are correct.
Frequency - Off line, every 12 hours

Methods:

Off line conventional analysis

Biomass is conventionally measured off-line, where the *E. coli* biomass is conventionally measured as the optical cell density in a spectrometer and the animal cell biomass is conventionally measured as the cell count using a haemocytometer.

On line non invasive method

Non-invasive methods are near Infra red spectroscopy, NAD(P)H dependent fluorescence and off gas analysis. Schmidt et al (1998) used near infra red to measure the optical density in a fermentation broth. Tartakovsky et al (1996) showed that scanning fluorometry is more informative than conventional NAD(P)H dependent fluorescence. In *E. coli* fermentations the tryptophan and riboflavin fluorescence was used to predict cell density (Tartakovsky et al, 1996). A chemical multisensor array together with an artificial neural network was used to estimate the biomass concentration and the specific growth rate by analysis of the off gas. An accuracy comparable to the conventional dry weight method was achieved (Bachinger et al 1998).

3.3.6 Substrate, Product etc.

Requirements

E. Coli

Why control: To check that there are no problems with the fermentation.

Frequency -Off line, typically retrospectively.

Animal cells

Why control: To check that there are no problems with the fermentation. Typical measurements are glucose, lactate, glutamine, ammonia

Frequency - Measured retrospectively off line

Methods:

Off line conventional analysis

All the measurements are conventionally measured off line.

At line methods

A stop flow analyser can measure the concentration of various substrates and products e.g. glucose and lactate. For example Ozturk et al (1997) measured the glucose and lactate concentration using an analyzer which removed cell free samples from a reactor via a 0·45 μm hollow fiber filtering system which was located in a circulation loop.

On line non invasive method

Near infra red spectroscopy can measured the concentration of products and nutrients in a conventional fermentation process. Schmidt et al (1998) measured the concentration of L-threonine, L-lysine in a fermentation broth whilst Hall et al (1996) mesured acetate and gycerol in *E. coli* fermentation. The technique can be accurate which was demonstrated by Riley et al (1998), where the concentration of alanine, glucose, glutamine and leucine was measured with a predition error of 1·4, 1·0, 1·1 and 0·3 mM respectively. According to Schmidt et al (1998) successful use of near infra red spectroscopy requires a calibration using at least 100 samples which cover the whole range of concentrations. The author also stated that this type of spectroscopy doesn't replace chemical analytical methods since they are required for the initial calibration and for peroidic recalibration.

3.3.7 Foam control

Requirements

E. Coli

Why control: Foam must not reach the air outlet filter.

Frequency -Continuous.

Animal cells

Why control: Foam must not reach the air outlet filter.

Frequency - Continous

Methods:

Disposable method

The height of the foam can be measured using a conductivity strip, which runs along the inside of the bioreactor and is connected to a disposable foam probe at the top of the bioreactor.

Non invasive method

An optical method using an optical window.

4. Materials and Methods

The aim of this chapter is to present all the materials and methods used for the experimental work in chapters 5 to 7. Section 4.1 covers the methods and equipment used to measure the k_La, CO_2 stripping and mixing time in both the microbial and animal cell bioreactors which is presented in all three results chapters. Section 4.2 details the monitoring, control and operation of the plunging jet bioreactor and the stirred tank bioreactor that is presented in chapter 6. Section 4.3 and 4.4 detail the protocols used for the Wild Type and Fab fermentations and section 4.5 details methods used for further experiments performed on the Fab and Wild Type fermentations.

4.1 Measurement of Mass Transfer Coefficient, CO_2 Stripping and Mixing Time

This section details the methods and material used to measure the k_La, CO_2 stripping and mixing time for the plunging jet reactor as a microbial bioreactor and the airlift, bubble column and plunging jet reactor as animal cell bioreactors. The section includes a description of the reactors, which for the microbial plunging jet bioreactor were the plunging jet mimic and the disposable plunging jet bag, and for the animal cell bioreactor were an airlift, bubble column and plunging jet reactor (not the same as the microbial bioreactor). The disposable plunging jet bag was subsequently used for the microbial fermentations.

4.1.1 Principals of Measurement

Principals of measurement are the equations and the principles used to measure the k_La, a measure of the oxygen transfer, the CO_2 stripping, a measure of the carbon dioxide transfer and the mixing time, a measure of time taken for compete homogeneity of macro mixing to be achieved. Appendix 9.2 details the equation used for the k_La measurement that the CO_2 stripping equation is also based on.

4.1.1.1 Mass transfer coefficient, k_La

The rate of oxygen transfer from the air bubbles to the liquid is given by the following equation.

$$k_L a = \frac{\partial C_L}{\partial t}\left(\frac{1}{(C^* - C_L)}\right)$$

(Equ. 4.1)

Integrating equation 4.1 for the time taken (t) for the oxygen saturation to increase from 5% to 70%, the k_La can be calculated as follows.

$$k_L a t = -\int_0^t \ln(C^* - C_L)$$

(Equ. 4.2)

Since $C_{L1} = 0$

$$k_L a = \left(\frac{1}{t}\right)\ln\left(\frac{(C^* - C_L^\circ)}{(C^*)}\right)$$

(Equ. 4.3)

$$k_L a = \frac{1}{t}\ln\left(\frac{1}{Y_L}\right) \qquad Y_L = \frac{(C^* - C_L)}{C^*}$$

(Equ. 4.4)

$$k_L a = \frac{1}{t}\ln\left(\frac{1}{Y_L}\right)$$

Define the probe response time, r_2

Let $r_2 = 1/Yp$

$$Y_P = \left(\frac{C^* - C_L}{C^*}\right)$$

(Equ. 4.5)

$Y_L = \exp(-k_L at)$

(Equ. 4.6)

As a first order process strictly exponential with a lag where K_P is the probe constant

$$\frac{\partial Y_p}{\partial t} = Kp(Y_L - Y_p)$$

(Equ. 4.7)

Equation 4.8 results from integrating equation 4.7 as shown in the appendix 2 and substituting for Y_L as given by equation 4.6.

$$Y_P = \frac{1}{r_1 - r_2}\left[r_1 \exp\left(\frac{-t}{r_1}\right) - r_2 \exp\left(\frac{-t}{r_2}\right)\right]$$

Where the resistances' r_1 and r_2 are defined as:

$r_1 = 1/k_La$ and $r_2 = 1/Kp$

(Equ. 4.8)

r_2 is the probe response time, which can be measured so that equation 4.8 reduces to

$$Y_p = \exp\left[\frac{-t}{r_2}\right]$$

When $t = r_2$, $Yp = \exp(-1) = 0{\cdot}368$

(Equ. 4.9)

The value of r_1 (or k_La) can be determined from equation 4.9.

Where:-

k_La = Volumetric mass transfer coefficient (s^{-1})

C* = Oxygen concentration of the liquid when it is in equilibrium with the gas (Mol L^{-1})

C_L = Oxygen concentration in the liquid (Mol L^{-1})

C_{L1} = Oxygen concentration in the liquid (Mol L^{-1}) at time t = 0

C_{L2} = Oxygen concentration in the liquid (Mol L^{-1}) at time t = t

r_2 = Probe response time from 100% to 36.8% (s)

Kp = Probe constant, $1/r_2$ (s^{-1})

The k_La is measured by the dynamic gassing out method where the dissolved oxygen tension, DOT is reduced to 0 % by dissolving nitrogen gas into the liquid. The time and DOT are measured using a chart recorder. The k_La is calculated from the probe response time, r_2 , and changes in the DOT with time by using the program shown in the appendix 9.3 which calculated the k_La on the basis of equation 4.9.

For each set of data the probe response time was measured. This was the time taken for the DOT to fall from 100% to 37% immediately after the probe was moved from water with DOT at 100% to water with the DOT at 0%. The temperature was measured using a temperature logger, (Squirrel, SQ1 600 Grant Instrument, Cambridge, UK).

The k_La values measured for the bubble column, airlift and plunging jet for animal cell culture were considerably lower than for the disposable plunging jet mimic and bag. The DOT probe response time of eight seconds was considered to be within the error of the k_La. Thus the probe response time was not taken into consideration, so the k_La for successive 10% increments in the DOT was measured using equation 4.3.

4.1.1.2 CO_2 stripping coefficient, CO_2 stripping

CO_2 stripping coefficient measures the rate of Carbon Dioxide transfer from the liquid to the air bubbles. It is based on the same principles as the k_La and thus equation 4.3 was adjusted so that it measured the CO_2 stripping coefficient. The dissolved oxygen tension was replaced by the dissolved partial pressure of CO_2.

$$k_L a = \frac{1}{t}\left[\ln\frac{\left(pCO_2^* - pCO_2^\circ\right)}{\left(pCO_2^* - pCO_2^t\right)}\right]$$

(Equ. 4.10)

Where

CO_2stripping = CO_2 stripping coefficient (s^{-1})

pCO_2^* = partial pressure of CO_2 in the liquid when it is saturated with CO_2 (mm Hg)

pCO_2° = partial pressure of CO_2 in the liquid at time, t = 0 (mm Hg)

pCO_2^t = partial pressure of CO_2 in the liquid at time, t = t (mm Hg)

t = time, (s)

4.1.1.3 Mixing time

The mixing time measures the time taken for a component to mix in the bioreactor and achieve complete homogeneity. The mixing time was measured as the time taken for sodium sulphite to mix with potassium triioxide solution. This was shown by a change in the solution colour from red to clear. This occurred because reaction 'a' was pulled to the right by the removal of iodine from the solution by reaction 'b'.

Reaction a: $KI + I_2 \rightarrow KI_3$

b: $Na_2SO_3 + I_2 + H_2O \rightarrow Na_2SO_4 + 2HI$

4.1.2 Plunging jet mimic

A perspex vessel was constructed with an outlet that was connected in a loop to a pump and nozzle. This was used to perform an initial series of studies on the design and operation of the plunging jet reactor as a disposable microbial bioreactor.

4.1.2.1 Description of the plunging jet mimic

A cylindrical vessel of diameter 0·2 m and height 0·7 m was used as a plunging jet mimic where the total volume was between 6 L and 9 L. The vessel had several outlets at the bottom, which were all positioned at 30 mm from the edge. Initially the outlet was 3·85 mm in diameter but was later increased to 16 mm. Nozzle diameters of 3·85 mm and 8·0 mm were used. A nozzle diameter smaller than 3·85 mm generated too higher a pressure for the pipe work. A peristaltic pump (Watson Marlow series 605Di/R peristaltic pump, Falmouth, Cornwall) was initially used. This pump was used in conjunction with an accumulator, which was essentially a plastic sealed bottle with two pipes. The inlet pipe was shorter than the outlet pipe so that only the outlet pipe was below the liquid level in the accumulator. The accumulator and peristaltic pump were replaced by a mono pump.

4.1.2.2 Measurement of k_La

The dissolved oxygen tension was reduced to zero by sparging nitrogen through the liquid using an air stone. Changes in the dissolved oxygen tension, (DOT) were measured with an Ingold probe (Mettler Toledo Ltd., Leicester, UK.) connected to a chart recorder. Thus with the DOT at 0 % the pump and chart recorder were simultaneously switched on so that the rate of change of the DOT were measured and the k_La was determined as described in section 4.1.1.1.

4.1.2.3 Measurement of mixing

As discussed above the mixing time was measured as the time taken for sodium sulphite to mix with potassium triioxide solution. This was shown by a change in the solution colour from red to clear. A 200 mL volume of potassium triioxide which consisted of 0·0375 mol L^{-1} of Potassium Iodide and 0·0125 mol L^{-1} of Iodine was added to the fermenter volume of 6 L of deionised water. The pump was switched on and the mixing time was started when 20 mL of sulphite solution of concentration 0·100 mol L^{-1} was added.

4.1.3 Disposable plunging jet bag

A disposable plunging jet bag was constructed by Hyclone Europe for use as the disposable microbial bioreactor which was compared with the stirred tank bioreactor in chapter 6. The design is detailed in chapter 6 and shown in figures 14 to 16. In addition to the microbial fermantions, the disposable plunging jet bag was used for k_La and mixing studies.

4.1.3.1 Description of disposable plunging jet bag

The disposable plunging jet bag, which is shown in figures 14 to 16, consisted of a square, bottomed plastic bag, which was inserted into a cylindrical perspex support. The

plastic bag was 0·66 m in height with a square based bottom of width 0·25 m and was constructed by Hyclone Europe (Newcastle, UK) for our personal use. The sides of the bag were constructed from four panels, which were welded along the sides. The bottom and top of the bag was a pyramid base of four equal triangles. Both the base and the top could be pulled out to form a flat square bottom and top. The bag was stretched into a cylindrical support of 0·29 m in diameter and 0·66 m in height. Due to the bags flexibility it stretched into the support so that it fitted the support tightly. In the top of the bag holes were mounted for the addition of the nozzle and for feed streams such as the alkali, acid, inoculum and fermentation feeds. At a distance of 0·05 m from the top at either side of the bag, two holes allowed attachment of an air inlet and outlet. The outlet to the pump was located at a distance of 0·05m from the bottom on one side of the bag. The DOT probe and pH probes were positioned on the opposite side at a distance of 0·05 m from the bottom. The outlet was connected in series to the mono pump and the process side of a heat exchanger (Alfa laval type POI-VL, Manufacturing no. 30100-14060, Alfa laval, Sharples, Camberley, UK) before being connected to the inlet of the plunging jet, which consisted of a nozzle. The cooling side of the heat exchanger was connected to a water bath, (F6, haarke, Germany) which was set at 20°C. The temperature of the liquid inside the plunging jet bag was measured with a temperature logger, (Squirrel, SQ1 600 Grant instrument, Cambridge, UK). Four nozzles were constructed with diameters of 2·4 mm, 2·8 mm, 3·2 mm and 4·0 mm, where the length of the nozzle was 15 times the nozzle diameter. The nozzles were lengthened by 35 times the nozzle diameter with a length of pipe of 4·0 mm in diameter, which proceeded the narrower diameter of between 2·4 mm to 4·0 mm. A fifth nozzle of 2·4 mm and 15 times the diameter in length was lengthened by 0·45 m with a pipe of 4·0 mm in diameter. This fifth nozzle was used for experiments investigating the height of fall.

4.1.3.2 Measurement of k_La

The k_La was measured in the disposable plunging jet by the same method as the disposable plunging jet mimic with several exceptions. The dissolved oxygen tension

was reduced to 0 % by putting nitrogen gas across the headspace and operating the mono pump so that the plunging jet entrained the nitrogen gas. When the DOT reached 0% the pump was switched off and air was blown across the headspace for a fixed time so that the nitrogen gas in the headspace was replaced by air. With the liquid at 0 % and the headspace full of air, the k_La was measured by simultaneously switching on the mono pump and chart recorder. As before changes in the dissolved oxygen tension, (DOT) were measured with an Ingold probe (Mettler Toledo Ltd., Leicester, UK.) which was connected to a chart recorder. Although the temperature of the water was maintained at 20 °C by the heat exchanger and water bath, it was recorded for each run.

4.1.3.3 Measurement of mixing

The disposable plunging jet bag was relatively opaque so the mixing time could not be measured by colour changes associated with a sodium sulphite solution mixing with a potassium triioxide solution. The mixing time was measured as the time taken for a pulse of sodium hydroxide to raise the pH to an equilibrium value. For each run the pH of the water in the plunging jet was adjusted to 6·0 units with concentrated alkali and acid. With the mono pump running 10 mL of 6 M NaOH was added and the time was measured for the pH to increase from 6·0 to 11·0 units. After each run liquid was removed via the sample line so that the liquid volume was fixed. The pH was measured with an Ingold probe (Mettler Toledo Ltd., Leicester, UK.) connected to a chart recorder. The pH probe had a probe response time, which unlike with the oxygen probe could not be describe by a simple mathematical function. Thus the probe response time was included in the final mixing time

4.1.4 Plunging jet, bubble column and airlift for use in suspension culture

As detailed in chapter 7 a comparison was made between the plunging jet reactor, bubble column reactor and airlift reactor which was based on the suitability of each reactor as a disposable animal cell bioreactor. The comparison was based on measurements of the

k_La, CO_2 stripping and mixing time. This section details the equipment and methods used for this comparison.

4.1.4.1 Description of airlift, bubble column and plunging jet reactor

A comparison was made between a 26 L airlift, bubble column and plunging jet reactor. All three reactors had the same vessel geometry of 1 m height and 0·185 m diameter. The airlift and bubble column had an identical perforated pipe gas sparger at the bottom. For the airlift the sparger was positioned in the middle of the riser, 0·05 m above the bottom of the baffle. For the bubble column the sparger was positioned 0·03 m off centre. The airlift was a spilt cylinder where a baffle of 0·7 m in length was positioned 0·1 m above the bottom so that there was 0·2 m of liquid above the baffle. The baffle was positioned across the centre so that the riser and downcomer were equal in area. For the plunging jet a peristaltic pump (Watson Marlow series 605Di/R, Falmouth, Cornwall) was used. For plunging jet reactor an accumulator was used when necessary to smooth the pulse of the jet. The plunging jet reactor was similar to the plunging jet mimic since it had an open headspace. The same 2·4 mm and 4·0 mm nozzles were used. Additional experiments were performed for the plunging jet reactor where the same vessel was used but at a reduced volume and thus aspect ratio of between 6 L to 20 L and 4·30 to 1·44 respectively.

4.1.4.2 Solutions used for the measurement of k_La, CO_2 stripping and mixing

Both the k_La and CO_2 stripping coefficient was measured in a buffer solution consisting of NaCl 6·4 g L^{-1}, $NaHCO_3$ 2·0 g L^{-1} and Pluronic F68 1·0 g L^{-1} dissolved in RO water; whilst the k_La was additionally measured in RO water. The mixing time was measured in Pluronic F68 1·0 g L^{-1} dissolved in RO water.

4.1.4.3 Measurement of k_La

As with the plunging jet mimic and the disposable plunging jet bag, the dynamic gassing out method was used to measure the k_La. The dissolved oxygen tension was reduced to zero by sparging nitrogen gas into the vessel for all three reactors. An Ingold DOT probe (Mettler Toledo Ltd., Leicester, UK.) measured the changes in DOT and was connected to a chart recorder. For the bubble column and airlift the chart recorder was started as the sparging gas was switched from nitrogen to air. For the plunging jet reactor the peristaltic pump and chart recorder was switched on simultaneously. The k_La values measured were considerably lower than for the disposable plunging jet mimic and bag. As discussed in section 4.1.1.1 the DOT probe response time of 8 seconds was considered within the error of the k_La. Thus the probe response time was not taken into consideration, so the k_La was measured using equation 4.3.

4.1.4.4 Measurement of CO_2 stripping

The CO_2 stripping coefficient was measured using equation 4.10. The partial pressure of CO_2 in the liquid was adjusted to 110 mm Hg, which corresponded to a pH of 6·95 units by sparging a combination of nitrogen and carbon dioxide. The partial pressure of CO_2 was measured using a BGA monitor (Radiometer, Radiometer AS, Copenhagen, Denmark). The decline in the partial pressure of CO_2 was measured from the moment the sparging gas was switched to air for the bubble column and airlift and when the peristaltic pump was switched on for the plunging jet reactor.

4.1.4.5 Measurement of mixing

The mixing time was measured as the time taken for potassium triioxide solution to mix with an addition of sodium sulphate. This was shown by a change in the solution colour from red to clear. Potassium triioxide with a concentration of 1·00 mol L^{-1} of Iodine and 1·20 mol L^{-1} of Potassium Iodide was added to the bioreactor at a volume of 0·300 ml per Litre of liquid in the reactor. With the bubble column and airlift at the required gas flow

rate and the plunging jet at the required pump flow rate, the mixing time was measured from the time of addition of sodium sulphate. The sodium sulphate of concentration 1·36 mol L^{-1} was added at a volume of 0·250 mL per Litre of liquid in the reactor. The mixing time was stopped when the whole liquid volume was clear.

4.2 Fermentations

This section details the materials and methods used to monitor and operate both the conventional stirred tank bioreactor and the disposable plunging jet reactor. These bioreactors were used for the comparison between the disposable and conventional bioreactors presented in chapter 6. The comparison was based on performing both the Fab and Wild Type fermentations in these reactors.

4.2.1 On line monitoring and operation of the bioreactors for the *E. coli* fermentations

Both the stirred tank reactor and plunging jet reactor were controlled and monitored by on line equipment. For both bioreactors the airflow rate, pH, temperature, stirrer speed for the stirred tank and pump flow rate for the plunging jet reactor were controlled. The on line monitoring was used to obtain the oxygen uptake rate, OUR, the carbon dioxide evolution rate, CER, the respiratory quotient, RQ and the dissolved oxygen uptake rate, DOT.

4.2.1.1 Operation of the stirred tank reactor

A 7 L LH fermenter (Adaptive Biosystems, Luton) was used with a 5 L working volume for the stirred tank reactor. The bioreactor had 3 rushton turbines and a perforated pipe sparger to provide the agitation and aeration. The airflow was fed via a 0.2 μm (emflon 11, DFA 300 1V00 2PV filter, Pall, Portsmouth) membrane into the sparger and via an outlet with a 0.2 μm (2MTB-0202Y-A, Domink Hunter, Country Durham) filter. A bleed from the outlet was fed into a mass spectrometer (MM8-80 Instrument, VG Gas Analysis Ltd., Winsford, Cheshire, UK.). The temperature changes were made by a heating element and coiling coils which were connected to process water. Acid, Alkali, Inoculum and Feed vessels were attached to the top of the fermenter via LH needles, which were inserted aseptically into their septums. Samples were removed via a LH sampling device

which was connected to a sampling tube and employed a membrane to remove samples aseptically.

4.2.1.2 On line monitoring and control of fermentation parameters for the stirred tank reactor

Both the dissolved oxygen tension and the pH were measured by Ingold probes (Mettler Toledo Ltd., Leicester, UK.). The temperature was measured by a thermacouple. Off line gas analysis was preformed by a mass spectrometer (MM8-80 Instrument, VG Gas Analysis Ltd., Winsford, Cheshire, UK.) which measured the partial pressure of nitrogen, oxygen, carbon dioxide and argon.

The temperature, pH, airflow rate and agitation rate were all controlled by the software package, Adaptive Biosystem (Adaptive Biosystems, Luton) via a 6358 eight loop controller (Turnbull Control Systems Ltd. Worthing). The software package, RTDAS or Real Time Data Acquisition Systems (Aquisistion Systems, Camberley, UK.) logged data from both the mass spectrometer and the TCS controller. The oxygen uptake rate, OUR and carbon dioxide evolution rate, CER were calculated using the RTDAS program. The software package, Adaptive Biosystem (Adaptive Biosystems, Luton) logged the temperature, pH, airflow rate, agitation rate and dissolved oxygen tension.

4.2.1.3 Operation of the plunging jet reactor

The disposable plunging jet was connected to the mono pump via the side outlet as shown in figure 16. The mono pump was in series with the process side of a heat exchanger followed by a 2·4 mm nozzle at the inlet of the disposable plunging jet. The cooling side of the heat exchanger was connected to a water bath (F6, Haake, Germany). Acid, Alkali, Inoculum and Feed vessels were connected to the disposable plunging jet at the top near the inlet. Air was pumped across the headspace via an inlet with a membrane and an outlet positioned either side of the vessel, 0·05 m from the top. A bleed from the outlet was then connected to a mass spectrometer (MM8-80 Instrument,

VG Gas Analysis Ltd., Winsford, Cheshire, UK.). Samples were removed from a sampling tube.

4.2.1.4 On line monitoring and control of fermentation parameters for the plunging jet reactor

As with the stirred tank reactor both the dissolved oxygen tension and the pH was measured by Ingold probes (Mettler Toledo Ltd., Leicester, UK.). The temperature was measured by a temperature logger, (Squirrel, SQ1 600 Grant Instruments Ltd., Cambridge, UK). Off line gas analysis was preformed by a mass spectrometer (MM8-80 Instrument, VG Gas Analysis Ltd., Winsford, Cheshire, UK.) which measured the partial pressure of nitrogen, oxygen, carbon dioxide and argon. The pH and airflow rate were controlled by the software package, Adaptive Biosystem (Adaptive Biosystems, Luton) via a 6358 eight loop controller (Turnbull Control Systems Ltd. Worthing). Both the temperature and the pump flow rate were controlled manually by adjusting the temperature of the water bath (F6, Haake, Germany) and the pump flow rate of the mono pump. The software package, RTDAS or Real Time Data Acquisition Systems (Aquisistion Systems, Camberley, UK.) logged data from both the mass spectrometer and the TCS controller. The oxygen uptake rate and carbon dioxide evolution rate was calculated using the RTDAS program. The software package, Adaptive Biosystems (Adaptive Biosystems, Luton) logged the pH, airflow rate and dissolved oxygen tension. The squirrel logged the temperature.

4.2.2 Off line monitoring of the *E. coli* fermentations

For both reactors off line monitoring was used to obtain further information on the resultant performance of both the Wild Type and Fab fermentions. This monitoring included the dry weight and optical density, which are both measures of the microbial concentration, the concentration of protein in both the supernatant and solid fractions and

for the Fab fermentation, the concentration of the Fab product in both the solid and supernatant fractions measured by an ELISA.

4.2.2.1 Dry weight

The dry cell weight was measured by the following method:

1. 1 ml of fermentation broth was transferred into an eppendorf whose mass was known.
2. The eppendorf was spun in a centrifuge at 1300 rpm for 10 minutes
3. The resulting supernatant was removed and the solid pellet was resuspended in 1 ml of RO water.
4. The suspension was spun in a centrifuge at 1300 rpm for 10 minutes.
5. The resulting supernatant was removed and the eppendorf with the lid open was put in an oven at 109 °C.
6. The eppendorfs were removed from the oven 24 hours later and immediately transferred to a desicator until they cooled. They were subsequently weighed, so that the mass of pellets was determined, by subtracting the original mass of the eppendorf.

4.2.2.2 Optical Density, OD

The optical density was measured as the reflectance of light at a fixed wavelength of 600nm, using a spectrometer (Beckman DU64, Beckman Instruments (UK.) Ltd., High Wycombe, UK.) In order to maximize the accuracy of the spectrometer, samples whose spectroscopic reading was above 1.0, were diluted with deionised water.

4.2.2.3 Total Protein measurement

The total protein concentration was measured using a reagent, Bio-Rad (Bio-Rad laboratories Ltd., Hemel Hempstead, Hertfordshire, UK.) diluted 1 in 5 times with deionised water. The light transmittance at a fixed wavelength of 595 nm was measured

between 5 and 60 minutes after addition of 2 mL of the dilute Biorad solution to 40μL of sample. In order to maximize the accuracy of the spectrometer, samples whose spectroscopic reading was above 1.0, were diluted with deionised water. The amount of protein was calculated using a standard curve of known protein standards. The concentration of protein was measured for both supernatant and homogenized samples where the latter gave the total protein in a sample. The same spectrometer was used as for the optical density.

4.2.2.4 ELISA

For the Fab fermentation an ELISA was used to measure the concentration of the Fab product in the supernatant and solid fractions. Prior to the ELISA the solid fraction was incubated overnight with 1 mL of periplasmic extraction buffer (table 2A) at 60°C and 50 rpm. The following method was used for both the solid and supernatant fractions:

Method

1. A NUNC 96 well maxisorp immunoplates (Life Technologies Ltd., Paisely, UK) was loaded with 100 μL of HP6045 coating solution (a mouse antihuman monoclonal antibody supplied by Celltech Chiroscience Ltd.) which had a dilution of 2 μg mL^{-1} in PBS (table 2C). The plate was stored overnight at 4°C.
2. The plate was then washed with PBS tween (table 2C) using a plate washer, (Columbus Tecan, UK Ltd. Reading, UK).
3. The first row of the plate was loaded with 200 μL of sample and standard, where the first two columns were used for the standard of know Fab concentration. 100 μL of sample conjugated buffer (table 2B) was then loaded into the remaining rows. A 1 in 2 dilution series was performed down the plate, so that each well had a 100 μL sample where the first row was the same concentration as the original sample or standard. The plate was put on an orbital shaker (Luckman 4RT rocking table,

Denley Instruments Ltd., Billinghurst, UK) at 300 rpm at room temperature for one hour.

4. The plates were washed in PBS tween using the plate washer. 100 µL of revealing antibody GD12 peroxidase (The Binding site Ltd., Birmingham, UK) diluted 1 in 2000 in sample conjugate buffer was loaded into each well of the plate. The plate was incubated for one hour on an orbital shaker at 300 rpm at room temperature.
5. The plate was washed in PBS tween using the plate washer. 100 µL of the substrate solution (table 2G) was added down the plate to each well. The absorbance at 630 nm was then read using a Dynatech MR 7000 microplate reader, (Dynex Technologies, Billingshurst, UK) after 4 to 10 minutes. The concentration of Fab in the samples was determined using an equation derived from the absorbance measured for the standards of known Fab concentration.

ELISA solutions

Table 2A - Periplasmic extration buffer

Component	Concentration g L^{-1}
Tris amino-methane	12·1
EDTA	2·92

pH to 7·4 with HCl, store 4°C

Table 2B - Sample conjugate buffer

Component	Concentration g L^{-1}
Tris amino-methane	6·05
NaCl	2·92
Tween – 20	0·1
Casein	1.0

pH to 7·0 with HCl, store 4°C

Table 2C - PBS, Phosphate buffer saline

Component	Concentration g L^{-1}
NaCl	8·0
KCl	0·2
Na_2HPO_4	1·15
KH_2PO_4	0·2

PBS tween additionally contains 0·5 ml L^{-1} of tween 20

Table 2D - TMB

Component	Additions
Tetramethylbenzidine	10 mg
Dimethylsulphoxide	1 mL

Table 2E - Sodium acetate/citric buffer

Component	Concentration
Sodium acetate	8·204 g L^{-1}

pH to 6·0 with citric acid

Table 2F - Hydrogen peroxide solution

Component	Concentration
30 % H_2O_2	1 in 50 dilution

Table 2G - Substrate solution

Solution	Addition
Acetate/citrate buffer (table 2E)	10·785 mL
H_2O_2 solution (table 2F)	107·85 µL
TMB (table 2D)	107·85 µL

4.3 Wild Type Fermentation Protocol

This section details the methods and materials for the Wild Type fermentation, which was performed in the conventional stirred tank bioreactor and the disposable plunging jet bioreactor. Whilst the protocol for Wild Type fermentation was the same for both reactors, due to differences in the operation of the stirred tank and plunging jet reactor, the methods are discussed separately.

4.3.1 5L stirred tank bioreactor

4.3.1.1 Inoculum

Procedure

- Cells were transferred from frozen glycol stocks to agar plates containing 28 g L^{-1} of nutrient agar (see below). These plates were incubated at 30° C, for 24 hours.
- The contents of the one plate were ascetically transferred into its own 2 L shaker. Each autoclaved shaker contained 0·250 L of shaker media (table 3A), where a solution of glucose and $MgSO_4.7H_2O$ and yeast extract were autoclaved separately and added prior to inoculation.
- The shakers were incubated at 30° C and an agitation speed of 200 rpm, for 15 hours.

Nutrient agar, (Oxoid, Unipath Ltd., Basingstoke, consists of 1 g L^{-1} powder 'Lab Lemco', 2 g L^{-1} yeast extract, 5 g L^{-1} Peptone, 5 g L^{-1} NaCl, 15 g L^{-1} Agar).

Table 3A - Wild Type - media for shakers

Component	Concentration ($g\ L^{-1}$ or $ml\ L^{-1}$)
$(NH_4)_2SO_4$	8·0 $g\ L^{-1}$
NaCl	2·5 $g\ L^{-1}$
Na_2HPO_4	2·16 $g\ L^{-1}$
KH_2PO_4	0·64 $g\ L^{-1}$
Yeast Extract (table 3B)	2·0 $g\ L^{-1}$
Trace elements	0·5 $ml\ L^{-1}$
$Fe_2SO_4.7H_2O$	0·2 $g\ L^{-1}$
Citric Acid	0·2 $g\ L^{-1}$
$MgSO_4.7H_2O$	0·2 $g\ L^{-1}$
Glucose	5·0 $g\ L^{-1}$

Note: a solution of glucose and $MgSO_4.7H_2O$ were autoclaved separately.

a solution of yeast extract was autoclaved separately.

$Fe_2SO_4.7H_2O$ and Citric Acid were dissolved separately.

Yeast Extract, 'Diffco Bacto Yeast Extract Technical (Becton Dickinson, Microbiology Systems, Sparks, MD, USA)

Table 3B - Wild Type - trace elements

Component	Concentration ($g\ L^{-1}$)
$CaCl_2$	10 $g\ L^{-1}$
H_3BO_3	4·0 $g\ L^{-1}$
$MnCl_4.4H_2O$	2·0 $g\ L^{-1}$
$ZnSO_4.7H_2O$	2·0 $g\ L^{-1}$
$CuSO_4.5H_2O$	0·4 $g\ L^{-1}$
$CoCl_2.6H_2O$	0·4 $g\ L^{-1}$
$NaMoO_4.2H_2O$	0·2 $g\ L^{-1}$

4.3.1.2 Fermentation

Procedure

The fermenter was sterilized with the wild type fermentation media (table 3D) in situ, with the exception of glucose and magnesium sulphate and a solution of yeast extract, which were autoclaved and added aseptically, prior to inoculation. The fermenter was inoculated aseptically with a 10% inoculum at the set points shown in table 3C. The fermenter was sampled every hour where the optical density was measured and a dry cell weight was performed. Samples were also frozen for subsequent protein analysis. The aeration and agitation were increased to there permitted maximum in order to maintain the DOT above 10%. Although the stirred tank reactor had a maximum operating aeration and agitation of 8 L min^{-1} and 1400 rpm respectively, due to foaming in the headspace the permitted maximum may be below these levels. When the DOT reached 10% at the maximum permitted aeration and agitation the fermentation was stopped. During the fermentation if there was a sudden drop in the OUR (oxygen uptake rate) which indicated that the carbon source was limited, glucose was added at a concentration of 5·0 g L^{-1} (table 3F).

Table 3C - Wild Type, STR - Initial fermentation set points

Parameter	Setpoint
pH	7.0
Temperature	30 °C
Agitation	500 rpm
Airflow rate	5 L min^{-1}

Fermentation media

Table 3D - Wild Type - fermentation media

Component	concentration ($g\ L^{-1}$ or $ml\ L^{-1}$)
$(NH_4)_2SO_4$	8·0g L^{-1}
NaCl	2·5 g L^{-1}
Na_2HPO_4	2·16 g L^{-1}
KH_2PO_4	0·64 g L^{-1}
Yeast Extract	5·0 g L^{-1}
Trace elements	1·0 ml L^{-1}
$Fe_2SO_4.7H_2O$	0·2 g L^{-1}
Citric Acid	0·2 g L^{-1}
$MgSO_4.7H_2O$	0·2 g L^{-1}
Glucose	10·0 g L^{-1}

Table 3F - Wild Type - Batch feed

Component	Concentration ($g\ L^{-1}$)
Glucose	500 g L^{-1}

4.3.2 14L disposable plunging jet bioreactor

4.3.2.1 Inoculum

The inoculum for the 14 L plunging jet reactor was exactly the same procedure as in the fermentation for the 5 L stirred tank bioreactor where the media and initial set points were not changed.

4.3.2.2 Fermentation

Procedure

The fermentation media (table 3D) was sterilized in an autoclave at 121°C for 20 minutes. The fermentation media was added and circulated through the heat exchanger so that its temperature was brought to 30°C. The pH, airflow rate and pump rate was adjusted to the set points shown in table 4A. The disposable plunging jet bioreactor was inoculated with a 10% inoculum taken from inoculum train. As with the stirred tank reactor the fermenter was sampled every hour where the optical density was measured and a dry cell weight was performed. Samples were also frozen for subsequent protein analysis. The pump rate was increased to keep the DOT above 10 %. When the DOT reached 10 % at the maximum permitted pump flow rate of 500 L hr^{-1} the fermentation was stopped. During the fermentation if there was a sudden drop in the OUR (oxygen uptake rate) indicating that the carbon source was limited, glucose was added at a concentration of 5·0 g L^{-1} (table 3F).

Table 4A -Wild Type, PJR - Initial fermentation set points

Parameter	Setpoint
PH	7·0
Temperature	30°C
Pump flow rate	390 L hr^{-1}
Airflow rate	10 L min^{-1}

4.4 Fab Fermentation Protocol

This section details the methods and material for the Fab fermentation, which was performed in the conventional stirred tank bioreactor and the disposable plunging jet bioreactor. As with the Wild Type fermentation, whilst the same protocol was used for both reactors, there were differences in the operation of the two reactors and thus the methods are discussed separately for each reactor.

4.4.1 Stirred tank reactor

4.4.1.1 Inoculum

Procedure

- Cells were transferred from frozen glycol stocks to agar plates containing complex media as given in table 5A. These plates were incubated at 30 °C, for 24 hours.
- The contents of the one plate were ascetically transferred into there own 2 L shaker. Each autoclaved shaker contained 0·200 L of shaker media (table 5B), where a solution of $MgSO_4.7H_2O$ was autoclaved separately and added prior to inoculation. The chloraphemical was dissolved separately in 2·5 mL of ethanol per shaker and sterilized by filtration prior to inoculation.
- The shakers were incubated at 30 °C and an agitation speed of 250 rpm, for 15 hours.

Table 5A - Fab - media for complex plates

Component	concentration ($g\ L^{-1}$)
Tryptone	16·0 $g\ L^{-1}$
Yeast Extract	10·0 $g\ L^{-1}$
NaCl	5·0 $g\ L^{-1}$
Agar no. 1	10·0 $g\ L^{-1}$
Chloramphenicol	0·03 $g\ L^{-1}$

Chloramphenicol was dissolved in ethanol and added to complex plate media when it had cooled to 40°C

Tryptone, (Oxoid, Unipath Ltd., Basingstoke, UK)

Agar no. 1 (Unipath Ltd., Oxoid)

Chloramphenicol, (BDH, Merck, Poole, UK)

Table 5B - Fab - media for shakers

Component	concentration ($g\ L^{-1}$ or $ml\ L^{-1}$)
$(NH_4)_2SO_4$	5·0 $g\ L^{-1}$
NaH_2PO_4	2·88 $g\ L^{-1}$
KCl	3·870 $g\ L^{-1}$
Citric Acid	4·0 $g\ L^{-1}$
Trace elements (table 5C)	10 $mL\ L^{-1}$
Glycerol	30 $g\ L^{-1}$
$MgSO_4.7H_2O$	1·0 $g\ L^{-1}$
Chloramphenicol	0·03 $g\ L^{-1}$

Note: pH to 6·80 media with the exception of MgSO4.7H2O and Chloramphenicol.

A solution of $MgSO_4.7H_2O$ was autoclaved separately.

Chloramphenicol was dissolved in ethanol and sterile filtered prior to use.

Table 5C - Fab - Trace elements

Component	Concentration ($g\ L^{-1}$)
Citrate	100 $g\ L^{-1}$
$CaCl_2.6H_2O$	5 $g\ L^{-1}$
$ZnSO_4.7H_2O$	2·46 $g\ L^{-1}$
$MnSO_4.4H_2O$	2·0 $g\ L^{-1}$
$CuSO_4.5H_2O$	0·5 $g\ L^{-1}$
$CoSO_4.7H_2O$	0·427 $g\ L^{-1}$
$FeCl_3.6H_2O$	9·67 $g\ L^{-1}$
H_3BO_3	0·03 $g\ L^{-1}$
$Na_2MoO_4.2H_2O$	0·024 $g\ L^{-1}$

4.4.1.2 Fermentation

Procedure

The fermenter was sterilized with the fermentation media in situ (table 5E), with the exception of the magnesium sulphate and chloramphenicol. The magnesium sulphate was autoclaved separately whilst the chloramphenicol was dissolved in ethanol and filter sterilized prior to use with a 0·2 μm syringe filter (Whatman Scientific Ltd. Maidstone, UK). The fermenter was inoculated aseptically with a 10% inoculum at the set points shown in table 7A. After an initial lag phase of 15 hours the fermenter was sampled every three hours. The optical density was measured and a dry cell weight was performed. Samples were also frozen for protein analysis and in the induction phase additionally for an ELISA. At specific optical densities various additions were made which are detailed in table 5F. At optical density of 15 and 35 glycerol additions were made. At an optical density of 40 additional $MgSO_4.7H_2O$ and $CaCl_2.6H_2O$ were added and the temperature was reduced to 27°C. At an optical density of 50 additions of glycerol and lactose were made. Throughout the fermentation the aeration and agitation were increased to there permitted maximum in order to maintain the DOT above 10%. Although the stirred tank reactor had a maximum operating aeration and agitation of 8 L

min^{-1} and 1400 rpm respectively, due to foaming in the headspace the permitted maximum may be below these levels.

Table 5D - Fab, STR - Initial fermentation set points

Parameter	Setpoint
pH	6·95
Temperature	30 °C
Agitation	750 rpm
Airflow rate	4 L min^{-1}

Fermentation media

Table 5E - Fab - fermentation media

Component	concentration (g L^{-1} or ml L^{-1})
$(NH_4)_2SO_4$	5·0 g L^{-1}
NaH_2PO_4	2·88 g L^{-1}
KCl	3·87 g L^{-1}
Citric Acid	4·0 g L^{-1}
Trace elements (table 5C)	10 ml L^{-1}
Glycerol	30 g L^{-1}
$MgSO_4.7H_2O$	1·0 g L^{-1}
Chloramphenicol	0·03 g L^{-1}

Note: pH to 6·80 media with the exception of MgSO4.7H2O and Chloramphenicol.

A solution of $MgSO_4.7H_2O$ was autoclaved a separately.

Chloramphenicol was dissolved in ethanol and sterile filtered prior to use.

Table 5F - Fab - additions

OD	Component	Concentration
15	Glycerol	30·0 g L^{-1}
35	Glycerol	20·0 g L^{-1}
40	$MgSO_4.7H_2O$	14·4 mM L^{-1}
	$CaCl_2.6H_20$	1·7 mM L^{-1}
50	Glycerol	10·0 g L^{-1}
	Lactose	50·0 g L^{-1}

4.4.2 14L disposable plunging jet bioreactor

4.4.2.1 Inoculum

The inoculum for the 14 L plunging jet reactor was inoculated by exactly the same procedure as in the fermentation for the 5 L stirred tank bioreactor where the media and initial set points were not changed.

4.4.2.2 Fermentation

Procedure

With the exception of chlorophenicol and MgSO4.7H2O, the fermentation media (table 5E) was sterilized in an autoclave at 121°C for 20 minutes. As with the stirred tank $MgSO_4.7H_2O$ was autoclaved separately and chloroamphencol was dissolved in ethanol and filter sterilized with a 0·2 μm syringe filter, (Whatman Scientific Ltd., Maidstone, UK) before addition. The fermentation media was added and circulated through the heat exchanger so that its temperature was brought to 30°C. The pH, airflow rate and pump rate was adjusted to the set points shown in table 6A. The disposable plunging jet bioreactor was inoculated with a 10% inoculum taken from inoculum train. After an initial lag phase of 15 hours the fermenter was sampled every three hours and the pump

rate was increased to a maximum 500 L hr^{-1} so that when possible the DOT was maintained above 10%. As with the stirred tank reactor the samples were used to measure the optical density and dry cell weight. Samples were also frozen for protein analysis and additionally for ELISA in the induction phase. As with the stirred tank reactor the same additions were made at optical densities of 15, 35, 40 and 50 (table 5F). At an optical density of 40 the temperature was reduced to 27°C.

Table 6A - FAB, PJR - Initial fermentation set points

Parameter	Setpoint
pH	6·95
Temperature	30°C
Pump flow rate	330 L hr^{-1}
Airflow rate	10 L min^{-1}

4.5 Other methods used

This section details methods and materials used to perform other experiments associated with the microbial fermentations that are detailed in chapter 6. These were the measurement of the strength of the Wild Type and Fab microbial cells in their respective fermentations and the shear sensitivity of the Fab product.

4.5.1 Measurement of visocity

Liquid visocity was measured using a Rheomat 115 viscometer (Contraves Industrial Products Ltd., Middlesex, UK). The measuring cyclinder rotated at 15 pre set speeds from 5 to 780 rpm, producing a shear rates over the range 24·3 s^{-1} to 3680 s^{-1}. The corresponding shear stress for each speed was recorded. Sample visocity was determined from the gradient of the linear regresssion of shear stress against shear rate. The measuring system was maintained at a constant temperature using a Haake re-circulating glycol/water bath (Haake, Germany).

4.5.2 Operation of shear device and calculation of shear

The shear sensitivity of Fab was measured in a shear device. This consisted of a spinning flat disk of radius 0·015 m and thickness 0·0012 m in a chamber of volume 15 mL. The volume of liquid was 13 mL with no air liquid interface and 6·5 mL with an air liquid interface. The disk was rotated using an electric motor for a fixed time of 20 seconds. The sample was then removed and an ELISA was performed. This maximum and average shear rate can be calculated using a model developed described in Boychyn et al (2001). According to this model significant turbulent shear forces are predicted within a very thin boundary layer at the disk surface. This model was based on the specific Navier Stokes equation of Cochran (in Schlichling 1979) to calculate the layer thickness and the maximum shear force developed.

4.5.3 Lysis of cells for shear experiment

Small scale periplasmic extraction for measurement of Fab in the solid phase.

1 mL of periplasmic extraction buffer (table 2A) was added to the cell pellet and incubated overnight at 60 C and 250 rpm.

Large scale periplasmic extraction for use in the shear experiment.

A 2L periplasmic extraction was performed in a 2L LH stirred tank reactor. Cell paste was produced by passing the fermentation broth through a centrifuge, CARR P6 Powerfuge (CARR Separations Inc., Franklin, MA) and freezing the samples. The cell paste was then thawed and 280 g were added per 1 L of periplasmic extraction buffer. This was put into the stirred tank reactor overnight, where the temperature and agitation speed was maintained at 60 C and 300 rpm.

4.5.4 Operation of homogenizer for cell strength experiments

Cell disruption was achieved using a Gaulin Micron Lab 40 homogeniser (APV Gaulin GMbH, Lubeck, Germany). 40 mL samples were passed once through the homogenising valve at an operating pressure of 110 bar to 1200 bar. Glycol cooling was supplied to the equipment to reduce the disruption temperature to 4° C. Samples were stored on ice.

5. *Design and Operation of a Microbial Disposable Plunging Jet Bioreactor*

5.1 Overview and aims

The aim of this chapter was to design a disposable plunging bioreactor for use with microbial fermentations and determine how it should be operated during the comparison with the conventional system. The plunging jet bioreactor was designed using a combination of published and experimental data performed in perspex plunging jet mimics. Modifications were then made to the original design, so that the bioreactor could be manufactured by Hyclone Europe. Subsequent to the bioreactor manufacture, a series of experiments were performed in the actual disposable plunging jet reactor to determine the nozzle configuration and operating power that should be used for the comparison with the conventional system. These experiments were performed whilst a delay in obtaining the disposable bioreactors (for use in performing the microbial fermentations presented in chapter 6) from Hyclone Europe was resolved.

5.2 Design of Disposable Plunging Jet Bioreactor

5.2.1 Design Considerations

In designing the plunging jet bioreactor, consideration was given to the work published on the plunging jet reactor. This published work is detailed in chapter 3, the theory of the plunging jet. The initial considerations were that the bioreactor must provide the basic

requirements of transfer of mass, heat and oxygen which are detailed further in chapter 1. In this system heat transfer occurs principally in the heat exchanger which is situated in the plunging jet loop. The heat transfer is determined by the heat exchange area, the temperature and heat capacity of the coolant stream and the flow rates of both the process and coolant streams. Thus it should be possible to design the heat exchanger to remove the heat generated by the microbial fermentation. Mass transfer occurs by the plunging jet and movement of liquid caused by the action of the pump on the outlet. Oxygen transfer occurs by the plunging jet entraining air bubbles as it hits the pool of liquid. The oxygen transfer rate is measured as the k_La, the oxygen transfer coefficient and the mass transfer is measured as the mixing time. A microbial fermentation has a high oxygen demand so that typically the productivity of the fermentation is linked to the oxygen transfer rate. Thus the oxygen transfer rate is a critical design factor.

The oxygen transfer coefficients value is determined by the rate of air entrainment and the residence time of the entrained air. The residence time of the entrained air is determined by how far the entrained air bubbles move vertically downwards and outwards before moving up and then subsequently how long the bubbles take to move upwards and outwards. The distance that the entrained air bubbles take to move vertically downwards is measured as the depth of bubble penetration and is proportional to the momentum of the jet. The residence time for the bubbles moving upwards is determined by the buoyancy force and thus is inversely proportional to the size of the secondary bubbles. Since the size of these bubbles are independent of the jet velocity and nozzle diameter, the residence time of the entrained air can only be increased by increasing the depth of the bubble penetration.

The plunging jet reactor was designed using information from the literature, as discussed in chapter 3 and using data collected from a series of experiments. Although there is a lot of data on the plunging jet, it mostly concerns the effect of the nozzle configuration and power input on one part of the oxygen transfer process such as the rate of air entrainment or the depth of bubble penetration. The data, which determines the effect of the nozzle

configuration and power input on the whole oxygen transfer process, is expressed in terms of the mass transfer factor, K_LA, which defines the rate of oxygen transfer per unit volume. To avoid confusion with the mass transfer coefficient or k_La, in this thesis the mass transfer factor, K_LA has the nomenclature Q_{KLA}. These equations and other equations that were used in the design process are listed below. Figure 7 shows the nozzle angle, height of fall and depth of bubble penetration, which are all measurements investigated in this chapter.

k_La, oxygen transfer rate

$$k_L a = \left(\frac{1}{t}\right) \ln\left(\frac{(C^* - C_L^\circ)}{(C^*)}\right)$$

(Equ. 4.3)

Power of the jet

$Po = 1/2\rho Vo^2 Q$ (Equ. 2.0)

(Bin, 1993)

Mass transfer factor, Q_{KLA}

$Q_{KLA\ 20^\circ} = 9 \times 10^{-5} Po$ (Equ. 2.1)

(Bin and Smith (1982))

$Q_{KLA\ 20^\circ} = 4{\cdot}28 \times 10^{-4} Po^{0{\cdot}71} do^{0{\cdot}2} Lj^{0{\cdot}2}$ (Equ. 2.4)

This is valid for Po = 0·2 to 100 W

Lj = 0·025 to 0·8 m.

(Bin, 1993)

Depth of bubble penentration

$$hp = C_{54} Vo^{n} do^{p}$$

(Equ. 2.14)

For $Vodo \geq 0{\cdot}01\ m^2 s^{-1}$, $n = p = 0{\cdot}66$, $C_{54} = 2{\cdot}4$

$Vodo < 0{\cdot}01\ m^2 s^{-1}$, $n = p = 1{\cdot}36$, $C_{54} = 61$

(Bin (1983), Bonsignore et al (1985), McKeogh and Ervine (1981), van de Donk (1981), van de Sande and Smith (1974))

Notation for the above equations are:

$Q_{KLA\ 20°}$ = mass transfer factor at 20°C, ($m^3\ s^{-1}$)

do = nozzle diameter (m)

Lj = length of jet (m)

Hp = maximum depth of bubble penetration (m)

Vo = velocity ($m\ s^{-1}$)

Po = power of the jet (W)

Q = volumetric flow rate ($m^3\ s^{-1}$)

k_La = oxygen transfer coefficient (s^{-1})

C* = oxygen concentration of the liquid when it is in equilibrium with the gas ($Mol\ L^{-1}$)

C_L° = oxygen concentration of the liquid at time t = 0 ($Mol\ L^{-1}$)

t = time (s)

Although the mass transfer factor, Q_{KLA} (units : $m^3\ s^{-1}$) and the mass transfer coefficient, k_La (units : s^{-1}) both measure the rate of dissolved oxygen transfer, they are not interchangeable. Thus a series of investigations were carried out to determine the effect of the nozzle configuration and power input on the k_La.

Figure 7 – Plunging jet reactor dimensions used in design work

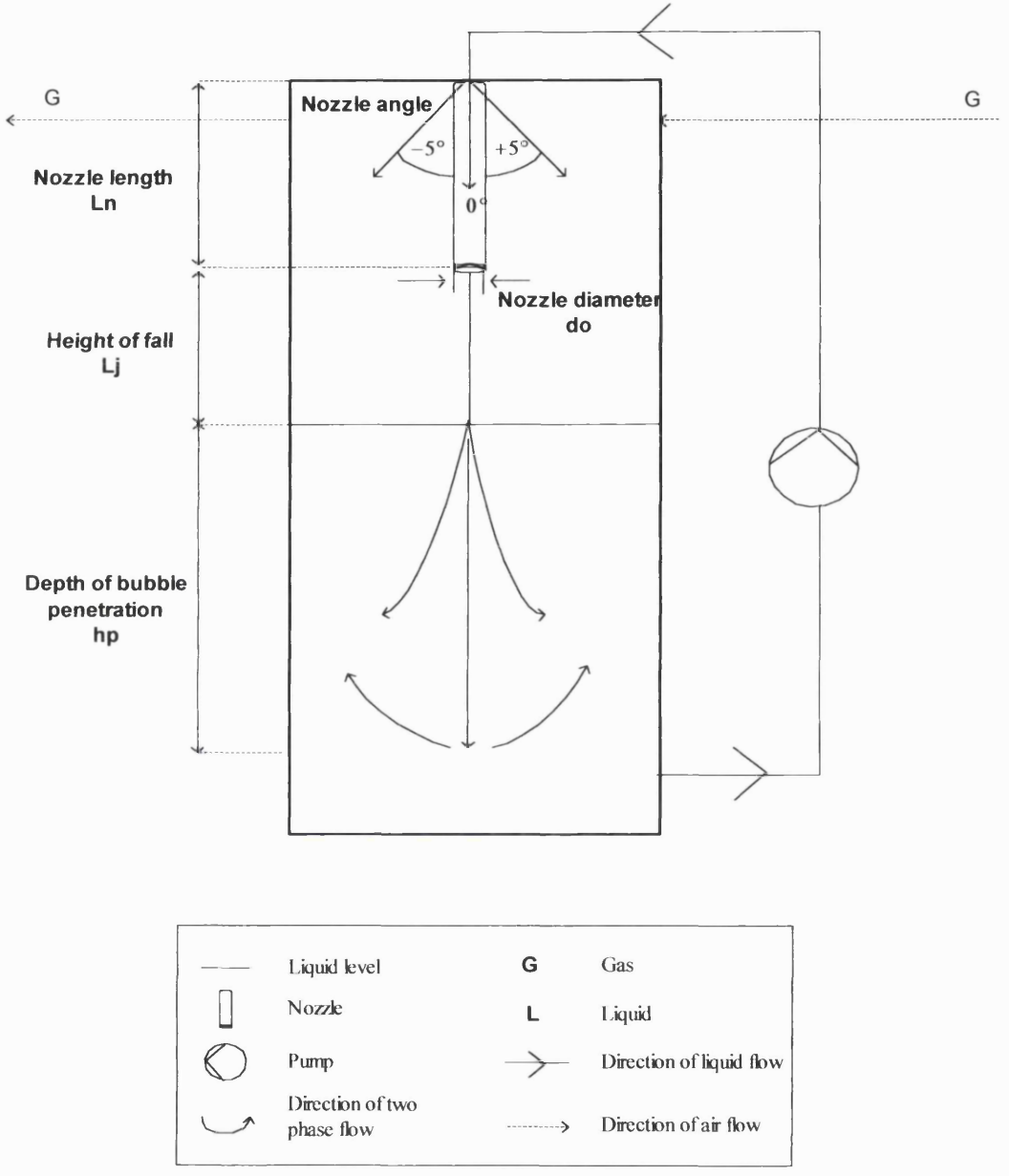

Figure 7
The figure shows the plunging jet reactor dimensions used in the design work presented in this chapter. The plunging jet reactor is not to scale, where the nozzle is enlarged to show its dimensions.

5.2.2 Investigations using the plunging jet mimic

An initial investigation measuring the effect of the nozzle configuration and power input on the k_La was performed using a plunging jet mimic and a peristaltic pump. The peristaltic pump was subsequently replaced with a mono pump. This initial experimental data is detailed below and is followed by the results in tables 7 to 11 and figures 8 to 11 on pages 126 to 133.

Table 7 shows that a peristaltic pump requires an accumulator for oxygen transfer to occur. Without an accumulator the pump produces a pulsating jet which results in the air bubbles moving in and out of the liquid at the same frequency as the pulse. Table 8 shows that reducing the nozzle diameter at a fixed pump rate results in an increase in the k_La.

Tables 7 and 8 suggest that the k_La increases with the velocity and power of the jet, so that a high volumetric flow rate through a small diameter nozzle is required. For the peristaltic pump feeding a 3·85 mm nozzle, the velocity does not increase significantly with the pump rate. This is because at the higher pump rates, the small inlet causes a large back pressure, which reduces the flow rate. Thus the flow rate through the nozzle was increased by replacing the peristaltic pump with a mono pump, which can pump against a relatively high back pressure. As table 9 shows this resulted in a higher flow rate and k_La value. The flow rate through the mono pump was increased further by increasing the outlet diameter from 4 to 16 mm (data not shown). Table 10 shows that with an identical nozzle configuration and flow rate, the k_La is increased by moving the nozzle from pointing directly over the outlet to pointing on the opposite side. Table 11 shows that for both the peristaltic pump without the accumulator and the mono pump, the mixing times are fairly short. At comparable pump flow rates, the mixing time was significantly greater for the peristaltic pump with the accumulator than the same pump rate without the accumulator.

Figure 8 shows that the k_La increases with the volumetric flow rate. At a maximum flow rate of 5 L min^{-1} which corresponds to a power per unit volume of 0·36 kW m^{-3}, the k_La was 185 hr^{-1} ± 48 hr^{-1}. At lower flow rate of 4·3 L min^{-1} which corresponds to a power per unit volume of 0·22 kW m^{-3}, the k_La was 50 hr^{-1} ± 10 hr^{-1}. Thus there is considerable error as the volumetric flow rate is increased to 5 L min^{-1}.

Figure 9 shows that the k_La increases with the height of fall for a 3·85 mm nozzle at two different flow rates. For a flow rate of 4·2 L min^{-1}, increasing the height of fall from 0·15 m to 0·37 m results in an increase in the k_La from 10 hr^{-1} to 40 hr^{-1}. A further increase in the height of fall to 0·45 m results in no further increase in the k_La. For a flow rate of 1·6 L min^{-1}, increasing the height of fall from 0·15 m to 0·37 m results in an increase in the k_La from 10 hr^{-1} to 20 hr^{-1}. As equation 2.4 shows a small rise in the oxygen transfer rate is expected with increasing the height of fall.

Figure 10 shows that both the maximum and constant depth of bubble penetration increases with the volumetric flow rate. The constant depth of bubble penetration is the length of the two-phase mixture that results when air is entrained by the jet as bubbles. At periodic time instants a few bubbles reach a lower depth before moving upwards, which was defined as the maximum depth of bubble penetration. These results were compared to predicted values using equation 2.14. As figure 10 shows the equation 2.14 predicts the depth to be between the maximum and constant depth across the range of power per unit volumes measured.

Figure 11 shows that at a fixed nozzle configuration and flow rate, the k_La decreases with the volume. This data shows that increasing the volume by increasing the liquid height results in a reduction in the k_La. The product of the k_La and volume was equal for the volumes of 7 L and greater. Tojo and Miyanami (1982) found that increasing the liquid volume by increasing the diameter of the liquid pool results in a reduction in the k_La.

Figure 12 shows the effect of the viscosity on the k_La. Increases in the viscosity of the solution were the result of increasing the concentration of PEG (polyethyleneglycol). The height of fall and volumetric flow rate were fixed at 0·14 m and 4·3 L min^{-1}. Increasing the viscosity from 0·002 Pa s, which is RO water to 0·012 Pa s results in an increase in the k_La from 100 hr^{-1} to 200 hr^{-1}. Further work is required to differentiate whether the increase in the k_La is due to an increase in the viscosity or an increase in the PEG concentration.

Table 7 - Oxygen transfer of a plunging jet using a peristaltic pump, with and without an accumulator

Presence of accumulator	Pump rate in (rpm)	Power per unit volume (kW m^{-3})	Volumetric flow rate (L min^{-1})	Velocity (m s^{-1})	time 0% to 1.5% (s)	k_La (s^{-1})
No	35	0·018	0·98	1·41	420 ± 31	
No	50	0·052	1·400	2·01	615 ± 27	
No	100	0·053	1·410	2·03	639 ± 36	
No	150	0·050	1·380	1·98	710 ± 38	
Yes	50	0·165	2·060	2·96	10 ± 1.0	(2·20 ± 0·105) $\times 10^{-3}$
Yes	100	0·242	2·340	3·4	10 ± 0.5	(3·92 ± 0·148) $\times 10^{-3}$
Yes	150	0·242	2·340	3·4	10 ± 1.0	(3·92 ± 0·299) $\times 10^{-3}$

Table 7
The oxygen transfer rate for a peristaltic pump with and without an accumulator, where the height of fall was fixed at 0·14 m and the nozzle diameter was 3·85 mm.
Without an accumulator there is virtually no oxygen transfer since it takes between 420 to 710 seconds for the DOT to increase from 0 to 1·5 %. With an accumulator oxygen transfer occurs with a k_La of between 2·2 $\times 10^{-3}$ s^{-1} to 3·92 $\times 10^{-3}$ s^{-1}, where the increase from 0 to 1·5% occurs in 10 seconds which is the probe response time.

Table 8 - Effect of nozzle diameter on oxygen transfer efficiency of a plunging jet with a peristaltic pump and an accumulator.

Nozzle diameter (mm)	pump rate (rpm)	k_La (s^{-1})
3·85	100	$(2·24 \pm 0·132) \times 10^{-3}$
8·00	100	$(1·80 \pm 0·109) \times 10^{-3}$
3·85	200	$(2·36 \pm 0·146) \times 10^{-3}$
8·00	200	$(1·97 \pm 0·168) \times 10^{-3}$

Table 8
The plunging jet used a peristaltic pump with an accumulator, where the height of fall was fixed at 0·14 m. Two nozzle diameters were used, which were 3·85 mm and 8·00 mm. The results show that reducing the nozzle diameter at a fixed pump rate results in an increase in the k_La.

Table 9 - Oxygen transfer of a plunging jet using a mono pump

Pump rate as percentage of output	Power per unit volume (kW m^{-3})	Volumetric flow rate (L min^{-1})	Velocity (m s^{-1})	k_La (s^{-1})
12·5 %	0·101	1·75	2·51	$(2·36 \pm 0·126) \times 10^{-3}$
25·0 %	0·248	2·360	3·40	$(3·64 \pm 0·153) \times 10^{-3}$
37·5 %	0·316	2·560	3·68	$(4·49 \pm 0·170) \times 10^{-3}$

Table 9
The flow rate through the 3·85 mm nozzle was increased by replacing the peristaltic pump with a mono pump which unlike the peristaltic pump, can pump against a relatively high back pressure generated by small nozzles. The data shows that the k_La increases with the volumetric flow rate where the height of fall was fixed at 0·14 m.

Table 10 - Effect of the outlet position on the oxygen transfer performance of a plunging jet with a perislaltic pump and an accumulator

Position	K_La (s^{-1})
Opposite	$(3{\cdot}57 \pm 0{\cdot}191) \times 10^{-3}$
Same side	$(2{\cdot}78 \pm 0{\cdot}123) \times 10^{-3}$

Table 10
The data shows that moving the nozzle from pointing directly above the outlet to pointing on the other side results in an increase in the k_La when the volumetric flow rate, height of fall and nozzle diameter are all fixed at 2·4 L min^{-1}, 0·14 m and 3·85 mm.

Table 11 - Mixing time for the plunging jet reactor

Pump	Addition	Pump rate (rpm)	Volumetric flow rate (L min^{-1})	Time (s)
Peristaltic	No accumulator	50	1·40	13 ± 1·0
Peristaltic	No accumulator	100	1·41	12 ± 1·0
Peristaltic	No accumulator	150	1·38	9 ± 1·0
Peristaltic	Accumulator	50	2·06	30 ± 1·0
Peristaltic	Accumulator	100	2·34	27 ± 1·0
Peristaltic	Accumulator	150	2·34	26 ± 1·0
Mono			3·30	9 ± 1·0
Mono			4·11	8 ± 1·0

Table 11
The table shows the mixing times for the peristaltic pump with and without an accumulator and with the mono pump. For all the measurements the nozzle diameter and height of fall were fixed at 3·85 mm and 0·14 m.
The data shows that for both the peristaltic pump without the accumulator and the mono pump, the mixing time are fairly short. At comparable pump flow rates, the mixing times were significantly greater for the peristaltic pump without the accumulator than the same pump with the accumulator.

Figure 8 - k_La versus volumetric flow rate

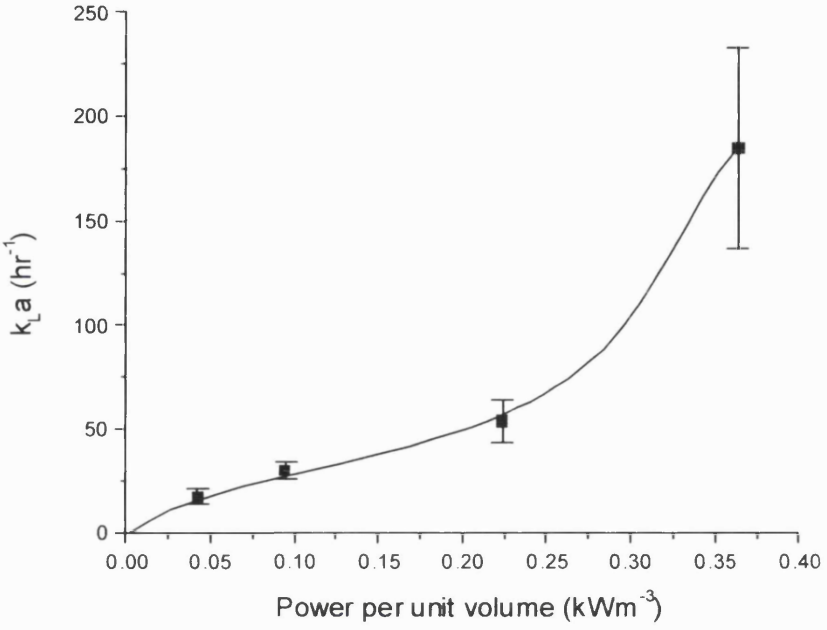

Figure 8
The figure shows the effect of increasing the volumetric flow rate on the k_La for the plunging jet mimic with the mono pump where the height of fall, liquid volume and nozzle diameter were fixed at 0·14 m, 6 L and 3·85 mm respectively.
Increasing the volumetric flow rate from 2·5 to 5·0 L min^{-1} results in an increase in the k_La from 20 ± 4 hr^{-1} to 184 hr^{-1} ± 48 hr^{-1}. The flow rate of 2·5 L min^{-1} to 5·0 L min^{-1} corresponds to a power per unit volume of 0·04 kW m^{-3} to 0·36 kW m^{-3}.

Figure 9 - Effect of height of fall on k_La using a mono pump

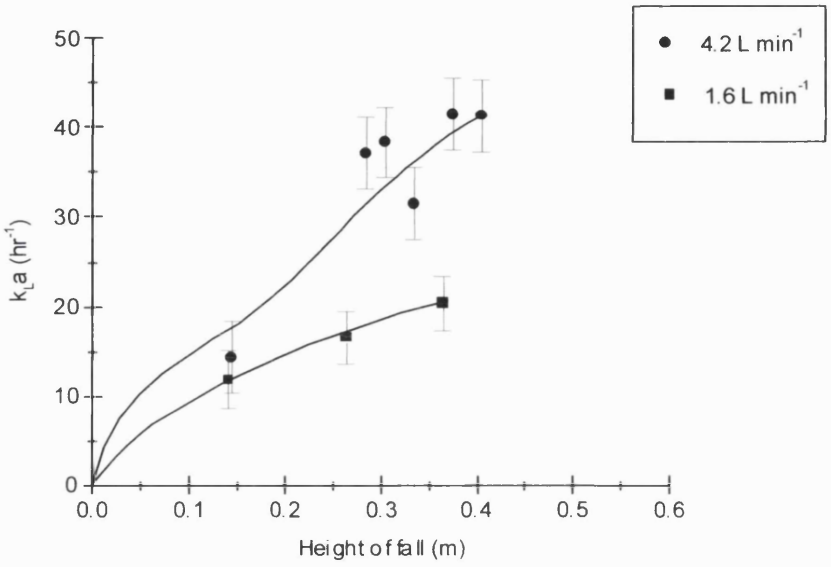

Figure 9
The figure shows the effect of the height of fall on the k_La for the plunging jet mimic with a fixed nozzle diameter of 3·85 mm. The mono pump was used for 4·2 L min^{-1} whilst the peristaltic pump was used for 1·6 L min^{-1}. Figure 7 shows that the height of fall is the distance between the nozzle and the liquid pool.
At a pump rate of 4·2 L min^{-1} increasing the height of fall from 0·14 m to 0·37 m results in an increase in the k_La of 10 hr^{-1} to 40 hr^{-1}. At a pump rate of 1·6 L min^{-1} increasing the height of fall from 0·14 m to 0·37 m results in an increase in the k_La from 10 hr^{-1} to 20 hr^{-1}.

Figure 10 - Effect of power per unit volume on depth of bubble penetration and comparison with calculated values

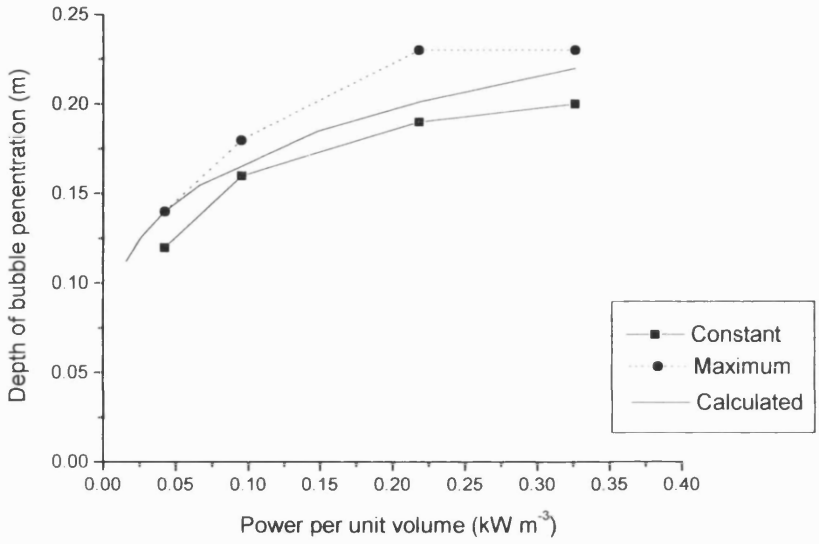

Figure 10
The figure shows the measured constant depth of bubble penetration, which is the length of the two-phase mixture that results when air bubbles are entrained. At some time instants a few bubbles reach a lower depth before moving upwards, this was measured as the maximum depth of bubble penetration. Both the constant and maximum depth of bubble penetration increases with the power per unit volume. The figure also shows the calculated depth using equation 2.14. For the range of power per unit volume measured of 0.05 kW m^{-3} to 0.35 kW m^{-3}, the calculated values are between the constant and maximum depth of bubble penetration measured.

Figure 11 - Effect of volume of the reactor on the k_La

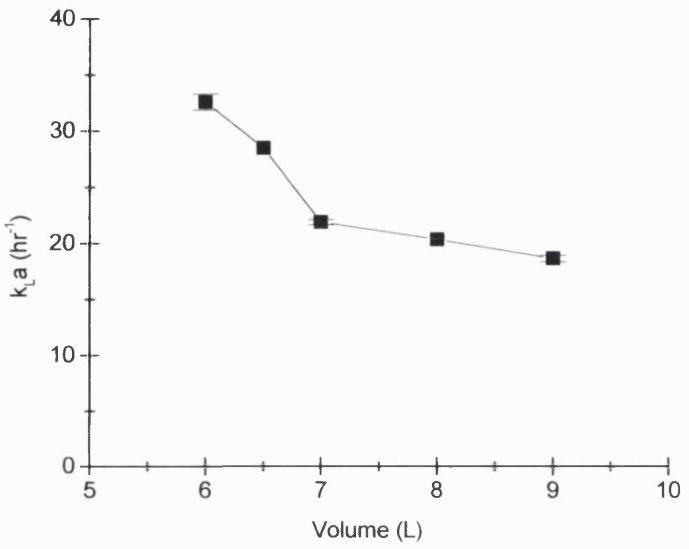

Figure 11
The figure shows the effect on increasing the volume of the reactor from 6 to 9 L on the k_La. The nozzle diameter, volumetric flow rate, power and height of fall were fixed at 3·85 mm, 3·2 L min^{-1}, 0·57 kW and 0·4 m respectively.
Increasing the working volume of the reactor results in a decrease in the k_La. From a volume of 7 L and greater the k_La times the volume is equal to a constant value.

Figure 12 – Effect of viscosity of the k_La

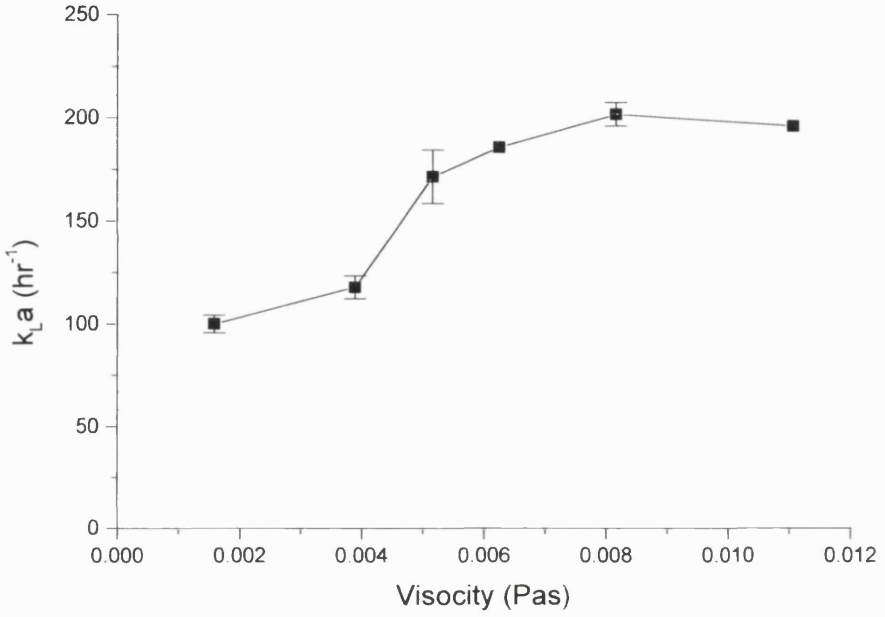

Figure 12
The figure shows the effect of the viscosity on the k_La. Increases in the viscosity of the solution were the result of increasing the concentration of PEG (polyethyleneglycol). The height of fall and volumetric flow rate were fixed at 0·14 m and 4·3 L min^{-1}.
The graph shows that the k_La increases with either the viscosity or the increase in the concentration of PEG.

5.2.3 Original design

The experimental data and published information on plunging jets that are both presented above were used to design the disposable plunging jet reactor with a working volume of 10 L, which is shown in figure 13, page 137. This section discusses how the original design was determined.

The plunging jet reactor was designed with a single nozzle. This is because both Van de Donk (1981) and Tojo et al (1982) found that vertical double jets had a lower mass transfer factor, Q_{KLA} than a single jet operating at the same power as the two combined. Additionally Tojo et al (1982) found that the single jet system had a slightly lower mixing time. The aspect ratio was determined by setting the height of liquid so that it was equal or slightly greater than the depth of the bubble penetration. The depth of bubble penetration was estimated to be between 0·25 m to 0·33 m. The lower estimate is based on the actual data presented in figures 8 and 10. The upper estimate was based on data from Tojo and Miyanami (1982) presented in figure 2 (Bin, 1993). This data showed that a power per unit volume of 2 kW m^{-3} resulted in a k_La of 0·04 s^{-1}. For a nozzle of 2·4 mm operating at a flow rate and power per unit volume of 5·6 L min^{-1} and 1·99 kW m^{-3}, the depth of bubble penetration was estimated to be 0·33 m using the equation 2·14. For the 10 L working volume reactor the diameter of the cylindrical vessel was 0·20 m, so that the height of the liquid was 0·32 m. The height of the bioreactor was 0·60 m, so that the vessel had a standard 1 : 3 aspect ratio and a headspace of 0·28 m. At this stage it was not necessary to specify the nozzle configuration which was the height of fall, nozzle angle, nozzle diameter and nozzle length. The outlet was positioned on the bottom, 0·03 m from the edge so that the jet was not pointing directly over the outlet. Two ports were positioned on opposite sides of the reactor, 0·05 m from the bottom, which were for the pH and DOT probe. Both the sample tube and the air inlet and outlet were positioned so that they did not interfere with the jet. The sample tube was positioned near one side of the bioreactor and the air inlet and outlet were positioned, at the top so that the air

circulation was not pointing directly at the jet. The bag was to be supported by a cylindrical perspex vessel of the same size and shape as the disposable bag.

5.2.4 The final design

This section discusses how modifications were made to the original design so that Hyclone Europe could manufacture the bioreactor. This final design which is shown in figures 14 to 16 (pages 138 to 140) was then used in the comparison of the disposable plunging jet reactor with the conventional stirred tank system.

A comparison between Figure 13 and 14 shows that the disposable bag supplied from Hyclone Europe had several changes from the original design. The cross sectional area was square rather than circular. According to Hyclone Europe cylindrical bag could not be constructed because it would require a circular weld at the bottom, which is difficult to construct and lacks strength. As shown in figure 15 the square bag was formed by a pyramid base, which could be pulled out to form a flat base. The actual shape of the plunging jet reactor is determined by the support, which could either be square or circular. A square support would have a width of 0·25 m and thus fit the bag exactly so that there would be no folds in the side or corners of the bag. For the circular support, the bag could either be larger than the support, so that it is folded into the support or smaller so that it stretched into the support. Since folds are likely to trap cells and thus promote heterogeneity, stretching the bag is the better option. Although with a square support the bag would not be stretched, its shape may result in dead zones in the corners as a result of poor mixing. Thus since the disposable bags are fairly strong and can be stretched, a larger circular support was used. For the bag to stretch into the circular support, its diagonal length must be a few centimeters greater than the diameter of the support. This resulted in a circular support of 0·29 m in diameter and 0·66 m in height as shown in figure 16.

Using a circular support resulted in increasing the cross sectional area of the plunging jet reactor. To counteract this increase, the working volume of the reactor was increased from its original volume of 10 L to 14 L so that the depth of the liquid pool was 0·21 m. Operating the plunging jet with the outlet at the bottom resulted in the sample tube being entrained in the jet, so that its oxygen transfer was seriously compromised. By positioning the outlet at the same side as the sample tube, at a 14 L volume the sample tube was kept away from the jet. Increasing the volume beyond 14 L resulted in an occasional and random entrainment of the sample tube in the jet, causing a random reduction in the oxygen transfer capacity.

Figure 13 - Original design of the plunging jet bioreactor

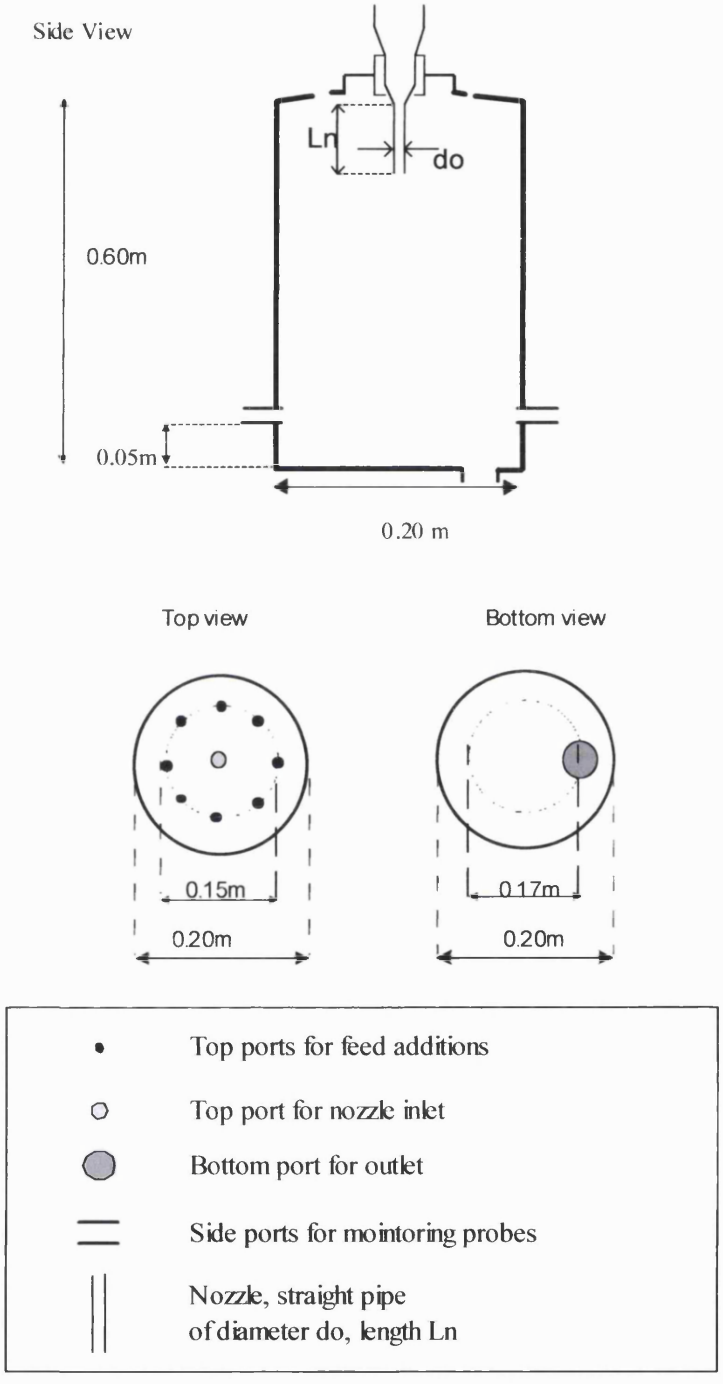

The figure shows the original design for the plunging jet bioreactor. The side view, bottom and top views are all shown. The nozzle is a straight pipe with a diameter do and length Ln. There are two side ports for the insertion of a pH and DOT probe for monitoring and control of the bioreactor.

Figure 14 - Actual Design of the plunging jet bioreactor

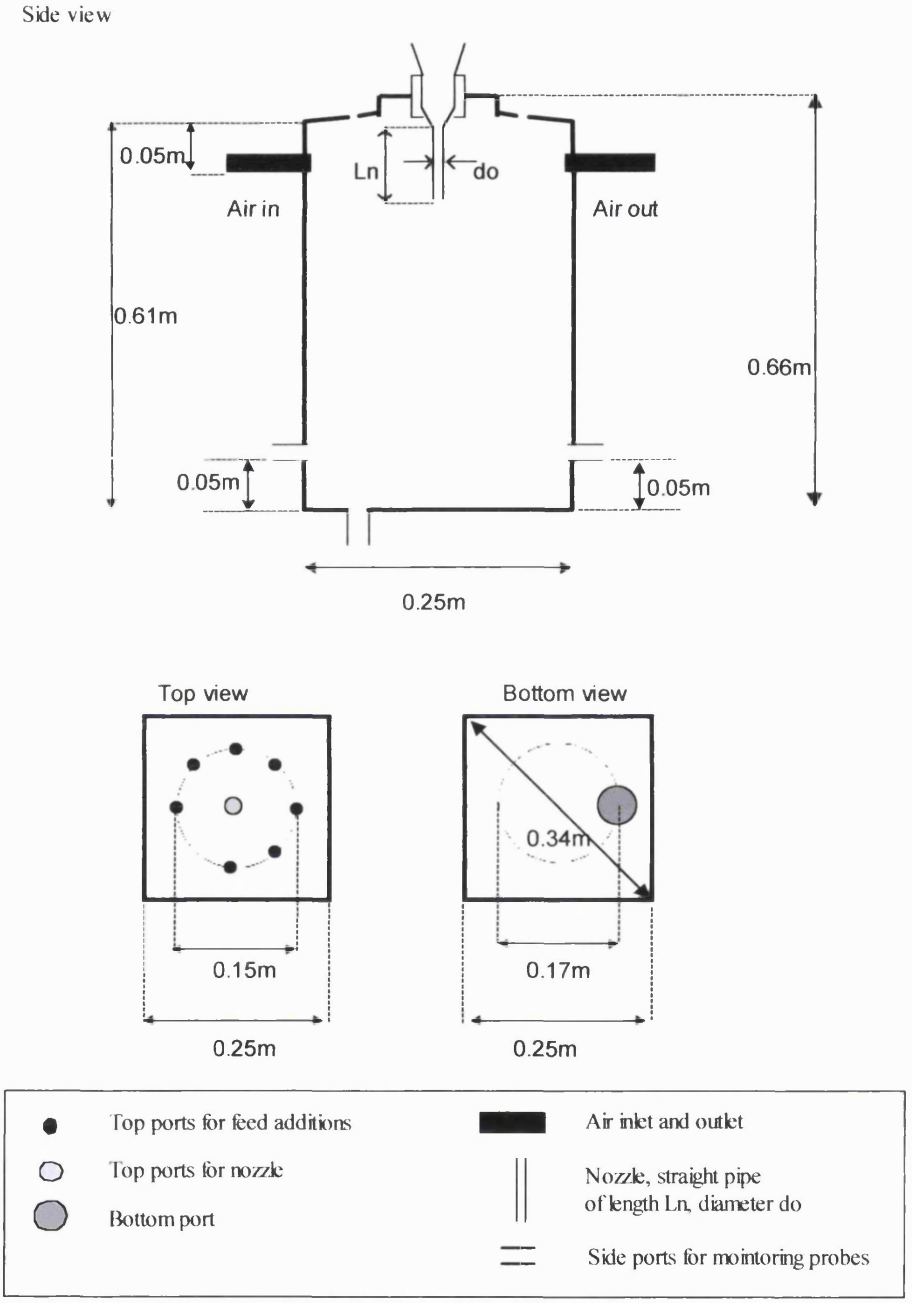

Figure 14
Changes were made to design so that Hyclone Europe could manufacture the bag and thus this figure shows the actual design of the disposable plunging jet bioreactor. As with figure 13 the side view, bottom and top views are all shown. The nozzle is a straight pipe with a diameter do and length Ln. The bioreactor has two side ports for insertion of a pH and DOT probe. The cross sectional area was changed from circular to square. The welding in shown in figure 15

Figure 15 – Welding line for the plunging jet bioreactor

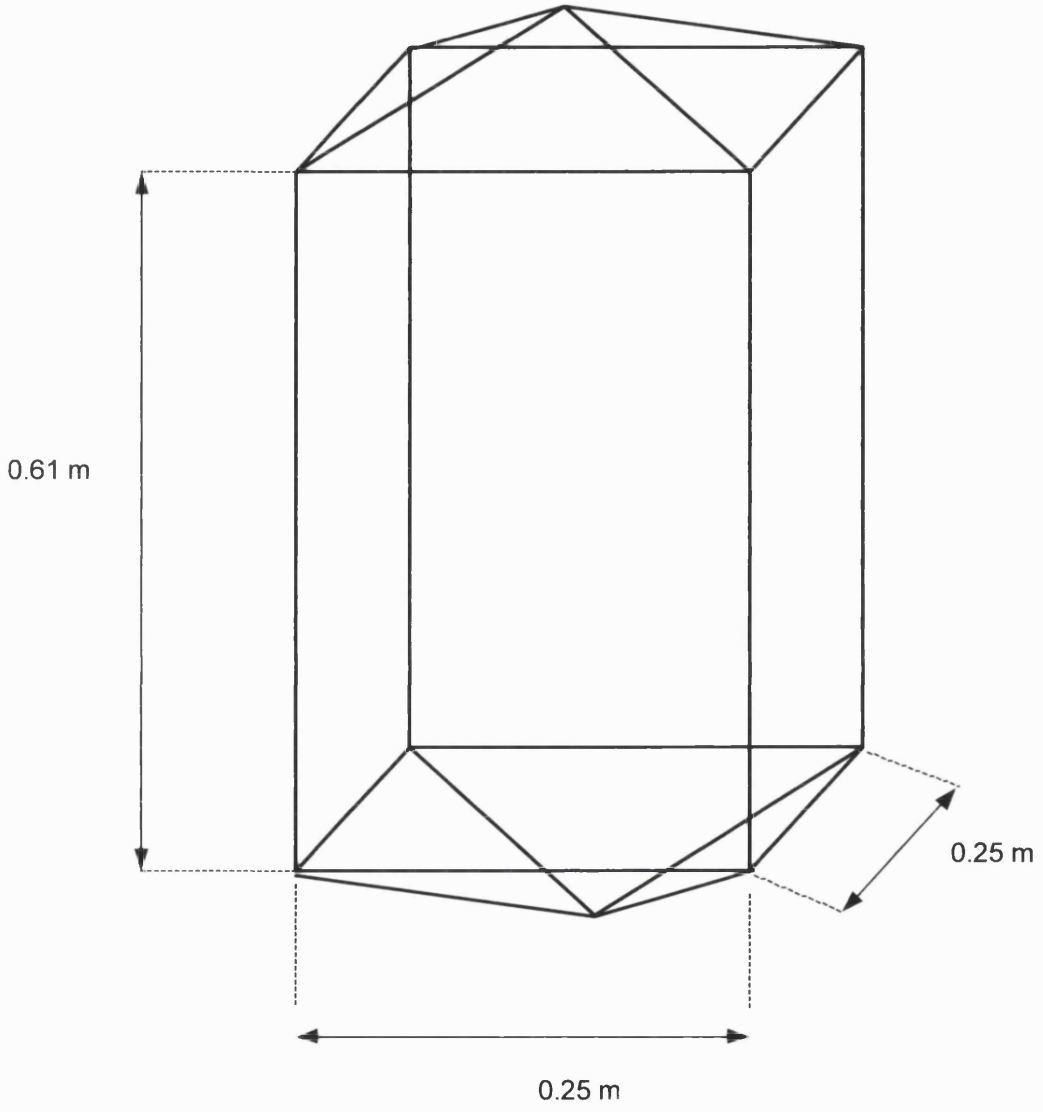

Figure 15
This figure shows how the bag was welded together to form the square cross section plunging jet bioreactor. All the lines shown are where the bag has been welded. The bottom and top pyramid base were pulled out so that both the top and bottom were flat in the perspex support.

Figure 16 - Actual design of plunging jet reactor with the perspex support, pump and heat exchanger

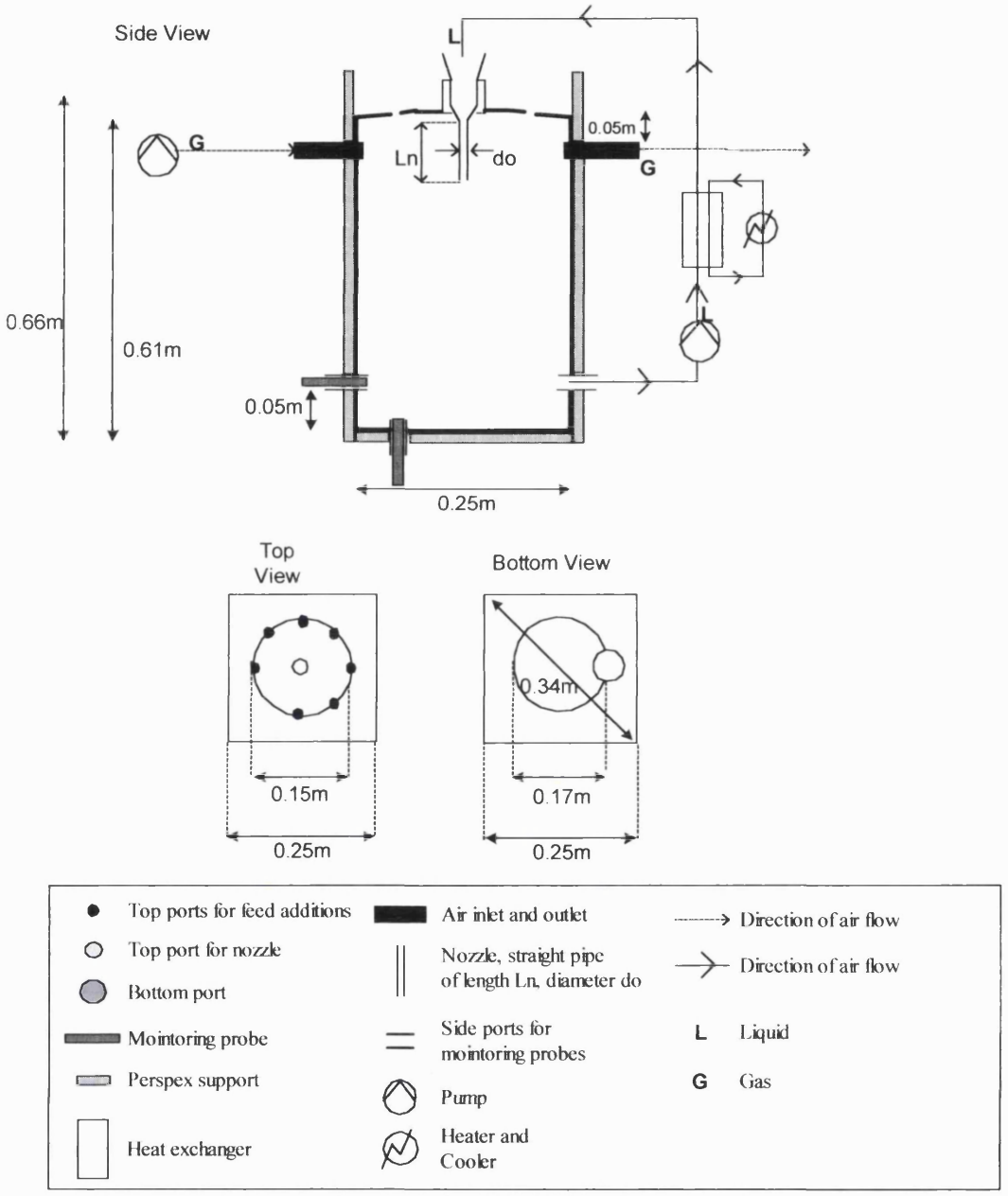

Figure 16
This figure shows how the plunging jet bioreactor bag fits into the perspex support. It also shows how the pump, heat exchanger, heater and cooler are connected in a loop to the nozzle and outlet of the plunging jet bioreactor. The liquid is circulated in the loop, which is shown by the 'L' for liquid and the arrows. Air is pumped across the head space as shown by the dotted lines (……), 'G' for gas and the arrows.

5.3 Determining the nozzle configuration and operating power

Subsequent to the manufacture of the final disposable plunging jet reactor by Hyclone Europe, a series of experiments was performed. Whilst experimental data has been obtained from the plunging jet mimics, it was considered important to perform experiments in the actual disposable plunging jet bioreactor. The aim of these experiments was to determine the nozzle configuration and the power per unit volume at which the bioreactor should be operated for the comparison with the conventional stirred tank bioreactor. The results are shown in figures 17 to 23 (pages 145 to 154).

Four nozzles were constructed for these experiments, which had a diameter of 2·4 mm, 2·9 mm, 3·2 mm and 4·0 mm. The nozzles were a simple pipe construction rather the nozzle proposed by Kenyres et al (1989). This is because although more complex nozzles will have a higher oxygen transfer efficiency their complex construction makes them unsuitable for disposable use. The nozzle length was designed so that the nozzle length divided by the nozzle diameter was 15. This is because according to Bin (1993) although the roughness of the jet is not fully developed until the nozzle's length to diameter ratio is 50 (van de Sande 1974); the entrained gas flow rate does not differ significantly for jets produced from nozzles with a length to diameter ratio greater than 15. The nozzle angle was initially set at 0° so that the jet was vertical because this was the most reproducible angle.

Figure 17 shows the how the k_La alters with the power per unit volume for a 2·4 mm nozzle at a 0·4 m height of fall. The graph shows five data sets which each represent a different run. Different runs are defined as data that were measured with the same bioreactor and nozzle configuration (height of fall, nozzle diameter and angle) but the plunging jet reactor was disassembled between runs. Each data point is a mean of several values, where the error bars shows the range of these values. The error bars were relatively short so that the error within one run is small. With the exception of the values

at the lowest power per unit volume of 0·03 kW m^{-3}, the error between different runs at equivalent power per unit volumes was relatively large. Thus subsequent comparisons were performed within the same run so that the error was minimized.

Figure 18A shows that for a fixed volumetric flow rate reducing the nozzle diameter results in a greater k_La. Figure 18B shows that the k_La is proportional to the power per unit volume for nozzle diameters between 2·4 mm and 4·0 mm. This agrees with several authors, including Bin and Smith (equation 2.1, Bin and Smith 1982), who have found that the mass transfer factor is proportional to the power of the jet. Thus in order to maximize the k_La, the 2·4 mm nozzle was selected for the fermentations.

Figure 19 shows the measured mixing time for the plunging jet reactor with a 2·4 mm nozzle and a 0·4 m height of fall. The measured mixing time includes a probe response time of 9 ± 1 seconds. Thus the data shows that increasing the power per unit volume from 0·025 kW m^{-3} to 0·161 kW m^{-3} results in a decrease in the mixing time. Beyond a power per unit volume of 0·161 kW m^{-3} the measured mixing time was equivalent to the probe response time and thus could not be measured. For a power per unit volume between 0·025 kW m^{-3} to 4·65 kW m^{-3}, the mixing times are sufficiently short demonstrating that the k_La measured at the DOT probe reflects the k_La across the whole plunging jet reactor.

Figure 20A is the plunging jet mimic with four different volumes, where the flow rate, power and nozzle diameter are fixed at 3·2 L min^{-1}, 0·57 kW and 3·85 mm respectively. With the exception of one outlying point at 9 L, for each of the volumes, the k_La was constant for a height of fall between 0·12 m to 0·4 m.
Figure 20B is the plunging jet reactor operating at three different power per unit volumes with a fixed nozzle diameter of 2·4 mm. Each power per unit volume was measured as a different run. For each of the power per unit volumes between 0·15 to 2·2 kW m^{-3}, increasing the height of fall from 0·1 to 0·4 m resulted in no significant change in the k_La whilst from 0·01 to 0·1 m the k_La increased significantly. For the power per unit volume

2·2 kW m^{-3}, the k_La was additionally measured for a second run and showed the same results as the first run.

Both figures show that k_La is unchanged by increasing the height of fall from 0·1 to 0·4 m. This differs from the equation 2.4 where increasing the height of fall results in an increase mass transfer factor, Q_{KLA}. Further analysis of this equation reveals that the power of the jet has a much greater influence than the height of fall. Figure 20B also shows that for a height of fall from 0·01 to 0·1 m the k_La increases. Thus the k_La does not decrease for a height of fall between 0·01 to 0·4 m demonstrating that the jet does not break up within this range. These results rather than the results shown in figure 9 were used to specify the height of fall. The height of fall was set at 0·4 m for the fermentations since a shorter nozzle was used that had a lower pressure drop.

Figure 21 shows the k_La measured in the Fab media and RO water under identical nozzle configurations. Apart from two outlying points that occurred with run 1 at equivalent power per unit volumes, the k_La measured in the Fab media was greater than in the RO water. This compares to work by Van de Donk et al (1979), Van de Donk (1981), who found that the k_La increased with the addition of salts.

Figure 22 shows the k_La versus the power per unit volume for a 5 L working volume stirred tank reactor. For specific airflow rates the k_La is proportional to the power per unit volume.

The plunging jet reactor was initially operated with a nozzle angle of 0° since this was the simplest construction. As discussed in chapter 6 both Fab PJR Run 1 and Wild Type Run 1 had a low oxygen transfer capacity. Thus further experiments were performed to investigate the effect of nozzle angle. Figure 23A shows how the k_La is affected by the nozzle angle for two different runs when the nozzle diameter, height of fall and power per unit volume were fixed at 2·4 mm, 0·4 m and 4·6 kW m^{-3} respectively. Both runs show that the k_La is reduced from 0·05 s^{-1} to 0·03 s^{-1} by moving the nozzle from 0° to +2.5°

towards the outlet. The only discrepancy between the runs is at an angle of +1·5° towards the outlet, where the k_La is 0·05 s^{-1} for run 2 but 0·03 s^{-1} for run 1. Thus the k_La decreases around the +1·5 ° angle. For both runs moving the nozzle angle from 0° to –2·5° results in no change in the k_La excepted for an outlying point at –0·9° for run 2. At an angle of –5·0° the two runs have different results. For run 1 the k_La is virtually unchanged whilst for run 2 it increases significantly to 0·085 s^{-1}. Figure 23B resolves this confusion between the two runs for the –5·0° angle away from the outlet. This figure shows two runs, which measure the k_La at angle of –5·0° away from the outlet and compares this with other data, which is at an equivalent height of fall and nozzle diameter but has a nozzle angle of 0°. The data shows that at a variety of power per unit volumes between 0·025 kW m^{-3} to 4·65 kW m^{-3} there is no difference between the k_La measured at the 0° and –5·0°. Thus the k_La value at –5·0° away from the outlet for run 2 was an outlying point. The overall conclusion is that moving the nozzle from 0° to angle greater than 1·5° towards the outlet results in a decrease in the k_La, whilst moving the nozzle away from the outlet to an angle of +1·5° results in no change in the k_La. Figure 22B also suggests that there is much less variation in the k_La at an angle of –5·0° away from the outlet rather than vertical with an angle of 0°. Since only two runs were performed at the angle of –5·0° further repeats are required to confirm this statement.

Figure 17 - Effect of volumetric flow rate on k_La

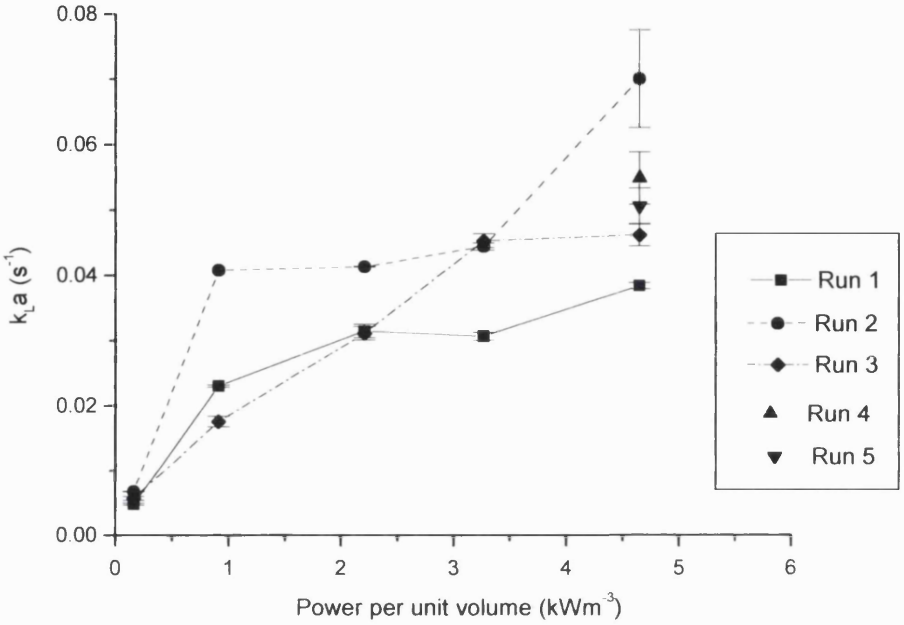

The figure shows the measured k_La for different setups where the nozzle diameter and height of fall was fixed at 2·4 mm and 0·4 m. The error bars show that for an individual run at a specific power per unit volume, the measured k_La values are fairly close together. With the exception of the k_La values measured at the lowest power per unit volume, the k_La values for different runs at equivalent power per unit volumes, are significantly different. Thus the error within one individual run is small whilst the error between the different runs is large.

Figure 18 A – k_La versus volumetric flow rate for four nozzle diameters

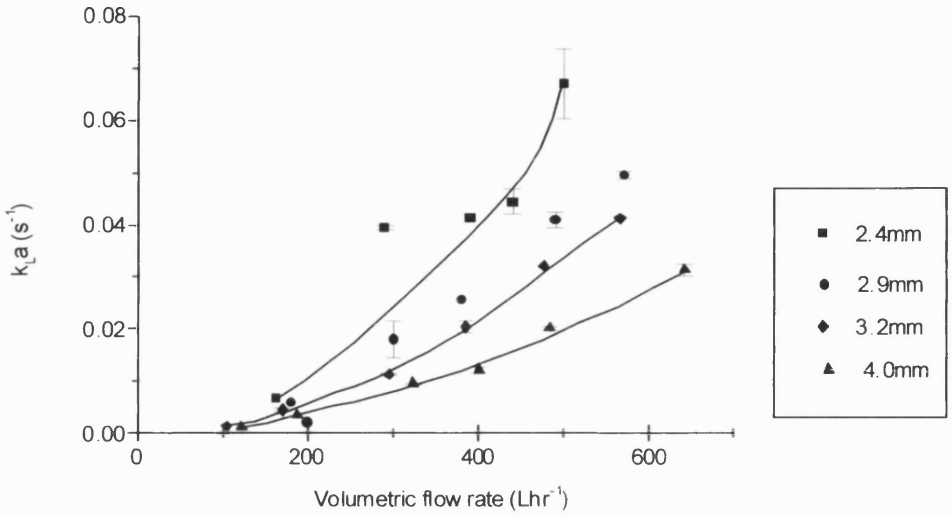

This figure shows the k_La values versus the volumetric flow rate for a range of nozzle diameters between 2.4 mm and 4.0 mm with a fixed height of fall of 0.4m.
The graph shows that for a fixed volumetric flow rate reducing the nozzle diameter results in an increase in the k_La.

Figure 18 B – k_La versus power per unit volume for four nozzle diameter

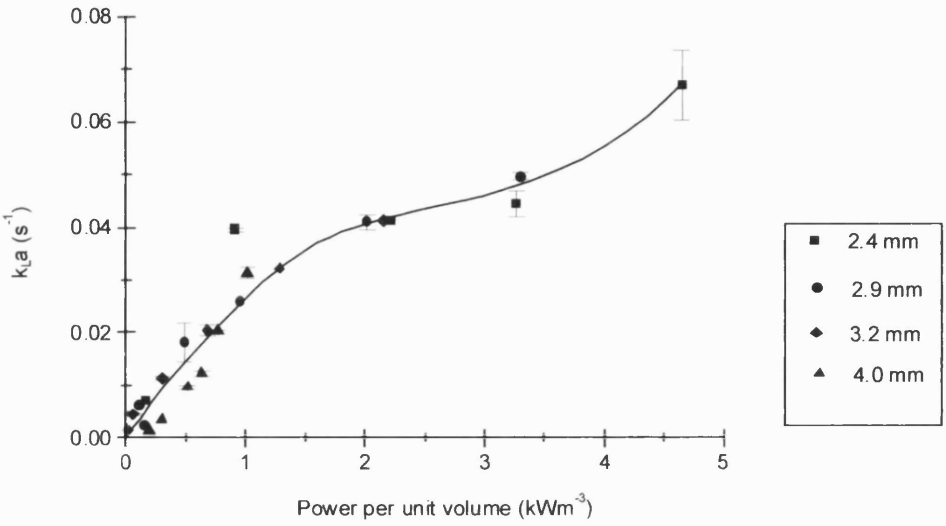

This figure shows the k_La values versus the power per unit volume for the same range of nozzle diameters between 2.4 mm and 4.0 mm as figure 15 A and with a fixed height of fall of 0.4 m.
The graph shows that for a range of nozzle diameters between 2·4 mm to 4·0 mm, the k_La is proportional to the power per unit volume of the jet.

Figure 19 - Mixing time

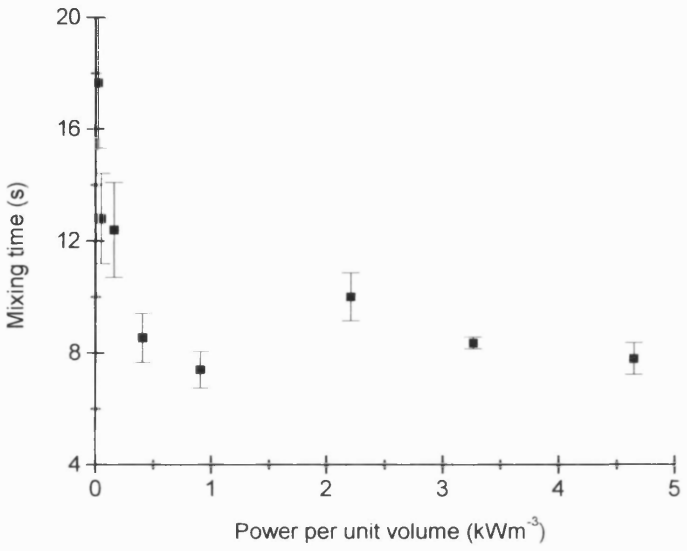

The figure shows the measured mixing time for a plunging jet reactor with a 2·4 mm nozzle and 0·4 m height of fall, operating at a range of power per unit volumes between 0·025 kW m^{-3} and 4·65 kW m^{-3}. The measured mixing time includes the probe response time, which was measured as 9 ± 1 seconds.
The graph shows that increasing the power per unit volume from 0·025 kW m^{-3} to 0·161 kW m^{-3} results in a decrease in the mixing time. Beyond a power per unit volume of 0·161 kW m^{-3} the measured mixing time is equivalent to the probe response time and thus the actual mixing time can not be measured. The mixing times are sufficiently short so that the k_La measured at the DOT probe reflects the k_La across the whole plunging jet reactor.

Figure 20 A - Effect of height of fall on k_La in the plunging jet mimic

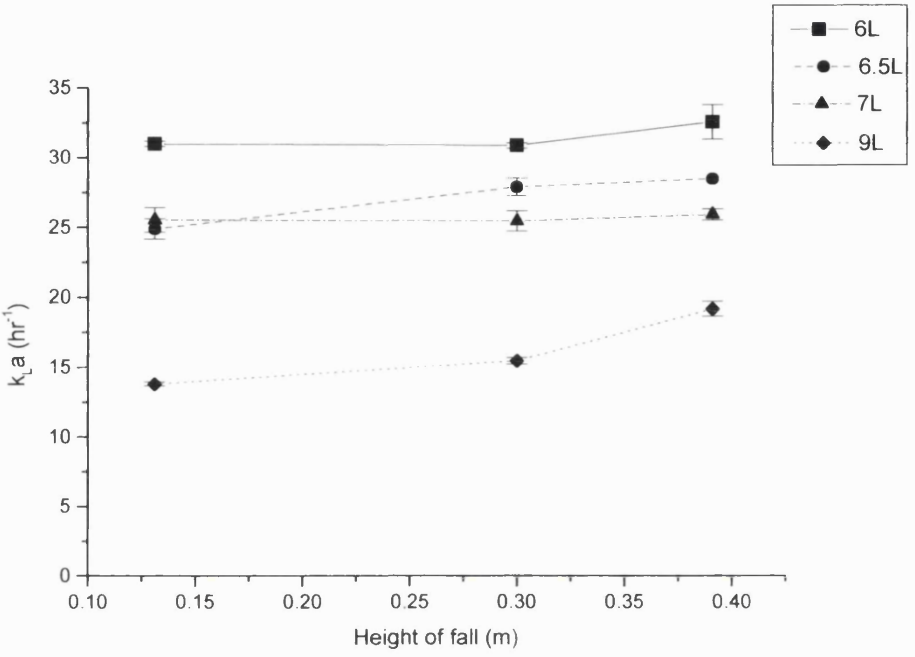

This figure shows how the k_La varies with the height of fall for the plunging jet mimic with four different volumes. Both the flow rate and nozzle diameter were fixed at 3·2 L min^{-1} and 3·85 mm respectively. Figure 7 shows that the height of fall is the distance from the nozzle to the liquid pool.
For a volume between 6 L to 9 L increasing the height of fall from 0·12 m to 0·4 m resulted in no change in the k_La. The only exception, which is an obvious outlying point is at 9 L where the k_La increases at a height of fall of 0·4 m.

Figure 20 B - Effect of height of fall on k_La for the plunging jet reactor

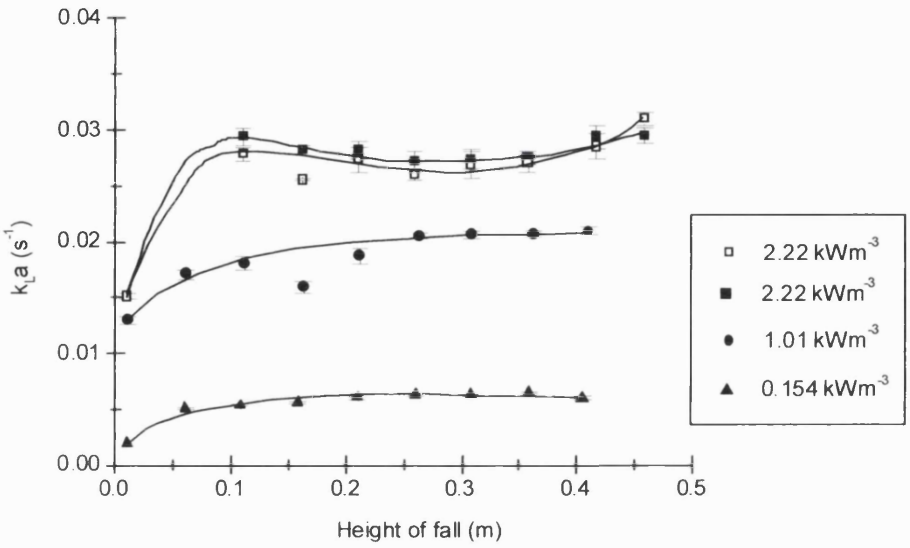

This figure shows how the k_La varies with the height of fall for the plunging jet reactor operating at three different power per unit volumes, where the nozzle diameter was fixed at 2·4 mm. Figure 7 shows that the height of fall is the distance from the nozzle to the liquid pool.

Increasing the height of fall from 0·1 to 0·4 m results in no change in the k_La for a power per unit volume between 0·15 to 2·2 kW m^{-3}. For a height of fall from 0·01 m to 0·10 m the k_La increases for the three power per unit volumes. For the highest power per unit volume of 2·22 kW m^{-3}, the k_La was additionally measured for a second run which had comparable results to the first run.

Figure 21 – Comparison between RO water and Fab media

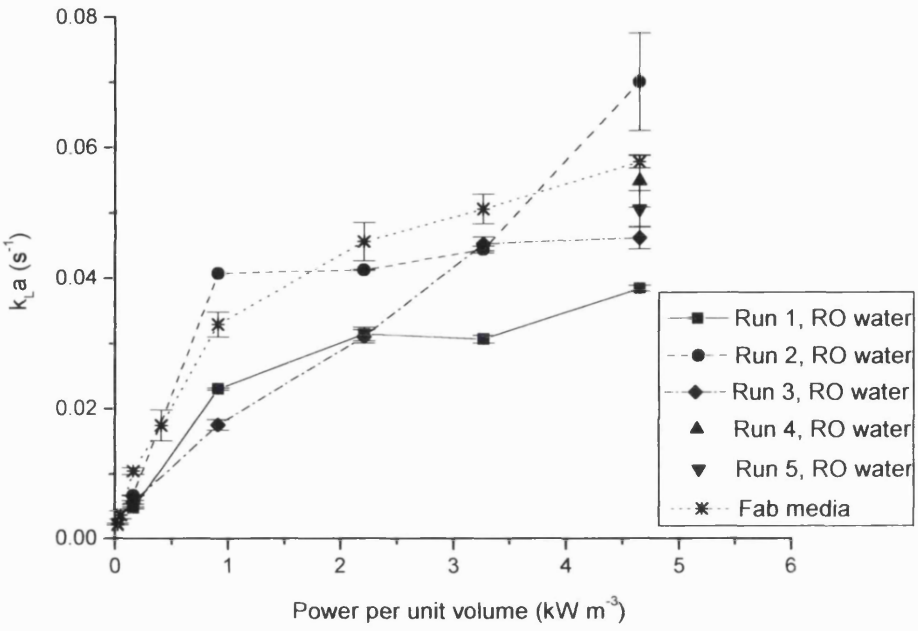

This figure shows the k_La measured in the Fab media compared to RO water for different runs with a 2.4 mm nozzle.

Figure 22 – k_La for stirred tank reactor

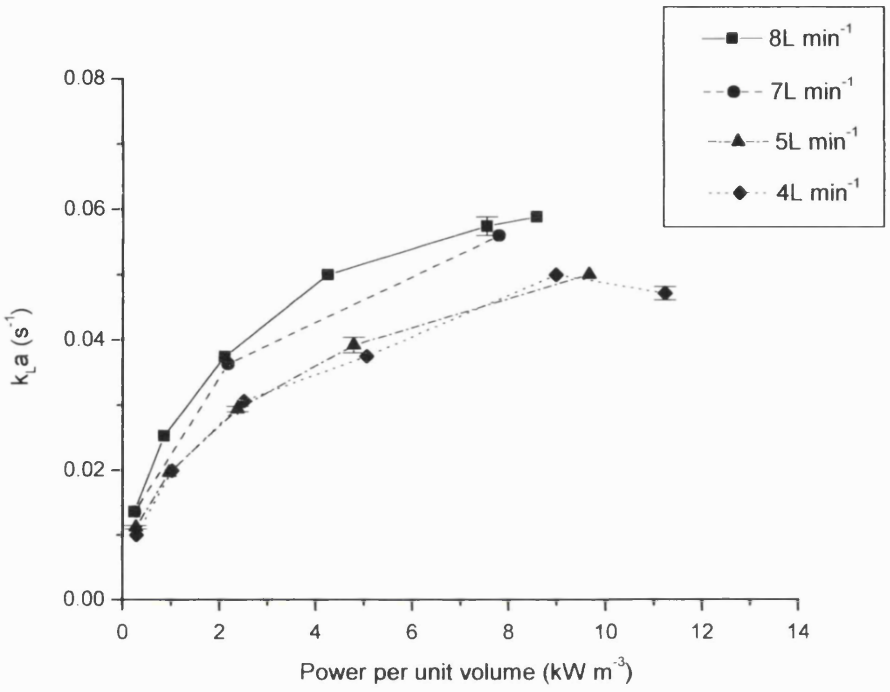

This figure shows the k_La measured in RO water for a 7L LH stirred tank reactor with a 5 L working volume. The data shows that for a specific airflow rate the k_La is proportional to the power per unit volume.

Figure 23 A - Effect of nozzle angle on the k_La

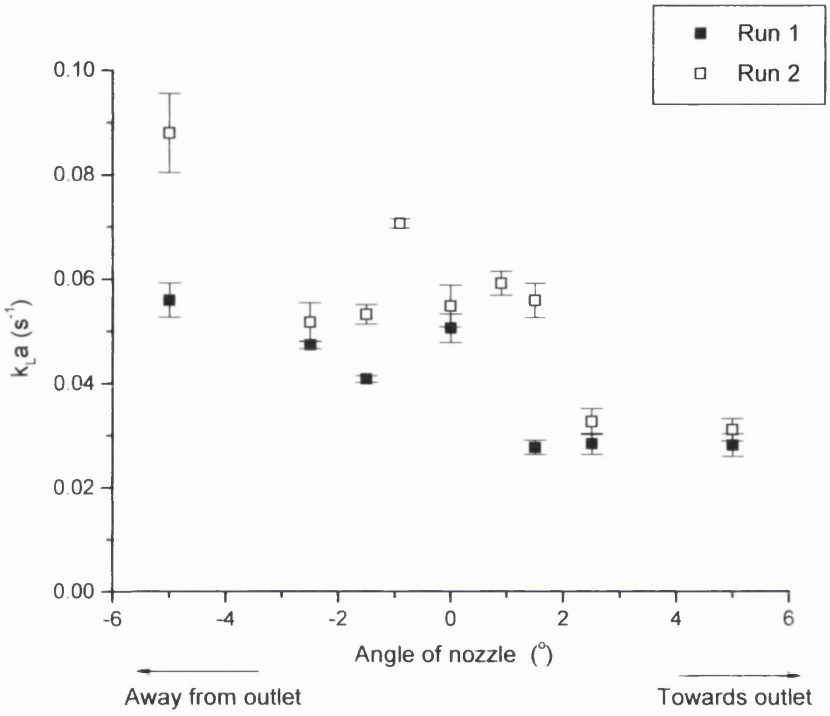

This figure shows how the k_La varies with the angle at a fixed power per unit volume, nozzle diameter and height of fall of 4.6 kW m^{-3}, 2.4 mm and 0.4 m respectively for two runs. Figure 7 shows that an angle of 0° corresponds to a vertical nozzle whilst a positive angle corresponds to the nozzle bent towards the outlet and a negative angle corresponds to the nozzle bent away from the outlet.
For both runs moving the nozzle angle from 0° to +2.5° towards the outlet results in a significant decrease in the k_La from 0.05 s^{-1} to 0.03 s^{-1}. The only discrepancy between the two runs is at an angle of +1.5° where the k_La is 0.05 s^{-1} for run 2 but 0.03 s^{-1} for run 1. Thus around an angle of +1.5° the k_La decreases significantly. Moving the nozzle from an angle of 0° to –2.5° away from the outlet results in no change in the k_La for both runs, with the exception of -0.9°, which is an obvious outlying point. At angle of –5.0° away from the nozzle the two runs show different results. For run 1 the k_La is virtually unchanged whilst for run 2 the k_La increases significantly to 0.085 s^{-1}.

Figure 23 B - Comparison between angle of jet at 0° and -5°

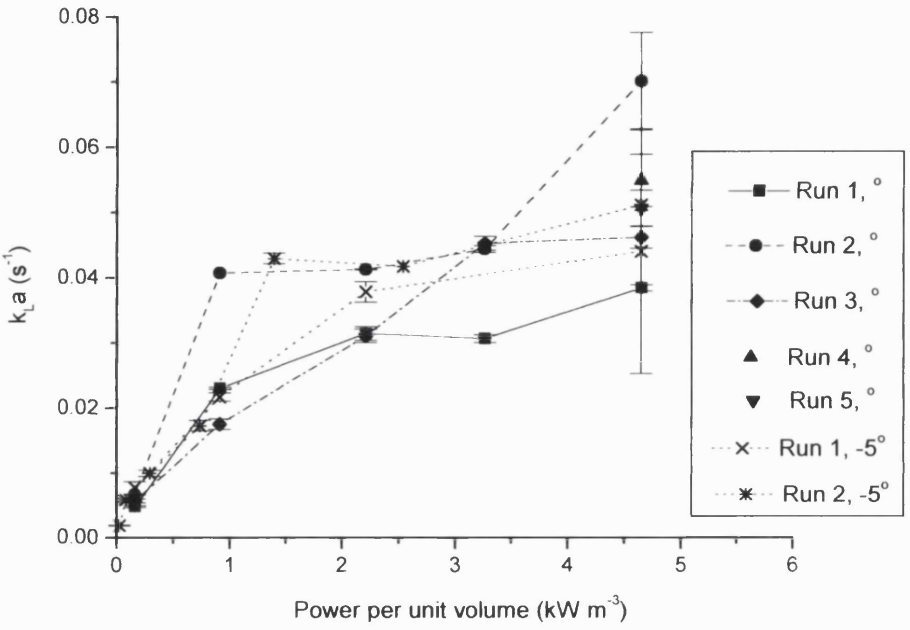

This figure shows the k_La measured at an angle of +5° for two different runs and is compared with k_La data measured at an angle of 0° for several runs. The height of fall and nozzle diameter were fixed at 0.4m and 2.4 mm respectively. Figure 7 shows that an angle of 0° corresponds to a vertical nozzle whilst a positive angle corresponds to the nozzle bent towards the outlet and a negative angle corresponds to the nozzle bent away from the outlet.
The data for the angle at +5° lies within the range of the majority of the data for the angle at 0°.

5.4 Summary of the Design and Operation of the Disposable Plunging Jet Bioreactor

The final design for the bioreactor is shown in Figure 16. The disposable plunging jet bioreactor is a square plastic bag of width 0.25 m that was stretched into a circular support of diameter 0.29 m and height 0.66 m. The bioreactor had a working volume of 14 L and an outlet positioned at the side that could be connected to a pump and heat exchanger, which would be positioned in series to the bioreactor. An inlet was positioned at the top of the bioreactor, which held a nozzle. The nozzle was a straight pipe of 2.4 mm in diameter and 36mm in length. The nozzle was positioned with a height of fall (distance between nozzle tip and liquid pool) of 0.4 m and at angle of 0° (i.e. pointing straight down). This height of fall was selected as the experimental data showed that the k_La did not vary with a height of fall between 0.1 m to 0.4 m. The nozzle to length ratio of 15 was selected because according to Bin (1993) the entrained gas flow rate does not increase beyond a ratio of 15. The smallest nozzle diameter was selected because experimental data and published work presented in section 5.2.1, both show that the k_La increases with the power per unit volume. As equation 2.1 shows, for a fixed volumetric flow rate reducing the nozzle diameter increases the power per unit volume. The nozzle angle was initially 0° as this was the most reproducible angle to achieve. Subsequent to the first disposable plunging jet runs, Fab run 1 and Wild Type run 1, the nozzle angle was changed to –5°. Figure 24 shows the 14 L disposable plunging jet bioreactor is operation with a microbial fermentation.

Figure 24 – 14 L plunging jet bioreactor in operation with a microbial fermentation

Figure 24
Picture of the 14 L disposable plunging jet bioreactor in operation with a microbial fermentation. The disposable bag is supported in a perspex support. The outlet is positioned at the bottom side port facing away from the picture, which connects to a heat exchanger behind the bioreactor and then in a loop to the nozzle shown at the top of the picture. The air inlet and outlet are located at the top side ports facing away from the picture and towards the picture respectively.

6. *Experimental Comparison of a Disposable and Conventional Microbial Bioreactor*

6.1 Overview and Aims

The aim of this chapter is to compare the disposable plunging jet bioreactor (PJR) with a conventional stirred tank reactor (STR) of similar scale. The comparison is based on the physical performance of the bioreactor and the resultant performance of the fermentation. The physical performance of the bioreactor is a comparison between the oxygen transfer performance of the bioreactor, the operating variables (airflow rate, stirrer speed and pump flow rate), the power per unit volume and the shear rate incurred. The resultant performance of the fermentation is how the fermentation responds to the bioreactor and thus a variety of measures are included such as the OUR profile, the RQ profile, the final dry weight and the growth rate. Two fermentations; a fragmented antibody fermentation, called the Fab fermentation and a Wild Type fermentation were used for the comparison. These two fermentations were selected because of their differing growth rates. The Fab fermentation is an industrial strain which is relatively slow growing with a 3 hour doubling time whilst the Wild Type fermentation has a 1 hour doubling time. Additionally the Fab fermentation is a typical example of a biopharmaceutical industrial process since it produces a fragmented antibody that is retained within the microbe during the fermentation and subsequently isolated during downstream processing.

6.2 The Fragmented antibody (Fab) fermentation

The fermentation studied is the Bacteria *E. coli* W3110 containing a plasmid, which incorporates ompA and a tac promotor. This is for the IPTG/lactose induction of a humanised antibody fragment. This antibody fragment is produced in the cytoplasm and is then exported to the periplasmic space. The fermentation is an industrial strain and thus is a useful one with which to test the plunging jet bioreactor as a microbial bioreactor.

For convenience of presentation the fermentation is divided into three phases: lag, growth and induced. During the lag phase no cell growth occurs, so that the OUR (oxygen uptake rate) and RQ (respiratory quotient) remain at zero. The majority of the biomass growth occurs in the growth phase, whilst the Fab product is only produced in the induction phase. The start of the growth phase is defined as the point when the OUR increases above zero. During the growth phase additions of glycerol occur at optical densities of 15, 35 and 50. Lactose is also fed at an optical density of 50. The transition from the growth to induction occurs beyond an optical density of 50 when the carbon source switches from glycerol to lactose. During this switch, the OUR falls and the fermentation switches from producing acid to producing alkali. Subsequently the OUR rises and the fermentation switches back to producing acid. It is this acid switch that defines the end of the growth and the start of induction. At an optical density of 45, the temperature is reduced from 30°C to 27°C and additions of $CaCl_2$ and $MgSO_4$ are made. These additions and a reduction in the temperature strengthen the walls of the bacteria, so that the percentage of the total Fab released into the supernatant is reduced. This reduction in the temperature also causes a decrease in the growth rate.

All the fermentations were monitored by continuously measuring the OUR, CER (carbon evolution rate) and RQ from off gas samples. Periodically the dry cell weight, optical density, concentration of total protein in the supernatant and solid fractions were measured from samples removed from the bioreactor. The percentage protein released is

the concentration of protein in the supernatant as a percentage of the total protein located in both the supernatant and solid fraction. During the induction phase additionally the concentration of the product Fab was also measured in the supernatant and solid fractions.

The performance of the two bioreactors will be judged both in terms of the physical performance of the bioreactor and the resultant performance of the fermentation. The physical performance of the bioreactor is a comparison between the oxygen transfer performance of the bioreactor, the operating variables, (airflow rate, stirrer speed and pump flow rate) the power per unit volume and the shear rate incurred. The oxygen transfer performance is determined by measuring the k_La directly in the fermentation and by a comparison between the OUR and the DOT (dissolved oxygen tension). The power per unit volume is estimated using engineering correlations and the shear rate from an empirical expression. The resultant performance of the fermentation is essentially how the fermentation grows and the cells response to the bioreactors shear environment. The cell growth rate is equivalent to the gradient of the log plot of the dry cell weight versus the fermentation time. The OUR which is an instantaneous measure of the amount of oxygen taken up by the fermentation at any given time, gives an indication of the rate of cell growth and metabolic activity. The RQ which is the ratio of the CER to the OUR, gives an indication of the fermentations carbon source. The percentage protein released, the concentration of protein in the supernatant and the concentration of Fab in the respective locations of solid and supernatant all give an indication of the cell integrity and the response of the cells to the bioreactors shear environment.

For both the STR and PJR the Fab fermentations are presented in six graphs as follows. Unless stated the same axes are used throughout to help in the comparison between the STR and PJR. For each fermentation a full description is given in the figure legends.

Figure A shows the key operating variables for the bioreactor. For both reactors this includes the air flow rate and additionally the stirrer speed and pump flow rate for the STR and the PJR respectively.

Figure B shows the calculated values for the power per unit volume, the shear rate and the k_La.

Figure C shows the results from direct monitoring of the off gas, which are the respiratory quotient (RQ) and the oxygen uptake rate (OUR). The dissolved oxygen tension (DOT) is plotted so that a comparison with the OUR can be made.

Figures D, E and F show the resultant performance characteristics for the fermentation. Figure D shows a log plot of the dry cell weight where the gradient is the growth rate. Figure E shows the protein concentration in the supernatant both as a log plot and expressed as the percentage of the total protein. Figure F shows the concentration of the product Fab in both the solid and the supernatant. For all three figures the OUR is additionally plotted for ease of comparison between the figures.

6.2.1 Fab fermentations in Stirred tank reactor (STR)

Fab STR Run 1 and Fab STR Run 2 are both Fab fermentation performed in the conventional stirred tank reactor or STR (7 L LH fermentor). For both fermentations the initial volume was 4.35 L including a 10% inoculum; this volume increases as the result of further additions so that the final volume is 5 L.

All the fermentations were monitored with off gas analysis and analysis of off line samples as described in section 4.2.1. The power per unit volume, Po_{str} the shear rate, G and the k_La were all calculated throughout the fermentation using the empirical equations shown below. The power per unit volume increases with both the air flow rate and the stirrer speed. The STR was controlled by increasing either or both the stirrer speed and airflow rate, each time the DOT fell below 20 to 30%. Although the STR has a maximum operating of speed and airflow rate of 1400 rpm and 8 L min^{-1} respectively due to foaming in the headspace, the STR may be limited below these levels.

Power, P_{str}

$$P_{str} = [(Pug^2 \times N \times di^3) \backslash (Q^z)]^x \times y \qquad \text{(Equ 6.1)}$$

(Michel and Miller 1962)

where $x = 0.45$

$y = 0.72$

$z = 0.56$

$$Pug = 6 \times \rho \times N^3 \times di^5, \qquad \text{(Equ. 6.2)}$$

(Rushton et al 1950, Zlokarnik and Judat, 1988)

Oxygen transfer coefficient, k_La

$k_La = OUR\backslash(C^*-C_L)$ (Equ. 6.3)

where $C^* = 0.252$ mmol L^{-1} hr^{-1} (Int. Critical Tables, 1928)

$C_L = (DOT\backslash 100) \times C^*$

Shear rate, G

$G = [(e_i \times \rho)\backslash \mu]^{0.5}$ (Equ. 6.4)

(Perry and Clinton, 1973)

where $e_i = e \times 15$ (Equ. 6.5)

$e = Po/(\rho \times V)$ (Equ. 6.6)

Where

P_{str} = power (W)

Pug = ungassed power (W)

N = agitation rate, stirrer speed (s^{-1})

di = impeller diameter (m)

Q = volumetric flow rate of air (m^3 s^{-1})

k_La = oxygen transfer coefficient (s^{-1})

C^* = oxygen concentration of the liquid when it is in equilibrium with the gas (Mol L^{-1})

C_L = oxygen concentration of the liquid (Mol L^{-1})

OUR = oxygen uptake rate (mol L^{-1} s^{-1})

DOT = dissolved oxygen tension (%)

G = shear rate (s^{-1})

e_i= energy dissipation rate at the impellar (m^2 s^{-3})

e= energy dissipation rate (m^2 s^{-3})

V= volume (m^3)

ρ= density ($kg\ m^{-3}$)

μ= viscosity, ($N\ s\ m^{-2}$)

Assumed ρ=1000 $kg\ m^{-3}$

μ=0.001 $N\ s\ m^{-2}$

6.2.1.1 Comparison between Fab STR Run 1 and Fab STR Run 2

The two Fab fermentations performed in the conventional stirred tank bioreactor, STR Run 1 and STR Run 2 are shown in Figures 25 and 26 respectively. Table 12 shows a comparison of the two fermentations which highlights the key physical performance variables of maximum power, shear rate, k_La and the key resultant performance variables of OUR, RQ, growth rate, final biomass and final Fab concentration. Both fermentations have characteristic features, which are described below and are followed by table 12 and figures 25 and 26 (pages 166 to 172).

Physical performance of the bioreactor

The k_La was constant at a fixed power whilst increasing the power resulted in an instantaneous increase in the k_La. For both runs the maximum k_La measured with the STR operating at its maximum power and the DOT at 5% to 10%, was 0.12 s^{-1}. The maximum operating power per unit volume and shear rate incurred for Run 1 was 12.7 kW m^{-3} and 13500 s^{-1} whilst for Run 2 the respective values were 11.2 kW m^{-3} and 13000 s^{-1}. Thus the STR used for Run 2 had a slightly better k_La performance since whilst the k_La values were equivalent, Run 2 used a lower maximum operating power per unit volume than Run 1. The DOT fell to 0% at 1980 minutes for Run 1 and 1650 minutes for Run 2, so that both fermentations were DOT limited as they entered the end of the growth phase. This was an expected result and since this microbial fermentation can grow under DOT limiting conditions, was not a problem.

Resultant performance of the fermentation

Both the RQ and the OUR showed characteristic patterns which were consistent between the two fermentations. The RQ was 0·8 during growth and 1·1 during induction; where the switch in the RQ value indicates a switch in the carbon source from glycerol to lactose. In the growth phase the OUR increased in an exponential manner to a peak of 155 mmol L^{-1} hr^{-1} for Run 1 and 170 mmol L^{-1} hr^{-1} for Run 2. At the end of the growth phase the OUR decreased sharply to 60 mmol L^{-1} hr^{-1} for Run 1 and 70 mmol L^{-1} hr^{-1} for

Run 2. For both runs as the fermentation started the induction phase the OUR increased sharply back to 120 mmol $L^{-1} hr^{-1}$. Subsequently the OUR increased at a significantly slower rate than in the growth phase. At 400 minutes into the induction phase for Run 1 and 360 minutes for Run 2, the OUR rapidly decreased indicating lactose limitation. For both fermentations addition of lactose resulted in the OUR rapidly increasing back to 120 mmol $L^{-1} hr^{-1}$ from which it continued to increase as before. For the first couple of hours of the growth phase, the cell growth rate for Run 1 and 2 were comparable at 0.20 hr^{-1} and 0.18 hr^{-1} respectively. As the growth phase progressed this growth rate decreased to 0.05 hr^{-1} for Run 1 and 0.12 hr^{-1} for Run 2. For the induction phase the growth rate decreased further to 0.026 hr^{-1} and 0.015 hr^{-1} for Run 1 and 2 respectively. Thus Run 1 had a lower growth rate at the end of the growth phase but a higher growth rate at the end of the induction phase.

Both fermentations showed similar profiles of both the percentage of released protein and the concentration of Fab. The percentage of released protein fell from an initial high of 10% for Run 1 and 7.5% for Run 2 to 4% for Run 1 and 1% for Run 2 as growth commenced. For Run 1 the percentage remained at roughly 4% for the rest of the fermentation whilst for Run 2 the percentage increased to 4% at the end of the fermentation. The concentration of the product Fab increased in both the solid and supernatant factions as the induction phase progressed where the concentration was consistently higher in the solid fraction. The final concentration in the solid and supernatant for Run 1 was 75 mg L^{-1} and 22 mg L^{-1} respectively. For Run 2 the final concentrations were 75 mg L^{-1} for the solid fraction and 14 mg L^{-1} for the supernatant. Thus although the final concentrations in the solid fractions were similar, Run 1 had a greater concentration of Fab in the supernatant than Run 2.

Table 12 - Summary of the stirred tank bioreactor performance for Fab STR Run 1 and 2

Parameter	STR Run 1	STR Run 2
Maximum power per unit volume	12.7 kW m^{-3}	11.2 kW m-3
Maximum shear rate incurred	13500 s^{-1}	13000 s^{-1}
Maximum k_La At fixed power per unit volume	0.12 s^{-1} k_La is fixed	0.12 s^{-1} k_La is fixed
Maximum OUR	155 mmol L^{-1} hr^{-1}	170 mmol L^{-1} hr^{-1}
RQ - during growth - during induction	0.8 1.1	0.8 1.1
Growth rate - initial growth - final growth - induction	0.20 hr^{-1} 0.05 hr^{-1} 0.026 hr^{-1}	0.18 hr^{-1} 0.12 hr^{-1} 0.015 hr^{-1}
Total fermentation time in growth phase	21.7 hrs	20.7 hrs
Percentage final growth to total growth	31 %	19 %
Final biomass - end growth - end induction	31 g L^{-1} 39 g L^{-1}	31 g L^{-1} 42 g L^{-1}
Final Fab concentration - supernatant - solid	 22 mg L^{-1} 75 mg L^{-1}	 14 mg L^{-1} 75 mg L^{-1}

Table 12
The table shows a comparison between Fab STR run 1 and Fab STR run 2, which are two Fab fermentations performed in the same 5 L stirred tank bioreactor. These fermentations are shown in figure 25 for Fab STR run 1 and 26 for Fab STR run 2.

Figure 25 - Fab STR Run 1

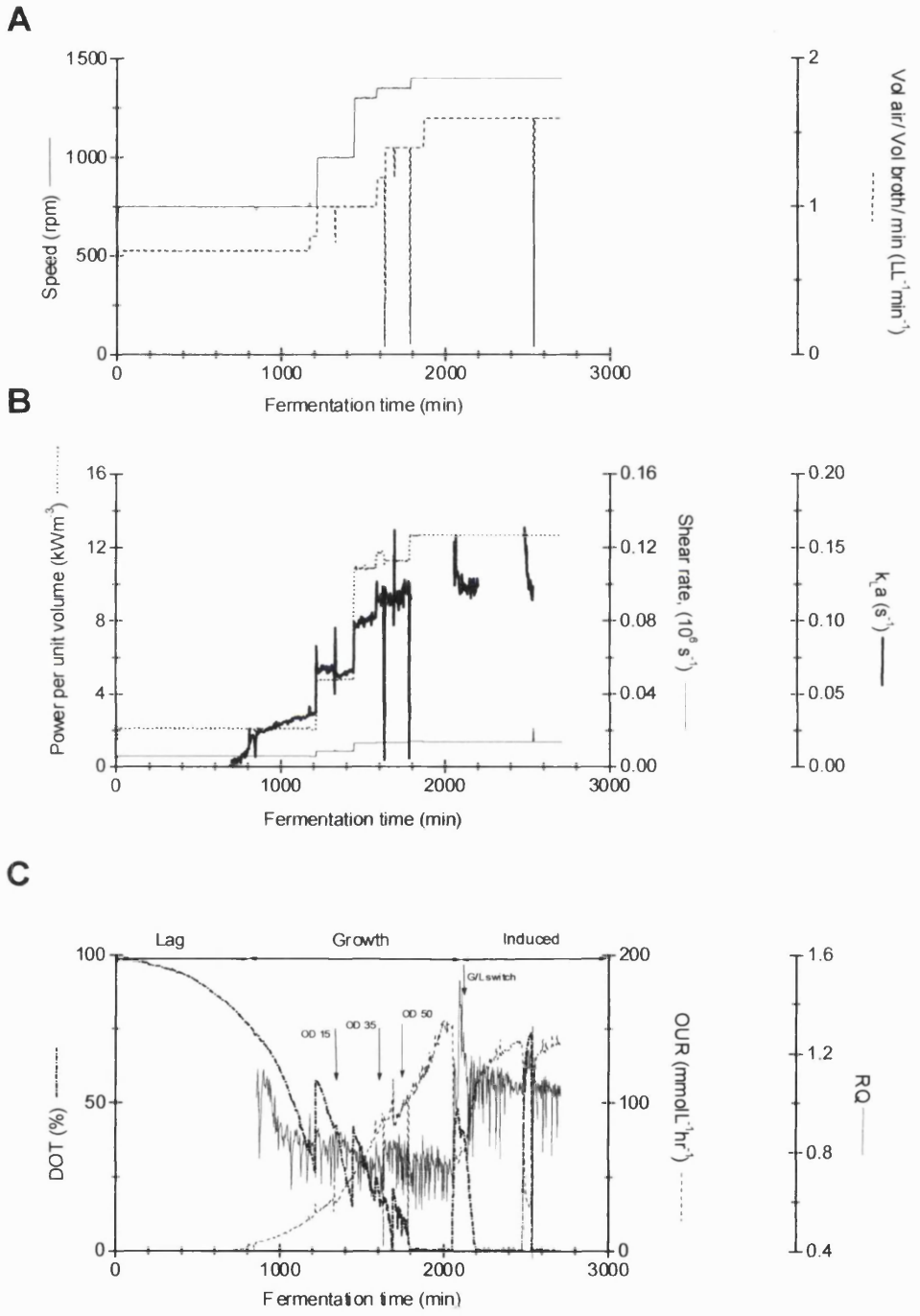

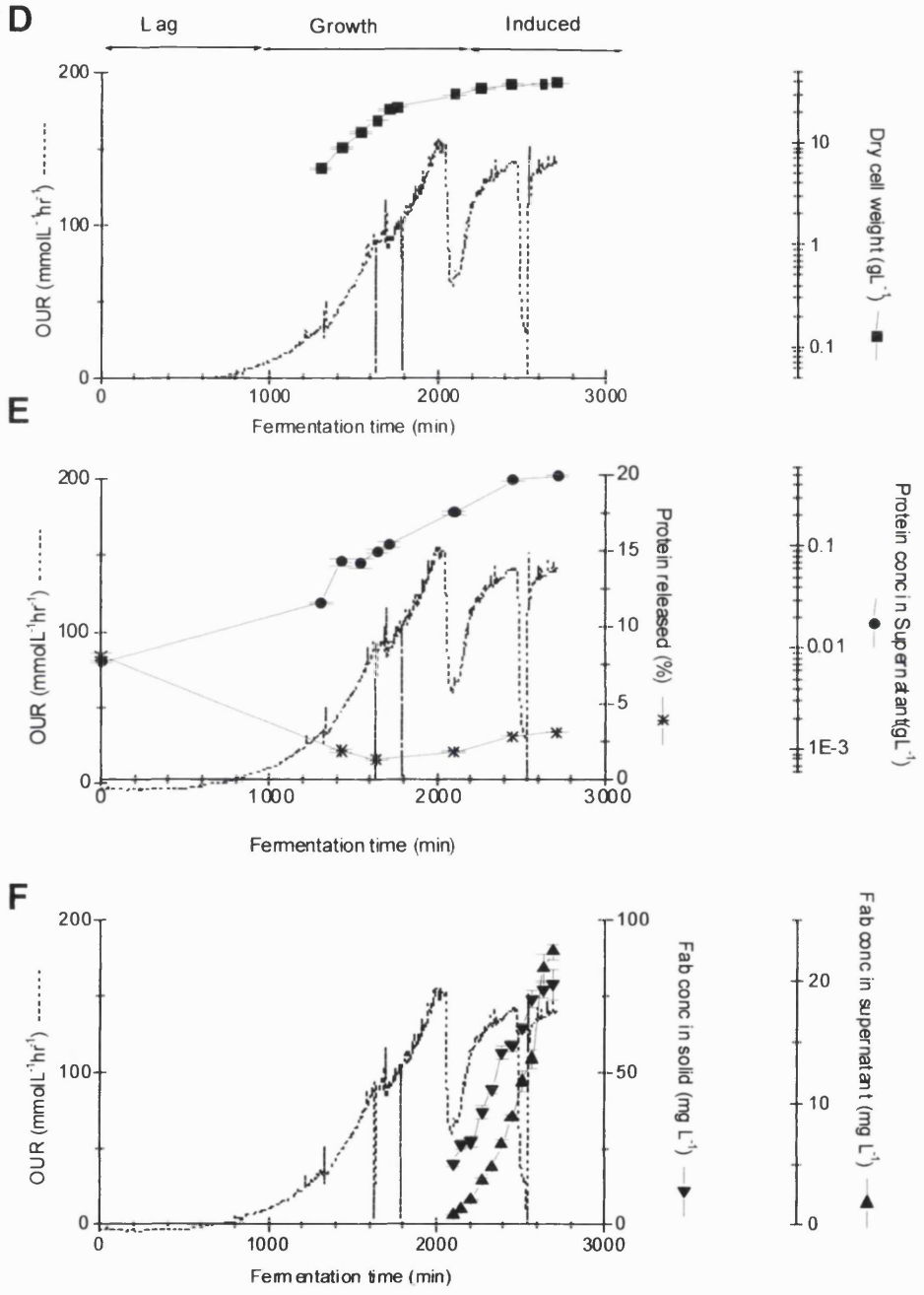
D
Lag
Growth
Induced
OUR (mmolL⁻¹hr⁻¹)
Dry cell weight (gL⁻¹)
Fermentation time (min)
E
Protein released (%)
Protein conc in Supernatant (gL⁻¹)
F
Fab conc in solid (mg L⁻¹)
Fab conc in supernatant (mg L⁻¹)

Figure 25 Fab STR Run 1 (stirred tank reactor 5L).
Figures A, B and C show that the bioreactors oxygen transfer performance was sufficient for the complete Fab protocol to be performed.

Figure A shows the operating variables speed and airflow rate. Both the speed and airflow rate was increased so that the DOT was maintained above 20%.

Figure B shows the calculated values for the Po_{str} power per unit volume, k_La and G, shear rate. At a fixed power per unit volume, the k_La is constant, whereas increasing the power per unit volume results in an increase in the k_La. The highest k_La was 0.12 s^{-1} when the bioreactor was operating at its maximum power and shear of 12.7 kW m^{-3} and 13500 s^{-1} respectively

Figure C shows how the DOT, OUR and RQ vary between the different fermentation phases. This fermentation shows a clear trend that as the OUR increases, at a fixed power the DOT falls, whilst increasing the power results in an instant increase in the DOT.
From 0 to 800 minutes the OUR and RQ are zero and thus this is the lag phase. At 800 minutes the OUR increases above zero and this is the start of the growth phase. The growth phase continues until 2100 minutes, where induction phase starts which is defined as the point when the acid switch occurs. Feed additions of glycerol at optical densities of 15, 35 and 50 were at the fermentation times of 1315 minutes, 1600 minutes, and 1760 minutes respectively (see arrows on Figure C). The RQ was 0.8 for the growth phase and at the start of induction increases to 1.1 where it remained for the induction phase.

Figure D shows a log plot of the resulting dry cell weight. At the end of the growth phase the biomass is 30.2 g L^{-1} (optical density of 63) whilst at the end of the induction phase it is 39.4 g L^{-1} (optical density of 88). The growth phase has a growth rate of 0.20 hr^{-1} between the fermentation times 800 minutes and 1700 minutes and a slower growth rate of 0.05 hr^{-1} between 1700 and 2100 minutes. The growth rate for the induction phase 0.026 hr^{-1}.

Figure E shows the protein concentration in the supernatant both as a log plot and expressed as a percentage of the total protein. From an initial 10%, the protein disruption subsequently fell to about 4% as growth commenced. Through the course of the fermentation it remained at about 4% with a small increase as the fermentation entered the induction phase.

Figure F shows the concentration of the product Fab in the supernatant and solid during the induction phase. As the phase progresses the concentration of Fab in both the supernatant and the solid increases. Throughout the induction phase the Fab concentration was significantly greater in the solid fraction.

Figure 26 - Fab STR Run 2

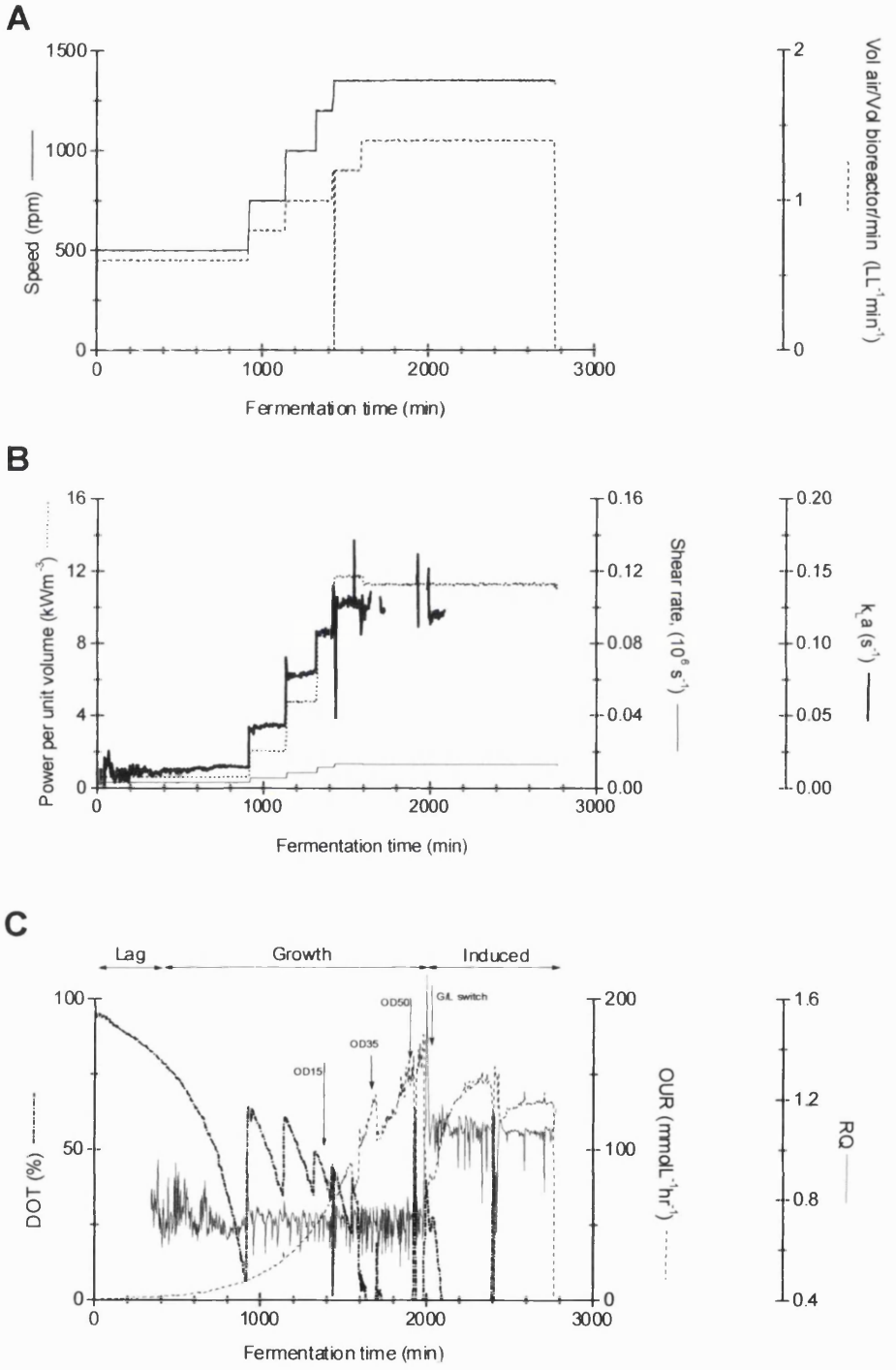

D

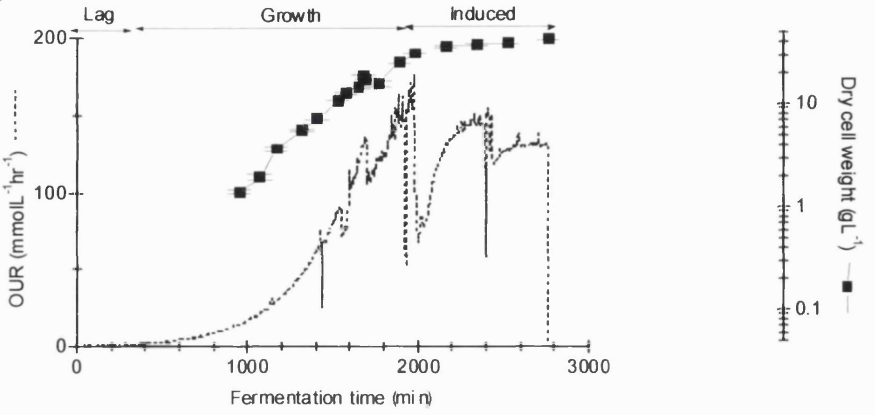
Lag
Growth
Induced
OUR (mmolL-1hr-1) ------
Fermentation time (min)
Dry cell weight (gL-1)

E

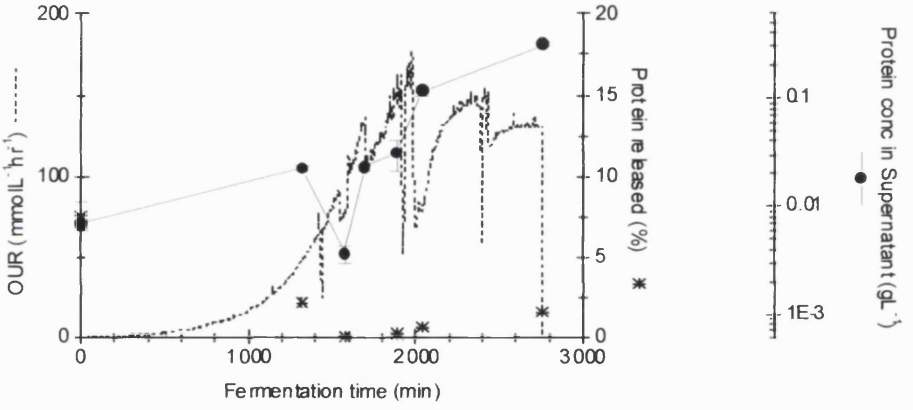
OUR (mmolL-1hr-1) ------
Protein released (%)
Fermentation time (min)
Protein conc in Supernatant (gL-1)

F

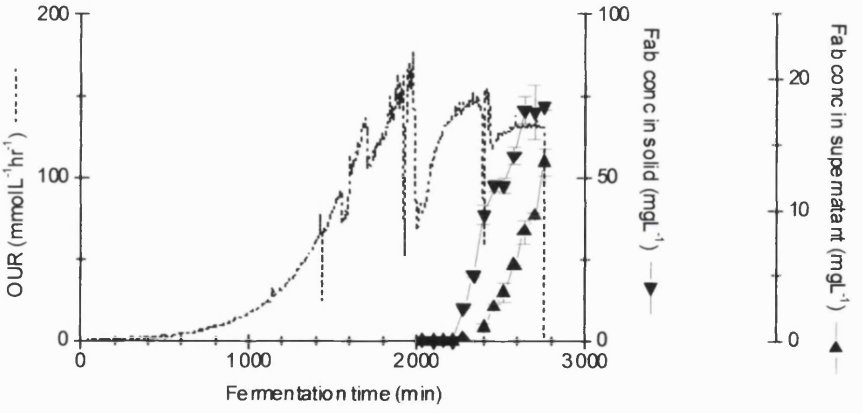
OUR (mmolL-1hr-1) ------
Fab conc in solid (mgL-1)
Fermentation time (min)
Fab conc in supernatant (mgL-1)

Figure 26 Fab STR Run 2 (stirred tank reactor 5L).
Figures A, B and C show that the bioreactors oxygen transfer performance was sufficient for the complete Fab protocol to be performed.

Figure A shows the operating variables speed and airflow rate. Both the speed and airflow rate was increased so that the DOT was maintained above 20%.

Figure B shows the calculated values for the Po_{str} power per unit volume, k_La and G, shear rate. At a fixed power per unit volume, the k_La is constant, whereas increasing the power per unit volume results in an increase in the k_La. The highest k_La was 0.12 s^{-1} with the bioreactor operating at its maximum power and shear rate of 11.2 kW m^{-3} and 13000 s^{-1} respectively.

Figure C shows how the DOT, OUR and RQ vary between the different fermentation phases. This fermentation shows a clear trend that as the OUR increases, at a fixed power the DOT falls, whilst increasing the power results in an instant increase in the DOT. From 0 to 400 minutes the OUR and RQ are zero and thus this is the lag phase. At 400 minutes the OUR increases above zero and this is the start of the growth phase. The growth phase continues until 2040 minutes, where the induction phase starts which is defined as the point when the acid switch occurs. Feed additions of glycerol at optical densities of 15, 35 and 50 were at the fermentation times of 1400 minutes, 1700 minutes, and 1900 minutes respectively (see arrows on Figure C).
The RQ was 0.8 for the growth phase and increased to 1.1 at the start of the induction phase, where it remained for the induction phase.

Figure D shows a log plot of the resulting dry cell weight. At the end of the growth phase the biomass is 31.0 g L^{-1} (optical density of 63) whilst at the end of the induction phase it is 42.1 g L^{-1} (optical density of 69.8). The growth phase has a growth rate of 0.18 hr^{-1} between the fermentation times 800 minutes and 1800 minutes and a slower growth rate of 0.12 hr^{-1} between 1800 and 2040 minutes. The growth rate for the induction phase is 0.015 hr^{-1}.

Figure E shows the protein concentration in the supernatant both as a log plot and expressed as a percentage of the total protein. From an initial disruption of 7.5% the percentage of protein disrupted fell to about 1% as growth commenced. Through the course of the growth phase it remained at about 1%. As the fermentation entered induction this percentage rose to a protein disruption of 4% by the end of the fermentation

Figure F shows the concentration of the product Fab in the supernatant and solid during the induction phase. As the phase progresses the concentration of Fab in both the supernatant and the solid increases. Throughout the induction phase the Fab concentration was significantly greater in the solid fraction.

6.2.2 Fab fermentations in Plunging jet reactor (PJR)

The four Fab fermentations performed in the disposable plunging jet bioreactor, which are called PJR Runs 1-4, are shown in Figures 27-30 respectively. A comparison between PJR Run 1 and 2 is shown in Table 13, whilst Table 14 shows a comparison between PJR Runs 2, 3 and 4. As before these tables highlight the key physical performance variables of maximum power, shear rate, k_La and the key resultant performance variables of OUR, RQ, growth rate, final biomass and final Fab concentration. A comparison between the four fermentations is discussed below which is subsequently followed by the tables 13-14 (page 178 to 179) and the figures 27 – 30 (180 to 191).

The four Fab fermentation runs, Fab PJR Runs 1-4, were all Fab fermentations performed in the disposable plunging jet bioreactor or PJR (Disposable bag). For all the fermentations the initial volume was 12.35 L including a 10% inoculum; this volume increased as the result of further additions so that the final volume was 14 L. All the fermentations were monitored with off gas analysis and analysis of off line samples as described in section 4.2.1. The power per unit volume, Po_{str} the shear rate, G and the k_La (oxygen transfer coefficient) were all calculated throughout the fermentation. The k_La was calculated using the equation 6.3 on page 162 whilst the power per unit volume and shear rate used the empirical equations below. The power per unit volume increased with the pump flow rate. Thus the pump flow rate is controlled so that the DOT was maintained above 20%. The airflow rate was maintained at its maximum flow rate of 10 L min^{-1}, so that the mass spectrometer received an adequate off gas sample.

Power per unit volume, Po/V

$Po/V = (½ \times \rho \times Q \times Vo^2)/V$ (Equ. 6.7)

(Bin, A. K., 1993)

Shear rate, G

$G = [(e \times \rho)\backslash\mu]^{0.5}$ (Equ. 6.4)

Where $e = (128 \times Q^3 \times f) \backslash (\pi^3 \times do^7)$ (Equ. 6.8)

(Perry and Clinton, 1973)

Units as follows:-

ρ= density (kg m^{-3})

μ= viscosity (N s m^{-2})

Q = volumetric flow rate (m^3 s^{-1})

Po/V = Power per unit volume (W m^{-3})

Vo = velocity (m s^{-1})

V = volume (m^3)

f = friction factor

do = nozzle diameter (m)

G = shear rate (s^{-1})

e = energy dissipation rate (m^2 s^{-3})

Assumed ρ = 1000 kg m^{-3}

μ = 0.001 N s m^{-2}

6.2.2.1 Comparison between Fab PJR Run 1 and Fab PJR Run 2

The two runs Fab PJR Run 1 and 2 are shown in figures 27 and 28 (pages 180 to 185) respectively and a comparison is shown in table 13 (page 178). Fab PJR Run 1 showed poor oxygen transfer performance so that the Fab protocol could not be completed. From 1000 to 1400 minutes with the power fixed at its operating maximum of 4.7 kW m^{-3}, the k_La varied significantly. This variation is shown by a comparison of the OUR and DOT at 1000, 1070 and 1250 minutes. At 1000 minutes with the OUR at 10 mmol L^{-1} hr^{-1} the DOT fell below 5% prompting an increase in the volumetric flow rate from 330 L hr^{-1} to 500 L hr^{-1}. This resulted in an increase in the power per unit volume from 1.4 to 4.7 kW m^{-3}. Despite this increase in the power, the DOT remained at 0% whilst the OUR continued to increase. At 1070 minutes with the OUR at 22 mmol L^{-1} hr^{-1} the DOT increased above 0%. From 1070 to 1170 minutes the k_La increased significantly, so that

both the DOT and OUR increased to a peak of 40% and 40 mmol L^{-1} hr^{-1} respectively at 1170 minutes. From 1170 minutes the DOT decreased so that by 1250 minutes with the OUR at 54 mmol L^{-1} hr^{-1} the DOT was at 0%. Clearly there is a significant difference in the oxygen transfer performance of the PJR at 1000 and 1250 minutes.

This poor oxygen transfer performance was repeated in the Wild Type PJR Run 1 and in other fermentations not included in the thesis. After careful analysis this poor performance was attributed to air being drawn down the outlet, where it escaped the fermentation broth at either the pump or the nozzle outlet. It was thought that pointing the nozzle away from the outlet would minimise this effect. Thus for Fab PJR Run 2 the nozzle angle was moved from 0° to -5° away from the outlet. This resulted in good oxygen transfer performance so that the complete Fab protocol could be performed in the PJR. A comparison of the two runs at the same OUR and power per unit volume of 5 mol L^{-1} hr^{-1} and 1.4 kW m^{-3} respectively, show that moving the angle form 0° to -5° results in an increase in the k_La from 0.005s^{-1} to 0.045 s^{-1}.

6.2.2.2 Comparison between Fab PJR Run 2, 3 and 4

Fab PJR Runs 2, 3 and 4 were all operated in an identical manner. For Runs 2 and 3, the complete Fab protocol was performed so that each fermentation had the three phases, lag, growth and induction. For Run 4 due to equipment failure (heat exchanger) the fermentation was terminated at 2000 minutes so that only the lag and the vast majority of the growth phase occurred. The three fermentations were shown in figures 28, 29 and 30 (pages 183 to 192) respectively and table 14 (page 179) shows a comparison between these fermentations.

Physical performance of the bioreactor

For all three fermentations the PJR was operated at a fixed power and shear rate of 1.40 kW m^{-3} and 85000 s^{-1} respectively, where the nozzle was angled at 5° away from the outlet. This nozzle angle significantly improved the oxygen transfer performance of the PJR, since for each run the DOT did not fall below 20% despite a maximum OUR of between 90 and 100 mmol L^{-1} hr^{-1}. For all three runs although the PJR was operated at a fixed power, the k_La increased significantly where increases in the k_La and OUR coincided. For the fermentations Runs 2 and 3 the maximum k_La values were 0.13 s^{-1} and 0.15 s^{-1} respectively. For both runs the maximum k_La coincided with a maximum OUR of 90 mmol L^{-1} hr^{-1} for Run 2 and 100 mmol L^{-1} hr^{-1} for Run 3.

Resultant performance of the fermentation

The three fermentations showed characteristic patterns for both the OUR and RQ. For the growth phase the RQ varied between 0.5 and 1.0 where addition of glycerol resulted in an increase in the RQ. For runs 2 and 3 the RQ was 1.0 for all of the induction phase. In the growth phase the OUR initially increased rapidly to 80 mmol L^{-1} hr^{-1} for Run 2 and 95 mmol L^{-1} hr^{-1} for Runs 3 and 4. The OUR then increased at a significantly slower rate to a peak of 90 mmol L^{-1} hr^{-1} for Run 2 and 100 mmol L^{-1} hr^{-1} for Runs 3 and 4. Subsequently the OUR decreased until the start of the induction phase, where the OUR remained fixed at 75 mmol L^{-1} hr^{-1} for Run 2 and 80 mmol L^{-1} hr^{-1} for Run 3. For all three fermentations the growth phase had two growth rates. The initial growth rate was 0.48 hr^{-1} for Run 2, 0.31 hr^{-1} for Run 3 and 0.42 hr^{-1} for Run 4. Subsequently the growth rate decreased significantly to 0.079 hr^{-1} for Run 2, 0.053 hr^{-1} for Run 3 and 0.050 hr^{-1} for Run 4. The growth rate for the induction phase decreased further to 0.041 hr^{-1} for Run 2 and 0.034 hr^{-1} for Run 3.

For all three fermentations the percentage of protein in the supernatant increased significantly at the end of the lag phase. These increases were from 8% to 80% for Run 2, 6% to 75% for Run 3 and 10% to 60% for Run 4. As the growth phase commenced the percentage of protein in the supernatant decreased to 4% for Runs 2 and 3 and 8% for

Run 4. For all three fermentations the percentage then remained at these levels for the rest of the growth phase and the induction phase. For both Run 2 and 3 throughout the induction phase, the concentration of Fab in the supernatant was negligible (0.005 mgL^{-1}) whilst in the solid fraction it was zero.

Table 13 Comparison between Fab PJR Run 1 and Fab PJR Run 2

Parameter	PJR Run 1	PJR Run 2
Nozzle angle	0°	-5°
Maximum power per unit volume	4.7 kW m^{-3}	1.4 kW m^{-3}
Maximum shear rate incurred	150000 s^{-1}	85000 s^{-1}
Maximum OUR	54 mmol L^{-1} hr^{-1}	90 mmol L^{-1} hr^{-1}
Maximum k_La At fixed power per unit volume	0.06 s^{-1} k_La increases with OUR	0.13 s^{-1} k_La increases with OUR
k_La at power per unit volume of 1.4 kW m^{-3} and OUR of 5 mmol L^{-1} hr^{-1}	0.005 s^{-1}	0.045 s^{-1}
RQ - during growth - during induction	1.1 to 0.6	0.55 to 0.95 1.0
Growth rate - initial growth - final growth - induction	0.58 hr^{-1} no induction	0.48 hr^{-1} 0.079 hr^{-1} 0.041 hr^{-1}
Final biomass - end growth - end induction	1.6 g L^{-1} no induction	22 g L^{-1} 30 g L^{-1}
Final Fab concentration - supernatant - solid	 no induction no induction	 0.005 mg L^{-1} 0 mg L^{-1}

Table 13
The table shows a comparison between Fab PJR run 1 and Fab PJR run 2, which are two Fab fermentations performed in the 14 L plunging jet bioreactor. The table shows the effect of moving the nozzle angle form 0° for Fab PJR run 1 to an angle of -5° for the Fab PJR Run 2. As shown in figure 7 the nozzle angle of 0° is vertical and -5° is 5° away from the nozzle outlet. These fermentations are shown in figure 27 for Fab PJR run 1 and figure 28 for Fab PJR run 2.

Table 14 Comparison between Fab PJR Run 2, 3 and 4

Parameter	PJR Run 2	PJR Run 3	PJR Run 4
Nozzle angle	-5°	-5°	-5°
Maximum power per unit volume	1.4 kW m^{-3}	1.4 kW m^{-3}	1.4 kW m^{-3}
Maximum shear rate incurred	85000 s^{-1}	85000 s^{-1}	85000 s^{-1}
Maximum OUR	90 mmol L^{-1} hr^{-1}	100 mmol L^{-1} hr^{-1}	90 mmol L^{-1} hr^{-1}
Maximum k_La At fixed power per unit volume	0.13 s^{-1} k_La increases with OUR	0.15 s^{-1} k_La increases with OUR	0.15 s^{-1} k_La increases with OUR
RQ - during growth, varies - during induction	0.55 to 0.95 1.0	0.60 to 0.90 1.0	0.53 to 0.92
Growth rate - initial growth - final growth - induction	0.48 hr^{-1} 0.079 hr^{-1} 0.041 hr^{-1}	0.31 hr^{-1} 0.053 hr^{-1} 0.034 hr^{-1}	0.48 hr^{-1} 0.050 hr^{-1} equipment failure
Total growth time	21.3 hrs	18.8 hrs	
% of final growth to total growth	50 %	42 %	
Final biomass - end growth - end induction	22 g L^{-1} 30 g L^{-1}	19 g L^{-1} 31 g L^{-1}	22 g L^{-1} 30 g L^{-1}
Final Fab concentration - Supernatant - Solid	 0.005 mg L^{-1} 0 mg L^{-1}	 0.005 mg L^{-1} 0 mg L^{-1}	 equipment failure

Table 14
The table shows a comparison between Fab PJR run 2, Fab PJR run 3 and Fab PJR run 4 which are three Fab fermentations performed in the 14 L plunging jet bioreactor. For all three runs the plunging jet reactor was operated in an identical manner. As shown in figure 7 the nozzle angle of -5 ° is 5 ° away from the nozzle outlet. These fermentations are shown in figure 28 for Fab PJR run 2, figure 29 for Fab PJR run 3 and figure 30 for Fab PJR run 4.

Figure 27 - Fab PJR Run 1

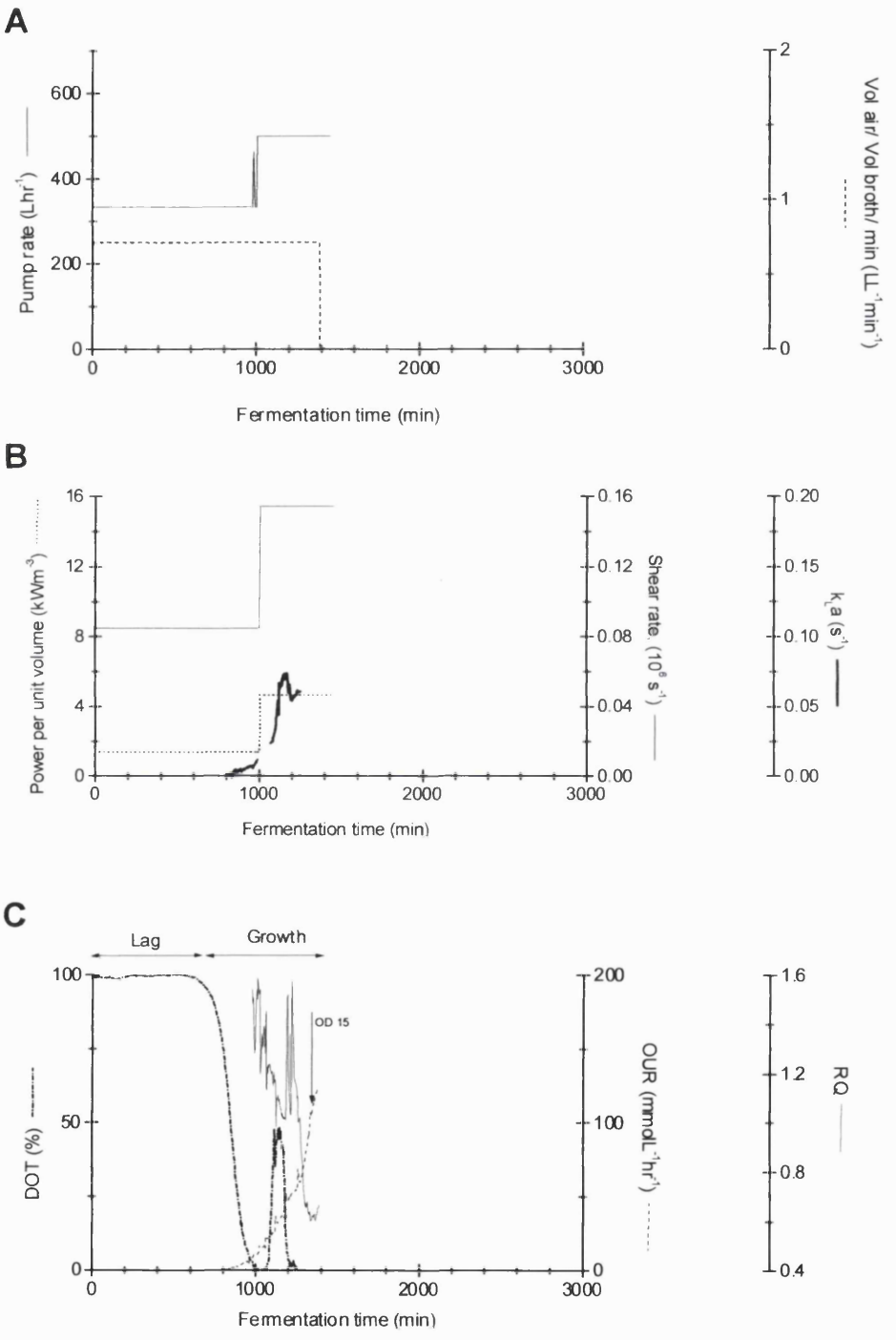

D

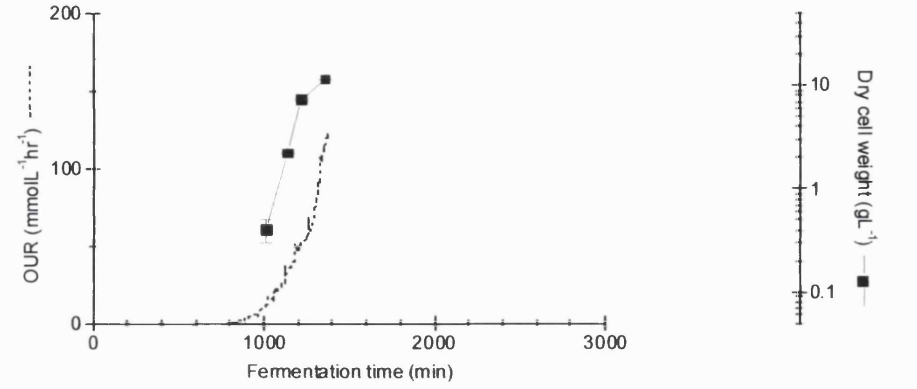
200
100
0
OUR (mmolL-1hr-1)
0
1000
2000
3000
Fermentation time (min)
10
1
0.1
Dry cell weight (gL-1)

E

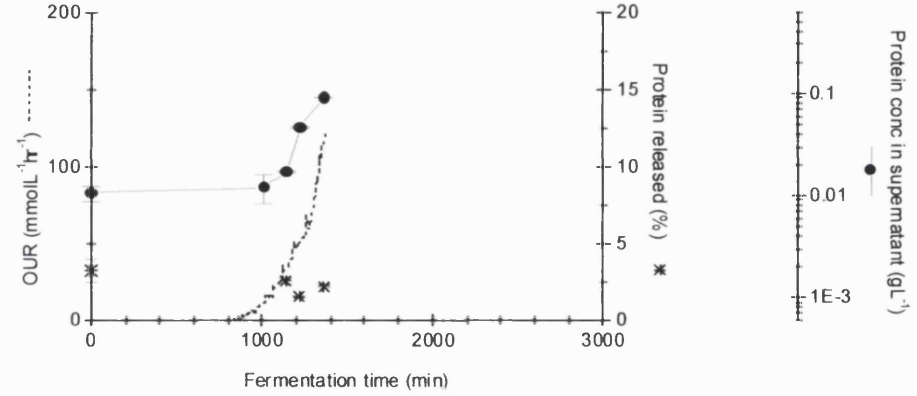
200
100
0
OUR (mmolL-1hr-1)
20
15
10
5
0
Protein released (%)
0
1000
2000
3000
Fermentation time (min)
0.1
0.01
1E-3
Protein conc in supernatant (gL-1)

Figure 27 Fab PJR Run 1 (14 L plunging jet reactor).
The nozzle configuration was a nozzle diameter of 2.4 mm and the nozzle was pointing straight down so that it had a nozzle angle of 0°.
Figures A, B and C show that the oxygen transfer performance of the bioreactor was not sufficient to allow the complete Fab protocol to be performed so that the fermentation was stopped in the growth phase at 1400 minutes.

Figure A shows the operating variables pump flow rate and airflow rate. The pump flow rate was initially fixed at 330 L hr^{-1}. At 1000 minutes the pump flow rate was increased to 500 L hr^{-1} for the remainder of the fermentation.

Figure B shows the calculated values for the Po_{pjr} power per unit volume, k_La and G, shear rate. The power per unit volume and hence the shear rate was initially fixed at 1.4 kW m^{-3} and 80000 s^{-1} respectively. At 1000 minutes the power per unit volume was increased to its maximum of 4.7kW m^{-3} with a shear rate of 150000 s^{-1}. The increase in the power per unit volume at 1000 minutes did not result in an increase in the k_La until 1070 minutes. The k_La then increased from 1070 to 1170 minutes.

Figure C shows how the OUR, DOT and RQ vary between the different fermentation phases. At the beginning of the growth phase the DOT fell sharply to below 5% at 1000 minutes. An increase in the power per unit volume failed to increase the DOT above 0% until 1070 minutes. From 1070 minutes to 1170 minutes both the DOT and the OUR increased to 40% and 40 mmol L^{-1} hr^{-1} respectively; indicating that the oxygen transfer in the bioreactor was increasing. From 1170 minutes the DOT decreased whilst the OUR increased so that at 1250 minutes the OUR and DOT were 54 mmol L^{-1} hr^{-1} and 0% respectively.
From 0 to 840 minutes the OUR and RQ were zero and thus this was the lag phase. At 840 minutes the OUR increased above zero and this was the start of the growth phase. A feed addition of glycerol at an optical density of 15 was made at the fermentation time of 1320 minutes (see arrows on Figure C). For the growth phase the OUR increased whilst the RQ fell from 1.1 at 1100 minutes to 0.6 at 1330 minutes.

Figure D shows a log plot of the resulting dry cell weight plotted with the OUR profile. The growth phase resulted in a final biomass of 11.6 g L^{-1} (optical density of 17). The growth phase had a growth rate of 0.58 hr^{-1} between the fermentation times 1010 minutes and 1360.

Figure E shows the protein concentration in the supernatant both as a log plot and expressed as a percentage of the total protein. The percentage of protein released was measured at 5% for four time intervals across the whole fermentation.

Figure 28 - Fab PJR Run 2

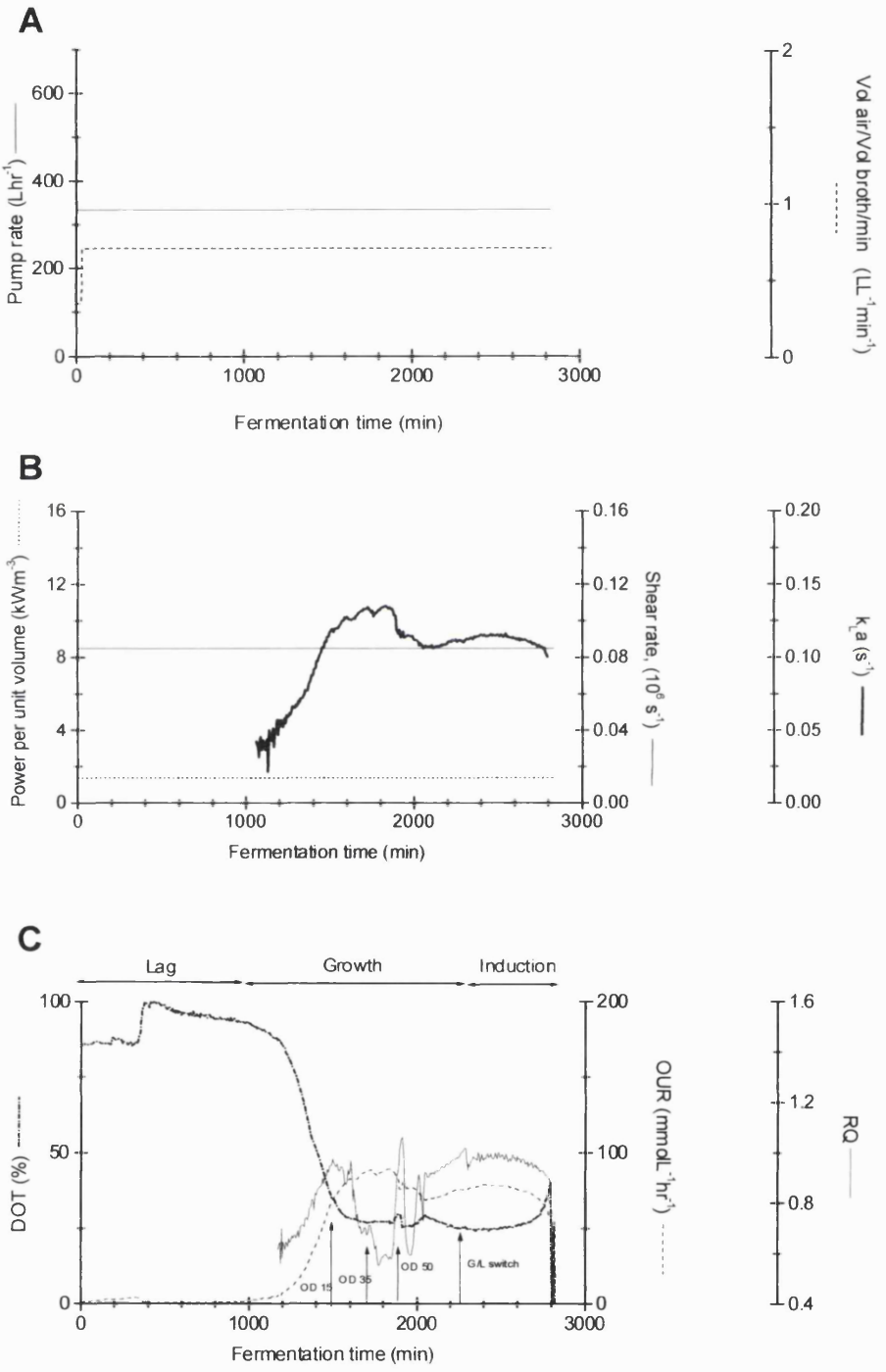

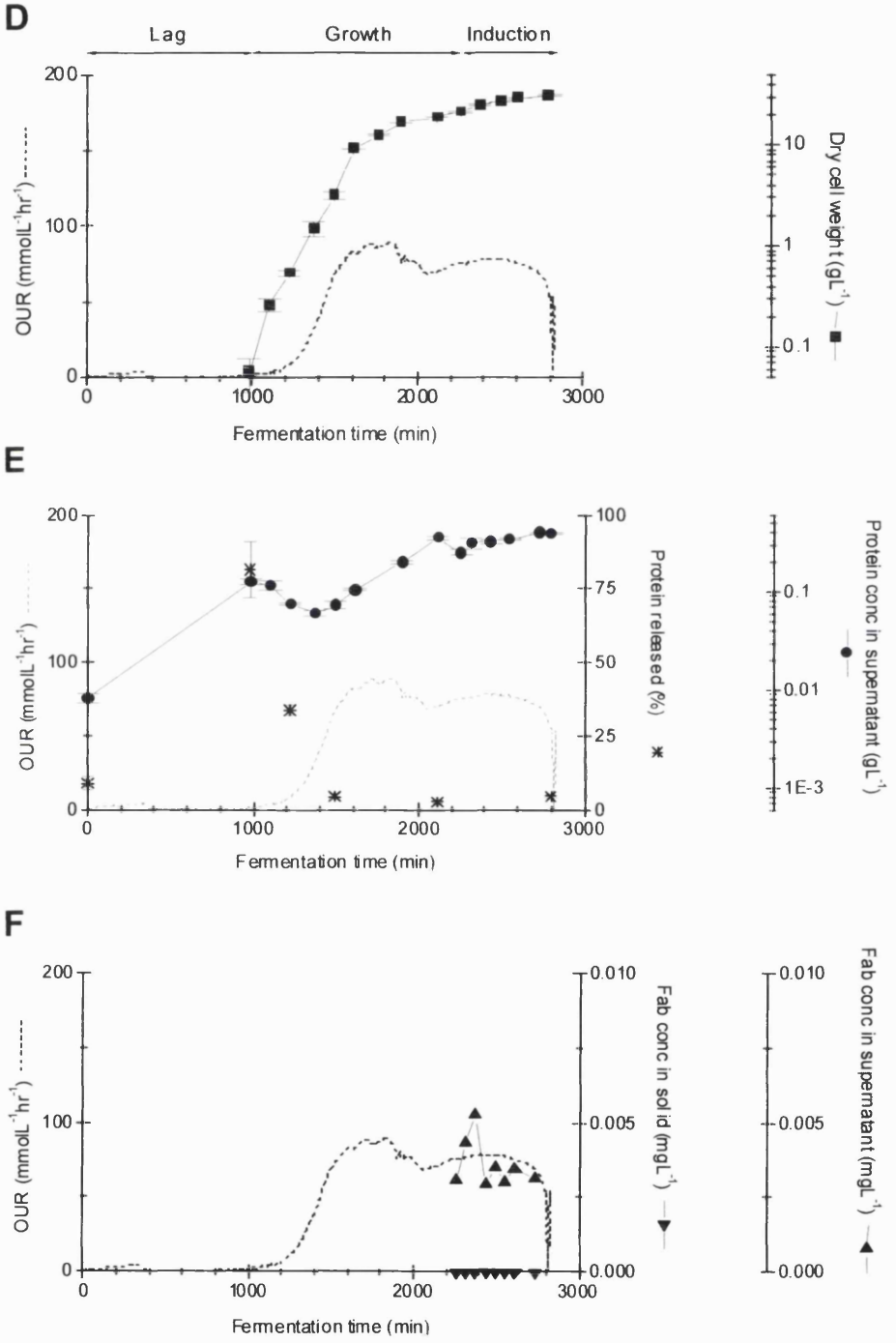
D
Lag
Growth
Induction
OUR (mmolL-1hr-1)
Dry cell weight (gL-1)
Fermentation time (min)
E
OUR (mmolL-1hr-1)
Protein released (%)
Protein conc in supernatant (gL-1)
Fermentation time (min)
F
OUR (mmolL-1hr-1)
Fab conc in solid (mgL-1)
Fab conc in supernatant (mgL-1)
Fermentation time (min)

Figure 28 Fab PJR Run 2 (14 L plunging jet reactor).
The nozzle configuration was a nozzle diameter of 2.4 mm and a nozzle angle of 5 ° away from the outlet. Figure A, B and C show that the oxygen transfer performance of the bioreactor was sufficient to allow the complete Fab protocol to be performed.

Figure A shows the operating variables pump flow rate and airflow rate. The pump flow rate was initially fixed at 330 L hr^{-1} and was not increased further since the DOT did not fall below 20%.

Figure B shows the calculated values for the Po_{pjr} power per unit volume, k_La and G, shear rate. The power per unit volume and hence the shear rate were fixed for the entire fermentation at 1.40 kW m^{-3} and 85000 s^{-1} respectively. A comparison of the k_La with the OUR in figure C shows that the k_La appeared to increase with the OUR. The maximum k_La was 0.13 s^{-1} measured at 1800 minutes when the OUR was at its maximum of 90 mmol L^{-1} hr^{-1}.

Figure C shows how the OUR, DOT and RQ vary between the different fermentation phases. Throughout the fermentation the DOT remained above 20%.
From 0 to 980 minutes the OUR and RQ were zero and thus this was the lag phase. At 980 minutes the OUR increased above zero and this was the start of the growth phase. The transition from the growth to the induction phase occurred at 2255 minutes when the acid switch occurred. Feed additions of glycerol at optical densities of 15, 35 and 50 were at the fermentation times of 1520 minutes, 1730 minutes, and 1895 minutes respectively (see arrows on Figure C).
For the growth phase, the RQ varied between 0.95 and 0.55 where addition of glycerol at 1520 minutes, 1730 minutes and 1895 minutes all coincided with a drastic fall in the RQ value. For the induction phase it remained roughly constant at 1.0.

Figure D shows a log plot of the resulting dry cell weight. The growth and induction phases resulted in a final biomass of 21.5 g L^{-1} (optical density of 60) and 30.1 g L^{-1} (optical density of 90) respectively. The growth phase had a growth rate of 0.48 hr^{-1} between the fermentation times 980 minutes and 1610 minutes and a slower growth rate of 0.079 hr^{-1} between 1610 and 2255 minutes. The growth rate for the induction phase is 0.041 hr^{-1}.

Figure E shows the protein concentration in the supernatant both as a log plot and expressed as a percentage of the total protein. From an initial protein disruption of 8% the protein disruption increased to 80% at the end of the lag phase. The protein disruption then decreased as the growth phase progresses to 4% at 1500 minutes, where it remained at this level for the rest of the fermentation.

Figure F shows the concentration of the product Fab in the supernatant and solid during the induction phase. The concentration of Fab in the supernatant was negligible whilst there was no detectable Fab in the solid phase.

Figure 29 - Fab PJR Run 3

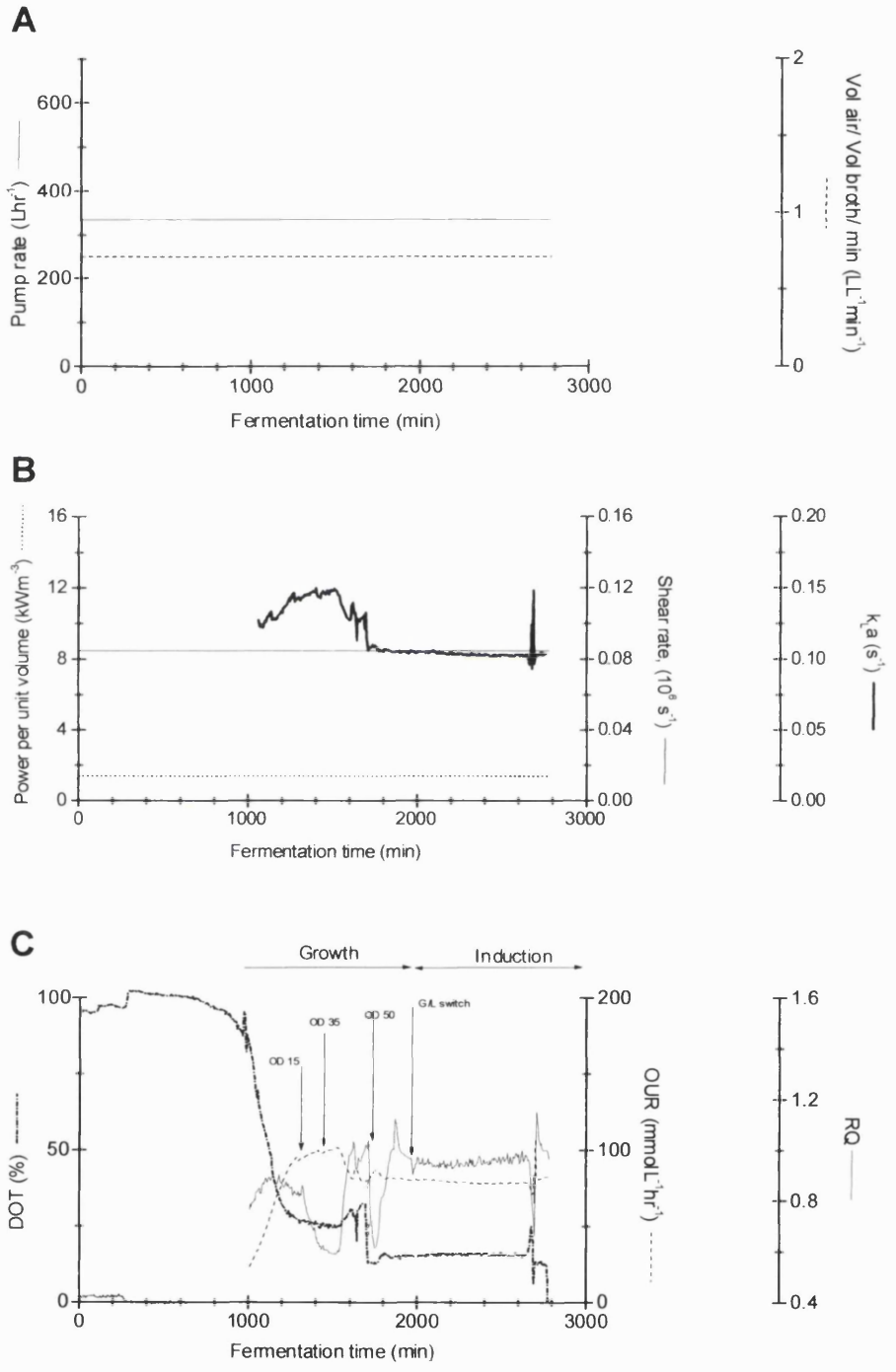

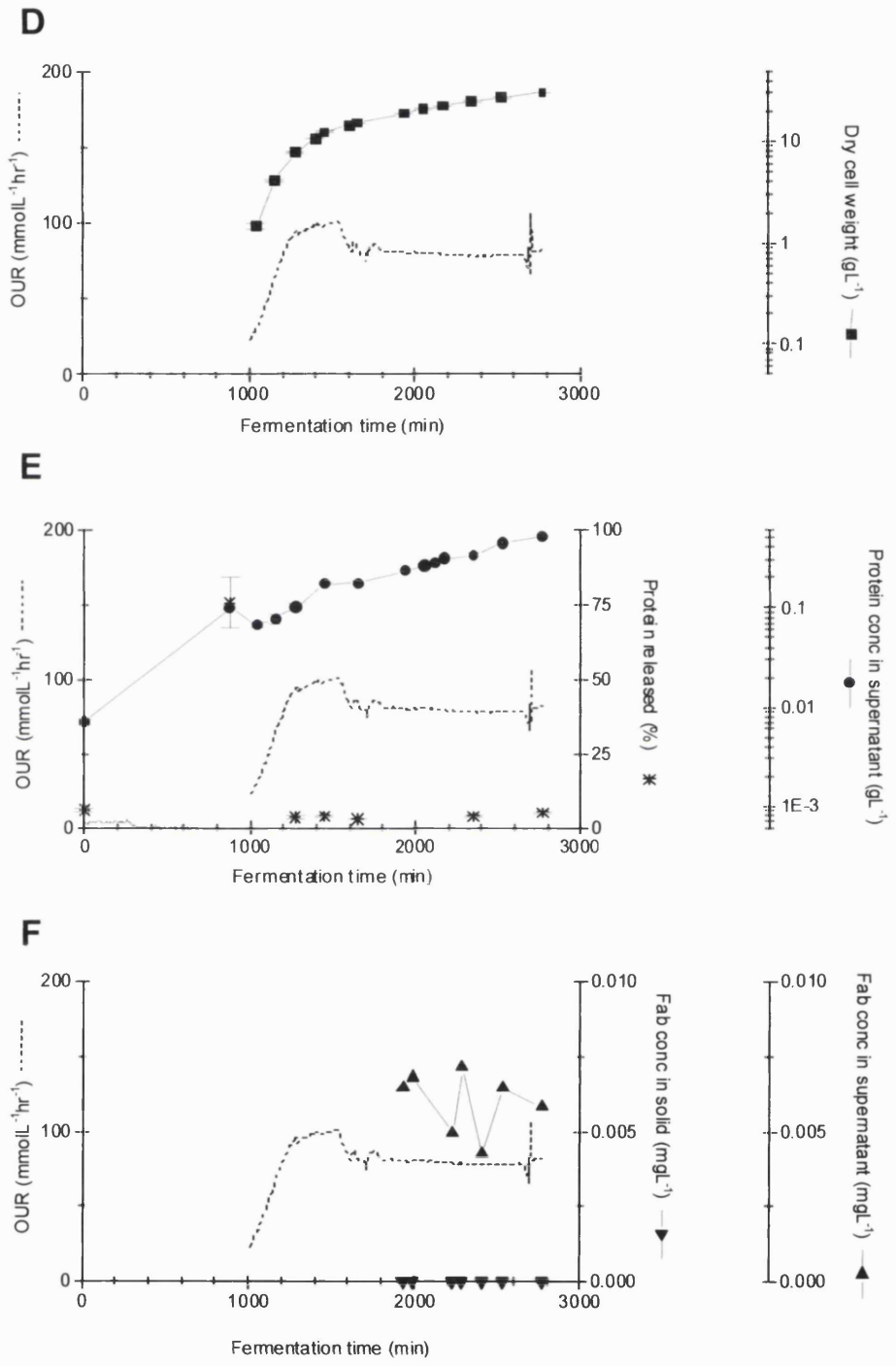
D
OUR (mmolL-1hr-1)
Dry cell weight (gL-1)
Fermentation time (min)
E
OUR (mmolL-1hr-1)
Protein released (%)
Protein conc in supernatant (gL-1)
Fermentation time (min)
F
OUR (mmolL-1hr-1)
Fab conc in solid (mgL-1)
Fab conc in supernatant (mgL-1)
Fermentation time (min)

Figure 29 Fab PJR Run 3 (14 L plunging jet reactor).
The nozzle configuration was a nozzle diameter of 2.4 mm and a nozzle angle of 5 ° away from the outlet. Figure A, B and C show that the oxygen transfer performance of the bioreactor was sufficient to allow the complete Fab protocol to be performed

Figure A shows the operating variables pump flow rate and airflow rate. The pump flow rate was initially fixed at 330 L hr^{-1} and was not increased further since the DOT did not fall below 20%.

Figure B shows the calculated values for the Po_{pjr} power per unit volume, k_La and G, shear rate. The power per unit volume and hence the shear rate were fixed for the entire fermentation at 1.4kW m^{-3} and 85000 s^{-1} respectively. A comparison of the k_La with the OUR in figure C, shows that the k_La appeared to increase with the OUR. The maximum k_La was 0.15 s^{-1} measured at 1500 minutes when the OUR was at its maximum of 100 mmol L^{-1} hr^{-1}.

Figure C shows how the OUR, DOT and RQ vary between the different fermentation phases. Throughout the fermentation the DOT remained above 20%.
Due to a temporary problem with the mass spectrometer there was no gas analysis from 600 minutes to 1000 minutes. From 0 to 600 minutes the OUR and RQ were zero and thus this was the lag phase. From 1000 minutes the OUR increased so that the fermentation was in the growth phase. Thus the switch from the lag to growth phase occurred at some time between 600 to 1000 minutes. The transition from growth to induction occurred at 1930 minutes when the acid switch occurred. Feed additions of glycerol at optical densities of 15, 35 and 50 were at the fermentation times of 1290 minutes, 1425 minutes, and 1700 minutes respectively (see arrows on Figure C).
For the growth phase the RQ varied between 0.90 and 0.60 where addition of glycerol at 1290 minutes and 1700 minutes both coincided with a drastic fall in the RQ value. For the induction phase the RQ remained roughly constant at 1.0.

Figure D shows a log plot of the resulting dry cell weight plotted. The growth and induction phase resulted in a final biomass of 19.0 g L^{-1} (optical density of 51.5) and 30.5 g L^{-1} (optical density of 76.5) respectively. The growth rate for the growth phase was 0.31 hr^{-1} between the fermentation times of 800 minutes and 1450 minutes and 0.053 hr^{-1} between 1450 and 1930 minutes. For the induction phase it was 0.034 hr^{-1}.

Figure E shows the protein concentration in the supernatant both as a log plot and expressed as a percentage of the total protein. The percentage of protein released increased from 6% at time zero to 75% at 880 minutes which is the end of the lag phase. The percentage then decreased to 4% at 1270 minutes, where it remained at this level for the rest of the fermentation.

Figure F shows the concentration of the product Fab in the supernatant and solid during the Fab production phase. The concentration of Fab in the supernatant was negligible whilst there was no detectable Fab in the solid phase.

Figure 30 - Fab PJR Run 4

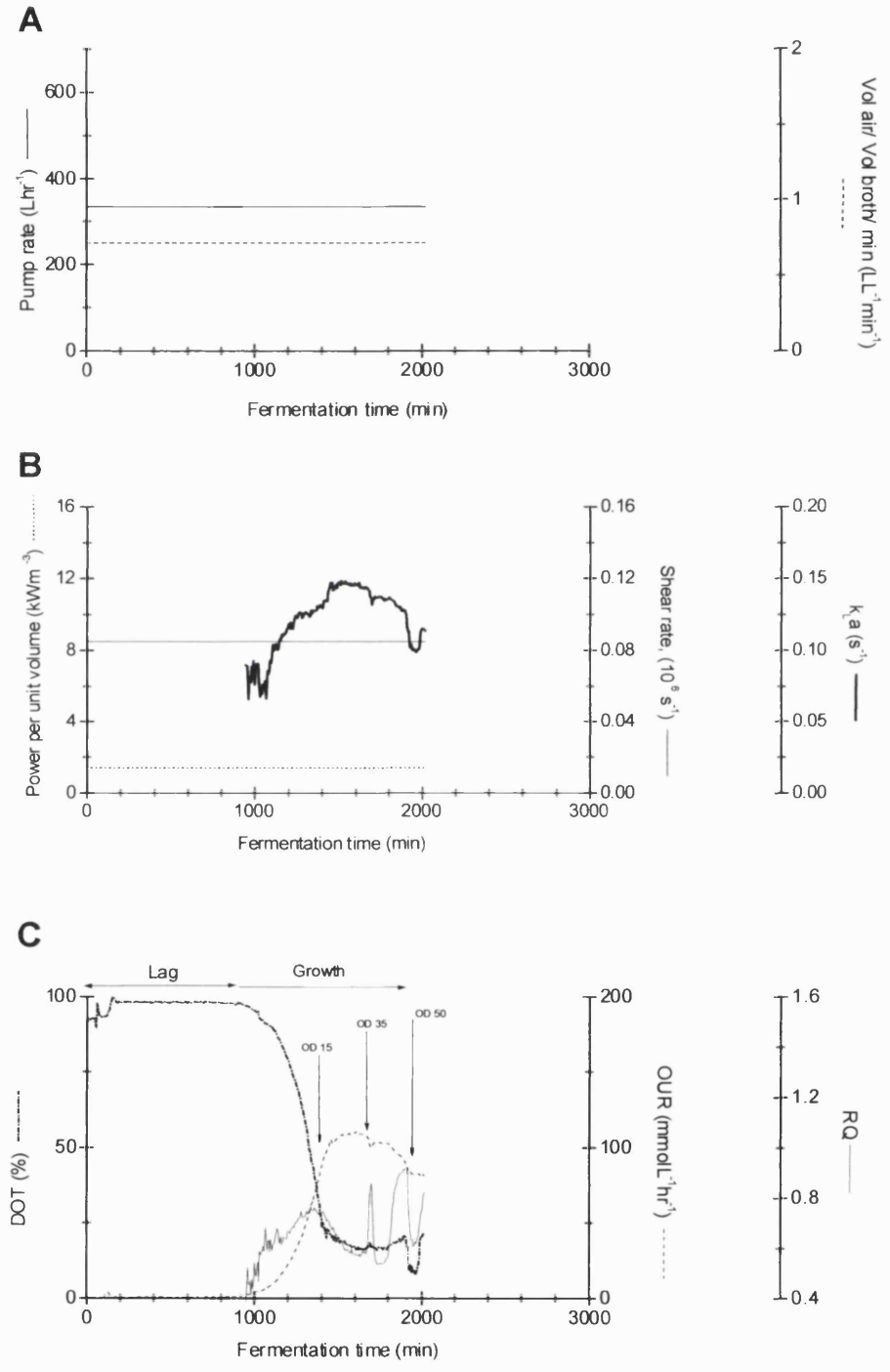

D

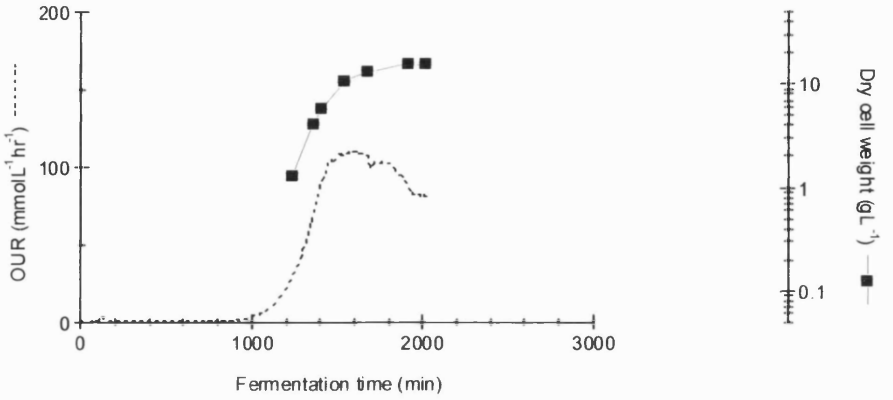
200
100
0
OUR (mmolL-1hr-1) ------
0
1000
2000
3000
Fermentation time (min)
10
1
0.1
Dry cell weight (gL-1)

E

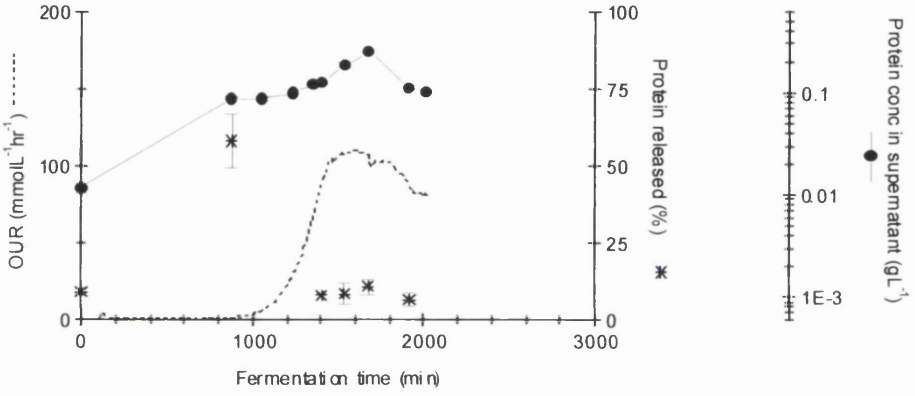
200
100
0
OUR (mmolL-1hr-1) ------
100
75
50
25
0
Protein released (%)
0
1000
2000
3000
Fermentation time (min)
0.1
0.01
1E-3
Protein conc in supernatant (gL-1)

Figure 30 Fab PJR Run 4 (14 L plunging jet reactor).
The nozzle configuration was a nozzle diameter of 2.4 mm and a nozzle angle of 5 ° away from the outlet. Due to an equipment failure this fermentation was terminated at 2000 minutes.

Figure A shows the operating variables pump flow rate and airflow rate. The pump flow rate was initially fixed at 330 L hr^{-1} and was not increased further since the DOT did not fall below 20%.

Figure B shows the calculated values for the Po_{pjr} power per unit volume, k_La and G, shear rate. The power per unit volume and hence the shear rate was fixed for the entire fermentation at 1.40 kW m^{-3} and 85000 s^{-1} respectively. A comparison of the k_La with the OUR in figure C shows that the k_La appeared to increase with the OUR.

Figure C shows how the OUR, DOT and RQ vary between the different fermentation phases. The DOT remained above 20% for the whole fermentation.
From 0 to 850 minutes the OUR and RQ were zero and thus this was the lag phase. At 850 minutes the OUR increased above zero and this was the start of the growth phase. Feed additions of glycerol at optical densities of 15, 35 and 50 were at the fermentation times of 1400 minutes, 1685 minutes, and 1910 minutes respectively (see arrows on Figure C).
For the growth phase the RQ varied between 0.92 and 0.53 where addition of glycerol at 1400 minutes, 1685 minutes and 1910 minutes all coincided with a drastic fall in the RQ value.

Figure D shows a log plot of the resulting dry cell weight plotted. At the end of the fermentation the biomass was 16.0 g L^{-1} (optical density of 42.0). The growth phase has a growth rate of 0.42 hr^{-1} between the fermentation times 1235 minutes and 1535 minutes and a slower growth rate of 0.050 hr^{-1} between 1535 minutes and 2015 minutes.

Figure E shows the protein concentration in the supernatant both as a log plot and expressed as a percentage of the total protein. The percentage of protein released increased from 10% at time 0 to 60% at 880 minutes, which is the end of the lag phase. The percentage then decreased to 8% at 1400 minutes, where it remained at this level for the rest of the fermentation.

6.3 Wild Type fermentations

The Wild Type fermentation is a K12 strain, JM107 that differs from the Fab W3110 since it has a higher intrinsic growth rate and has no product. As with the Fab fermentation for convenience of the results presentation the fermentations are divided into phases. For the Wild Type fermentation these are the lag and growth phase and for some of the fermentations there is an additional second lag phase and second growth phase. The lag phase in which there is no cell growth and the OUR remains at zero, is very short and is quickly followed by the growth phase. During the growth phase, the biomass and thus the OUR increase exponentially, so that the maximum capacity of the bioreactor can be determined. This is achieved by stopping the fermentation when the bioreactor becomes DOT limiting; defined as a DOT of 10% and falling, with the bioreactor operating at its maximum power.

All the fermentations were monitored by continuously measuring the OUR, CER and RQ from the off gas analysis. Periodically the dry cell weight, optical density, concentration of protein in the supernatant and solid fractions were measured from samples removed from the bioreactor.

As with the Fab fermentation the two bioreactors are judged on both their physical performance and the resultant performance of the fermentation. As before the physical performance is a comparison between the oxygen transfer performance of the bioreactor (k_La and comparison between OUR and DOT), the operating variables, (airflow rate, stirrer speed and pump flow rate), the power per unit volume and the shear rate incurred. The resultant performance of the fermentation is the log plot of the dry cell weight, OUR, RQ and the concentration of protein in the supernatant.
For both the STR and PJR the Wild Type fermentations are presented in five graphs which follow the same format as the Fab fermentations. As before a full description of each fermentation is given in the figure legend.

Figure A presents the key operating variables for bioreactor. For both reactors this includes the airflow rate and additionally the stirrer speed and pump flow rate for the STR and the PJR respectively.
Figure B shows the calculated variables power per unit volume, shear rate and k_La.
Figure C shows the RQ, OUR and DOT.
Figure D shows the log plot of both the dry cell weight and the optical density.
Figure E shows the protein concentration in the supernatant both as a log plot and expressed as the percentage of the total protein.
For figures D and E the OUR is also plotted for comparative purposes.

6.3.1 Wild Type fermentations in Stirred tank reactor

Wild Type STR Run 1 and Wild Type STR Run 2 are both Wild Type K12 JM107 fermentations performed in a STR (7L LH fermentor). Both fermentations were run with a 5 L total volume including a 10% inoculum.

All fermentations were monitored with continuous off gas analysis and periodic analysis of off line samples as described in section 4.2.1. The power per unit volume, Po_{str} the shear rate, G and the k_La were all calculated throughout the fermentation using the same equations as used for the Fab STR fermentations in section 6.2.1. The power per unit volume increased with both the air flow rate and the stirrer speed. As before although the STR has a maximum operating speed and airflow rate of 1400 rpm and 8 L min^{-1} respectively; due to foaming in the headspace, the STR may be limited below these levels.

6.3.1.1 Comparison between Wild Type Run 1 and Wild Type Run 2

Wild Type STR run 1 and 2 are shown in figures 31 and 32 (pages 196 to 201) respectively and table 15 (page 195) shows the comparison between the two

fermentations. Both fermentations had characteristic features, which are described as follows.

Physical performance of the bioreactor

As with the Fab fermentations in the STR discussed in section 1.1.1, the k_La was constant at a fixed power whilst it instantly increased as the power increased. For both runs the maximum k_La was measured when the DOT was 10% and the bioreactor was operating at its maximum power per unit volume. The maximum power and k_La for Run 1 was 9.2 kW m^{-3} and 0.16 s^{-1} whilst for Run 2 it was 0.14 s^{-1} and 11.2 kW m^{-3} respectively.

Resultant performance of the fermentation

For Run 1 the OUR increased in an exponential manner to a final OUR of 140 mmol L^{-1} hr^{-1}. For Run 2 the OUR increased in an exponential manner to an OUR of 100 mmol L^{-1} hr^{-1} at 370 minutes. From 370 minutes to 420 minutes when the fermentation was stopped, apart from a short peak, the OUR increased only slightly. For both fermentations the RQ had a mean of 1.0 throughout the fermentation. For the first two hours the growth rate for Run 1 and Run 2 was 1.00 hr^{-1} and 0.87 hr^{-1} respectively. For the remainder of the fermentation the growth rate decreased to 0.66 hr^{-1} for Run 1 and 0.56 hr^{-1} for Run 2. Thus Run 1 had a slightly higher growth rate.

The two fermentations had very similar profiles for the percentage of protein in the supernatant. For both fermentations the percentage of supernatant protein decreased from 20% at 0 minutes to 5% at 120 minutes and then remained below 5% for the rest of the fermentation.

Table 15 - Comparison between STR Wild Type run 1 and STR Wild Type run 2

Parameter	STR Run 1	STR Run 2
Maximum power per unit volume	9.2 kW m^{-3}	11.2 kW m-3
Maximum shear rate incurred	11500 s^{-1}	13000 s^{-1}
Maximum OUR	140 mmol L^{-1} hr^{-1}	100 mmol L^{-1} hr^{-1}
Maximum k_La At fixed power per unit volume	0.16 s^{-1} k_La is fixed	0.14 s^{-1} k_La is fixed
RQ	1.0	1.0
Growth rate - First 2 hours - After 2 hours	1.00 hr^{-1} 0.66 hr^{-1}	0.87 hr^{-1} 0.56 hr^{-1}
Final biomass - end growth - optical density	9.7 g L^{-1} 23	13.0 g L^{-1} 26

Table 15
This table shows a comparison between Wild Type STR run 1 and Wild Type STR run 2, which are two Wild Type fermentations performed with the same 5 L stirred tank bioreactor. These fermentations are shown in figure 31 for Wild Type STR run 1 and figure 32 for Wild Type STR run 2.

Figure 31 - Wild Type STR Run 1

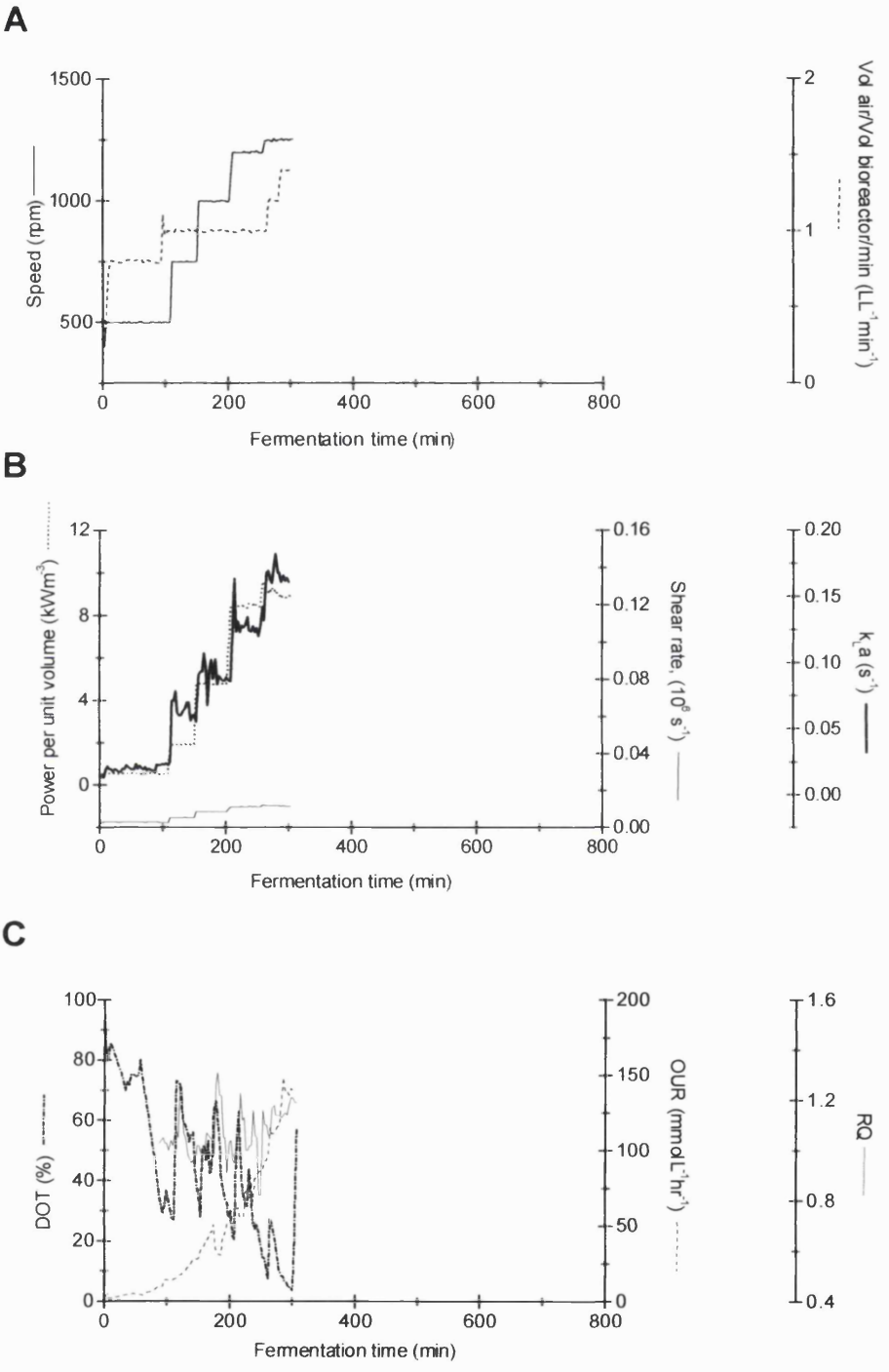

D

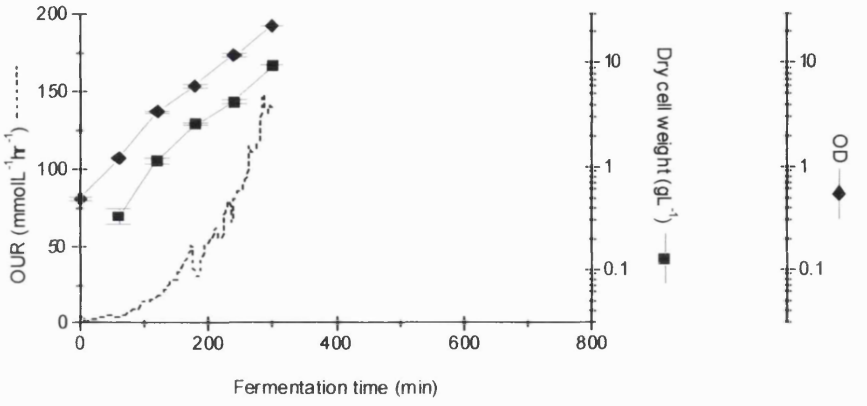
OUR (mmolL-1hr-1)
Dry cell weight (gL-1)
OD
Fermentation time (min)

E

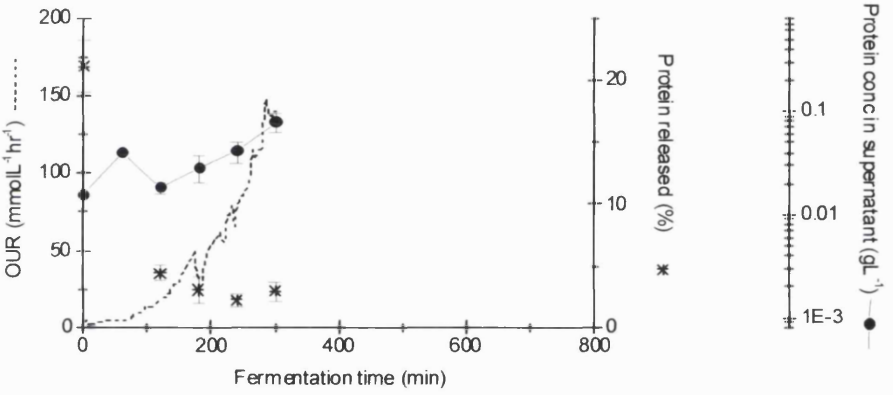
OUR (mmolL-1hr-1)
Protein released (%)
Protein conc in supernatant (gL-1)
Fermentation time (min)

Figure 31 Wild Type STR Run 1 (stirred tank reactor 5 L).
Figure A shows the operating variables speed and airflow rate. Both the speed and airflow rate were increased so that the DOT was maintained above 20%.

Figure B shows the calculated values for the Po_{str} power per unit volume, k_La and G, shear rate. At a fixed power per unit volume, the k_La was constant; where as increasing the power per unit volume resulted in an increase in the k_La measured. The k_La reached a maximum of 0.16 s^{-1} with the bioreactor operating at its maximum power per unit volume and shear rate of 9.2 kW m^{-3} and 11500 s^{-1} respectively.

Figure C shows the OUR, DOT and RQ.
At the start of the fermentation the OUR was above 0 mmol L^{-1} hr^{-1} so that there was no lag phase. The OUR increased in an exponential manner to a final OUR of 140 mmol L^{-1} hr^{-1}. The RQ varied with a mean of 1.0.

Figure D shows a log plot of the dry cell weight and the optical density. For the first two hours the growth rate was 1.00 hr^{-1} which slowed to a growth rate of 0.66 hr^{-1} for the remainder of the fermentation. The final biomass was 9.7 g L^{-1} (optical density of 23).

Figure E shows the concentration of the protein in the supernatant both as a log plot and expressed as a percentage of the total protein. The percentage of protein disrupted decreased from 20% at 0 minutes to 5% at 120 minutes. It then remained below 5% for the rest of the fermentation.

Figure 32 - Wild Type STR Run 2

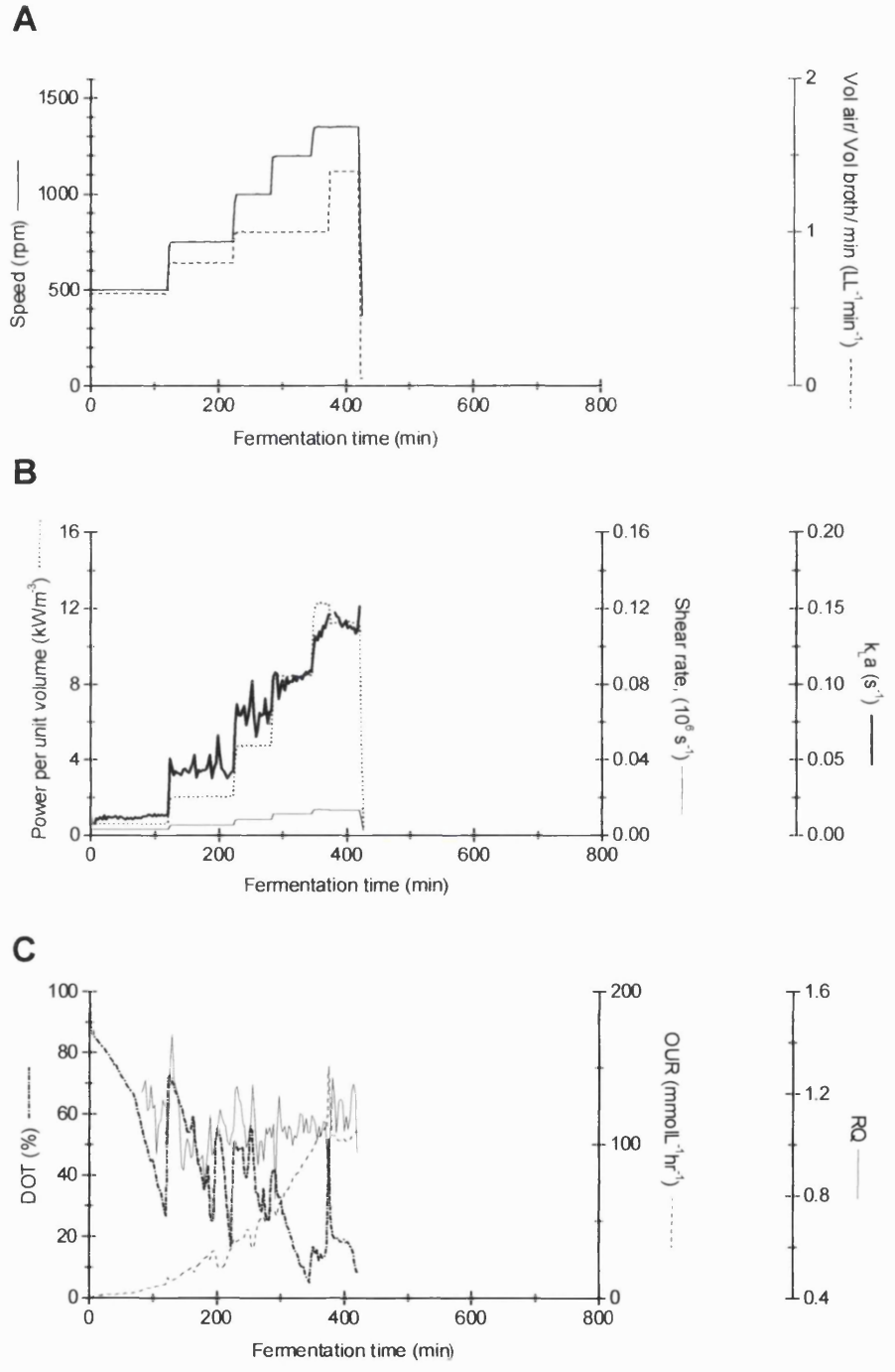

D

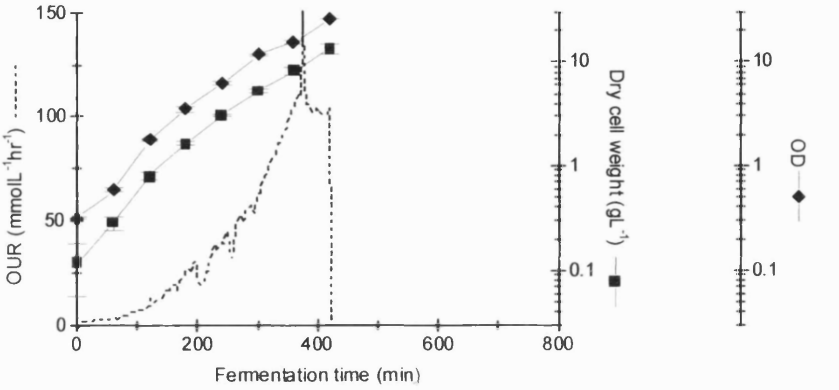
OUR (mmolL-1hr-1) ------
Dry cell weight (gL-1) —■—
OD —◆—
Fermentation time (min)

E

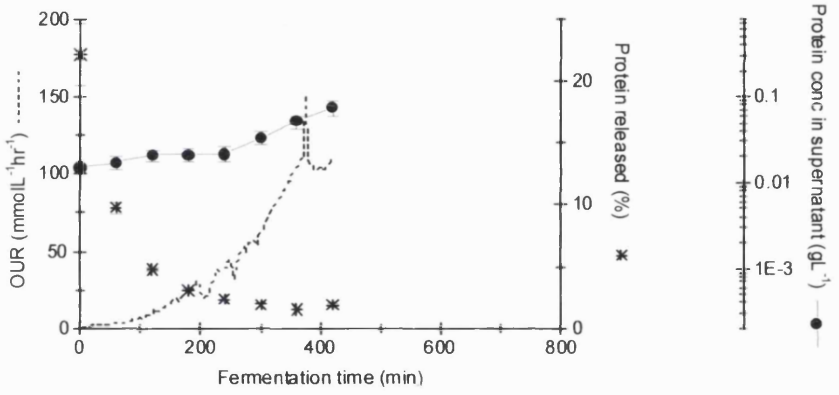
OUR (mmolL-1hr-1) ------
Protein released (%) *
Protein conc in supernatant (gL-1) —●—
Fermentation time (min)

Figure 32 Wild type STR Run 2 (stirred tank reactor 5 L)
Figure A shows the operating variables speed and airflow rate. Both the speed and airflow rate were increased so that the DOT was maintained above 20%.

Figure B shows the calculated values for the Po_{str} power per unit volume, k_La and G, shear rate. At a fixed power per unit volume, the k_La was constant; where as increasing the power per unit volume resulted in an increase in the k_La measured. The k_La reached a maximum of 0.14 s^{-1} with the bioreactor operating at its maximum power per unit volume and shear rate of 11.2 kW m^{-3} and 13000 s^{-1} respectively.

Figure C shows the OUR, DOT and RQ.
The OUR increased above 0 mmol L^{-1} hr^{-1} after 9 minutes so that the lag phase was 0 to 9 minutes and the growth phase was 9 minutes onwards. From 9 to 370 minutes the OUR increased in an exponential manner to a maximum OUR of 100 mmol L^{-1} hr^{-1}. From 370 to 420 minutes when the fermentation was stopped, with the exception of a short spike, there was no significant increase in the OUR. The RQ varied with a mean of 1.0.

Figure D shows a log plot of the dry cell weight and the optical density. For the first two hours the growth rate was 0.87 hr^{-1} which slowed to a growth rate of 0.56 hr^{-1} for the remainder of the fermentation. The final biomass was 13.0 g L^{-1} (optical density of 26).

Figure E shows the concentration of the protein in the supernatant both as a log plot and expressed as a percentage of the total protein. The percentage of protein disruption decreased from 20 % at 0 minutes to 5% at 120 minutes. It then remained significantly below 5% for the rest of the fermentation.

6.3.2 Wild Type fermentations in plunging jet reactor

Wild Type PJR Runs 1 to 4 are all Wild Type fermentations performed in a PJR (14 L Disposable bag). All the fermentations were run with a 14 L total volume including a 10% inoculum. The nozzle configuration differed between runs whilst the height of fall was kept constant.

All the fermentations were monitored with off gas analysis and analysis off line of broth samples as described in section 4.2.1. The power per unit volume, Po_{str}, the shear rate, G and the k_La were all calculated throughout the fermentation using the equations in section 6.2.2. As before the power per unit volume increased with the pump flow rate. The pump flow rate was controlled so that the DOT was maintained above 20%. The airflow rate was maintained at its maximum flow rate of 10 L min^{-1}, so that the mass spectrometer received an adequate off gas sample. The four fermentations, Wild Type PJR runs 1 to 4 are shown in figures 33 to 36 respectively (pages 207 to 218). Table 16, page 205 shows the comparison between Wild Type PJR runs 1 and 2 whilst table 17 page 206 shows the comparison between Wild Type PJR runs 2, 3 and 4.

6.3.2.1 Physical performance of the Wild Type PJR Run 1

Like Fab PJR Run 1, Wild Type PJR Run 1 showed poor oxygen transfer performance. As discussed in section 6.2.2.1 this poor oxygen transfer performance was attributed the nozzle angle so that for Wild Type PJR Run 2 the nozzle angle was moved from 0° to 5° away from the outlet.

6.3.2.2 Comparison between Wild Type PJR Run 2, 3 and 4

Wild Type PJR Run 2 is shown in figure 34, page 210. For this run the plunging jet bioreactor was operated with a nozzle which was 2.4 mm in diameter and with an angle of -5°. The bioreactor was operated with a low level of control, which means that the power per unit volume was initially fixed at a relatively high level of 0.9 kW m^{-3} and was increased periodically by large increments. For PJR Run 2 from 0 to 130 minutes the fermentation was in the first growth phase where the OUR increased in an exponential manner and the optical density increased with a growth rate of 0.88 hr^{-1}. At 130 minutes with the OUR at 14 mmol L^{-1} hr^{-1} and the power per unit volume and shear rate at 1.4 kW m^{-3} and 85000 s^{-1} respectively; cell lysis occurred. This was indicated by a simultaneous increase in the percentage of the protein in the supernatant, a decrease in both the OUR and optical density and significant foam production. Shear was identified as a possible reason for the cell lysis. Thus for successive fermentations the calculated shear rate was reduced.

Wild Type PJR run 3 is shown in figure 35, page 213. For this run the same nozzle configuration was used as Wild Type PJR run 2 but the power per unit volume was controlled so that it was at its minimum and thus is called 'a high level' of control. This was done by starting the fermentation with the power per unit volume at its lowest setting of 0.02 kW m^{-3} and increasing it by small increments each time the DOT fell into the 20 to 30% range. For Run 3 from 0 to 80 minutes the fermentation was in the growth phase where the OUR increased in an exponential manner and the optical density increased with a growth rate of 0.44 hr^{-1}. At 80 minutes with the OUR at 5 mmol L^{-1} hr^{-1} and the power

per unit volume and shear rate at 0.027 kW m^{-3} and 11870 s^{-1} respectively; cell lysis occurred. As before this was indicated by a simultaneous increase in the percentage of the protein in the supernatant, a decrease in both the OUR and optical density and significant foam production.

Wild Type PJR run 4 is shown in figure 36, page 216. For this run the shear rate was reduced further by using the largest nozzle diameter of 4.0 mm, at the same height of fall and angle as used in Run 2 and 3. Figure 37 A, page 219 shows that for any nozzle with a nozzle diameter between 2.4 and 4.0 mm, operating at an equivalent power and volume, the k_La will be equivalent. Figures 37 A and 37 C show that increasing the nozzle diameter from 2.4 to 4.0 mm results in a lower shear rate for a given power. As with Run 3 the power per unit volume was controlled so that it was always at its lowest possible level. For this run the cell growth occurred from 0 to 140 minutes where the OUR increased in an exponential manner to 17 mmol L^{-1} hr^{-1} and the optical density increased with a growth rate of 0.78 hr^{-1}. At 140 minutes with the OUR, power per unit volume and shear rate at 17 mmol L^{-1} hr^{-1}, 0.31 kW m^{-3} and 18650 s^{-1} respectively; cell lysis occurred. This was indicated by the same change of factors as in Runs 2 and 3. It is noteworthy that lysis occurred at a higher shear rate of 85000 s^{-1} in Run 2 than in either Run 3 or 4 where the shear rate was 11870 s^{-1} and 18650 s^{-1} respectively.

Table 16 - Comparison between Wild Type PJR Run 1 and Wild Type PJR Run 2

Parameter	PJR Run 1	PJR Run 2
Nozzle angle	0°	-5°
Maximum power per unit volume	4.7 kW m^{-3}	1.4 kW m^{-3}
Maximum OUR for 2nd growth with DOT 25%	10 mmol L^{-1} hr^{-1}	50 mmol L^{-1} hr^{-1}
Fermentation time lysis occurred	1.8 hours	2.2 hours
Power per unit volume at which lysis occurred	1.4 kW m^{-3}	1.4 kW m^{-3}
Shear rate at which lysis occurred	85000 s^{-1}	85000 s^{-1}
OUR at which lysis occurred	3 mmol L^{-1} hr^{-1}	14 mmol L^{-1} hr^{-1}
Growth rate – First 2 hours	0.38 hr^{-1}	0.88 hr^{-1}
Final Optical density prior to lysis	0.33	1.2

Table 16
The table shows a comparison between Wild Type PJR run 1 and Wild Type PJR run 2, which are two Wild Type fermentations performed in the 14 L plunging jet bioreactor. The table shows the effect of moving the nozzle angle form 0° for Wild Type PJR run 1 to an angle of -5° for the wild PJR Run 2. As shown in figure 7 the nozzle angle of 0° is vertical and -5° is 5° away from the nozzle outlet. These fermentations are shown in figure 33 for Wild Type PJR run 1 and figure 34 for Wild Type PJR run 2.

Table 17 – Comparison between Wild Type PJR Run 2, Wild Type PJR Run 3 and Wild Type PJR Run 4

Parameter	PJR Run 2	PJR Run 3	PJR Run 4
Nozzle angle	-5°	-5°	-5°
Nozzle diameter	2.4 mm	2.4 mm	4.0 mm
Method of operation - Level of control of power per unit volume	Low level of control	High level of control	High level of control
Fermentation time lysis occurred	2.2 hours	1.3 hours	2.3 hours
Power per unit volume at which lysis occurred	1.4 kW m^{-3}	0.027 kW m^{-3}	0.31 kW m^{-3}
Shear rate at which lysis occurred	85000 s^{-1}	11870 s^{-1}	18650 s^{-1}
OUR at which lysis occurred	14 mmol L^{-1} hr^{-1}	5 mmol L^{-1} hr^{-1}	17 mmol L^{-1} hr^{-1}
Growth rate – First 2 hours	0.88 hr^{-1}	0.44 hr^{-1}	0.78 hr^{-1}
Biomass, Final Optical density -prior to lysis	1.2	0.7	2.3

Table 17
The table shows a comparison between Wild Type PJR run 2, Wild Type PJR run 3 and Wild Type PJR run 4 which are three Wild Type fermentations performed in the 14 L plunging jet bioreactor. For PJR Run 2 the plunging jet bioreactor was operated with a low level of control of the power per unit volume. This means that the initial power per unit volume of 0.9 kW m^{-3} was at a relatively high value and was increased periodically by large increments. For PJR Run 3 and 4 the plunging jet bioreactor was operated with a high level of control of the power per unit volume. This means that the initial power per unit volume of 0.02 kW m^{-3} for both Runs 3 and 4 was at a relatively low value and was increased by small increments to maintain the DOT above 20%. Thus for runs 3 and 4 the plunging jet reactor was operated at the lowest power per unit volume possible in order to maintain the shear rate at its lowest value. Whilst for PJR run 2 and 3 a 2.4 mm nozzle was used, for PJR run 4 a 4.0 mm nozzle diameter was used so that the shear rate incurred was reduced further. As shown in figure 7 the nozzle angle of -5° is 5° away from the nozzle outlet. These fermentations are shown in figure 34 for Wild Type PJR run 2, figure 35 for Wild Type PJR run 3 and figure 36 for Wild Type PJR run 4.

Figure 33 - Wild Type PJR Run 1

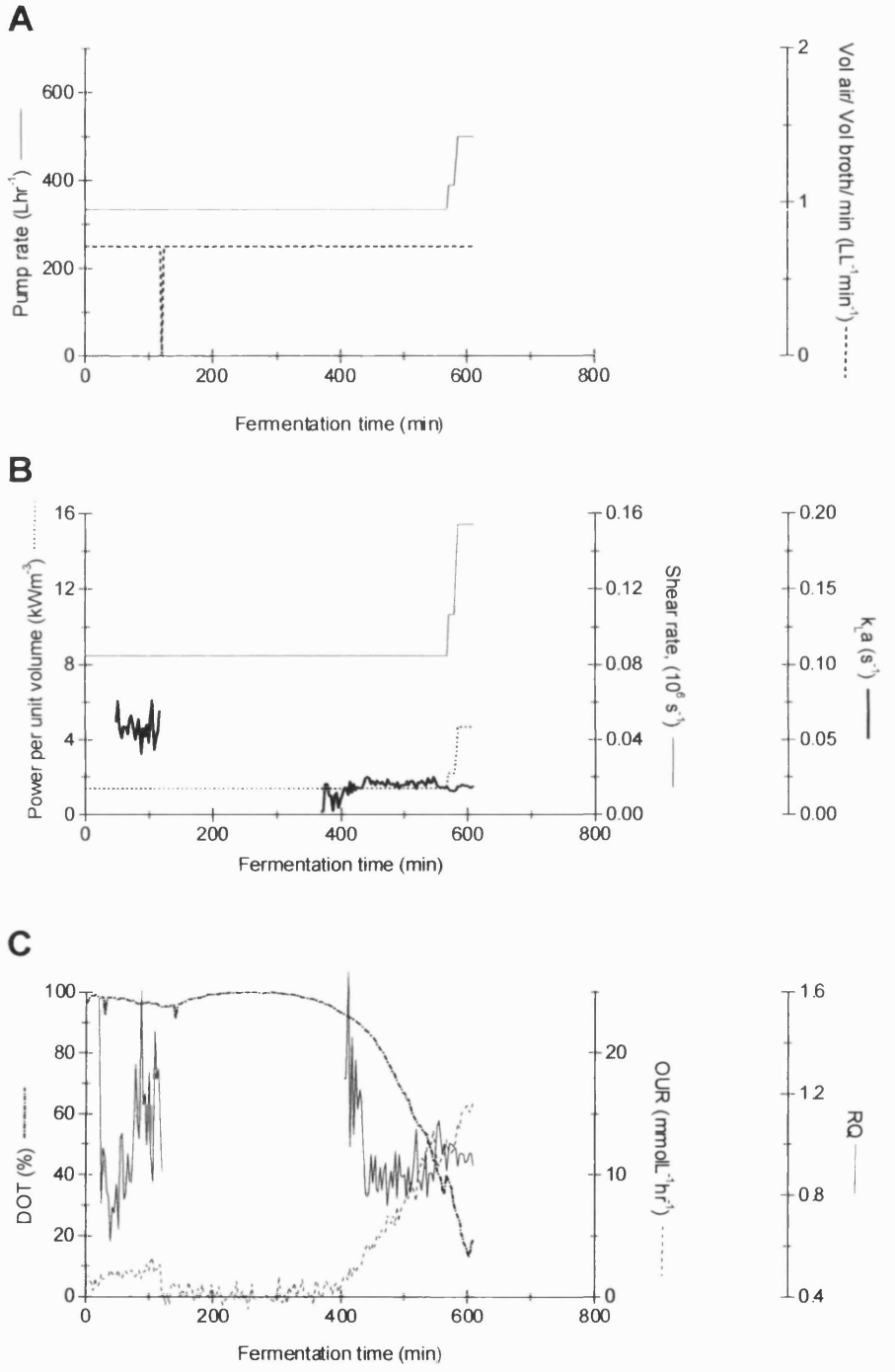

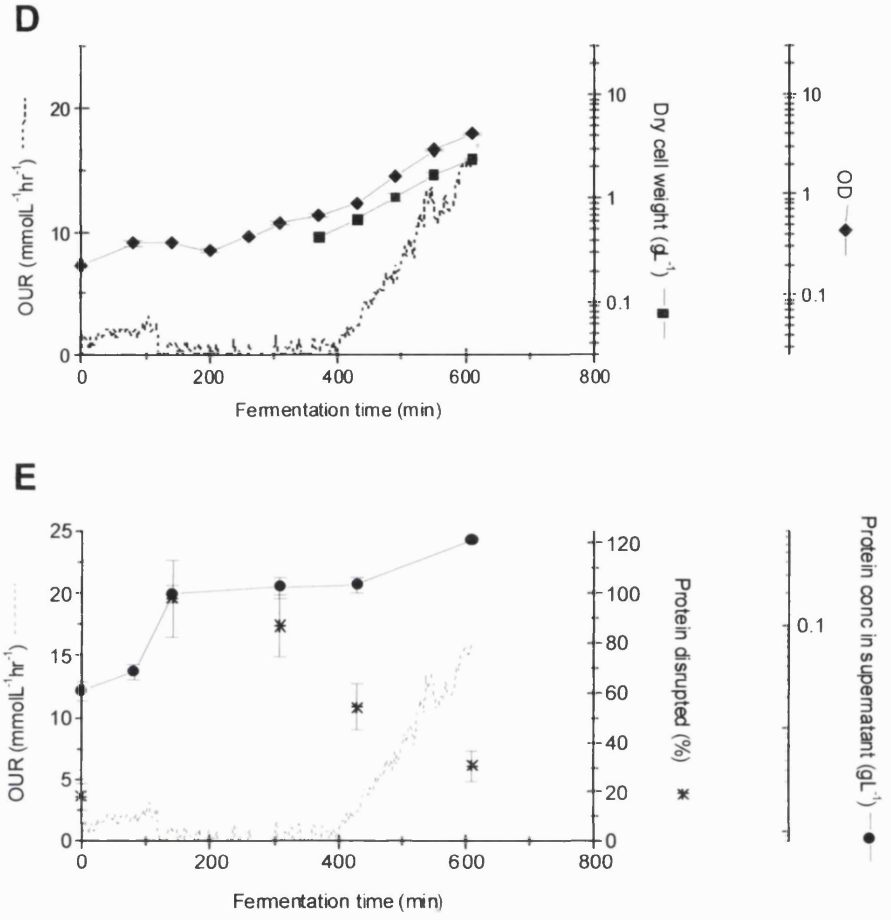
D
OUR (mmolL-1hr-1)
Dry cell weight (gL-1)
OD
Fermentation time (min)
E
OUR (mmolL-1hr-1)
Protein disrupted (%)
Protein conc in supernatant (gL-1)
Fermentation time (min)

Figure 33 Wild Type PJR Run 1(plunging jet reactor 14 L).
The nozzle configuration was a nozzle diameter of 2.4 mm and a nozzle angle of 0°.

Figure A shows the operating variables pump flow rate and airflow rate. The pump flow rate was initially fixed at 330 L hr^{-1}. At the end of the fermentation this was increased to 500 L hr^{-1} due to the DOT decreasing to 20%.

Figure B shows the calculated values for the Po_{str} power per unit volume, k_La and G, shear rate. The power per unit volume and shear rate incurred were initially fixed at 1.40 kW m^{-3} and 85000 s^{-1}. At the end of the fermentation this was increased to 4.7 kW m^{-3} and 155000 s^{-1} respectively. The two growth phases were not sufficient to produce reliable k_La data.

Figure C shows the OUR, DOT and RQ
At the start of the fermentation the OUR was above zero so that there was no lag phase. For the first 110 minutes the OUR increased in an exponential manner so that the fermentation was in the growth phase. From 110 minutes the OUR decreased to nearly 0 mmol L^{-1} hr^{-1} where it remained until 400 minutes. Thus cell death occurred where the fermentation was in a second lag phase from 130 to 400 minutes. From 400 minutes onwards the OUR increased in an exponential manner so that this was a second growth phase.
The first growth phase was too short to produce reliable RQ data. From 420 minutes onwards the RQ was approximately 0.9.

Figure D shows a log plot of the dry cell weight and the optical density.
For the first 110 minutes the growth rate was 0.38 hr^{-1} after which there was no growth until 400 minutes. The growth rate from 430 to 610 minutes was 0.54 hr^{-1}.

Figure E shows the concentration of the protein in the supernatant both as a log plot and expressed as a percentage of the total protein. At the onset of the second lag phase at 130 minutes the percentage of protein disruption increased from 20% at 0 minutes to 100% at 140 minutes. During the second growth phase the percentage of protein released decreased from 55% at 430 minutes to 30% at 610 minutes.

Figure 34 - Wild Type PJR Run 2

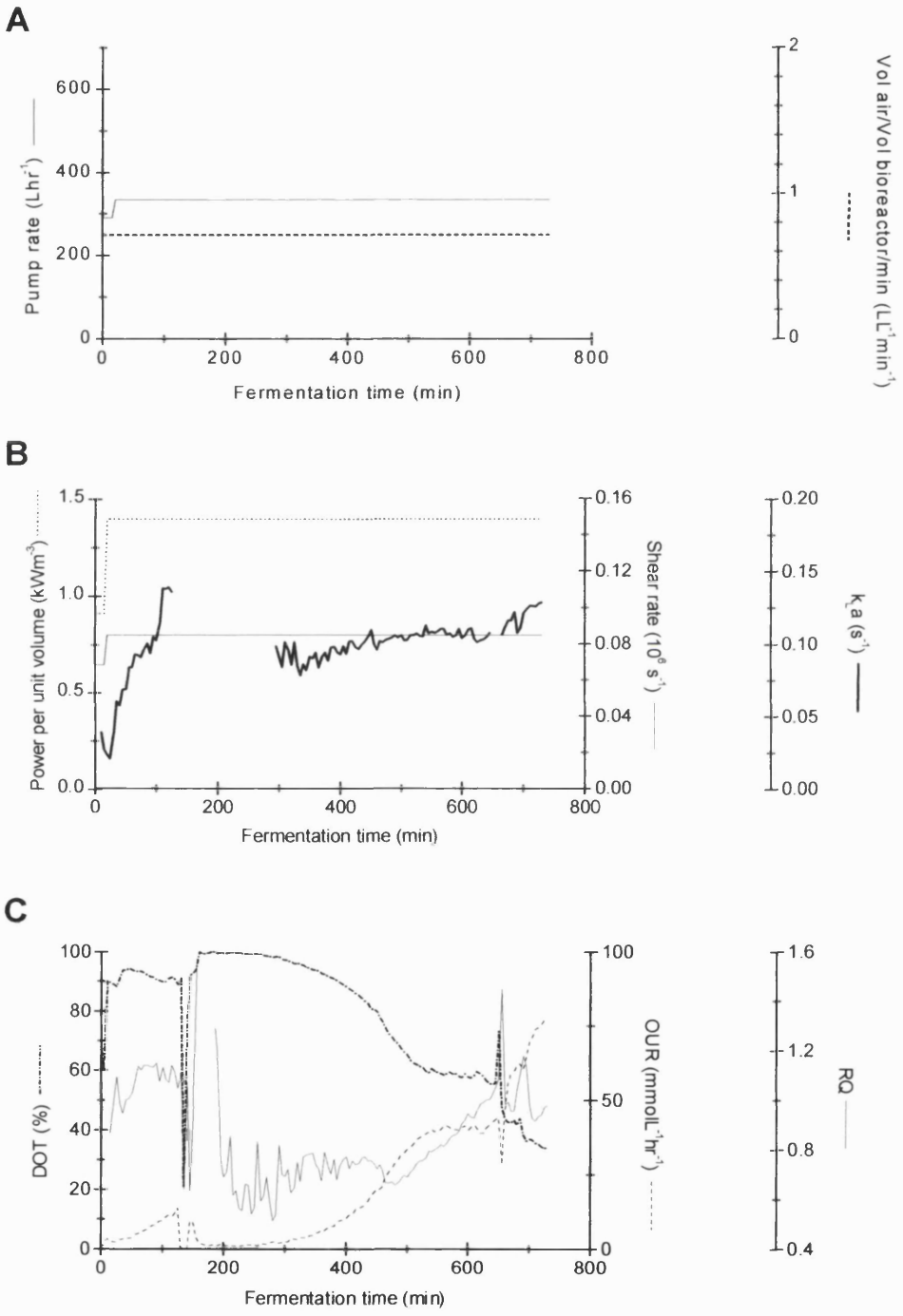

D

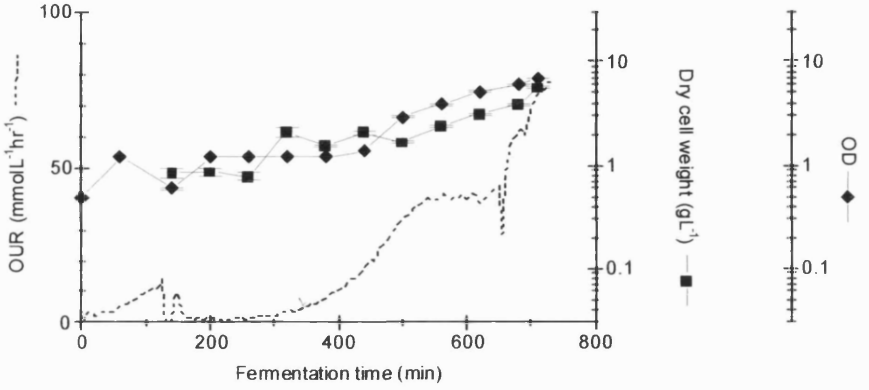
OUR (mmolL-1hr-1) ------
Dry cell weight (gL-1)
OD
Fermentation time (min)

E

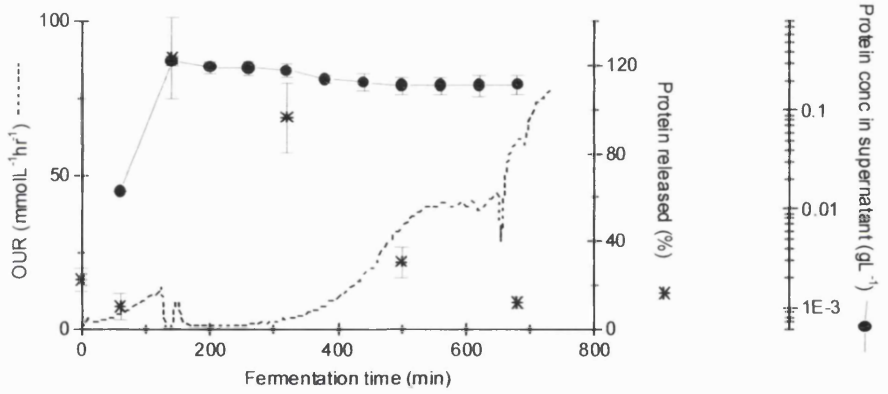
OUR (mmolL-1hr-1) ------
Protein released (%)
Protein conc in supernatant (gL-1)
Fermentation time (min)

Figure 34 Wild Type PJR Run 2 (plunging jet reactor 14 L).
The nozzle configuration was a nozzle diameter of 2.4 mm and a nozzle angle of 5 ° away from the outlet.

Figure A shows the operating variables pump flow rate and airflow rate. The pump flow rate was initially fixed at 290 L hr^{-1} but then quickly increased to 330 L hr^{-1} where it remained for the entire fermentation since the DOT did not fall below 20%.

Figure B shows the calculated values for the Po_{str} power per unit volume, k_La and G, shear rate. From 300 to 700 minutes the power per unit volume was fixed at 1.4 kW m^{-3} and results in a k_La which rose slightly from 0.08 to 0.13 s^{-1}. The shear rate increased with the power so that it was initially 68500 s^{-1} but quickly increased to 85000 s^{-1}.

Figure C shows the OUR, DOT and RQ.
At the start of the fermentation the OUR was above 0 mmol L^{-1} hr^{-1} so that there was no lag phase. For the first 130 minutes the OUR increased in an exponential manner so that the fermentation was in the growth phase. From 130 minutes the OUR decreased to nearly zero where it remains until 300 minutes. Thus cell death occurred where the fermentation was in a second lag phase from 130 to 300 minutes. From 300 minutes onwards the OUR increased in a exponential manner until 500 minutes, where the OUR remained roughly constant before increasing again from 650 minutes onwards. The increase in the OUR from 300 to 700 minutes was a second growth phase.
From 50 to 130 minutes the RQ remained roughly constant at 1.1. From the start of the second growth period at 300 minutes to 475 minutes the RQ was 0.8. From 475 to 650 minutes the RQ increased from 0.8 to 1.0.

Figure D shows a log plot of the, dry cell weight and the optical density, which is a measure of the bacterial cell concentration. For the first 60 minutes the optical density increased with a growth rate of 0.88 hr^{-1}. From 60 to 260 minutes neither the optical density nor the dry cell weight increased. From 440 minutes both the optical density and dry cell weight increased, where the growth rate from 440 to 710 minutes was 0.36 hr^{-1}.

Figure E shows the concentration of the protein in the supernatant both as a log plot and expressed as a percentage of the total protein. At the onset of the second lag phase at 130 minutes the percentage of protein disruption increased from 20% at 0 minutes to 120% at 140 minutes. During the second growth phase the percentage of protein released decreased from 100% at 300 minutes to 12% at 700 minutes.

Figure 35 - Wild Type PJR Run 3

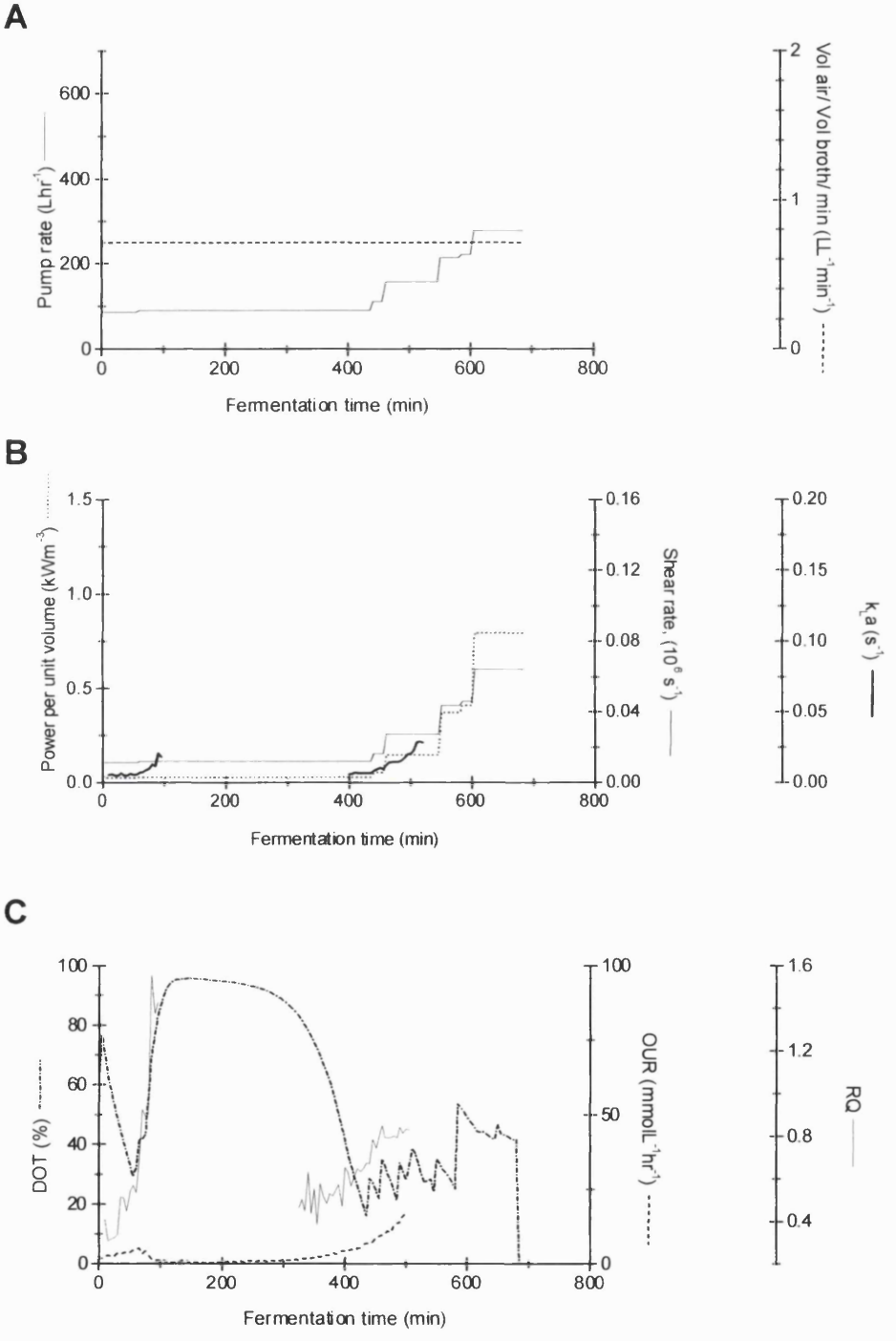

D

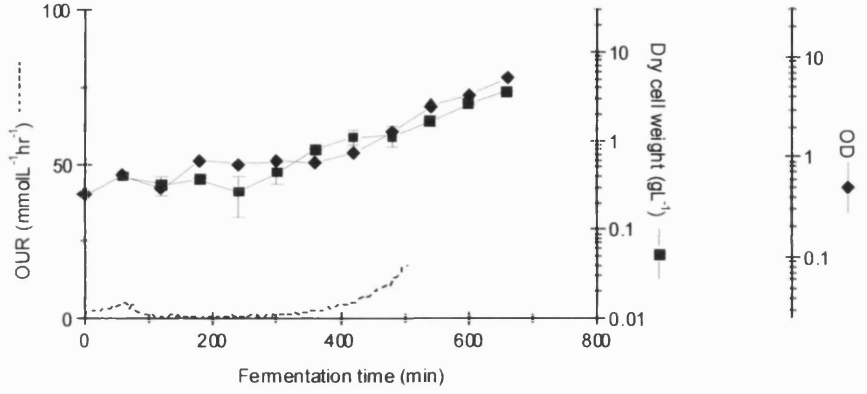
OUR (mmolL-1hr-1)
Dry cell weight (gL-1)
OD
Fermentation time (min)

E

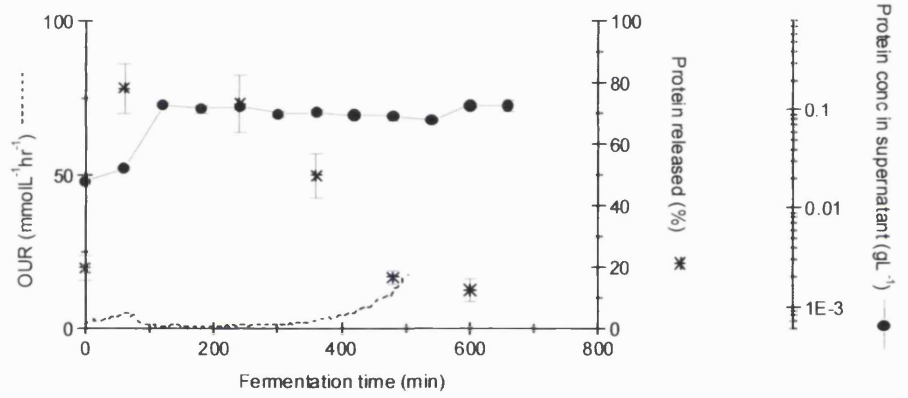
OUR (mmolL-1hr-1)
Protein released (%)
Protein conc in supernatant (gL-1)
Fermentation time (min)

Figure 35 Wild Type PJR Run 3 (plunging jet reactor 14 L).
The nozzle configuration was a nozzle diameter of 2.4 mm and a nozzle angle of 5° away from the outlet. The mass spectrometer failed at 500 minutes so that there is no OUR, RQ or k_La data from 500 minutes onwards.

Figure A shows the operating variables pump flow rate and airflow rate. The pump flow rate was initially fixed at the lowest possible flow rate and then increased each time the DOT fell into the 20 to 30% range.

Figure B shows the calculated values for the Po_{str} power per unit volume, k_La and G, shear rate. The two growth phases were not sufficient to produce reliable k_La data.

Figure C shows the OUR, DOT and RQ.
At the start of the fermentation the OUR was above 0 mmol L^{-1} hr^{-1} so that there was no lag phase. For the first 80 minutes the OUR increased in an exponential manner so that the fermentation was in the growth phase. From 80 minutes the OUR decreased to nearly 0 mmol L^{-1} hr^{-1} where it remained until 300 minutes. Thus cell death occurred where the fermentation was in a second lag phase from 80 to 300 minutes. From 300 to 500 minutes when the mass spectrometer failed, the OUR increased in a exponential manner. The first and second growth phase were too short to produce reliable RQ data

Figure D shows a log plot of the OUR, dry cell weight and the optical density which is a measure of the bacterial cell concentration. For the first 60 minutes the optical density increased with a growth rate of 0.44 hr^{-1}. From 60 to 300 minutes neither the optical density nor the dry cell weight increased significantly. From 420 minutes both the optical density and dry cell weight were increasing significantly, where the growth rate from 420 to 660 minutes was 0.43 hr^{-1}.

Figure E shows the concentration of the protein in the supernatant both as a log plot and expressed as a percentage of the total protein. The percentage of protein disrupted increased from 20% at 0 minutes to 80% at 60 minutes. During the second growth phase the percentage of protein released decreased from 50% at 360 minutes to 12% at 600 minutes.

Figure 36 - Wild Type PJR Run 4

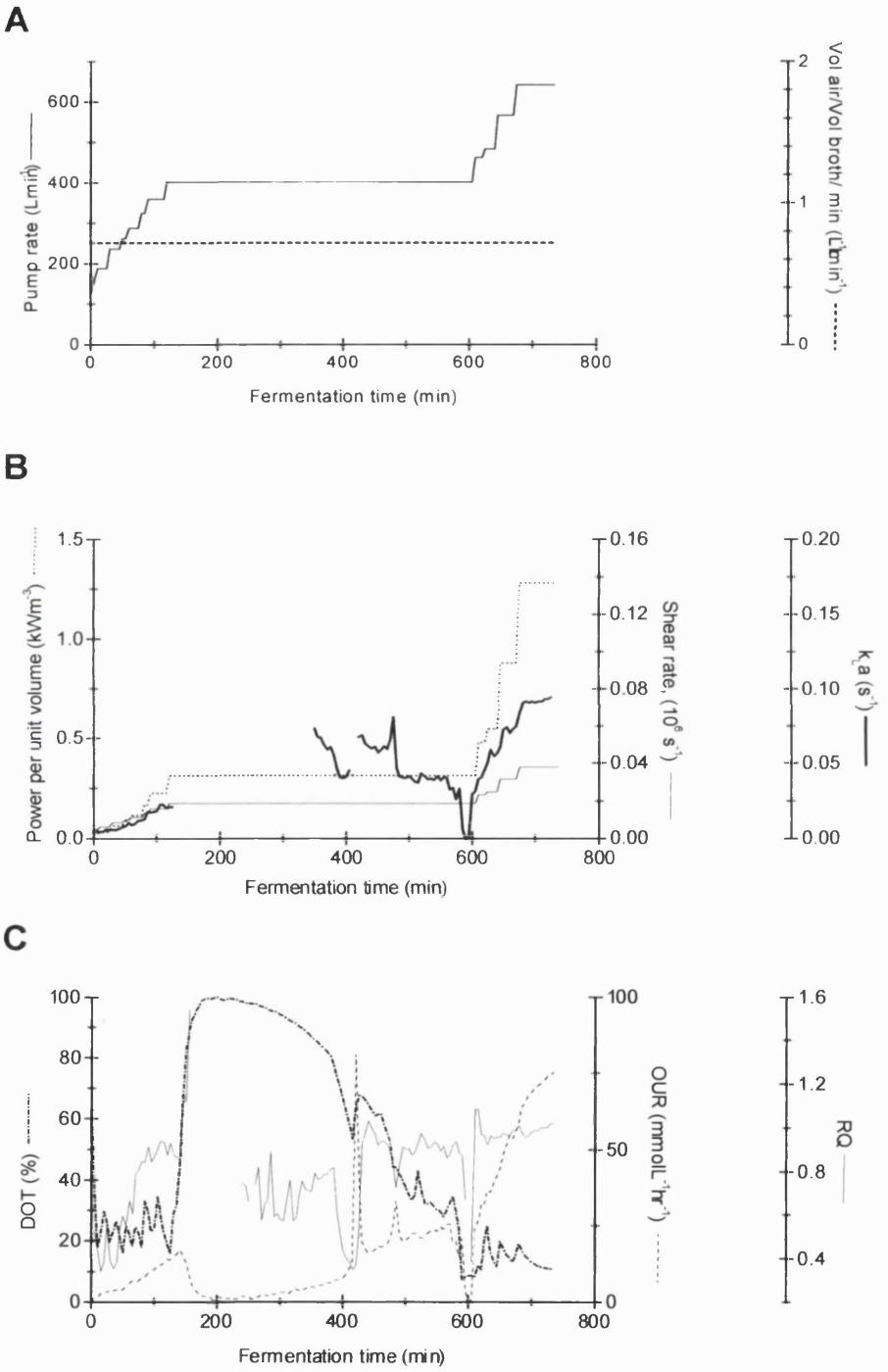

D

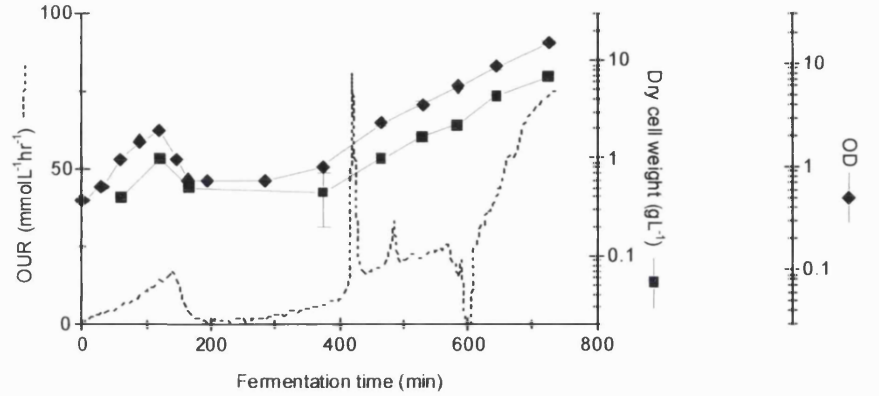
100
50
0
OUR (mmolL-1hr-1)
0
200
400
600
800
Fermentation time (min)
10
1
0.1
Dry cell weight (gL-1)
10
1
0.1
OD

E

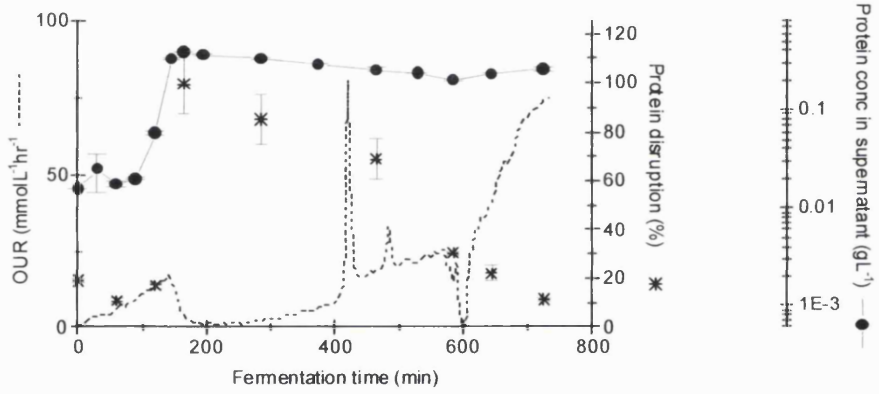
100
50
0
OUR (mmolL-1hr-1)
0
200
400
600
800
Fermentation time (min)
120
100
80
60
40
20
0
Protein disruption (%)
0.1
0.01
1E-3
Protein conc in supernatant (gL-1)

Figure 36 Wild Type PJR Run 4 (plunging jet reactor 14 L).
The nozzle configuration was a nozzle diameter of 4.0 mm and a nozzle angle of 5° away from the outlet.

Figure A shows the operating variables pump flow rate and airflow rate. The pump flow rate was initially fixed at the lowest possible flow rate and then increased each time the DOT fell into the 20% to 30% range.

Figure B shows the calculated values for the Po_{str} power per unit volume, k_La and G, shear rate. The two growth phases were not sufficient to produce reliable k_La data.

Figure C shows the OUR, DOT and RQ
At the start of the fermentation the OUR was above 0 mmol L^{-1} hr^{-1} so that there was no lag phase. For the first 140 minutes the OUR increased in an exponential manner so that the fermentation was in the growth phase. From 140 minutes the OUR decreased to nearly 0 mmol L^{-1} hr^{-1}, where it remained until 270 minutes. Apart from a short dip at 600 minutes, the OUR increased in an exponential manner from 270 minutes onwards. The first growth phase was too short to produce reliable RQ data. From 400 minutes the RQ had a mean of 0.9.

Figure D shows a log plot of the dry cell weight and the optical density. For the first 120 minutes the optical density increased with a growth rate of 0.78 hr^{-1}. From 120 to 465 minutes neither the optical density nor the dry cell weight increased significantly. From 465 minutes both the optical density and dry cell weight increased significantly where the growth from 465 to 725 minutes was 0.41 hr^{-1}.

Figure E shows the concentration of the protein in the supernatant both as a log plot and expressed as a percentage of the total protein. The percentage of protein disrupted increased from 20% at 0 minutes to 100% at 165 minutes. During the second growth phase the percentage of protein released decreased from 85% at 285 minutes to 11% at 725 minutes.

Figure 37 - Effect of nozzle diameter on the jet power, k_La and shear rate

A

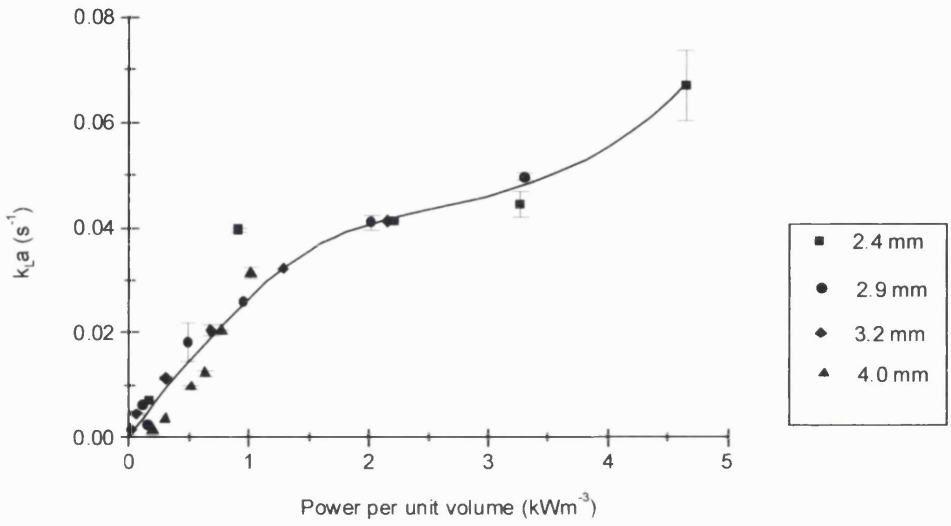

Figure 37 A
This figure shows how k_La measured in water varies with the power per unit volume for the nozzle diameters 2.4 mm, 2.9 mm, 3.2 mm and 4.0 mm in the 14 L plunging jet reactor where the nozzle angle is 0°. The graph shows that the k_La is proportional to the power per unit volume.

B

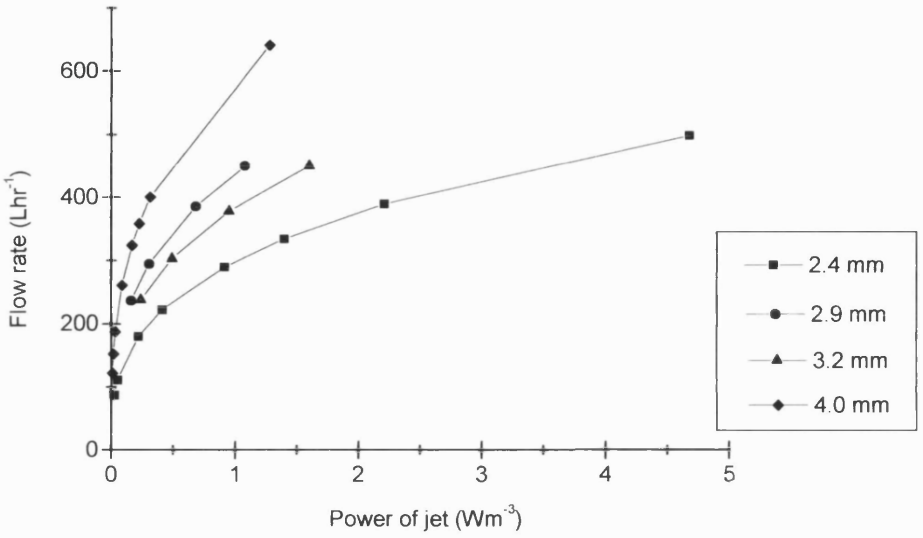
Flow rate (Lhr^{-1})
600
400
200
0
0
1
2
3
4
5
Power of jet (Wm^{-3})
2.4 mm
2.9 mm
3.2 mm
4.0 mm

C

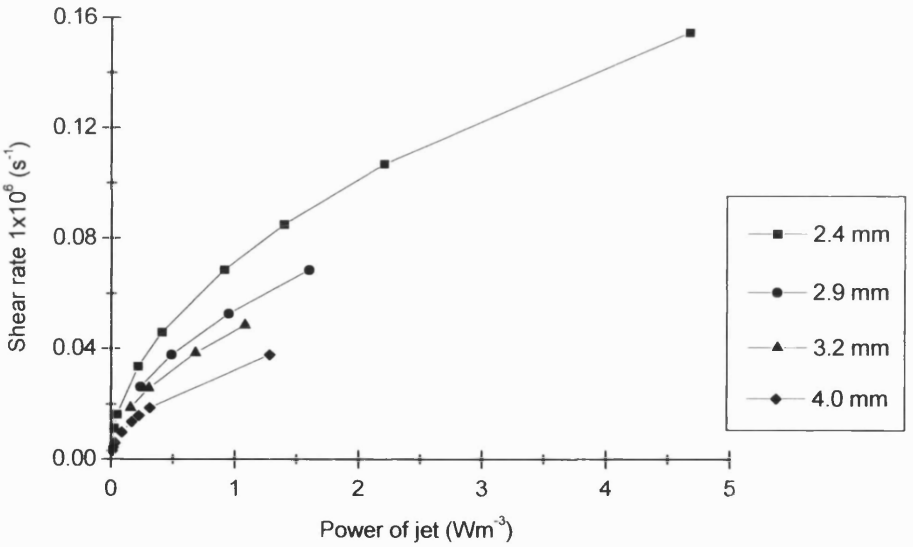
Shear rate 1x10^{6} (s^{-1})
0.16
0.12
0.08
0.04
0.00
0
1
2
3
4
5
Power of jet (Wm^{-3})
2.4 mm
2.9 mm
3.2 mm
4.0 mm

Figure 37 B
This figure shows the volumetric flow rate required for a specific power of the jet for four different nozzle diameters, which are 2.4 mm, 2.9 mm, 3.2 mm and 4.0 mm.
This graph shows that for an equivalent power of the jet, increasing the nozzle diameter requires higher volumetric flow rate.

Figure 37 C
This figure shows the shear rate incurred in the nozzle at a specific power of the jet for four different nozzle diameters, which are 2.4 mm, 2.9 mm, 3.2 mm and 4.0 mm.
This graph shows that for equivalent power of the jet, increasing the nozzle diameter results in a lower shear rate.
Thus figure B and C show that at an equivalent power of the jet, increasing the nozzle diameter requires a higher volumetric flow rate but results in a lower shear rate (calculated shear rate, G).

6.4 Comparison between the disposable and conventional bioreactor

The aim of this chapter was to compare the conventional stirred tank reactor with the disposable plunging jet reactor on the basis of both the physical performance of the bioreactor and the resultant performance of the fermentation. Two fermentations were used as the basis for this comparison, which were the Wild Type fermentation and the Fab fermentation. For the Fab fermentation, Fab STR runs 1 and 2 are shown in figures 25 and 26 respectively, and Fab PJR runs 1 to 4 are shown in figures 27 to 30 respectively. Table 18 on the following page shows a summary of the physical performance and resultant performance of the Fab fermentation in the STR and PJR. For the Wild Type fermentation, Wild Type STR runs 1 and 2 are shown in figures 31 and 32 respectively, and Wild Type runs 1 to 4 are shown in figures 33 to 36 respectively. For the Wild Type fermentation there is no table that summarises the physical and resultant performance of the Wild Type fermentation in the two reactors. This is because in the PJR the Wild Type fermentation terminates within the first 2 hours, so that no comparison can be made. This also means that the Wild Type fermentation can not be used to compare the physical performance of the PJR and the STR. A comparison between the physical performance and the resultant performance for the disposable and conventional bioreactors are discussed below.

Table 18 - Summary of the performance of the plunging jet and the stirred tank bioreactors with the Fab fermentation

Parameter	STR Fab Runs 1-2	PJR Fab Runs 2-4
Maximum power per unit volume	11.2 – 12.7 kW m^{-3}	1.4 kW m^{-3}
Maximum shear rate incurred	13000 – 13500 s^{-1}	85000 s^{-1}
Maximum OUR	155 – 170 mmol L^{-1} hr^{-1}	90 – 110 mmol L^{-1} hr^{-1}
Maximum k_La At fixed power per unit volume	0.12 s^{-1} k_La is fixed	0.13 – 0.15 s^{-1} k_La increases with OUR
RQ - during growth - during induction	0.8 1.1	Varied from 0.5 to 1.0 1.0
Growth rate - initial growth - final growth	0.18 – 0.20 hr^{-1} 0.12 – 0.05 hr^{-1}	0.31 – 0.48 hr^{-1} 0.050 – 0.079 hr^{-1}
Percentage of final growth to total growth	19 % to 31 %	42 % to 50 %
Growth rate - induction	0.015 – 0.026 hr^{-1}	0.034 – 0.041 hr^{-1}
Final biomass - end growth - end induction	30 – 31 g L^{-1} 39 – 42 g L^{-1}	19 – 22 g L^{-1} 30 – 31 g L^{-1}
Final Fab concentration supernatant solid	 14 – 22 mg L^{-1} 75 mg L^{-1}	 0.005 mg L^{-1} no Fab detected

Table 18
The table compares the performance from the STR Fab Runs 1 and 2 with the PJR Fab Runs 2, 3 and 4. For both the STR runs and the PJR runs, where there were different values for each run, the range of values is shown. For both the STR runs, the stirred tank configuration was the same. For all three PJR runs, the plunging jet bioreactor configuration was the same where the nozzle angle was -5°, which is 5° away from the outlet and the nozzle diameter was 2.4 mm.

6.4.1 The physical performance of the stirred tank reactor and the plunging jet reactor

6.4.1.1 Overview

The physical performance of the bioreactor is measured by the operating variables, (airflow rate, stirrer speed, pump flow rate) which are ultimately measured as the power per unit volume required to achieve oxygen transfer measured by the k_La and the shear rate incurred. Of the two fermentations used, only the Fab Fermentation can be used as a basis to compare the physical performance. This is because whilst the Fab fermentation was completed in the plunging jet reactor, the Wild Type fermentation terminated within the first two hours so that insufficient data on the physical performance of the plunging jet reactor was obtained.

6.4.1.2 Comparison between the plunging jet reactor and the stirred tank reactor

The bioreactors operated at a maximum power per unit volume in the range of 11.2 to 12.7 kW m^{-3} for the STR and 1.4 kW m^{-3} for the PJR. At their maximum operating power per unit volume the STR incurred a shear rate in the range of 13000 to 13500 s^{-1} whilst for the PJR it was 85000 s^{-1}. The maximum k_La values were in the range of 0.12 s^{-1} for the STR and 0.13 to 0.15 s^{-1} for the PJR. Thus although the maximum k_La values for the PJR and STR were comparable, the STR required a higher power per unit volume whilst the PJR incurred a higher shear rate.

The relationship between the power per unit volume, oxygen uptake rate (OUR) and k_La were different for the two reactors. For the stirred tank reactor the k_La increases with the power per unit volume, so that at a fixed power per unit volume the k_La is constant. This means that operation of the stirred tank reactor with a fermentation where the oxygen demand, OUR is increasing, requires the power per unit volume to be increased at successive intervals so that the DOT is maintained above 20 %. For the plunging jet reactor the k_La increased with the OUR where the power per unit volume was fixed. Thus

this reactor was operated at a fixed power per unit volume and the DOT was maintained above 20 %.

6.4.2 The resultant performance of the fermentation in the stirred tank reactor and plunging jet reactor

6.4.2.1 Overview

The resultant performance of the fermentation is how fermentation grows and responds to the bioreactor's shear environment. For both the Fab fermentation and the Wild Type fermentation, the comparison was based on the growth rate, final dry weight, OUR and RQ profiles and the percentage of protein released. Additionally for the Fab fermentation the concentration of Fab in the solid and supernatant is a comparison factor.

6.4.2.2 Fab fermentation

The OUR profile and the RQ profile were different in the PJR compared to the STR. For the lag phase and the first part of the growth phase the two reactors had similar OUR profiles. After which the OUR profiles differed significantly from 80 to 95 mmol $L^{-1} hr^{-1}$. In the STR the OUR continued to increase to a maximum of 155 to 170 mmol $L^{-1} hr^{-1}$ at the end of the growth phase. As the fermentation approached the induction phase, the OUR decreased to 60 to 70 mmol $L^{-1} hr^{-1}$ and subsequently increased to 120 mmol $L^{-1} hr^{-1}$ as induction started. In the PJR the OUR increased at a much slower rate to a maximum of 90 to 110 mmol $L^{-1} hr^{-1}$ before decreasing to 75 to 80 mmol $L^{-1} hr^{-1}$ at the end of the growth phase. The OUR then remains roughly constant at 75 to 80 mmol $L^{-1} hr^{-1}$ for induction. Additionally in the STR, the OUR had a short peak associated with lactose limitation whilst in the PJR there was no such peak. In the growth phase the RQ was 0.8 for the STR, whilst in the PJR the RQ varied between 0.5 and 1.0, where addition of glycerol resulted in an increase in the RQ. The varying RQ in the PJR may indicate that prior to each glycerol feed, the Fab fermentation is glycerol limited and is utilising different nutrients perhaps from the breakdown of other cells. During the induction phase the RQ was 1.0 both in the PJR and the STR.

The higher maximum OUR during the growth phase in the STR is associated with a higher final dry weight at the end of the growth phase. In the STR the final dry weight at the end of the growth phase was between 30 to 31 g L^{-1} for the STR whilst for the PJR it was between 19 to 22 g L^{-1}. At the end of the induction phase the dry weight was 39 to 42 g L^{-1} for the STR and 30 to 31 g L^{-1} for the PJR. Thus the final dry weight at the end of both the growth and induction phase was lower for the PJR than the STR. This difference in both the OUR profile and the final dry weight between the STR and the PJR is supported by an analysis of the growth rates. For the PJR whilst it has a higher initial growth rate compared to the STR, the fermentation switches to the lower growth rate, termed 'final growth', earlier in its growth phase. This earlier decrease in the growth rate for the PJR occurs at an OUR of about 75 to 80 mmol L^{-1} hr^{-1}, which is point that the OUR is increasing at a much slower rate.

For the PJR the percentage of protein in the supernatant increased from an initial value of between 6% and 10% to a value of between 60% and 80% at the end of the lag phase. This percentage then decreased to between 4% and 8% as the fermentation entered the growth phase where it remained within this range for the rest of the fermentation. In the STR the percentage of protein in the supernatant decreased from an initial value of between 7.5% and 10% to a value of between 1% and 4% as the growth phase commenced. For one of the fermentations the percentage remained at 4% for the rest of the fermentation whilst for the other, the percentage increased from 1% to 4% at the end of the fermentation. For the STR there was no measurement of the percentage of protein in the supernatant at the end of the lag phase so no comparison can made with the high value of between 60% and 80% measured in the PJR. Thus the percentages of protein in the supernatant in both the growth and induction phases were slightly higher in the PJR compared to the STR.

There was a significant difference in the concentration of Fab in both the solid and supernatant fractions for the PJR and STR. In the supernatant the final concentration in the STR was between 14 to 22 mg L^{-1} whilst in the PJR it was negligible (measured at

0.005 mg L^{-1}). In the solid fraction the final concentration in the STR was 75 mg L^{-1} whilst it was 0 mg L^{-1} in the PJR.

6.4.2.3 Wild Type fermentation

The resultant performance of the Wild Type fermentations in the STR differed significantly from those in the PJR.

In the STR the fermentations either started with the growth phase immediately or after a short lag phase. The fermentation then continued in the growth phase for the entire fermentation where the OUR increased in an exponential manner to a final OUR of between 100 to 140 mmol L^{-1} hr^{-1}.

In the PJR the fermentation started in the growth phase where the OUR increased in an exponential manner. After 80 to 140 minutes cell lysis occurred, where the OUR decreased from between 5 and 17 mmol L^{-1} hr^{-1} to nearly 0 mmol L^{-1} hr^{-1}. The OUR remained at nearly 0 mmol L^{-1} hr^{-1} for between 130 to 220 minutes so this was a second lag phase. Regrowth then occurred after the second lag phase where with the exception of a few instances, the OUR increased in an exponential manner. Samples of the fermentation were taken before and immediately after the lysis in the PJR and compared with a sample taken at the corresponding fermentation time in the STR. These were stained with a gram stain and examined under a microscope where all the microbes were gram negative. Before cell lysis, the microbes from the PJR were more elongated than those from the STR. Immediately after cell lysis in the PJR, the sample showed virtually no identifiable microbes indicating that the lysis process had destroyed the vast majority of the microbes.

The first growth phase in the PJR was similar to the start of the growth phase in the STR. For all of the fermentations the OUR increased in an exponential manner. For the PJR Runs 2 and 4 the initial growth rate was 0.88 hr^{-1} and 0.78 hr^{-1} respectively. This was

similar to the growth rate for the first two hours in the STR which were 1.00 hr^{-1} and 0.87 hr^{-1} for Runs 1 and 2 respectively. The PJR Run 3 had a growth rate of 0.44 hr^{-1}, which was lower than in the STR.
Due to the shortness of the PJR growth phase, a comparison can not be made based on either the RQ or the percentage of protein in the supernatant.

For Runs 3 and 4 the operation of the PJR was altered in order to minimise the shear rate. For Run 3 the same nozzle configuration was used but the power per unit volume was controlled so that it was at its minimum. For Run 4 in addition to controlling the power per unit volume, the nozzle diameter was increased from 2.4 mm to 4.0 mm. Despite these changes, lysis still occurred within the first two hours of growth so that the PJR fermentation was not comparable with the STR fermentation.

6.5 Other experiments performed subsequent to the fermentations

This chapter shows the resultant performance of the Fab fermentation and the Wild Type fermentation in the plunging jet reactor and the stirred tank reactor. Subsequently to performing these fermentations two further experiments were conducted. The first experiment was to compare the strength of the Fab and Wild Type cells whilst the second experiment was to determine whether the Fab products defined structure was sensitive to shear.

6.5.1 Comparison between the strength of the Fab and Wild Type bacterial cells

6.5.1.1 Overview and Aims

The results presented in this chapter show that there is a distinct difference in the performance of the Fab fermentation and Wild Type fermentation in the plunging jet reactor. The fermentation runs; Fab STR Runs 1 – 2 and Wild Type STR Runs 1 - 2

show that both the Fab fermentation and the Wild Type fermentation can be performed in the STR. The fermentation runs; Fab PJR Run 2 - 4 show that the Fab fermentation can be performed in the PJR although there are differences which include the RQ profile and the Fab product concentration. The fermentation runs; Wild Type PJR Runs 1 - 4 show that the Wild Type fermentation can not be performed in the PJR, since the fermentation undergoes lysis within the first two hours of growth. Thus there is a difference in the resultant performance of the two fermentations in the PJR.

A possible explanation for this difference is that the two fermentations have significantly different growth rates. The Fab fermentation has a slower growth rate, so that the cells are likely to be stronger and thus are less likely to lyse in the plunging jet reactor. The aim of the following experiment is to measure the relative strength of the cells in the Wild Type and Fab fermentations through the course of the respective fermentations. Since the Wild Type fermentation undergoes lysis in the plunging jet reactor the comparison was made in a stirred tank reactor.

6.5.1.2 Actual Comparison

The strength was measured by withdrawing samples from the stirred tank reactor at given time intervals and then immediately putting the samples through a homogenzier at a specified pressure for one pass. The percentage disruption is the amount of protein released at the pressure specified divided by the total protein. Both the amount of protein released at the specified pressure and the total protein are normalised with respect to the background protein concentration. Thus the strength of the cell is inversely proportional to the percentage disruption, since weaker cells will have a greater the amount of protein release at any given pressure. The three specified pressures were 110, 150 and 200 Pa. The total protein is measured from samples that have been put through the homogenzier for one pass at a pressure of 1200 Pa.

Figure 38 A, page 231 shows the cell strength of an entire Fab fermentation. For the first 1500 minutes the cell strength remained roughly constant. Between 1500 to 1700

minutes the cell strength appeared to increase so that the cells were stronger in the Fab induction phase than the growth phase.

Figure 38 B, page 231 shows the cell strength of the entire Wild Type fermentation. For the first 30 minutes the cell strength decreases significantly. This cell strength remained roughly constant until 100 minutes where the cell strength begins to increase. From 100 minutes onwards the cells gets progressively stronger as the fermentation progresses to the end. From 0 to 100 minutes the cell strength for the Wild Type fermentation is significantly lower than the cell strength for the entire Fab fermentation. This difference in cell strength may be why the Wild Type fermentation is susceptible to lysis at the 80 to 140 minutes into the fermentation in the plunging jet reactor. The cell strength in the stirred tank reactor decreases in a shorter time frame than lysis occurs in the plunging jet reactor. Thus the cell strength should be measured for the Wild Type fermentation and the Fab fermentation in the plunging jet reactor.

Figure 38 – Percentage disruption at three different pressures for Fab and Wild Type fermentations

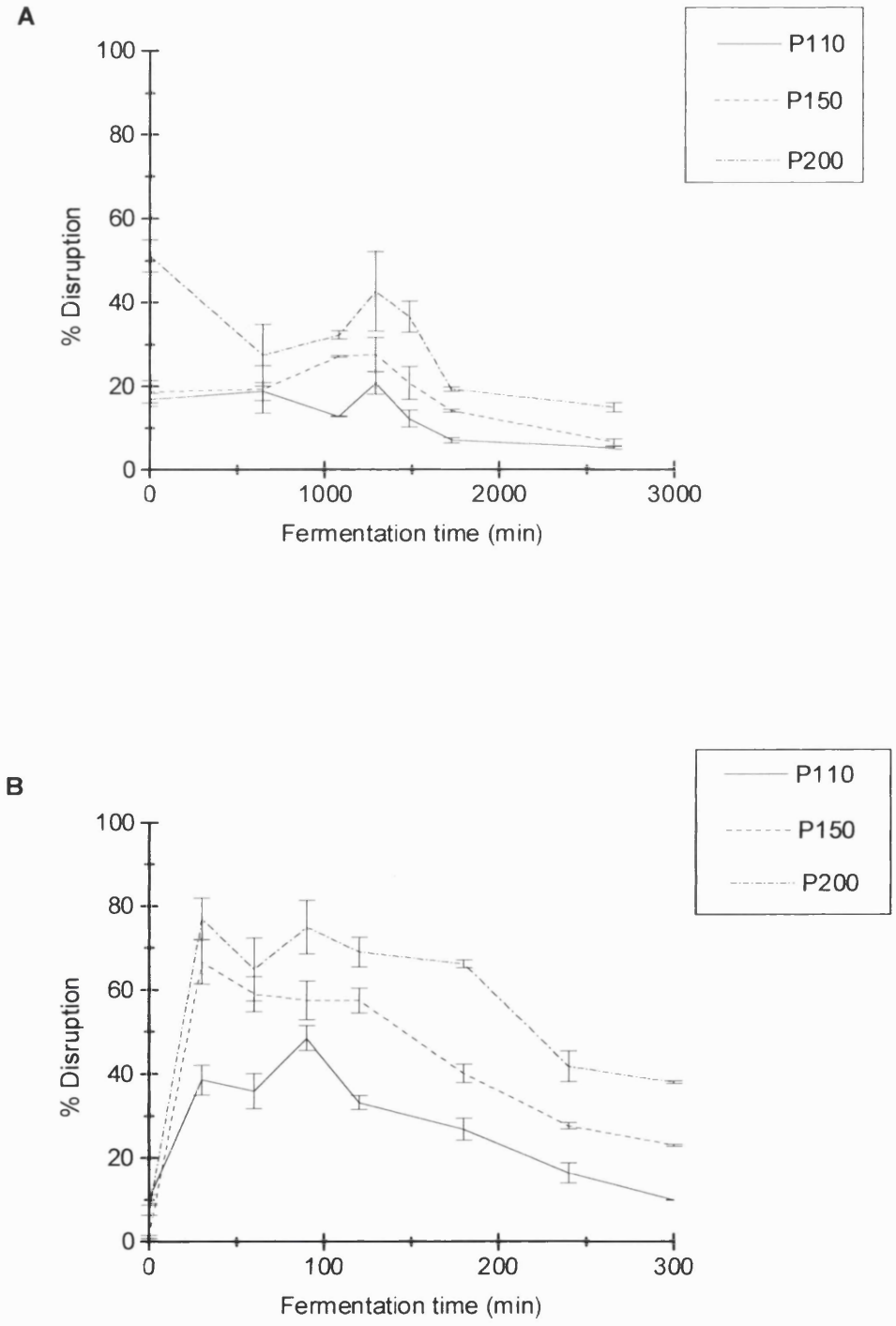

Figure 38 A
This figure shows the disruption of the Fab fermentation cells at three different specified pressures in a homogenzier. This is a measurement of the strength of the bacterial cells for the Fab fermentation in a stirred tank bioreactor

The fermentation can be divided into the lag phase from 0 to 650 minutes, the growth phase from 650 minutes to 1700 minutes and the Fab production phase from 1700 to 2650 minutes. For the first 1500 minutes the strength remains roughly constant. Between 1500 and 1700 minutes the cell strength appears to increase so that the cells are stronger in the Fab production phase compared to the growth phase.

Figure 38 B
This figure shows the disruption of the Wild Type fermentation cells at three different specified pressures in a homogenzier. This is a measurement of the strength of the bacterial cells for a Wild Type fermentation in a stirred tank bioreactor.

For the first 30 minutes the cell strength dramatically decreases. This cell strength remains roughly constant until 100 minutes where the cell strength begins to increase. From this point the cells get progressively stronger as the fermentation progresses to the end. Compared to the Fab fermentation these changes in the cell strength are more significant. Also the cell strength for the Wild Type fermentation between 0 and 100 minutes is lower than the cell strength observed in the entire Fab fermentation.

6.5.2 Shear sensitivity of the Fab product

6.5.2.1 Overview and Aims

A comparison of the Fab fermentation in the stirred tank reactor, Fab STR Runs 1 - 2 with the same fermentation in the plunging jet reactor, Fab PJR Runs 2 - 3 shows that there is a difference in the Fab product concentrations in both the supernatant and the solid fraction. Compared to the fermentations in the STR, the PJR fermentation had negligible Fab concentration in the supernatant and no detectable Fab in the solid fractions. This difference between reactors could be attributed to a higher shear in the PJR, which would degrade the Fab product. The aim of the following experiment is to test the integrity of the Fab product's defined structure to shear. This experiment only tested the sensitivity of the Fab product and did not mimic either the distribution or the residence time of the shear forces in the PJR.

6.5.2.2 Actual measurement of the shear sensitivity

The percentage Fab activity for Fab lysate was measured after it had been in a shear device at a specified shear rate for a residence time of 20 seconds. This percentage Fab activity is the activity of the Fab after it has been in the shear device as a percentage of the initial Fab activity. The volume of each sample was 13 ml for those samples with no air interface (without air interface) and 6.5 ml for those with an air liquid interface (with air interface). The Fab lysate is a Fab fermentation broth that has been exposed to a chemical lysis step followed by centrifugation. This results in disruption of the cells so that the Fab product is released into the supernatant where it is subsequently separated from the solid fraction. Figure 39, page 235 shows that the Fab product is sensitive to shear with and without an air liquid interface.

The average shear rate is calculated as follows:

$G_{average} = \gamma_{average}/\mu$ (Equ. 6.9)

$G_{average} = 1.25 \times 0.0294 \times \rho \times v^2 \times [v \times r/\upsilon]^{0.2}$ (Equ. 6.10)

$v = 2\pi N/60r$ (Equ. 6.11)

Where

Gaverage = Average shear rate (s^{-1})

$\gamma_{average}$ = Average shear stress (kg m^{-1} s^{-2})

μ = viscosity Ns m^{-2}

ρ = density, kg m^{-3}

v= velocity, m s^{-1}

r = radius, m

υ = kinematic viscosity, m^2 s^{-1}

N = Rotational speed, s^{-1}

Figure 39 – Percentage loss of Fab activity as a result of the shear device

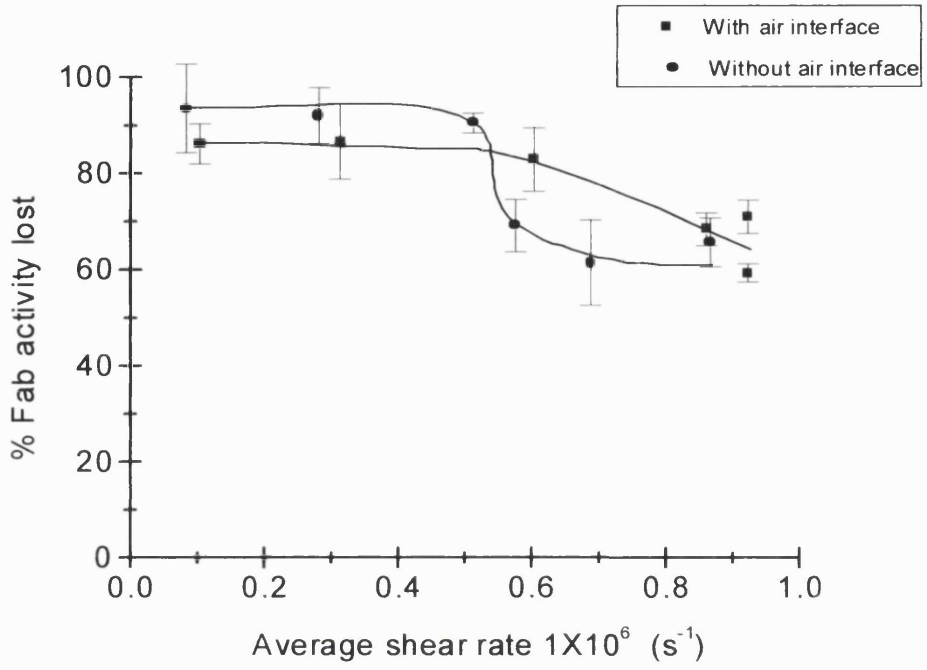

Figure 39
The figure shows the percentage Fab activity for Fab lysate after it has been in a shear device as a percentage of the initial Fab activity.
The graph shows that the activity of the Fab is sensitive to shear both in the presence and absence of an air liquid interface, where the Fab activity decreases as the maximum shear rate increases. This experiment shows no discernible difference in the percentage of Fab activity lost in the presence of shear with and without an air liquid interface.

6.6 Discussion

The aim of this chapter was to compare the PJR with the STR using both the Fab fermentation and the Wild Type fermentation. For the Fab fermentation, a comparison was made between the two bioreactors on the basis of both the physical performance of the bioreactor and the resultant performance of fermentation. For the Wild Type fermentation, a comparison could only be made on the basis of the resultant performance of the fermentation. This is because the Wild Type fermentation failed to grow sufficiently in the PJR.

6.6.1 Physical performance of the PJR in comparison with the STR

The oxygen transfer rate was the principal design factor, which was measured as the oxygen transfer coefficient, k_La. This is considered for this comparison as the physical performance of the bioreactor, which is defined as the operating variables (airflow rate, pump flow rate and stirrer speed) measured as the power per unit volume, required to achieve the k_La and shear rate incurred.

For the PJR the k_La is principally affected by the power per unit volume and the position of the nozzle with respect to the outlet. The results in chapter 5 show that in water, the k_La increases with the power per unit volume for both the STR and the PJR. This agrees with published work documented in chapter 2, including Bin and Smith, (1982), Bin, (1993) and Linek (1989). In the Fab fermentations, at a fixed power per unit volume with the OUR increasing, the k_La remains fixed in the STR but increases in the PJR. Thus during the growth phase of the Fab fermentation, the method of operation for the STR and PJR were different. In the STR, the increasing OUR resulted in a decrease in the DOT, so that the power per unit volume was increased each time the DOT decreased to between 10% and 20%. In the PJR, although the increasing OUR resulted in a decrease in the DOT, it was maintained above 20% throughout the fermentation so that the power per

unit volume remained fixed. This mode of operation in the PJR was possible because the k_La increased with the OUR at a fixed power per unit volume. At a power per unit volume of 1.4 kW m^{-3}, in water the k_La was 0.02 to 0.04 s^{-1} which agrees with the values presented in figure 2 from Bin, (1993). At the same power per unit volume in the fermentation, the k_La increased from 0.045 s^{-1} to 0.13 s^{-1} as the fermentation progressed and the OUR increased. Thus the fermentation broth had a considerable affect on the k_La. A possible reason for the k_La increasing with OUR at a fixed power per unit volume, is that viscosity increases with the biomass. This requires future work to be performed, which is discussed below.

For maximum oxygen transfer efficiency, the position of the nozzle with respect to the outlet is important. In water the results show that the k_La is decreased as the nozzle is angled towards the outlet by +5° and suggest that the k_La remains unchanged as the nozzle is angled away from the outlet by -5°. In the fermentation the k_La is increased as the nozzle is angled away from the outlet by -5°. PJR Runs 1 and 2 show that at the same OUR and power per unit volume of 5 mol L^{-1} hr^{-1} and 1.4 kW m^{-3} respectively; moving the nozzle from an angle of 0 to -5° (away from the outlet) results in an increase in the k_La from 0.005 s^{-1} to 0.045 s^{-1}. Whilst published work has raised the possible effect of the nozzle angle on the rate of air entrainment, as discussed in chapter 2, section 2.4, this is not thought to be the reason. In this case the effect of the nozzle angle on the k_La in the fermentation was attributed to the increased residence time of the entrained air bubbles as they had a greater distance to travel across the bioreactor to the outlet. Thus the position of the nozzle inlet with respect to the nozzle outlet is an important aspect of the disposable plunging jet bioreactor.

For roughly the same maximum k_La of 0.12 s^{-1} for the STR and 0.13 s^{-1} to 0.15 s^{-1} for the PJR, the PJR reactor had a lower maximum power per unit volume of 1.4 kW m^{-3} compared to 12.0 kW m^{-3} for the STR. The corresponding shear rate incurred was greater in PJR where the maximum rate was 85000 s^{-1} compared to 13000 s^{-1} for the STR. This

higher shear rate was attributed to the difference in the resultant performance of both the Wild Type and the Fab fermentations between the STR and PJR bioreactors.

6.6.2 Resultant performance of the fermentation for the PJR and the STR

For the PJR a comparison between the Fab and Wild Type fermentations suggests that the resultant performance is dependent on the strength of the fermentation cells. In the PJR, the complete Fab protocol was performed, where there was no significant lysis whilst for the Wild Type fermentation lysis occurred within the first two hours in the PJR. In the STR both these fermentations were completed according to the protocol with no significant lysis. Thus in the PJR there is a distinct difference in the resultant performance of the Wild Type and Fab fermentation. This difference is attributed to a difference in the strength of the cells since the Fab fermentation has an initial growth rate of 0.20 hr^{-1} and thus is likely to be stronger than the Wild Type with a growth rate of 0.90 hr^{-1}. This difference in strength was confirmed by a comparison between the strength of the Wild Type and the Fab cells through the course of the fermentation.

For the Wild Type fermentation lysis occurred within 2 hours, despite lowering the initial shear rate from 85000 s^{-1} for Run 2 to 11270 s^{-1} for Run 3 by controlling the power per unit volume and 5980 s^{-1} for Run 4 by additionally using a larger diameter nozzle. The highest shear rate at which lysis occurred was 85000 s^{-1} for Run 2, which was significantly higher that for Runs 3 and 4 where lysis occurred at a shear rate of 11870 s^{-1} and 18650 s^{-1} respectively. These results could indicate that the cells lysed at a particular time in their growth phase and were not sensitive to the difference in shear rate between the highest rate of 85000s^{-1} for Run 2 and the lowest rate of 11870 s^{-1} for Run 4. An alternative explanation is that for Run 2, the fermentation was started at a higher shear rate of 68500 s^{-1} compared to around 11000 s^{-1} for Run 3 and 4. This higher initial shear rate in Run 2 could have resulted in selecting cells that were stronger than in the other runs. If this alternative explanation is correct, then the plunging jet bioreactor should be operated with an initial power per unit volume that is sufficient to maintain the DOT

above 20 % for the entire fermentation. Thus further work is required to determine whether either hypothesis is valid.

Whilst the protocol for the Fab fermentation was completed in the PJR, there were distinct differences between the same fermentation in the PJR and the STR.
For the lag phase and the first part of the growth phase up to an OUR of 80 to 95 mmol L^{-1} hr^{-1}, the fermentations in the STR and PJR are broadly similar. In the STR the OUR increases in the growth phase to a maximum of 155 to 170 mmol L^{-1} hr^{-1}. In the PJR from an OUR of 80 to 95 mmol L^{-1} hr^{-1} there is a dramatic deceleration to a maximum OUR in the growth phase is 90 to 110 mmol L^{-1} hr^{-1}. For the PJR, this deceleration in the OUR coincides with an earlier decrease in the growth rate and hence a lower final dry weight at the end of the growth and induction phases compared to the STR. Unlike in the STR where the RQ was 0.8, in the PJR it varied between 0.5 and 1.0 where addition of glycerol resulted in an increase. This may indicate that prior to each glycerol feed in the PJR, the fermentation is glycerol limited and is utilising different nutrients perhaps from the breakdown of other cells. In summary the Fab fermentation is responding to a higher shear rate by reducing its growth rate in the latter half of the growth phase. A higher shear rate could incur a higher cell death rate (resulting in cell lysis) in the PJR compared to the STR. This higher death rate would reduce the overall growth rate and result in a different usage of the nutrients in the media where by the nutrients are utilised earlier in the fermentation, and then recycled by subsequent cell lysis. This could explain the varying RQ during the growth phase in the PJR.

The Fab fermentation is an industrial process to produce a fragmented antibody product; Fab. In the STR the majority of Fab is located in the periplasmic space, so that the final concentration in the solid fraction is 75 mg L^{-1}. There is some leakage of the Fab product into the supernatant where the final concentration is 14 to 22 mg L^{-1}. In the PJR no Fab product was detected in the solid fraction whilst in the supernatant negligible amounts were measured as approximately 0.005 mg L^{-1}. The shear sensitivity of the Fab product was measured, where it was found that its activity and hence its defined structure was

eroded by the action of shear both in the presence and absence of an air interface. Thus possible explanation for the negligible amount of Fab in the supernatant and no Fab in the solid is that shear in the PJR results in the outer polysaccharide layer on the cell being stripped away (as proposed in Hewitt et al, 1998). This would result in a cell that is still viable but the release of periplasmic proteins including the Fab product to the external media environment would occur. Shear forces could then break down the Fab product so that it no longer had its defined structure and hence activity. An alternative explanation is that the Lactose induction process, which produces the Fab product, is inhibited in the PJR but not in the STR.

6.7 Future Work

6.7.1 Physical performance of the PJR

One possible factor affecting the k_La of the plunging jet reactor is the viscosity. This is because the k_La appears to increase with the OUR at a fixed power per unit volume in the plunging jet reactor. The viscosity should be measured across the entire fermentation and then compared with the k_La profile. Then providing the Fab fermentation is unaffected by carboxymethlycellulose, (CMC) this should be added during the growth phase of fermentation in the PJR to investigate whether increasing the viscosity affects the k_La.

For roughly the same k_La, of 0.13 s^{-1} to 0.15 s^{-1} for PJR and 0.12 s^{-1} for the STR, the PJR incurred a higher maximum shear rate of 85000 s^{-1} in the PJR compared to 13500 s^{-1} in the STR. This higher shear rate is thought to have caused the difference in the resultant performance for both the Fab and Wild Type fermentations in the STR and the PJR. For the Wild Type fermentation, despite operating the PJR at the lowest power per unit volume with a larger nozzle diameter of 4.0 mm, lysis still occurred. The shear rate incurred can be reduced further by using the nozzle developed by Kenyeres et al (1989). This nozzle could increase the energy efficiency by between 30 % to 60 % and thus

require a lower flow rate and incur a lower shear rate. The reproducibility and ease of construction of such a nozzle should be examined. An alternative to replacing the nozzle is to increase the number of the basic nozzles, so that each nozzle is operating at a lower power per unit volume and thus the shear rate incurred is lower. The combined power per unit volume of the nozzles would be slightly greater than power per unit volume of the single nozzle that was replaced.

6.7.2 Resultant performance of the fermentation

As discussed above the lack of the Fab product in the PJR is attributed to two possible reasons. These are either that shear strips away the periplasmic membrane so that the Fab product is released and then its defined structure is destroyed by shear or alternatively the reactor's environment causes inhibition of the lactose induction process so that the Fab product is not produced. These two reasons can be resolved by transferring the fermentation from the plunging jet reactor to the stirred tank reactor during the induction phase. If negligible amounts of the Fab product were produced in the STR then this would indicate inhibition of the lactose induction process so that the fault lies with the fermentation rather than the reactor. Alternatively if the Fab product is produced in the STR, then this would indicate that shear in the plunging jet reactor is destroying the defined structure of the Fab product.

If the break up of the Fab product is attributed to shear, then further studies can be performed to further prove the role of shear. These are principally that the entire Fab fermentation is performed in the STR but during the induction phase samples can be withdrawn and put through a scaled down mimic of the plunging jet reactor. If shear associated with the reactor causes break down of the Fab product then it would be expected that the amount of Fab in both the supernatant and solid fraction is lower in the scale down samples than in the control samples from the STR. In addition by varying the residence time of the samples in the scaled down mimic, the effect of time exposure can be determined. Finally the shear rate in the mimic can be varied to determine the level at

which significant Fab destruction does not occur. Since animal cell cultures typically secrete their product, results from these experiments have major implications for a plunging jet animal cell bioreactor.

The resultant performance of the Fab fermentation in the PJR suggest that the fermentation may have different nutrient requirements compared to the same fermentation in the STR. In particular the varying RQ during the growth phase may suggest that the Fab fermentation is glycerol limited prior to each feed. Thus the Fab fermentation should be repeated with an increased number of glycerol feeds where the overall amount of glycerol is increased. Consideration should also be give to increasing the concentration of the inorganic salts in the media, particularly magnesium sulphate and calcium chloride. The concentration of these two salts could also be increased for the additional feed at an optical density of 40. This is because these salts are supposed to increase the strength of the outside wall of the cell and thus reduce leakage of the Fab product.

6.8 Summary

The comparison between the conventional stirred tank bioreactor and the disposable plunging jet bioreactor showed that the physical performance of the two bioreactors were comparable but that there were differences in the resultant performance of the Wild Type and Fab fermentations.

For the physical performance the maximum k_La values were comparable at 0.12 s^{-1} for the STR and 0.13 to 0.15 s^{-1} for the PJR. The plunging jet bioreactor operated at a lower power per unit volume of 1.4 kW m^{-3} compared to 11.2 to 12.7 kW m^{-3} for the STR but had a higher shear rate of 85000 s^{-1} compared to 13500 s^{-1} for the STR. The method of control of the power per unit volume was different for the two reactors. For the STR at a fixed power per unit volume, the k_La remained constant as the OUR increased. Thus the power per unit volume was periodically increased resulting in an instantaneous increase in the k_La. For the PJR at a fixed power per unit volume the k_La increased with the OUR. Thus the power per unit volume was fixed for the entire fermentation. For the PJR moving the nozzle from vertical (0°) to 5° away from the outlet (-5°) resulted in a substantial increase in the k_La for both the Fab and the Wild Type fermentations. Thus the position of the nozzle inlet with respect to the outlet is important.

For both the Wild Type and Fab fermentations there were differences in the resultant performance between the plunging jet bioreactor and the stirred tank bioreactor. Both fermentations were completed in the STR and were compared to the same fermentations in the PJR. In the PJR reactor, the Wild Type fermentation was terminated within the first 140 minutes due to lysis but the Fab fermentation was completed. This difference in response was attributed to the slower growth rate and stronger microbial cells of the Fab fermentation compared to the Wild Type fermentation. Although the Fab fermentation was completed in the PJR, there were differences between the two reactors, which are detailed in the discussion above. Principally these include a lower final dry weight and

virtually zero final Fab concentration in both the solid and supernatant fractions for the PJR. Further work is required to confirm whether these differences are due to the higher shear rate in the PJR.

7 Disposable Animal Cell Bioreactor

7.1 Overview and aims

The aim of this chapter was to evaluate which reactor should be used as the disposable animal cell bioreactor in a comparison with a conventional animal cell bioreactor. The possible options are the airlift, bubble column and plunging jet reactor. The basis of the comparison was the k_La, CO_2 stripping and mixing, which were measured for the conventional airlift bioreactor at typical superficial velocities used for large scale animal cell culture. A comparison between the airlift and bubble column was performed at a relatively small scale of 26 L to determine whether the two reactors have comparable performance. Although several authors have concluded that the airlift had better aeration and mixing than the bubble column, it was thought that at a relatively small scale they might be comparable. Whilst the plunging jet reactor's construction meant that it was the most suitable reactor for a disposable, there was concern that shear associated with the nozzle may be to high to support animal cell culture. Thus the power per unit volume required to match the k_La, CO_2 stripping and mixing of the conventional airlift bioreactor were measured. In terms of performance, at the large scale the airlift is more suitable than a bubble column, plunging jet reactor or rocker. Of these reactors, the airlift design is the most complex and thus its design, as a disposable was considered.

Due to difficulties in obtaining sterile disposable bioreactors, no actual cell culture in a disposable bioreactor could be performed so that a comparison between a disposable and a conventional bioreactor could not be made. Thus extensive work based on measuring the k_La, CO_2 stripping and mixing in perspex vessels was performed.

7.2 Comparison between an airlift, bubble column and plunging jet reactor

7.2.1 Overview and aims

An airlift, bubble column and plunging jet reactor were all compared at a 26 L volume. For each of these vessels the oxygen transfer coefficient, k_La, the CO_2 stripping coefficient, CO_2 stripping and the mixing time were measured. The aim of this work is to determine whether the plunging jet reactor can match the equivalent k_La, CO_2 stripping and mixing of the conventional airlift at a shear rate and power per unit volume that is likely to support an animal cell culture. The comparison between the airlift and the bubble column will also determine whether the bubble column's performance at small scale is equivalent to that of the conventional airlift.

7.2.2 Basis of the comparison

7.2.2.1 Physical performance factors

The comparison will be based on the oxygen transfer coefficient, k_La, CO_2 stripping coefficient, CO_2 stripping and the mixing time. These equations are shown below.

k_La, oxygen transfer coefficient

$$k_L a = \left(\frac{1}{t}\right) \ln\left(\frac{(C^* - C_L^\circ)}{(C^*)}\right)$$

(Equ. 4.3)

CO_2 stripping coefficient

$$k_L a = \frac{1}{t}\left[\ln\frac{\left(pCO_2^* - pCO_2^\circ\right)}{\left(pCO_2^* - pCO_2^t\right)}\right]$$

(Equ. 4.10)

Power for the plunging jet

$Po = 1/2\rho QVo^2$ (Equ. 2.0)

(Bin, 1993)

Power per unit volume for the airlift and bubble column

$$Po/V = \frac{1000VsRT}{22\cdot 4Z}\ln\left(\frac{\rho gZ}{p_u}\right)$$

(Equ. 7.0)

(Roels and Heijnen, 1980)

The above equations use the following notation

k_La = volumetric mass transfer coefficient (s^{-1})

C^* = oxygen concentration of the liquid when it is in equilibrium with the gas (Mol L^{-1})

C_L = oxygen concentration in the liquid at time t = 0 (Mol L^{-1})

CO_2stripping = CO_2 stripping coefficient (s^{-1})

pCO_2^* = partial pressure of CO_2 in the liquid when it is saturated with CO_2 (mm Hg)

pCO_2° = partial pressure of CO_2 in the liquid at time, t = 0 (mm Hg)

pCO_2^t = partial pressure of CO_2 in the liquid at time, t = t (mm Hg)

t = time (s)

ρ = density of liquid (kg m^3)

Po = power (W)

Po/V = power per unit volume (W m^{-3})

Vo = velocity of the jet (m s^{-1})

do = diameter of the jet (m)

Q = volumetric flow rate (m^3 s^{-1})

Vs = superficial gas velocity (m s^{-1})

R = universal gas constant (J mol^{-1} K^{-1})

T = temperature (K)

Z= ungassed height of liquid in the column (m)

g= gravitational accereration (m s^{-2})

Pu = pressure of gas at column outlet (Pa)

7.2.2.2 Design and operation of the bioreactors

All three reactors had the same vessel geometry of 1 m height and 0·185 m diameter. The airlift and bubble column had an identical gas sparger at the bottom. The airlift was a split cylinder so that it had a baffle that was 0·7 m in length and was positioned 0·1 m above the bottom, so there was a 0·2 m of liquid above the baffle. The baffle was positioned across the centre so that the riser and downcomer area were equal. For the plunging jet reactor a nozzle with a 4·0 mm diameter was selected. A nozzle with a larger diameter was not selected because the pump could not produce a large enough flow rate to achieve adequate k_La values. A smaller nozzle diameter was not used because of excessive foam production, where a large majority of the solution was foam.

For all three reactors the k_La, CO_2 stripping coefficient and the mixing time were measured. For the airlift and bubble column these parameters were measured versus the gas flow rate, whilst for the plunging jet reactor it was the pump flow rate. Both the CO_2 stripping coefficient and the k_La were measured in the buffer solution consisting of NaCl 6·4 g L^{-1}, $NaHCO_3$ 2·0 g L^{-1} and Pluronic F68 1·0 g L^{-1} (dissolved in RO water), whilst the k_La was additionally measured in RO water. This buffer was used since it mimics the buffers used in animal cell culture with airlifts. For the mixing time the salts NaCl and $NaHCO_3$ were omitted since they could interfere with the mixing time measurement and

their presence would have little effect on the mixing time. Thus the mixing time was measured in Pluronic F68 1·0 g L^{-1} (dissolved in RO water).

Airlifts are operated with a maximum superficial velocity, which is typically between 0·01 m s^{-1} to 0·015 m s^{-1} (personal communication, Lonza). The 26 L airlift is equivalent to industrial airlifts. Thus the k_La, CO_2 stripping and mixing time were measured at a superficial velocity of 0·01 ms $^{-1}$ and 0·015 m s^{-1}. These values were then used as targets for the bubble column and plunging jet reactor.

7.2.3 Airlift performance

The k_La, CO_2 stripping and mixing time were measured for an airlift operating at a gas flow rate and power per unit volume range of 3 L min^{-1} to 16 L min^{-1} and 0·02 kW m^{-3} to 0·10 kW m^{-3} respectively.

Figure 40 A and B, pages 257 to 258 show that the k_La increased with the gas flow rate and thus the power per unit volume in the airlift. Siegel and Merchuk (1987) observed this in a spilt cylinder airlift. For a superficial velocity and gas flow rate of 0·011 m s^{-1} and 9·0 L min^{-1}, the k_La was 6·3 ± 0·05 hr^{-1}. Increasing the superficial velocity and gas flow rate to 0·015 m s^{-1} and 12·0 L min^{-1} respectively resulted in an increase in the k_La to 8·9 ± 0·26 hr^{-1}.

Figure 41 A and B, pages 261 to 262 show that the CO_2 stripping coefficient increased with the gas flow rate and thus the power per unit volume. Operating at a superficial velocity and gas flow rate of 0·011 m s^{-1} and 9·0 L min^{-1} resulted in a CO_2 stripping coefficient of 0·34 ± 0·01 hr^{-1}. Increasing the superficial velocity and gas flow rate to 0·015 m s^{-1} and 12 L min^{-1} resulted in a CO_2 stripping coefficient of 0·49 ± 0·004 hr^{-1}.

As shown in figure 42 A and B, pages 263 to 264 the mixing time decreased with an increasing gas flow rate and thus with an increasing power per unit volume. Operating at a superficial velocity and gas flow rate of 0·011 m s^{-1} and 9·0 L min^{-1} respectively resulted in a mixing time of 15 ± 1 second. Increasing the superficial velocity and gas

flow rate to 0·015 m s^{-1} and 12 L min^{-1} respectively resulted in a mixing time of 13 ± 1 second.

These results at superficial velocities of 0·01 m s^{-1} and 0·015 m s^{-1} were the targets for the bubble column and the plunging jet reactor. Thus the k_La target was between 6·3 ± 0·05 hr^{-1} to 8·9 ± 0·26 hr^{-1}. The CO_2 stripping coefficient target was 0·34 ± 0·01 hr^{-1} to 0·49 ± 0·004 hr^{-1}. The target range for the mixing time was 15 to 13 ± 1 seconds. This is summarised in table 19, page 254.

7.2.4 Comparison between the airlift and the bubble column

7.2.4.1 Aims and Overview

The aim of this work was to determine whether the bubble column at small scale could be used as disposable bioreactor that had equivalent performance to the airlift. It has been well documented that at a large scale the airlift has greater aeration and mixing than the bubble column. The comparison between the airlift and bubble column is shown in figures 40 A and B (pages 257 to 258) for the k_La, 41 A and B (261 to 262) for CO_2 stripping and 42 A to E (pages 263 to 267) for mixing. The comparison is also summarised in table 20, page 255.

7.2.4.2 Results

There was no significant difference in performance between the bubble column and the airlift. At equivalent gas flow rates and power per unit volumes the bubble column had comparable k_La values. Thus the bubble column required a gas flow rate of 9·0 L min^{-1} for a k_La of 6·2 ± 0·08 hr^{-1} and 12·0 L min^{-1} for a k_La of 8·4 ± 0·36 hr^{-1}. The corresponding power per unit volumes, were 0·056 kW m^{-3} and 0·075 kW m^{-3} respectively. The CO_2 stripping coefficient values for the airlift and bubble column were comparable at equivalent gas flow rates and power per unit volumes below 9 L min^{-1} and 0·056 kW m^{-3} respectively. Above these ranges in the gas flow rate and power per unit

volume, the CO_2 stripping coefficients were greater in the airlift. The bubble column required a gas flow rate of between 9 and 12 L min^{-1} to achieve the lowest CO_2 stripping target of 0·34 hr^{-1}. At the highest gas flow rate of 16 L min^{-1} the CO_2 stripping coefficient was 0·45 ± 0·02 hr^{-1}. At the same gas flow rates and power per unit volumes, the bubble column had lower mixing times. The lowest mixing target of 13 seconds occurred in the bubble column at a gas flow rate of 3 L min^{-1}, whilst in the airlift this mixing time occurred at a gas flow rate of 12 L min^{-1}.

With the airlift operating at a fixed gas flow rate of 16 L min^{-1}, increasing the height of liquid above the baffle from 0·1 m to 0·5 m, resulted in a decrease in the mixing time from 13 to 7 seconds. Increasing the height of the liquid further to 0·6 m resulted in an increase in the mixing time to 8·5 seconds. These results differ from Varley and Birch (1999), where in a split cylinder the mixing time increased as the liquid height above the baffle increased from 0·1 m to 0·5 m. These results agree with Christi and Moo-Young (1987), where in a spilt cylinder the mixing time decreased with an increasing liquid height above the baffle up to 0·5 m. Weiland (1984) observed similar results in a draught tube airlift. Comparing the airlift and bubble column at a gas flow rate of 16 L min^{-1}, the mixing times were comparable when the airlift had a liquid height above baffle of between 0·4 and 0·5 m.

These results show that the bubble column either had better or comparable mixing to the airlift, depending on the height of liquid above the baffle in the airlift. These results contrast with several papers, which have stated that at comparable power per unit volumes, airlifts had lower mixing times (Varley and Birch (1999), Verlaan et al (1988)). The results also show that at equivalent power per unit volumes the airlift and bubble column had comparable k_La values and thus the two reactors have identical aeration efficiencies within the power per unit volumes of 0 to 0·1 kW m^{-3}. This contrasts with several authors who collectively have stated that airlifts, particularly of the spilt vessel type (cylinder or rectangular) have higher aeration efficiencies compared to conventional aeration tanks and bubble column (Margaritits and Sheppard (1981), Orazem and Erickson (1979), Hatch (1975) and Siegel and Merchuk (1988)). This result of

comparable performance between the bubble column and airlift is attributed to the small scale of the bubble column and airlift.

This work concludes that at a 26 L scale the bubble column and airlift have a comparable performance. Compared to the rocker, the bubble column has a greater k_La, since the maximum k_La measured in water for the rocker was 4.0 hr^{-1} whilst for the bubble column a k_La of 15 hr^{-1} was measured in water. Thus at small scale the bubble column can be used as a disposable bioreactor with an equivalent performance to the airlift.

7.2.5 Comparison between the airlift and the plunging jet reactor

7.2.5.1 Aims and Overview

The aim of this work was to determine the power per unit volume required for the plunging jet reactor to match the airlift's performance. The basis for this comparison was measuring the k_La, CO_2 stripping and mixing targets in the airlift at the superficial velocities of 0.01 m s^{-1} and 0.015 m s^{-1}. This comparison is shown in figures 40, 41 and 42 (pages 257 to 264) and is summarised in table 21, page 256.

7.2.5.2 Results

There was a significant difference in the performance of the airlift and plunging jet reactor. Compared to the airlift and bubble column, the plunging jet reactor had a significantly lower k_La, CO_2 stripping and mixing. The k_La increased with the power per unit volume from 0·05 to 0·15 kW m^{-3} but from 0·15 to 0·25 kW m^{-3} the k_La was flat. The maximum k_La achieved was 6·5 ± 0·42 hr^{-1} at a power per unit volume and pump flow rate of 0·15 kW m^{-3} and 6·5 L min^{-1} respectively. Operating the plunging jet reactor at a power per unit volume of 0·05 to 0·15 kW m^{-3} resulted in a CO_2 stripping and mixing time of 0·10 to 0·25 hr^{-1} and 220 to 120 seconds respectively. Thus whilst the lower k_La target was met, the CO_2 stripping and mixing were well below their target ranges.

For the plunging jet reactor the CO_2 stripping and mixing were well below their target ranges. Neither the CO_2 stripping coefficient nor the mixing times can be improved by changes in the partial pressures of the constituent gases that make up the air supply to the headspace. The mixing times are too high above the targets for improvements to be made by using multiple injections points as suggested by Christi and Moo-Young (1987). In fact the mixing times are so far below the target, that it is probable that the cells would not be sufficiently in suspension. Thus there are no possible alterations to the 26 L plunging jet reactor so that it could function as an animal cell bioreactor.

Table 19 – Target k_La, CO_2 stripping and mixing as measured in the 26 L airlift

Superficial velocity Gas flow rate	0·01 m s^{-1} 9·0 L min^{-1}	0·015 m s^{-1} 12·0 L min^{-1}
k_La	6·3 ± 0·05 hr^{-1}	8·9 ± 0·26 hr^{-1}
CO_2 stripping	0·34 ± 0·01 hr^{-1}	0·49 ± 0·004 hr^{-1}
Mixing	15 ± 1 s	13 ± 1 s

The table shows the k_La (hr^{-1}), CO_2 stripping (hr^{-1}) and mixing (s) measured in a 26 L airlift at the superficial velocities of 0.01 m s^{-1} and 0.015 m s^{-1} which spans the range of maximum superficial velocities that the airlift operates during an animal cell culture.

Table 20 – Comparison between the bubble column and the airlift based on k_La, CO_2 stripping and mixing

	Gas flow rate			
	3 L min^{-1}	9·0 L min^{-1}	12·0 L min^{-1}	16·0 L min^{-1}
k_La				
AR		6·3 ± 0·05 hr^{-1}	8·9 ± 0·26 hr^{-1}	
BCR		6·2 ± 0·08 hr^{-1}	8·4 ± 0·36 hr^{-1}	
CO_2 stripping				
AR		0·34 ± 0·01 hr^{-1}	0·49 ± 0·004 hr^{-1}	
BCR		0·32 ± 0·01 hr^{-1}	0·43 ± 0·02 hr^{-1}	0·45 ± 0·02 hr^{-1}
Mixing				
AR		15 ± 1 s	13 ± 1 s	
BCR	13 ± 1 s	9 ± 1 s	8 ± 1 s	

The table shows the k_La (hr^{-1}), CO_2 stripping (hr^{-1}) and mixing (s) measured at specified gas flow rates, (L min^{-1}) in the 26 L airlift, AR and 26 L bubble column, BCR. In the airlift the gas flow rates of 9.0 L min^{-1} and 12.0 L min^{-1} are equivalent to the superficial velocities of 0.01 m s^{-1} and 0.015 m s^{-1} respectively. These two superficial velocities span the range of maximum superficial velocities that an airlift typically operates during an animal cell culture.

Table 21 – Comparison between the plunging jet and the airlift

Reactor	PJR	AR	AR
Pump flow rate	6.5 L min^{-1}	-	-
Gas flow rate	-	9.0 L min^{-1}	12.0 L min-1
Power per unit volume	0.15 kW m^{-3}	0.056 kW m^{-3}	0.075 kW m^{-3}
k_La	6.5 ± 0.42 hr^{-1}	6·3 ± 0·05 hr^{-1}	8·9 ± 0·26 hr^{-1}
CO_2 stripping	0.25 ± 0.002 hr^{-1}	0·34 ± 0·01 hr^{-1}	0·49 ± 0·004 hr^{-1}
Mixing	120 ± 5 s	15 ± 1 s	13 ± 1 s

The table shows the highest k_La (hr^{-1}), CO_2 stripping (hr^{-1}) and mixing (s) measured in the 26 L plunging jet reactor, PJR. This is compared with the k_La (hr^{-1}), CO_2 stripping (hr^{-1}) and mixing (s) measured for the 26 L airlift reactor, AR at the gas flow rates of 9.0 L min^{-1} and 12.0 L min^{-1} which are equivalent to the superficial velocities of 0.01 m s^{-1} and 0.015 m s^{-1} respectively. These two superficial velocities span the range of maximum superficial velocities that an airlift typically operates during an animal cell culture.

Figure 40 – The k_La for the 26 L airlift, bubble column and plunging jet reactor

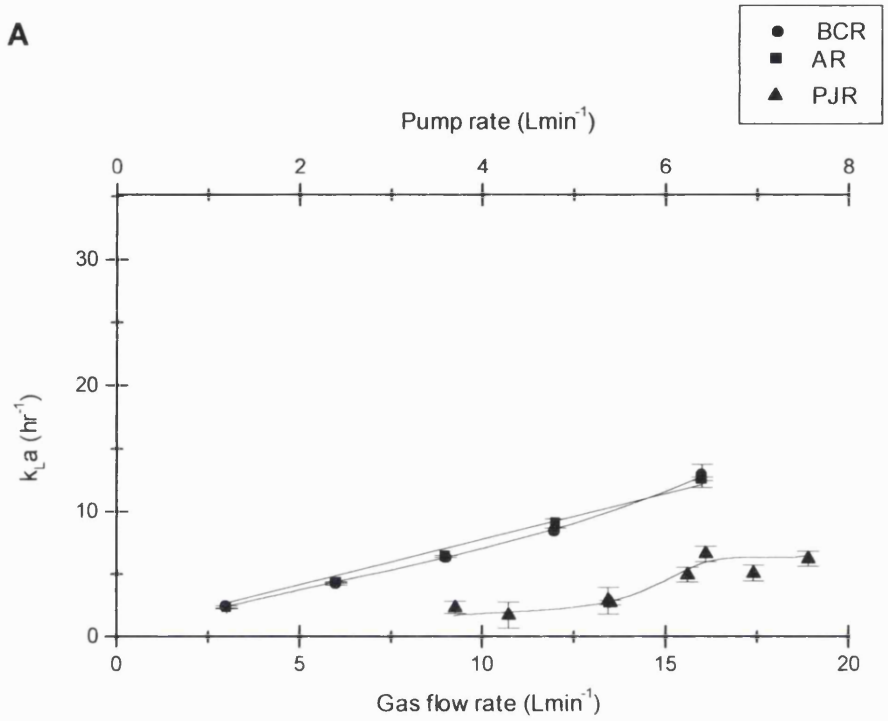

The figure shows the k_La values (hr^{-1}) versus the gas flow rate (L min^{-1}) for the 26 L airlift and bubble column and the pump flow rate (L min^{-1}) for the 26 L plunging jet reactor. The plunging jet reactor has a 4.0 mm diameter nozzle. The k_La values (hr^{-1}) were measured in a buffer solution (NaCl 6·4 g L^{-1}, $NaHCO_3$ 2·0 g L^{-1} and Pluronic F68 1·0 g L^{-1}).
At equivalent gas flow rates, the bubble column and airlift had comparable k_La values.

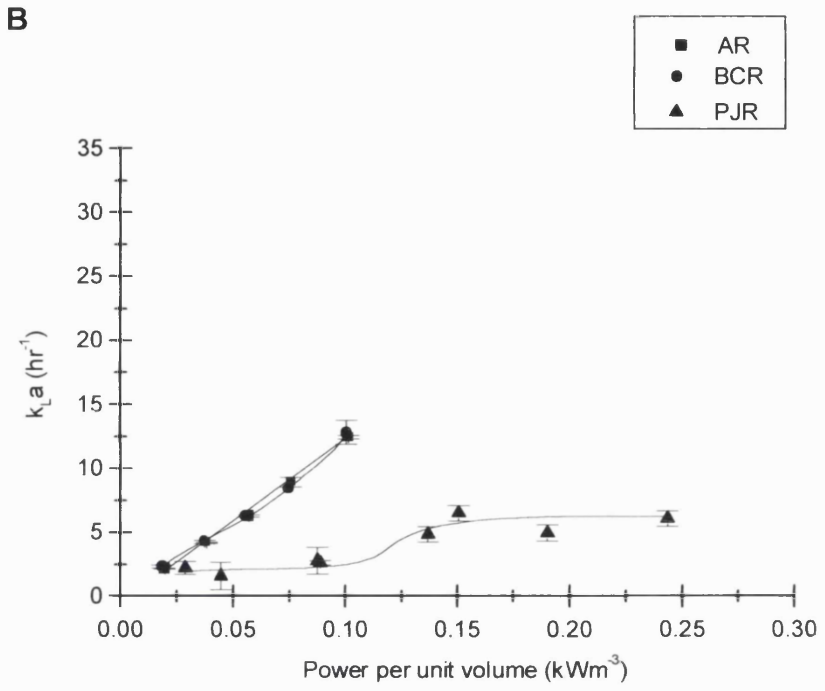

The figure shows the k_La values (hr^{-1}) versus the power per unit volume ($kW\ m^{-3}$) for the 26 L airlift, bubble column and plunging jet reactor. The plunging jet reactor has a 4.0 mm diameter nozzle. The k_La values (hr^{-1}) were measured in a buffer solution (NaCl 6·4 g L^{-1}, $NaHCO_3$ 2·0 g L^{-1} and Pluronic F68 1·0 g L^{-1}).
The figure shows that at equivalent power per unit volumes the bubble column and airlift had comparable k_La values. For both the bubble column and airlift, the k_La increased with the power per unit volume for the range measured. For the plunging jet reactor, the k_La increased with the power per unit volume from 0·05 kW m^{-3} to 0·15 kW m^{-3} but from 0·15 kW m^{-3} to 0·25 kW m^{-3} the k_La was flat.

C

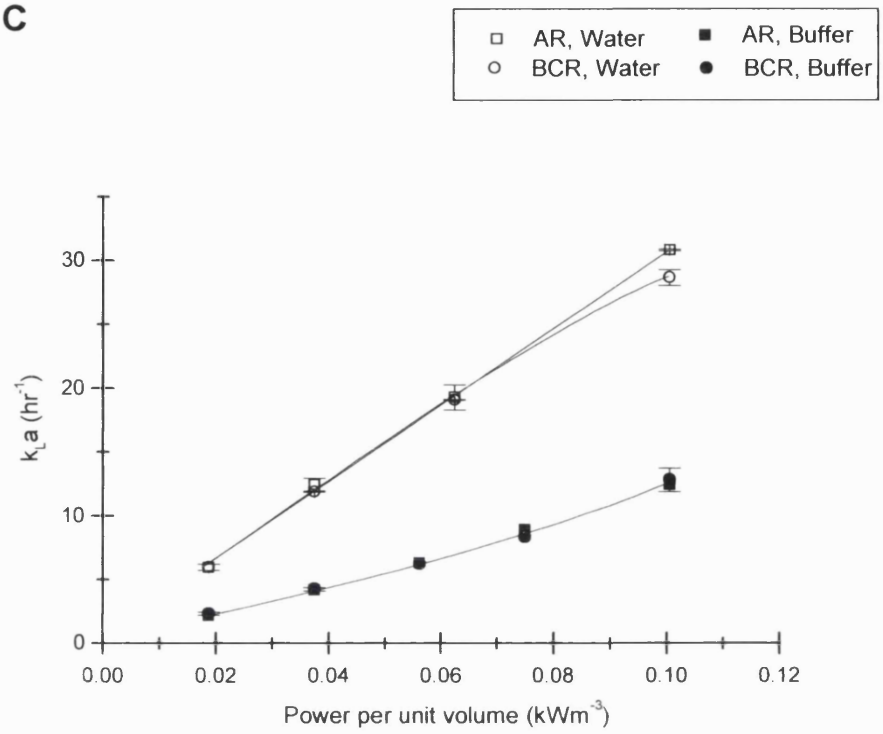

The figure shows a comparison of the k_La values (hr^{-1}) measured in the water and buffer (NaCl 6·4 g L^{-1}, $NaHCO_3$ 2·0 g L^{-1} and Pluronic F68 1·0 g L^{-1}) for the 26 L bubble column reactor (BCR) and 26 L airlift reactor (AR). The k_La values are shown versus the power per unit volume (kW m^{-3}).
The figure shows that for both the bubble column and the airlift, the k_La values measured in the RO water are significantly higher than those measured in the buffer solution at equivalent power per unit volumes.

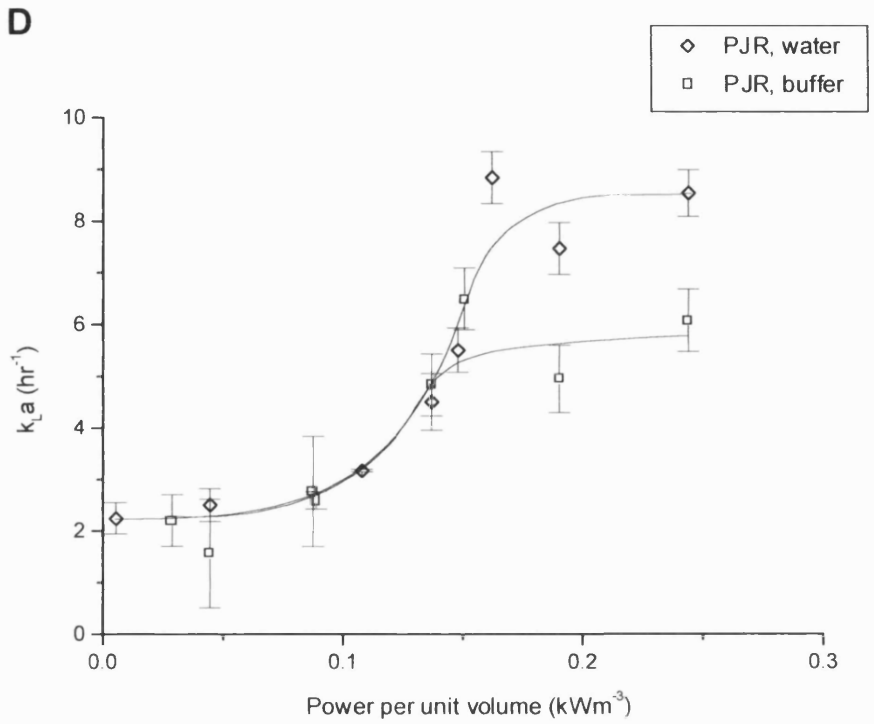

The figure shows a comparison of the k_La values (hr^{-1}) measured in the water and buffer (NaCl 6·4 g L^{-1}, $NaHCO_3$ 2·0 g L^{-1} and Pluronic F68 1·0 g L^{-1}) for the 26 L plunging jet reactor (PJR) with a 4.0 mm diameter nozzle. The k_La values are shown versus the power per unit volume (kW m^{-3}).
The figure shows that for the plunging jet reactor operating at a power per unit volume of less than 0·2 kW m^{-3} there is little difference between the k_La values in the RO water and in the buffer at equivalent power per unit volumes. For power per unit volumes greater than 0·2 kW m^{-3}, the k_La values are greater in the RO water.

Figure 41 – The CO_2 stripping coefficient for the 26 L airlift, bubble column and plunging jet reactor

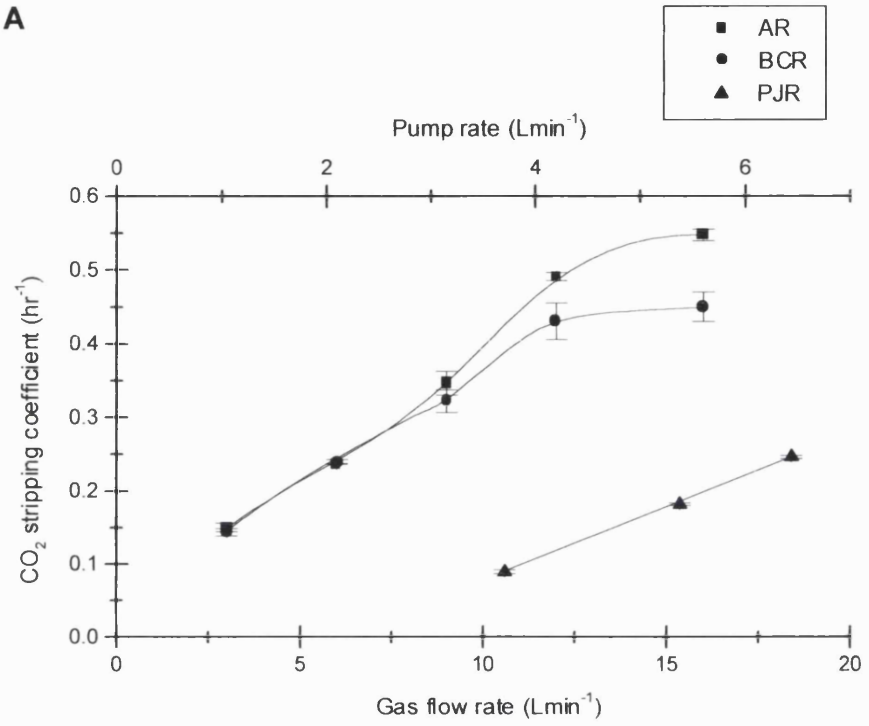

The figure shows the CO_2 stripping coefficient (hr^{-1}) versus the gas flow rate (L min^{-1}) for the 26 L airlift and bubble column and the pump flow rate (L min^{-1}) for the 26 L plunging jet reactor. The plunging jet reactor has a 4.0 mm diameter nozzle. The CO_2 stripping coefficient (hr^{-1}) measured in the buffer solution (NaCl 6·4 g L^{-1}, $NaHCO_3$ 2·0 g L^{-1} and Pluronic F68 1·0 g L^{-1}).
The figure shows that at a gas flow rate below 9 L min^{-1} the CO_2 stripping is comparable between the airlift and bubble column. At a gas flow rate of 9 L min^{-1} and greater, the CO_2 stripping is greater in the airlift than the bubble column.

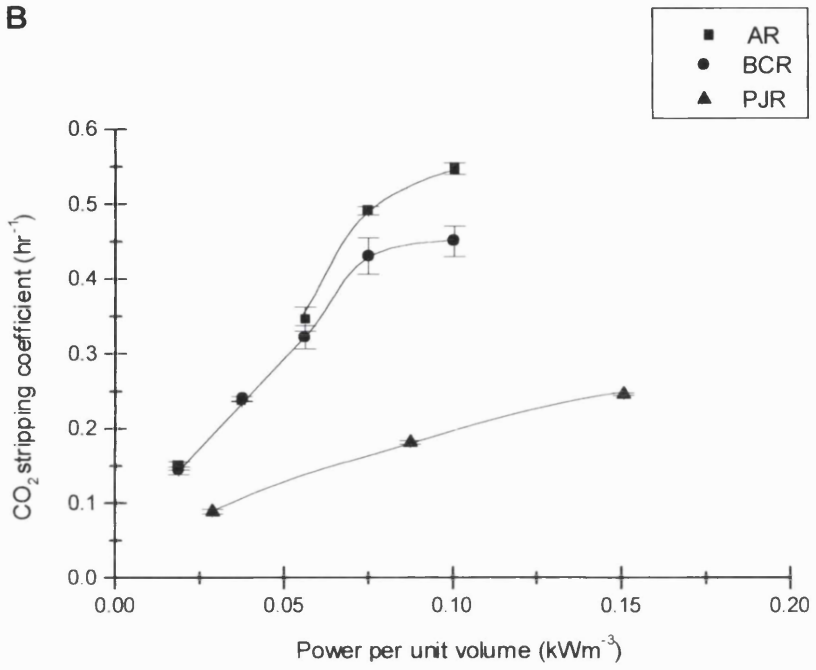

The figure shows the CO_2 stripping coefficient (hr^{-1}) versus the power per unit volume ($kW\ m^{-3}$) for the 26 L airlift, 26L bubble column and the 26 L plunging jet reactor. The plunging jet reactor has a 4.0 mm diameter nozzle. The CO_2 stripping coefficient (hr^{-1}) was measured in the buffer solution (NaCl 6·4 g L^{-1}, $NaHCO_3$ 2·0 g L^{-1} and Pluronic F68 1·0 g L^{-1}).

The figure shows that at equivalent power per unit volumes, the plunging jet reactor had a significantly lower CO_2 stripping coefficient than in the airlift reactor or bubble column reactor.

Figure 42 – The mixing time for the 26 L airlift, bubble column and plunging jet reactor

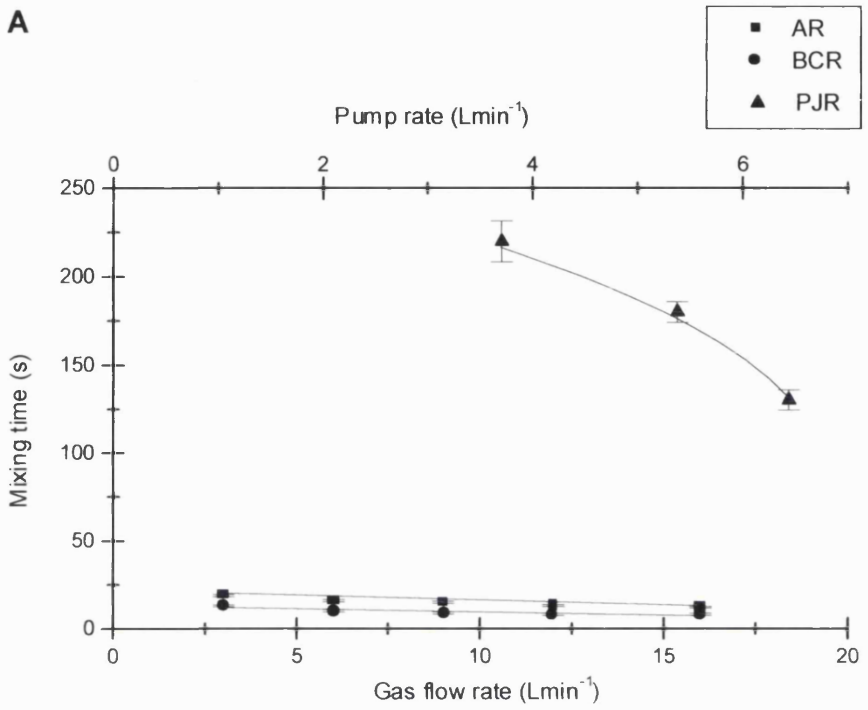

The figure shows the mixing time (s) versus the gas flow rate (L min^{-1}) for the airlift and bubble column and the pump flow rate (L min^{-1}) for the plunging jet reactor. The plunging jet reactor has a 4.0 mm diameter nozzle. The mixing times were measured in a solution of 1·0 g L^{-1} Pluronic F68

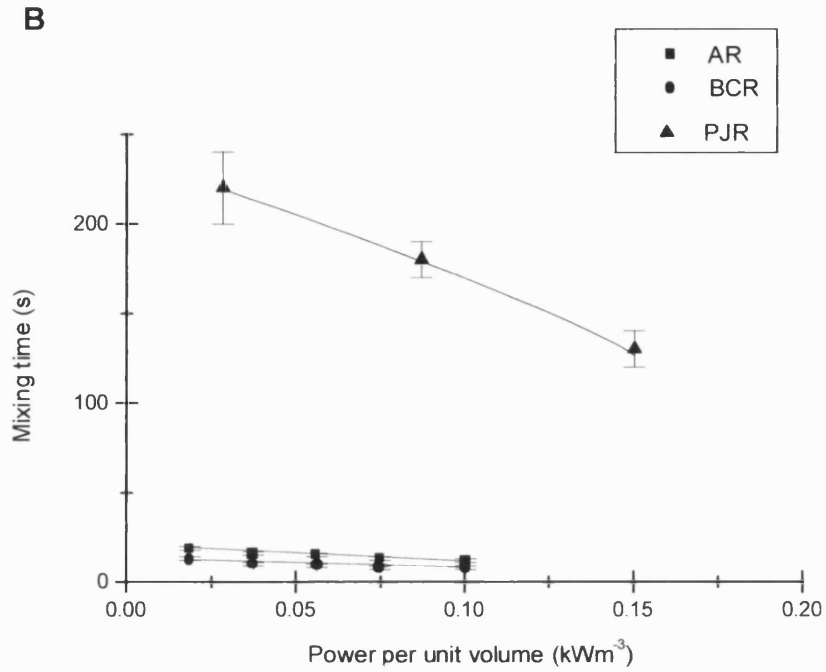

The figure shows the mixing time (s) versus the power per unit volume (kW m^{-3}) for the airlift, bubble column and the plunging jet reactor. The plunging jet reactor has a 4.0 mm diameter nozzle. The mixing times were measured in a solution of 1·0 g L^{-1} Pluronic F68

The figure shows that the plunging jet reactor has higher mixing times compared to either the bubble column or the airlift at equivalent power per unit volumes.

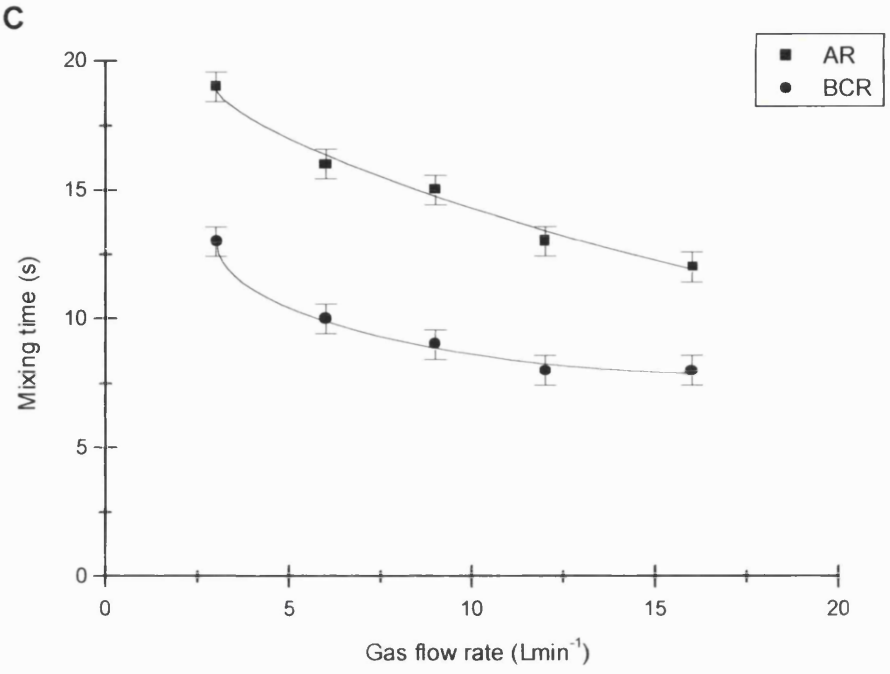

The figure shows the mixing time (s) versus the gas flow rate (L min^{-1}) in a solution of 1·0 g L^{-1} Pluronic F68 for the 26 L airlift reactor, AR and the 26 L bubble column reactor, BCR.
The bubble column had a lower mixing time than the airlift at all the equivalent gas flow rates measured.

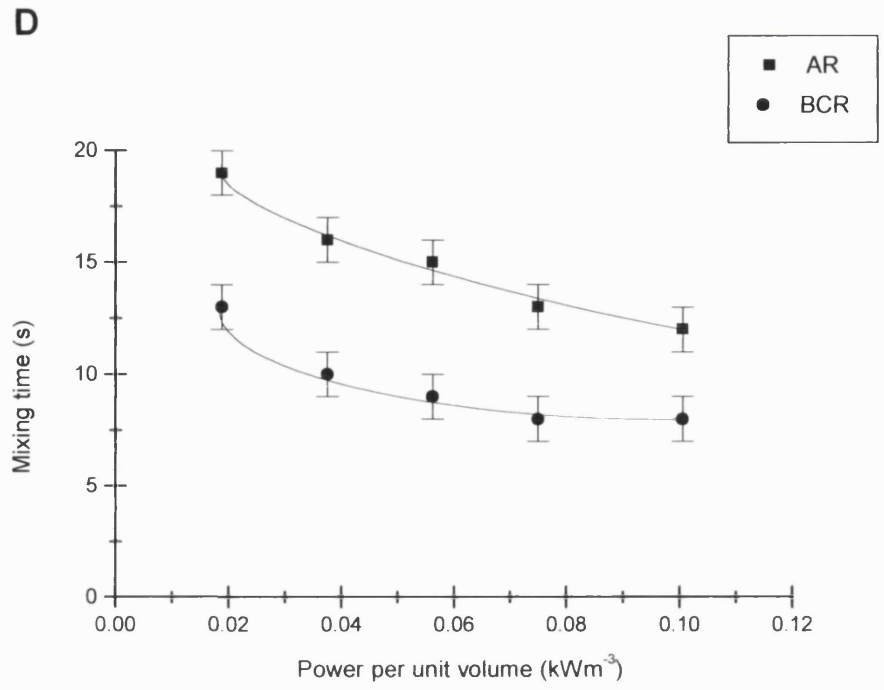

The figure shows the mixing time (s) versus the power per unit volume (kW m^{-3}) in a solution of 1·0 g L^{-1} Pluronic F68 for the 26 L airlift reactor, AR and the 26 L bubble column reactor, BCR.
The bubble column had a lower mixing time than the airlift at all the equivalent power per unit volumes measured.

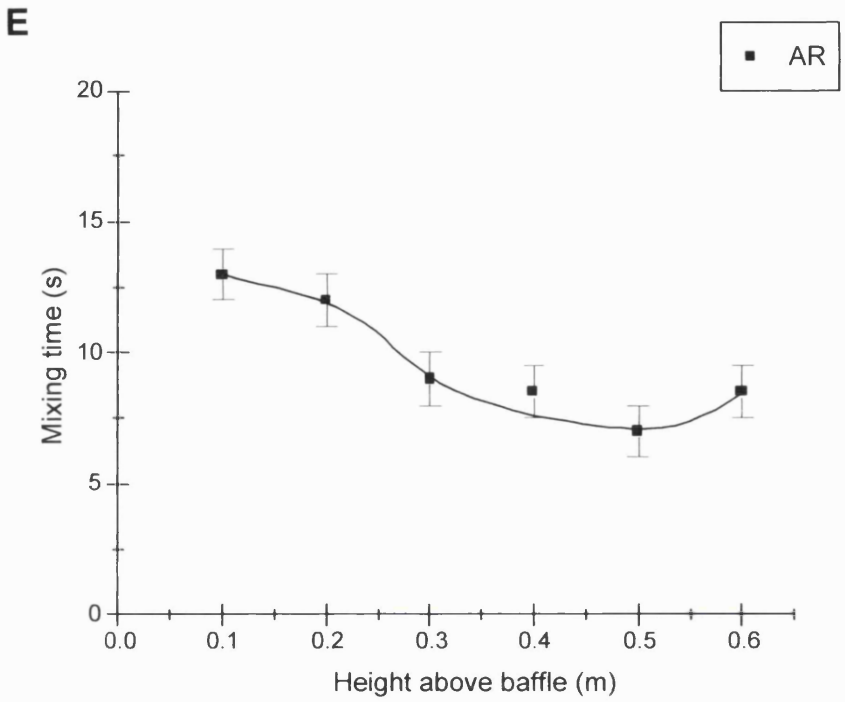

The figure shows for the 26 L airlift, AR the mixing time (s) at height of liquid above the baffle of between 0.1 m to 0.6 m, for a fixed gas flow rate of 16 L min^{-1}.
The figure shows that increasing the height above the baffle from 0·2 m to 0·5 m, results in a lower mixing time, which is equivalent to the bubble column at the same gas flow rate.

7.2.6 Improving the performance of the plunging jet reactor

7.2.6.1 Aims and Overview

As Figures 40, 41 and 42 (pages 257 to 264) show the performance of the plunging jet reactor is worse than both the bubble column and the airlift. The aim of this work is to improve the performance of the plunging jet reactor so that the k_La, CO_2 stripping and mixing are equivalent to the targets for the airlift shown in table 19, page 254.

7.2.6.2 Selection criteria for the nozzle diameter

In selecting a nozzle diameter for the animal cell plunging jet reactor both the shear in the nozzle and the pump flow rate must be minimised. A high shear rate in the nozzle could cause damage by shear. A high pump flow rate could cause damage primarily by excessive movement through the plume, which is a region of high shear damage due to the presence of bursting bubbles. The plume can be compared to the gas disengagement zone where according to Kioukia et al (1992), the more frequently the cells passed through this region, the greater the cell damage. Additionally a high pump rate could impart shear damage as the cells are circulated through the peristaltic pump.

The shear rate through the nozzle should not exceed 15000 s^{-1} since this corresponds to a shear stress of 15 N m^2, which has been set as the maximum limit for the animal cell plunging jet bioreactor. Figure 43, page 275 shows how the calculated shear rate in the nozzle increases with the power per unit volume. This is shown for the 26 L and 20 L with the 4·0 mm nozzle, the 8 L with the 2·4 mm nozzle and the 10 L and 6 L reactors with both the 2·4 mm and 4·0 mm nozzles. Table 23, page 273 shows the power per unit volume for each reactor at the maximum shear rate of 15000 s^{-1}.

7.2.6.3 Effect of aspect ratio

The poor performance of the plunging jet reactor was attributed to the high aspect ratio that allowed air bubbles to remain in the upper part of the column. Thus the same vessel was used but with reduced volumes so that the height to diameter ratio was decreased as

shown in the table 22 below. The k_La was used as a basis for the comparison. For the reactor volumes of 6 L and 10 L both the 2·4 mm and 4·0 mm nozzle diameters were used. For the reactor volumes of 20 L and 26 L only the 4·0 mm nozzle diameter was used since a 2·4 mm nozzle produced a too high pressure at the flow rates required and produced too much foaming.

Table 22 : The height to diameter ratio for the PJRs

Volume (L)	Height (m)	Diameter (m)	Height to diameter
26	1·010	0·185	5·5
20	0·800	0·185	4·30
10	0·415	0·185	2·20
8	0·340	0·185	1·80
6	0·266	0·185	1·44

Table 22
The height to diameter ratio for the plunging jet reactor, PJR for 6 L, 8 L, 10 L, 20 L and 26 L reactor volumes.

Figure 44 B, page 277 shows that for a power per unit volume between 0 to 0·1 kW m^{-3}, the k_La was more responsive to the power per unit volume for the 6 L reactor than the 10 L, 20 L and 26 L reactors. For the 6 L reactor for a given power per unit volume between 0 to 0·1 kW m^{-3} the k_La was comparable with the 2·4 mm and 4·0 mm nozzle. For the 10 L reactor for a power per unit volume between 0 to 0·3 kW m^{-3}, the k_La was greater in the 4·0 mm nozzle than with the 2·4 mm nozzle. Table 24, page 273 shows for each reactor volume, the power per unit volume required to match the lower and upper k_La targets of 6.3 hr^{-1} and 8.9 hr^{-1} respectively. This data shows that for the 6 L reactor the k_La target of 8.9 hr^{-1} can be produced within the power per unit volume specified by the shear rate using both the 2.4 mm and the 4.0 mm nozzles. For the 10 L reactor with the 2.4 mm nozzle, the required power per unit volume to achieve the k_La target of 8.9

hr^{-1} exceeds its specified maximum whilst with the 4.0 mm nozzle the upper k_La target is achieved with a power per unit volume below its specified maximum. For the 20 L reactor using the 4.0 mm nozzle, the upper k_La target was achieved with a power per unit volume which exceeds its specified maximum. Thus these results presented in both figure 44 and table 24 imply that increasing the volume of this reactor from 6 L to 10 L requires an increase in the nozzle diameter.

7.2.6.4 The 6 L reactor as a potential disposable animal cell bioreactor

The 6 L reactor was selected to determine whether the k_La, CO_2 stripping and mixing targets set in the airlift could be achieved in the plunging jet reactor. As discussed above in selecting the nozzle diameter both the shear rate in the nozzle and the pump flow rate must be minimised. Thus for the 6 L reactor the 2.4 mm nozzle was selected since the k_La target of 8.9 hr^{-1} was achieved within the specified maximum power per unit volume set by the shear rate of 15000 s^{-1} and with a lower pump flow rate than in the 4.0 mm nozzle. As a comparison the k_La, CO_2 stripping and mixing were also measured in the 8 L and 10 L reactors.

Figure 45, pages 278 to 281 shows the k_La, CO_2 stripping and mixing time for the 6 L, 8 L and 10 L reactors with the 2.4 mm nozzle. For the same reactors, table 25, page 274 shows the power per unit volume required for each reactor to match the upper and lower targets for the k_La and mixing. The table does not include CO_2 stripping since figure 45 shows that with the exception of the 6 L reactor, the lower CO_2 stripping target of 0.34 hr^{-1} was not attained in any of the reactors operating at power per unit volumes above their specified maximum.

The table 25 shows that for both the 6 L and 8 L reactors, the upper k_La target of 8.9 hr^{-1} and the upper mixing targets of 13 seconds were achieved within the respective maximum power per unit volumes specified of 0.10 kW m^{-3} and 0.075 kW m^{-3}. For the 10 L reactor operating at its specified maximum power per unit volume of 0.06 kW m^{-3}, the k_La, CO_2 stripping and mixing were all below their respective lower targets of 6.3 hr^{-1}, 0.34 hr^{-1} and 15 seconds.

Figure 45 shows that of the three reactors operating at their specified maximum power per unit volumes based on a shear rate of 15000 s^{-1}, the 6 L reactor had the best performance. The k_La range target of 6·3 hr^{-1} to 8·9 hr^{-1} required a power per unit volume range of 0·05 kW m^{-3} to 0·064 kW m^{-3} for both the 6 L and 8 L reactors. The lowest mixing time target of 13 seconds occurred at a power per unit volume of 0·038 kW m^{-3} and 0·060 kW m^{-3} for the 6 L and 8 L reactor respectively. For the 6 L reactor at its specified maximum of 0·10 kW m^{-3}, the CO_2 stripping value was 0·30 ± 0·04 hr^{-1}, which is just within range of the lower target of 0·34 ± 0·01 hr^{-1}. Operating the 8 L reactor at its specified maximum power per unit volume of 0·075 kW m^{-3}, resulted in a CO_2 stripping value of 0·25 ± 0·02 hr^{-1}. For the 10 L reactor the k_La, mixing and CO_2 stripping were all significantly below there targets, even with a power per unit volume that was significantly above its operational maximum of 0·060 kW m^{-3}. Increasing the power per unit volume from 0 to 0·27 kW m^{-3} resulted in virtually no increase in the k_La. For the mixing time increasing the power per unit volume from 0·05 kW m^{-3} to 0·1 kW m^{-3} resulted in an increase in the mixing time from 25 ± 3 seconds to 60 ± 4 seconds. Increasing the power per unit volume to 0·35 kW m^{-3} resulted in a decrease in the mixing time to 30 ± 4 seconds. For the CO_2 stripping coefficient increasing the power per unit volume from 0·057 kW m^{-3} to 0·12 kW m^{-3} resulted in an increase from 0·18 ± 0·02 hr^{-1} to 0·30 ± 0·045 hr^{-1}. Increasing the power per unit volume further resulted in a decrease in the CO_2 stripping coefficient.

This work concludes that operating the 6 L bioreactor with a power per unit volume at its specified maximum of 0·1 kW m^{-3} would result in bioreactor performance that is limited by its CO_2 stripping ability. This is because whilst the reactor matches the upper k_La and mixing targets of 8.9 hr^{-1} and 13 seconds respectively, the highest CO_2 stripping coefficient was 0·30 ± 0·04 hr^{-1}, which is just within range of the lower target of 0.34 hr^{-1}. In addition increasing the aspect ratio from 1.44 to 2.20 in order to increase the volume from 6 L to 10 L results in a dramatic deterioration in performance. Figure 45 shows that for the 10 L reactor the k_La, mixing and CO_2 stripping were all below the respective

lower targets even operating with a power per unit volume above its specified maximum of 0.60 kW m^{-3}. The poor performance in the 10 L reactor could be attributed to the observation that as the power per unit volume is increased, the presence of small bubbles located towards the top of the reactor increased in number so that a 'foam effect' was observed.

This is shown in figure 46 B (page 283) where there is a build up of small bubbles towards the top of the reactor volume so that the 'foam effect' is created and for comparative purposes figure 46 A (page 282) is shown where there in no 'foam effect' observed. At the time of performing these experiments, the flow rates at which this foam effect occurs were not recorded and thus a complete analysis of this problem can not be presented. For both the 20 L and 26 L plunging jet reactors operating at the power per unit volume between 0.05 to 0.25 kW m^{-3}, this foam effect was observed where the presence of small bubbles increased in the number as the power per unit volume was increased.

Table 23 : Power per unit volume at maximum shear rate of 15000 s^{-1} for various plunging jet reactors

Nozzle diameter	Volume	Power per unit volume at shear rate of 15000s^{-1}
2.4 mm	6 L	0.100 kW m^{-3}
2.4 mm	8 L	0.075 kW m^{-3}
2.4 mm	10 L	0.060 kW m^{-3}
4.0 mm	6 L	0.470 kW m^{-3}
4.0 mm	10 L	0.280 kW m^{-3}
4.0 mm	20 L	0.150 kW m^{-3}
4.0 mm	26 L	0.110 kW m^{-3}

The table shows the power per unit volume (kW m^{-3}), which corresponds, to the shear rate of 15000 s^{-1}. This is shown for the plunging jet reactor volumes of 6 L, 8 L and 10 L with the 2.4 mm nozzle and for the reactor volumes of 6 L, 10 L, 20 L and 26 L with the 4.0 mm nozzle.

Table 24 : The power per unit volume and pump flow rate that result in the lower and upper k_La targets for the plunging jet reactors

Nozzle diameter	Volume	Power per unit volume		Pump flow rate	
		6.3 hr^{-1}	8.9 hr^{-1}	6.3 hr^{-1}	8.9 hr^{-1}
2.4 mm	6 L	0.05 kW m^{-3}	0.06 kW m^{-3}	1.5 L min^{-1}	1.6 L min^{-1}
2.4 mm	10 L	0.32 kW m^{-3}	-	3.0 L min^{-1}	-
4.0 mm	6 L	0.05 kW m^{-3}	0.06 kW m^{-3}	2.5 L min^{-1}	2.9 L min^{-1}
4.0 mm	10 L	0.16 kW m^{-3}	0.20 kW m^{-3}	4.6 L min^{-1}	5.2 L min^{-1}
4.0 mm	20 L	0.16 kW m^{-3}	0.20 kW m^{-3}	6.0 L min^{-1}	6.5 L min^{-1}
4.0 mm	26 L	0.15 kW m^{-3}	-	6.5 L min^{-1}	-

The table shows the power per unit volume (kW m^{-3}) and pump flow rate (L min^{-1}) which results in the lower and upper k_La targets of 6.3 hr^{-1} and 8.9 hr^{-1}. This is shown for the plunging jet reactor volumes of 6 L and 10 L with the 2.4 mm nozzle and the reactor volumes of 6 L, 10 L, 20 L and 26 L with the 4.0 mm nozzle.

Table 25 : The power per unit volume that result in the lower and upper k_La and mixing targets for the 6 L, 8 L and 10 L plunging jet reactors

Nozzle diameter	Volume	k_La		Mixing	
		6.3 hr^{-1}	8.9 hr^{-1}	15 s	13 s
2.4 mm	6 L	0.05 kW m^{-3}	0.06 kW m^{-3}		0.03 kW m^{-3}
2.4 mm	8 L	0.05 kW m^{-3}	0.06 kW m^{-3}	0.03 kW m^{-3}	0.06 kW m^{-3}
2.4 mm	10 L	0.32 kW m^{-3}	-	-	-

The table shows the power per unit volume (kW m^{-3}), which results in the lower and upper k_La of 6.3 hr^{-1} and 8.9 hr^{-1} and the lower and upper mixing targets of 15 s and 13 s. This is shown for the plunging jet reactor volumes of 6 L, 8 L and 10 L with the 2.4 mm nozzle.

Figure 43 – The calculated shear rate for various reactors and nozzle diameters

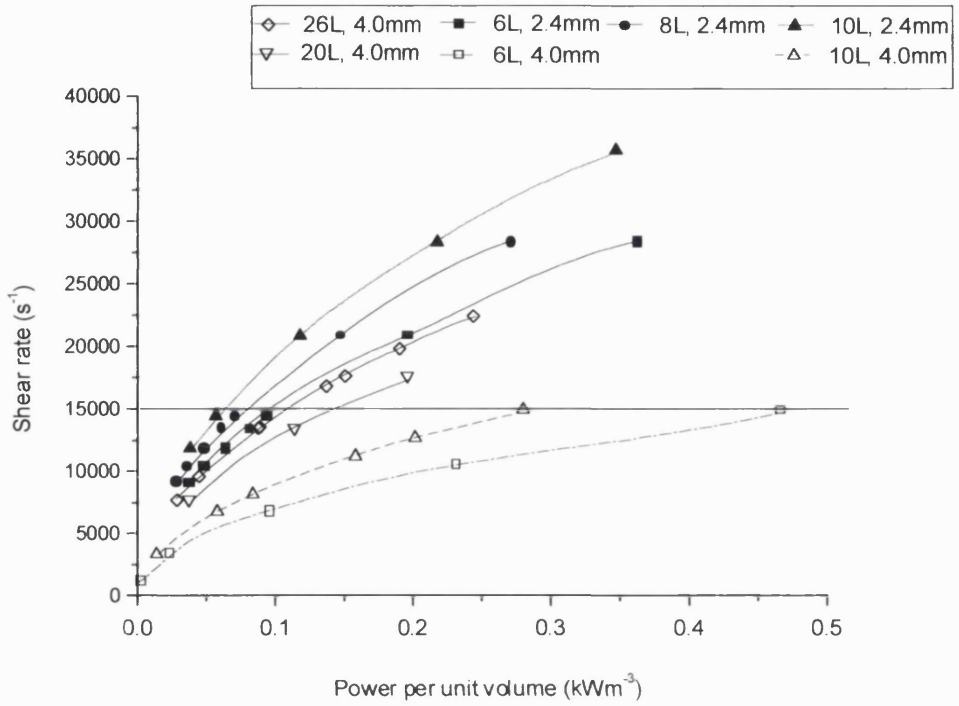

The figure shows the calculated shear rate incurred for the 26 L and 20 L reactor with the 4·0 mm nozzle, the 8 L reactor with the 2·4 mm nozzle and for the 6 L and 10 L reactor with both the 2·4 mm and 4·0 mm nozzle. A shear rate of 15000 s^{-1} is equivalent to a shear stress of 15 N m^2 and is the limit set for these experiments. The calculated shear rate of 15000 s^{-1} corresponds to a power per unit volume of 0·1 kW m^{-3}, 0·075 kW m^{-3} and 0·060 kW m^{-3} for the respective reactors 6 L, 8 L and 10 L with a 2·4 mm nozzle.

Figure 44 – Measurement of the k_La for a plunging jet reactor with different nozzle diameters and reactor volumes

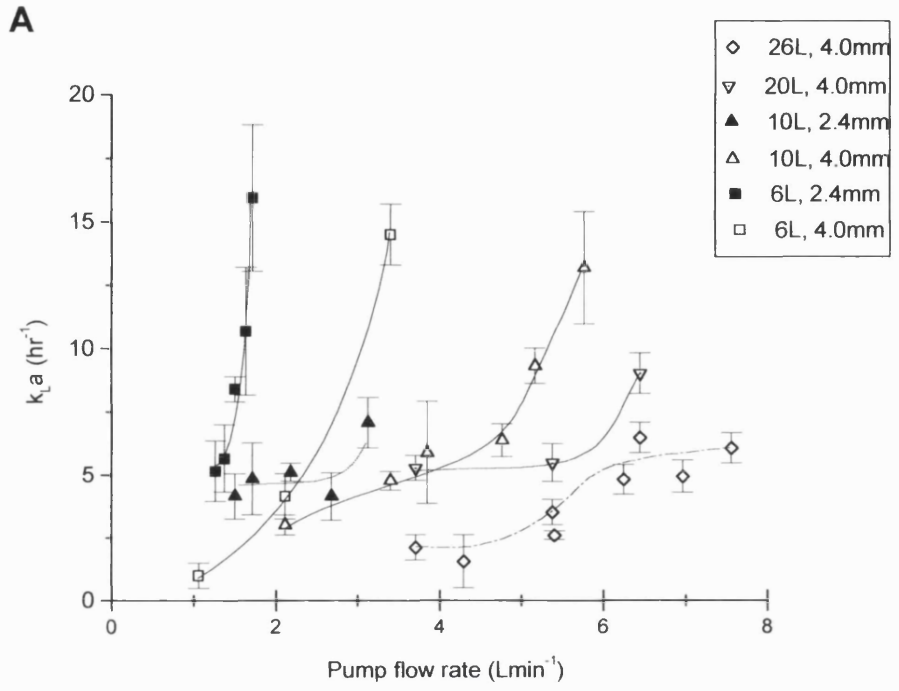

The figure shows respectively the effect of the pump flow rate (L min^{-1}) on the k_La (hr^{-1}) for various plunging jet reactors. The reactors are the 26 L, 20 L, 10 L and 6 L with the 4.0 mm diameter nozzle and the 6 L and 10 L reactors with the 2.4 mm diameter nozzle. The k_La was measured in buffer solution (NaCl 6·4 g L^{-1}, $NaHCO_3$ 2·0 g L^{-1} and Pluronic F68 1·0 g L^{-1}).

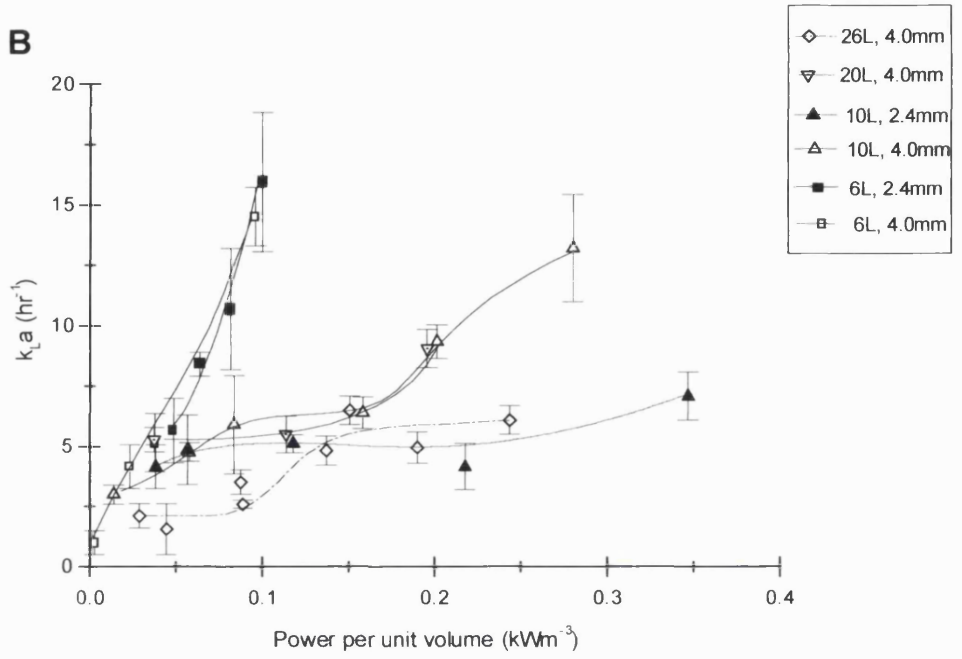

The figure shows the effect of the power per unit volume (kW m^{-3}) on the k_La (hr^{-1}) for various plunging jet reactors. The reactors are the 26 L, 20 L, 10 L and 6 L with the 4.0 mm diameter nozzle and the 6 L and 10 L reactors with the 2.4 mm diameter nozzle. The k_La was measured in buffer solution (NaCl 6·4 g L^{-1}, $NaHCO_3$ 2·0 g L^{-1} and Pluronic F68 1·0 g L^{-1}).

The figure shows that for a power per unit volume from 0 to 0·1 kW m^{-3} the k_La is greater in the 6 L reactor compared to the 10 L, 20 L and 26 L reactors.
For the 6 L reactor operating at specific power per unit volumes between 0 to 0·1 kW m^{-3}, the k_La values are comparable for the 2·4 and 4·0 mm diameter nozzle. For the 10 L reactor at fixed power per unit volumes between 0·1 to 0·3 kW m^{-3}, the reactor with the 4·0 mm diameter nozzle had a higher k_La than the reactor with the 2·40 mm diameter nozzle.

Figure 45 - Measurement of k_La, CO_2 stripping coefficient and mixing for three different volumes

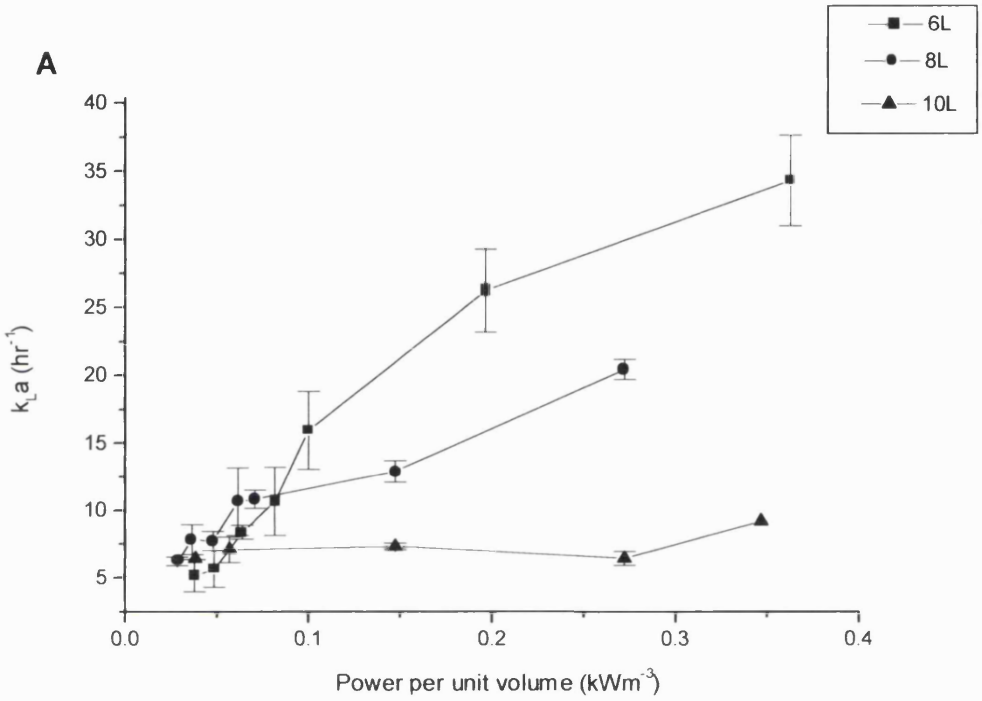

The figure shows the k_La (hr^{-1}) versus the power per unit volume ($kW\ m^{-3}$) for the plunging jet reactors 6 L, 8 L and 10 L with respective aspect ratios of 1.44, 1.80 and 2.20. The k_La values were measured in the buffer solution (NaCl 6·4 g L^{-1}, $NaHCO_3$ 2·0 g L^{-1} and Pluronic F68 1·0 g L^{-1}). All three reactors have a 2.4 mm diameter nozzle.

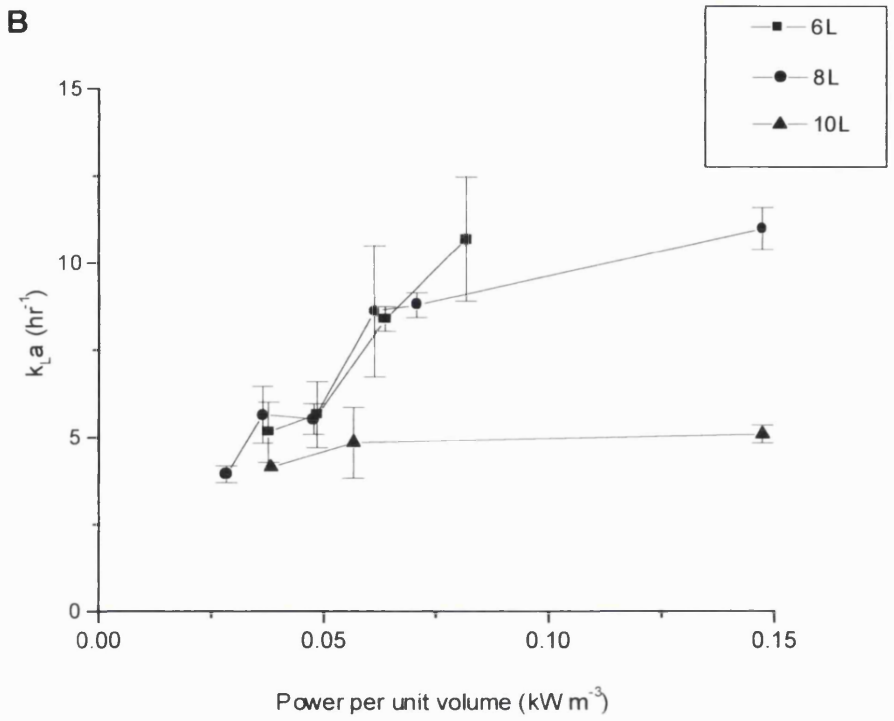

The figure shows the k_La (hr^{-1}) versus the power per unit volume ($kW\ m^{-3}$) for the plunging jet reactors 6 L, 8 L and 10 L with respective aspect ratios of 1.44, 1.80 and 2.20. The results are those of figure A but are presented at a smaller power per unit volume scale.

Both figures 45 A and B shows that at equivalent power per unit volumes the 6 L reactor has a significantly higher k_La than either the 8 L or the 10 L reactor. For the 10 L reactor increasing the power per unit volume results in virtually no increase in the k_La so that at comparable power per unit volume it has the lowest k_La. For the 6 L and 8 L reactors the k_La increases with the power per unit volume.

Figure 45 B shows at equivalent power per unit volumes from 0 to 0·1 $kW\ m^{-3}$, the k_La values for the 6 L and 8 L reactors are comparable; whilst for the 10 L reactor the k_La values are significantly lower.

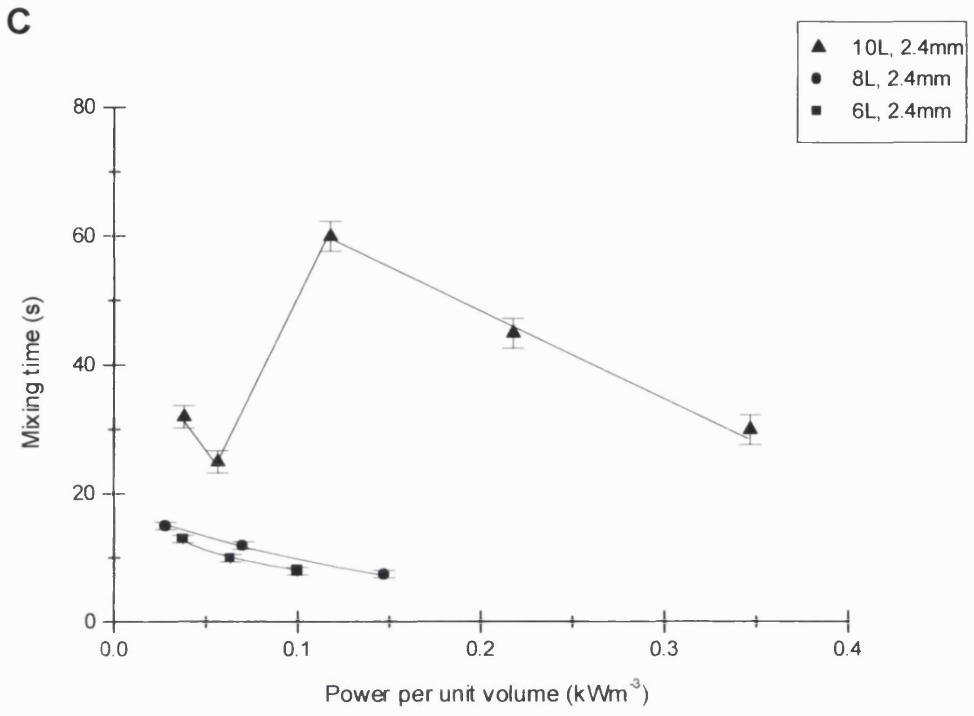

The figure shows the mixing time(s) versus the power per unit volume (kW m^{-3}) measured in the pluronic F68 solution for the 6 L, 8 L and 10 L plunging jet reactors with a 4.0 mm diameter nozzle.
At equivalent power per unit volumes the mixing times for 6 L and 8 L plunging jet reactors are virtually comparable. For both these plunging jet reactors increasing the power per unit volume results in a decrease in the mixing time.
At equivalent power per unit volumes, the mixing time for the 10 L plunging jet reactor are significantly greater. For this reactor an increase in the power per unit from 0·05 kW m^{-3} to 0·1 kW m^{-3}, results in an increase in the mixing time from 25 ± 3 seconds to 60 ± 4 seconds. Subsequent increases in the power per unit volume from 0·1 to 0·35 kW m^{-3} results in a decrease in the mixing time from 60 to 30 ± 4 seconds.

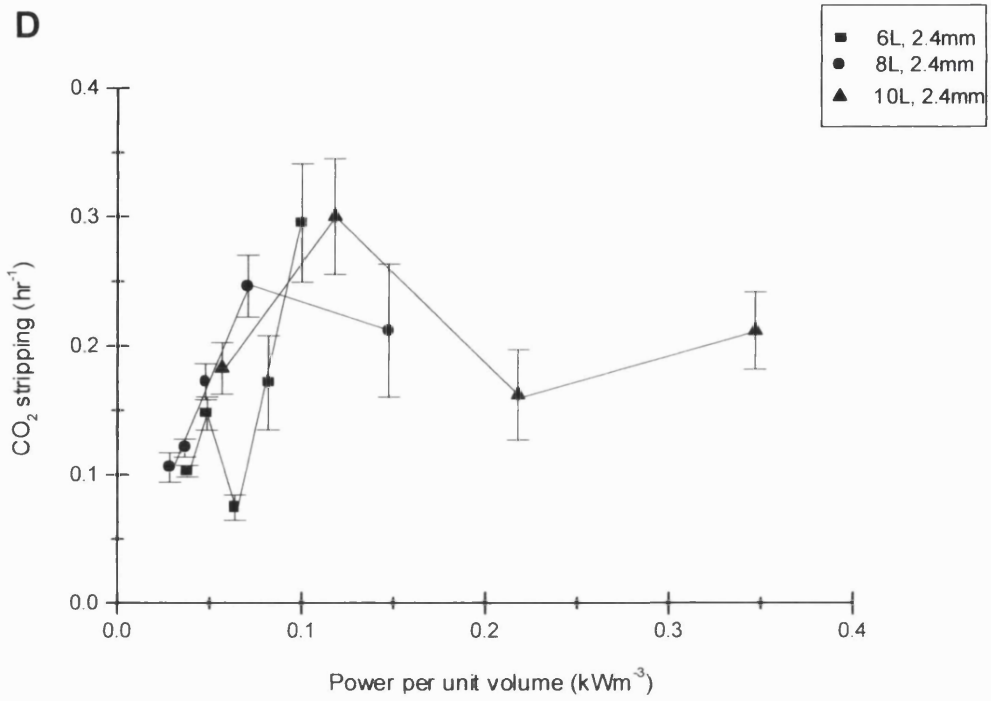

The figure shows the CO_2 stripping coefficient (hr^{-1}) versus the power per unit volume ($kW\ m^{-3}$) measured in the buffer solution (NaCl 6·4 g L^{-1}, $NaHCO_3$ 2·0 g L^{-1} and Pluronic F68 1·0 g L^{-1}) for the 6 L, 8 L and 10 L plunging jet reactors.

The figure shows that for all three reactors increasing the power per unit volume from 0 to 0·1 kW m^{-3}, results in an increase in the CO_2 stripping coefficient. For both the 10 L and 8 L reactor the power per unit volume was increased beyond 0·1 kW m^{-3}, which resulted in a decrease in the CO_2 stripping coefficient.

Figure 46 A – Picture of the plunging jet reactor without 'foam effect'

The figure shows the plunging jet reactor where there is no build up of the entrained air bubbles and thus no 'foam effect' at the upper part of the reactor.

Figure 46 B – Picture of the plunging jet reactor with the 'foam effect'

The figure shows the plunging jet reactor where there is a build up of entrained air bubbles, which create the 'foam effect' at the upper part of the reactor.

7.3 Conversion of an airlift from Conventional to Disposable

7.3.1 Aims and overview

The aim of this work is to design a disposable airlift bioreactor in order to evaluate whether the conventional airlift can be used as a disposable. The comparison between the airlift and bubble column shows that at a scale of 26 L, the performance of the two bioreactors were comparable. Thus at this scale both the airlift and bubble column are valid options for conversion into disposable equipment. As the scale increases it is likely that the airlift's performance will be better than that of the bubble column. This is because as discussed in section 7.2.4.2 several authors have stated that the airlift's mixing and aeration efficiency is superior to a bubble column (Varley and Birch, 1999; Verlaan et al, 1988; Margaritits and Sheppard, 1981; Orazem and Erickson, 1979; Hatch, 1975 and Siegel and Merchuk, 1988). In considering whether these two bioreactors can be converted to disposable equipment, the airlift presents the greater challenge because its construction is more complex. Thus this section considers how to convert an airlift from fixed stainless steel to disposable plastic. The two key issues are that the airlift must be easily constructed and must allow reproducible construction.

7.3.2 Design of a disposable airlift bioreactor

Figure 47 A to C, pages 289 to 291 shows the final design for the disposable airlift reactor. The airlift was an internal rather than an external airlift. This is because although an external airlift has a greater liquid circulation (Chisti and Moo-Young, 1987; Bello et al 1984) an internal airlift is easier to construct and is the conventional choice for an animal cell airlift. As described in chapter 5, according to Hyclone Europe a cylindrical shaped bag is difficult to construct and thus a circular airlift must be formed by stretching a square bag into a circular shaped support. Inserting a square airlift with a divider attached at two diagonally opposing corners, into a circular support, will result in the divider lacking tension. This is because the diagonal length of the square bag is

slightly greater than the diameter of the support. The divider could be tensioned, by using two anchored lines on either side of the spilt to support the divider. Alternatively the bag could be clamped into a hinged support along the axis of the split using the specially attached 'wings' on the bag. It was decided that both of these options were too complex and that a square bag should be inserted into a square support. Although a square airlift could have zones in the three corners for both the riser and downcomer, where the mixing was sufficiently less than in the bulk; it was thought that the airlift could be designed with sufficient mixing so that this difference in mixing was minimised. According to Christi and Moo-Young (1987), square and rectangular cross sections have practical applications in industry. A rectangular airlift was not used because although the mass transfer is increased, the amount of coalescence is reduced (Gasner, 1974). An increase in the mass transfer is not required but a reduced coalescence leads to smaller sized bubble. These smaller sized bubbles cause more damage to cells at the gas disengagement zone and have a greater tendency to be carried over into the downcomer, where they can cause an increase in the amount of CO_2 (Gray et al 1996; Aunins and Henzler, 1991; Handa et al 1987; Tramper et al, 1986; Chalmers and Bavarian, 1991; Bavarian et al, 1991; Orton and Wang, 1990; Newitt et al, 1954; Garner et al, 1954; Gardner et al, 1990; Murhammer and Goochee, 1988). The base had a flat rather than curved bottom. This is because although a flat bottom will give bubble free or dead zones at the corners, it is easier to specify a flat base so that the sparger pipes, drain tube and sample tube are attached to the bottom. The aspect ratio typically varies between 1:6 to 1:12 (Varley and Birch, 1999). An aspect ratio of 1:6 was chosen partly because a lower height airlift has a lower mixing time. In a concentric airlift increasing the height results in an increase in the mixing time, which is particularly pronounced at low gas flow rates typical of animal cell culture. This is because the circulation path is increased so that the distance between the end sections where the bulk of the dispersion occurs is increased (Russell et al, 1994; Verlaan et al, 1986).

The baffle was positioned so that the riser was equal to the downcomer. The divider is fixed at two opposing corners so that it diagonally dissects the airlift in two equal sized triangular cross sections, which are the downcomer and riser. By attaching the divider

into the corners the strength and complexity of the welds are not altered. Also the exact position at which the divider is positioned is very important to the performance of the airlift. The ratio of the riser to downcomer affects the specific mixing time, where for internal loop reactors, positioning the baffle so that the riser cross sectional area is equal to the downcomer area has the best mixing (Bello et al 1984; Varley and Birch, 1999). The riser to downcomer ratio has also been reported to affect the mass transfer (Chisti and Moo-Young, 1987; Griffiths, 1988). Thus by inserting the baffle in the corners, the area of the downcomer and riser will consistently be equal between different vessels. The vertical position for the baffle must also be consistent between vessels. This is because both the bottom and top clearance affects the performance of the airlift. For the clearance at the bottom, the cross sectional area for the fluid flow from the downcomer to the riser must not exceed 1·65 times the cross sectional area of the downcomer. An airlift with a downcomer clearance that exceeds these dimensions will have a large volume located between the lower end of the downcomer and reactor base, which is mainly free of bubbles (Christi and Moo-Young, 1987). For the clearance above the baffle, the height of liquid must not exceed 0·5 m because the mixing time will significantly increase (Christi and Moo-Young, 1987).

The sparger chosen was a perforated pipe because it is cheap to install and operate (Christi and Moo-Young, 1987). The sparger must be located above the divider rather than below it (Christi and Moo-Young, 1987). Since the air delivery effects the function of the airlift and therefore the reproducibility, the sparger must be fixed in place. In the design the sparger pipe runs down the divider so that it provides extra support for the divider. Since there is little information on sparger design the size of holes were determined by the size of bubbles required (Heijnen, and Van't Riet., 1984; Aunins and Henzler, 1991). Appendix 9.1 discusses the effect of the size of holes on the bubble size in greater detail. It is assumed that the culture media has properties, which are between coalescing and non-coalescing media. The airlift requires bubbles that at some distance from the sparger, have a diameter between 4 mm to 6 mm. In coalescing systems by a process of dispersion and coalescence, bubbles will have a diameter of about 6 mm. In non-coalescing systems, the bubbles remain at the same size that they were at the sparger.

Thus the equations 9.0 and 9.1 (page 304 to 305) which determine the size of the bubble at the sparger are used to set the bubble diameter between 4 mm to 6mm. Since the superficial velocity at which there is a transition from the separate bubble formation to the chain bubbling regime is not known both equations 9.0 and 9.1 are used. For a range of superficial velocities between 0·0037 m s^{-1} to 0·015 m s^{-1}, the equation 9.0 for the separate bubble formation specified the smallest bubble diameter and thus was used to set the hole diameter. For practical reasons the hole diameter was limited to a maximum of 2 mm (a larger hole allows water back up the sparger pipe).

Assuming separate bubble formation regime

$$db = 1.7\left(\frac{\sigma do}{\Delta \rho g}\right)^{1/3} \qquad \text{(Equ. 9.0)}$$

(van Krevelen and Hoftijzer, 1950; Perry and Chilton, 1973)

Assuming σ = 0·0727 N m^{-1}, $\Delta\rho$ = 1000 kg m^{-3} and g = 9·8 m s^{-1}
For a hole diameter, do = 2×10^{-3} m, the diameter of the bubbles produced at the sparger is calculated as 4·2 mm.

For a hole diameter of 2 mm the equation 9.1, page 305 for chain bubbling predicts that the diameter of the bubbles produced at the sparger to be 4·8 mm and 8·3 mm for superficial velocities of 0·0037 m s^{-1} and 0·0150 m s^{-1} respectively.
The number of holes was set so that the total area of the holes is equal to the area for the sparger pipe. For a sparger pipe of 6·4 mm in diameter, 10 × 2 mm holes were used. These ten holes were evenly spaced as shown in figure 47 C, page 291. The sparger pipe is also sloped downwards with an additional hole at the bottom (drain hole), so that water can be easily cleared from the sparger pipe.

The number of ports required was kept to a minimum, so that the design was as simple as possible. The ports were the sample tube, drain tube, gas inlet that connects to the sparger tube, the gas outlet and two ports, which connected to the headspace.

7.3.3 Method of monitoring the disposable airlift bioreactor

With current technology it is not possible to use monitoring systems which are installed prior to sterilisation by gamma irradiation or to insert sterile probes into a bag after gamma irradiation. Thus during the operation, samples are taken to determine the DOT, pCO_2, pH and temperature. A thermopocket where a thermacouple could be inserted, was not used in the design because it was too complicated for the manufacturers. The bag is well insulted since it consists of three layers of plastic. This means that whilst the temperature can't be measured reliably from the outside, the internal temperature can be maintained with a water jacket around the bag. A non-sterile version which has several additional inserts for thermacouples and DOT probes, must be used to determine the temperature of the jacket and the k_La of the airlift at different gas flow rates. This information can then be used to operate a sterile version, which has no internal DOT or temperature measurements.

Figure 47 – Disposable 10 L Airlift

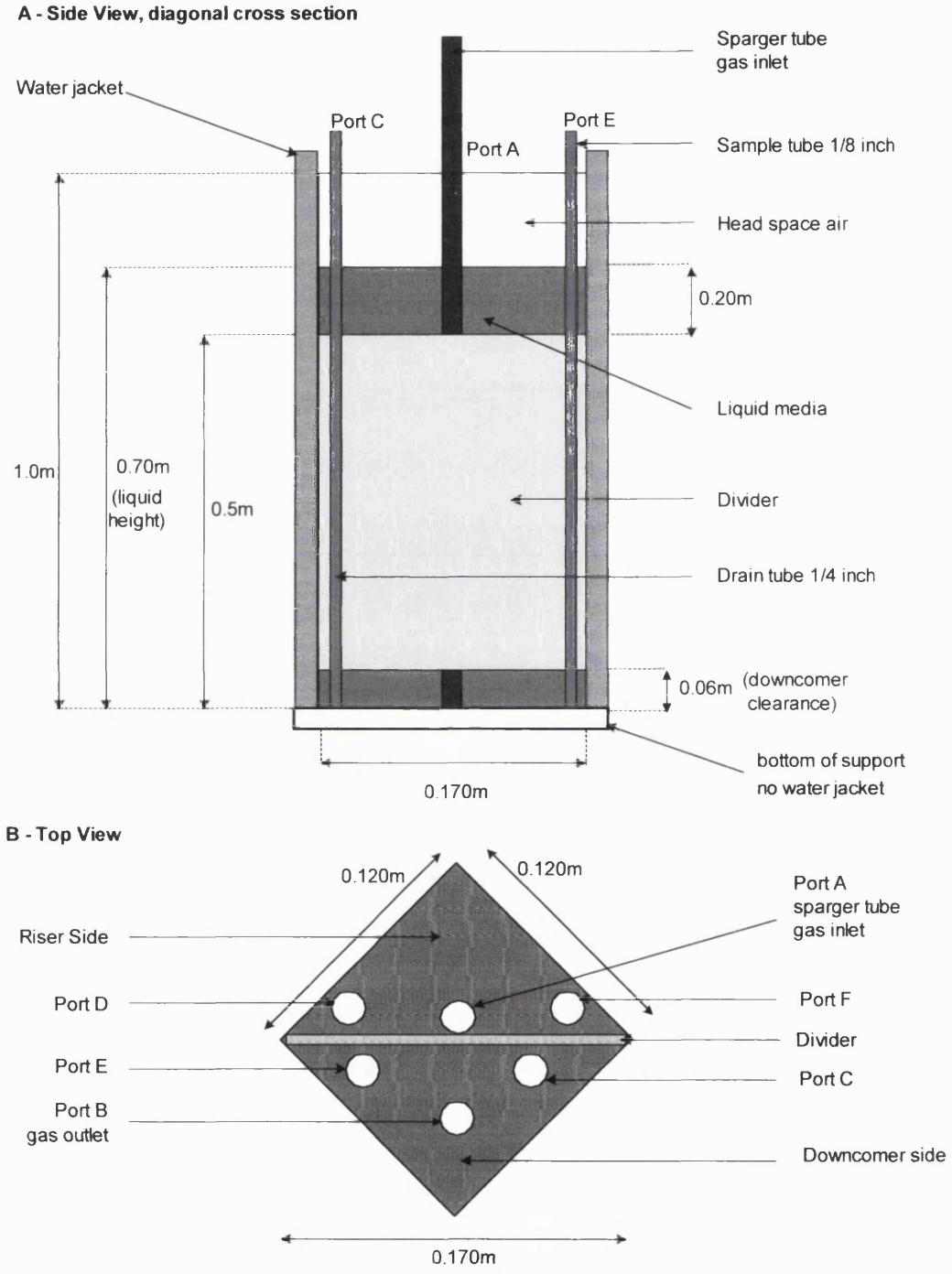

Figure 47 A

This figure shows the diagonal cross section of the 10 L disposable airlift reactor from the side view. The diagram shows the bag located in the perspex support, which has a water jacket along the two vertical sides. The diagram shows the internals, which are a divider, a sample tube, drain tube and sparger tube. The drain, sample and sparger tubes are all attached at the bottom of the bag.

Figure 47 B

This figure shows the diagonal cross section from the top view so that the location of each port is shown.

Port A is the gas inlet
¼ inch tubing of length 0.2m connects the sparger tube with the outlet end of a Millipore Millex FG50 0.2 μm Cat. No. SLFG85000. The inlet of this filter is connected to silicon tube of length 0.4m,

Port B is the gas outlet
½ inch tubing of length 0.4m connects head space to the inlet end of a Millipore Opticap 4 inch aervant Cat. No. KTGR04HB3. There is also two spare cflex tubes each 0.2m in length which branch off the ½ inch pipe and are sealed at the ends. This is so that additional outlet filters can be added if they are required. The outlet of the filter is connected to a ½ inch tubing of length 0.4m.

Port C
¼ inch tubing of length 0.2m connects drain pipe to a divider which splits into 4 cflex lines which are each 1 m in length (Hyclone UK Ltd. 1/8 inch Cat no. 082-125-2).

Port D
¼ inch tubing of length 0.2m connects headspace to a divider which spilts into 3 cflex lines which are each 1m in length (as before).

Port E
¼ inch tubing of length 0.1m connects the sample tube with a divider which spilts into 2 cflex lines each 0.5 m long. The free ends of the cflex is sealed.

Port F
¼ inch tubing of length 0.2m connects the headspace with 1m of cflex tubing (as before). The free end of the cflex is sealed.

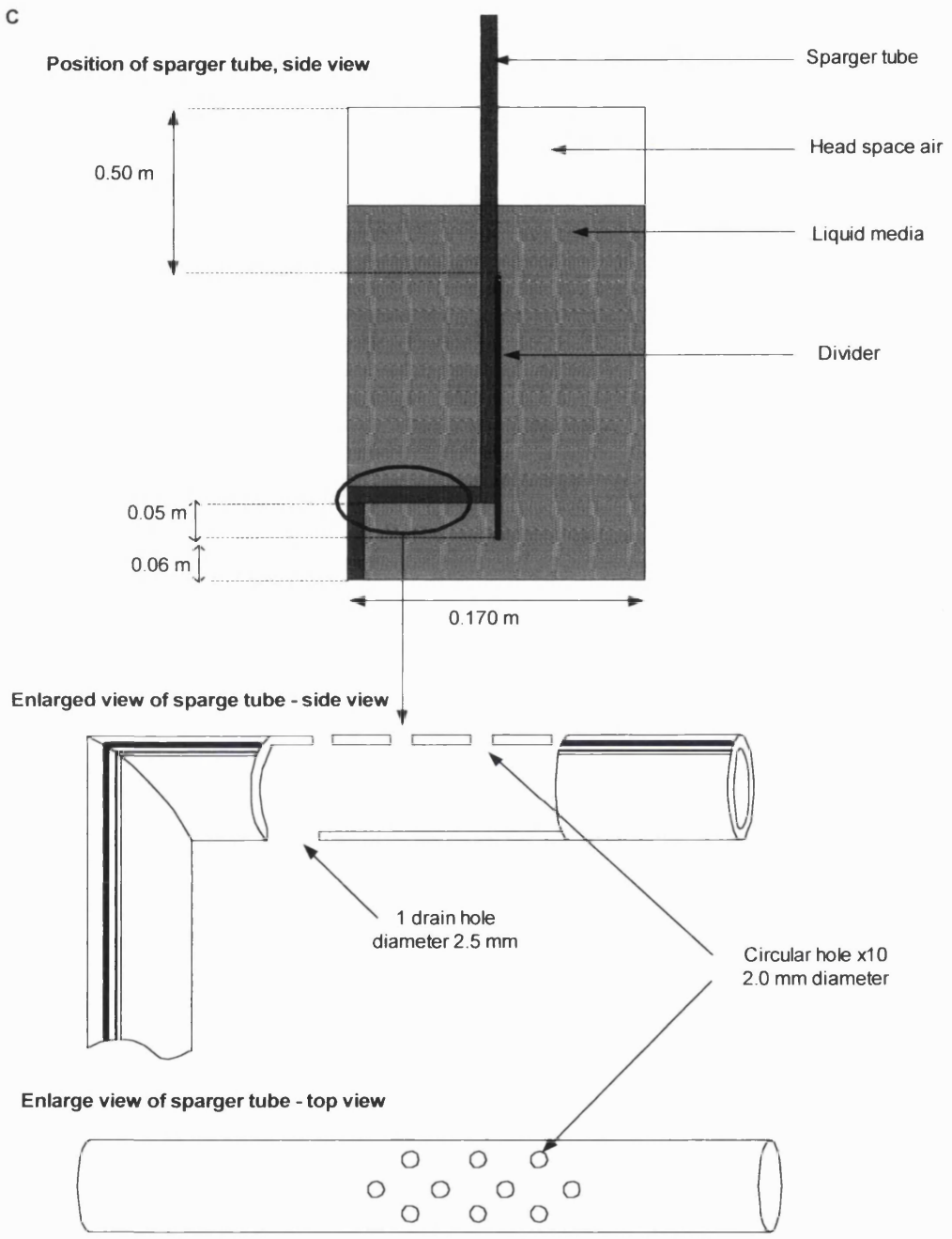

Figure 47 C
This figure shows the internal position of the sparger tube in the airlift and an enlarged diagram of the horizontal section of the sparger tube with the 10 sparger holes and the 1 drain tube from both the side and top view. The 10 sparger holes are all 2.0 mm in diameter whilst the drain tube is 2.5 mm in diameter. The sparger is positioned in the bag so that the middle section with the 10 holes is horizontal when the bag rests flat on the bottom of the perspex support.

7.4 Discussion

The aim of this chapter was to evaluate which of the bubble column, airlift and plunging jet reactor was the best option as a disposable animal cell bioreactor. The basis of this evaluation is whether each disposable animal cell bioreactor can match the k_La, CO_2 stripping and mixing targets measured in an airlift. These targets were measured in an airlift at superficial velocities of 0·01 m s^{-1} and 0·015 m s^{-1}, which are respectively the lower and upper maximum superficial velocities that an airlift is operated at during a large scale animal cell culture for biopharmaceutical manufacture. Table 19 page 254 shows the maximum targets, which are 6.3 to 8.9 hr^{-1} for k_La, 0.34 to 0.49 hr^{-1} for CO_2 stripping and 15 to 13 seconds for mixing.
Subsequently for the reactor selected, a disposable bioreactor should be designed and a comparison with a conventional airlift or stirred tank animal cell bioreactor should be performed. Due to the lack of available sterile bags, no such comparison could be performed. The work performed was sufficient to evaluate the merits of each reactor as an animal cell bioreactor, which is discussed below.

7.4.1 The plunging jet reactor

The work presented in this chapter culminates in evaluating whether a 6 L plunging jet reactor is a potential disposable animal cell bioreactor. The k_La, CO_2 stripping and mixing were measured for the 6 L reactor and both the 8 L and 10 L reactors as a comparison. Since animal cells are sensitive to shear, for animal cell culture the shear in the nozzle should be limited to 15000 s^{-1}, which corresponds to a shear stress of 15 N m^{-2}. For the 6 L, 8 L and 10 L reactors, table 23 page 273 shows for each reactor the power per unit volume that corresponds to this shear rate

Operating the 6 L reactor with the 2.4 mm nozzle at its maximum power per unit volume of 0.10 kW m^{-3} results in a k_La of 16 ± 2.90 hr^{-1}, mixing of 8 ± 1 seconds and CO_2 stripping of 0.30 ± 0.04 hr^{-1}. Thus whilst the upper targets for k_La and mixing are easily attained, the maximum stripping of 0.03 ± 0.04 hr^{-1} was just within range of the lower

target of 0.34 ± 0.01 hr^{-1}. Thus the performance of the bioreactor is limited by CO_2 stripping. The 10 L reactor with the 2.4 mm nozzle operating at its maximum power per unit volume of 0.06 kW m^{-3}, resulted in a k_La of 4.9 ± 1.4 hr^{-1}, CO_2 stripping of 0.18 ± 0.02 hr^{-1} and mixing of 25 ± 3 seconds. Thus the lower targets for k_La, CO_2 stripping and mixing were not attained by the 10 L reactor. For both the 6 L and 10 L reactor the k_La was measured using both a 2.4 mm nozzle and a 4.0 mm nozzle. These results show that for the 6 L reactor at equivalent power per unit volume below its maximum of 0.1 kW m^{-3}, the k_La values are the same for both the 2.4 mm and 4.0 mm nozzle. For the 10 L reactor at equivalent power per unit volume below 0.06 kW m^{-3}, the k_La values are the same for both the 2.4 mm and 4.0 mm nozzle. Operating the 10 L reactor at equivalent power per unit volume greater than 0.06 kW m^{-3}, the k_La values are greater with the 4.0 mm nozzle than the 2.4 mm nozzle. Thus for the 10 L reactor, the upper k_La target of 8.9 hr^{-1} is only achieved below the reactor's maximum power per unit volume with the 4.0 mm nozzle. These results imply that increasing the reactor volume requires an increase in the nozzle diameter. This requires further investigation by measuring the CO_2 stripping and mixing in the 10 L reactor with the 4.0 mm nozzle to determine whether the values at equivalent power per unit volumes are greater with the 4.0 mm nozzle than the 2.4 mm nozzle.

The poor performance in the 10 L reactor with the 2.4 mm nozzle could be attributed to the observation that as the aspect ratio increased from 1.44 to 2.20, the presence of small bubbles located towards the top of the reactor volume were observed which created a 'foam effect'. For the 10 L reactor it was observed that these small bubbles increased in number as the power per unit volume increased. This effect is not observed in water and was attributed to the surfactant in the media. This surfactant is present in the media to protect the cells from shear associated damage principally from bursting bubbles and thus must be present. This foam effect is shown in figures 46 A and B, pages 282 to 283.

The presence of small bubbles in the upper part of the 10 L reactor highlights that the entrained air bubbles could cause significant damage. As discussed in section 1.3.2.1 cell damage in suspension culture is almost entirely due to bubble aeration since in the

absence of bubbles extreme agitation is required to induce cell damage (Oh et al, 1989; Kunas and Papoutsakis, 1990). Thus the presence of these bubbles in the 10 L reactor with the 2.4 mm nozzle is likely to result in significant cell damage. According to Bin (1993), the diameter of the bubbles is less than 1 mm in the inner part of the plume and between 3 to 4 mm in the outer part. Another study measured the mean diameter of the bubbles to be 2 mm (Bonetto and Lahey (1993)). These bubble diameters are significantly greater than the 4 to 6 mm bubble diameters that occur in both an airlift and bubble column. Since cell death increases with a decreasing bubble diameter, the plunging jet bubbles are likely to cause more damage (Aunins and Henzler (1991), Tramper et al (1986), Chalmers and Bavarian (1991), Bavarian et al (1991), Orton and Wang (1990), Newitt et al. (1954), Garner et al. (1954), Gardner et al (1990), Murhammer and Goochee (1988)).

Whilst at a 6 L scale the plunging jet reactor's CO_2 stripping performance was below that of the airlift, this is not the only reason for concluding that this reactor is not a suitable option as a disposable animal cell bioreactor. The observations and results presented in this chapter suggest that there are significant problems in increasing the scale of the reactor. The results suggest that increasing the aspect ratio requires an increase in the nozzle diameter. Whilst increasing the nozzle diameter will reduce the shear in the nozzle, the higher volumetric flow rate may result in greater shear damage in the bubble plume and in the pump due to the faster circulation time. An animal cell bioreactor requires sufficient mass transfer and mixing so that the cells are in a homogeneous environment and remain in suspension. For a large scale plunging jet this would require multiple nozzles with a low aspect ratio vessel so that the shear rate in each nozzle did not exceed 15000 s^{-1} and to prevent the presence of small bubbles in the upper part of the reactor creating the 'foam effect'. If further work showed that the 6 L reactor could support an animal cell culture for a 7 day period, the operating window is likely to be highly constrained. This is because the reactor must be scaled up without shear damage from the nozzle and bubbles in the plume but with sufficient mass transfer and mixing. The principal reason for using a disposable bioprocess is flexibility and speed of manufacture from concept to delivery. Clearly a disposable animal cell bioreactor which

is likely to have a highly constrained operating window is not suitable as a disposable bioreactor.

7.4.2 Airlift versus bubble column

The work presented in this chapter shows that at a small scale the bubble column and airlift have equivalent physical performance. Published work has shown that at a larger scale, the airlift outperforms the bubble column for both aeration and mixing so that in industry the conventional non-mechanically aerated bioreactor is the airlift. Thus the airlift is more scaleable than the bubble column. The only structural difference between the bubble column and the airlift, is the presence of the divider in the airlift. The disposable airlift presented in this chapter has a square cross sectional area so that the divider is inserted across the diagonal. This insures that the divider is taut and can be welded as part of the seams. Thus the construction of this design is not sufficiently more complex than a bubble column that it can not be used as a disposable animal cell bioreactor. Since the airlift is more scaleable than the bubble column, it is the preferred choice as a disposable animal cell bioreactor. As discussed below a sterile version of the proposed airlift design should be used to determine whether it can support an animal cell culture and whether the culture can be monitored by taking samples from the sample tube.

7.5 Future Work

The airlift was selected as the most suitable option as an animal cell bioreactor. A non sterile version of the 10 L reactor should be obtained which has additional ports for DOT, pH and temperature probes so that a comparison with a 10 L conventional stainless steel airlift can be made on the basis of physical performance. The k_La, CO_2 and mixing times should be measured versus the gas flow rate for both the disposable and conventional airlift. The gas flow rate should be limited to a superficial velocity of 0.015 m s^{-1} in the conventional airlift.

A sterile version of the 10 L reactor should be obtained in order to perform a comparison with the conventional airlift on the basis of the resultant performance of the animal cell culture. This comparison should be based on performing the same animal cell culture, a hybridoma in suspension culture in both the conventional and disposable bioreactors. The comparison should be based on the growth rate and the concentration of product produced over the animal cell culture time. The conventional airlift should be operated with the typical control and monitoring equipment of an integral pH probe, DOT probe and temperature probe. Unlike with the plunging jet reactor, the airlift lacks a loop for insertion of a heat exchanger and monitoring and control equipment. The method of monitoring and control of the disposable animal cell bioreactor is particularly important since as discussed in animal cell requirements section 1.2.3.1, animal cells are sensitive to the concentration of carbon dioxide and pH. Since at the time of writing this thesis there was no suitable disposable integral monitoring equipment for the disposable airlift, the bioreactor should be monitored by taking samples via the sample tube to measure the DOT, pH, Carbon dioxide and temperature. If the airlift was successfully controlled by taking samples via the sample tube, then an at line monitoring device could be used in subsequent runs so that monitoring and control was more automated. The profile of the k_La versus the gas flow rate measured in the non sterile version of the disposable airlift should be used to determine the gas flow rates required throughout the animal cell culture.

7.6 Summary

A comparison between the airlift, bubble column and plunging jet reactor was performed to determine which reactor was the most suitable as a disposable animal cell bioreactor. The basis of the comparison was the k_La, CO_2 stripping and mixing, which were measured for an airlift at superficial velocities of 0.01 and 0.015 m s^{-1}, the typical maximum superficial velocities used for large scale animal cell culture. The resulting k_La, CO_2 stripping and mixing measurements were used as the targets for the bubble column and plunging jet reactor. These targets were 6·3 hr^{-1} to 8·9 hr^{-1} for the k_La target, 0·34 hr^{-1} to 0·49 hr^{-1} for the CO_2 stripping coefficient target and 15 to 13 seconds for the mixing time.

Whilst initial studies were performed on a 26 L plunging jet reactor, its performance was not comparable to the bubble column and airlift and thus 6 L to 10 L plunging jet reactors were used. For these reactors a maximum power per unit volume was determined which corresponded to a shear stress and rate of 15 N m^{-2} and 15000 s^{-1} respectively. Operating the 6 L reactor with the 2.4 mm nozzle below its maximum power per unit volume resulted in both the upper k_La and mixing targets but only the lower CO_2 stripping target. Operating the 10 L reactor with the 2.4 mm nozzle at its maximum power per unit volume resulted in k_La, CO_2 stripping and mixing values which were all above their targets. This poor performance for the 10 L reactor with the 2.4 mm nozzle, was attributed to the observation of small bubbles located towards the top the reactor volume, which created a 'foam effect'. The k_La was measured for the 10 L reactor with the 4.0 mm nozzle where the upper k_La target was achieved within the reactor's maximum operating power per unit volume. Thus these results indicate that increasing the scale of the reactor requires an increase in the nozzle diameter and thus the pump flow rate. Although this high pump flow rate would minimise shear in the nozzle, cell damage may result from excessive circulation of cells through the pump and bubble plume. Whilst further work is required to prove that a cell culture can not be supported by a plunging jet reactor, it was concluded that the plunging jet reactor was not a suitable option as a

disposable animal cell bioreactor since any operating window is likely to be highly constrained.

The 26L bubble column and airlift showed comparable performance. At equivalent power per unit volumes, the k_La values were comparable between the two reactors. The CO_2 stripping values were comparable at power per unit volumes less than 0.056 kW m^{-3} but at higher power per unit volumes the CO_2 stripping was greater in the airlift. At the equivalent power per unit volumes the mixing time was marginally lower in the bubble column than the airlift. Thus this work shows that at a small scale the bubble column reactor is suitable as a disposable animal cell bioreactor. Since published work has shown that at a larger scale, the airlift outperforms the bubble column for both aeration and mixing, the design of the airlift was evaluated as a potential disposable animal cell culture for large scale culture. Although the plunging jet reactor has the simplest construction, experimental work concluded that it was not a suitable disposable animal cell bioreactor and thus the construction of the airlift was compared with the bubble column. The only structural difference between these two reactors is the presence of the divider in the airlift. The design presented in this chapter has a square cross sectional area so that the divider is inserted in a diagonal position insuring that it is taut. The design also proposed a method of inserting the sparger so that it remained fixed during operation and could be reproducibly constructed between vessels. Thus it was concluded that the airlift was the preferred option for a disposable animal cell bioreactor. Future work should involve using a sterile version of the proposed airlift design to determine whether it can support an animal cell culture and whether the culture can be monitored and controlled by taking samples from the sample tube.

8 Discussion

For the microbial bioreactor further work is required to establish whether the plunging jet reactor is suitable as a disposable microbial bioreactor. The plunging jet bioreactor used for the comparison with the conventional stirred tank bioreactor presented in chapter 6 is not suitable as a disposable microbial bioreactor. This is because whilst the physical performance of the plunging jet bioreactor does meet the requirements of microbial bioreactor, the resultant performance of the fermentation does not.

The comparison between the physical performance of the plunging jet bioreactor and the stirred tank bioreactor showed that the maximum k_La were comparable where it was 0.12 s^{-1} in the stirred tank bioreactor and 0.13 to 0.15 s^{-1} in the plunging jet bioreactor. These comparable k_La values were achieved with a higher maximum power per unit volume in the stirred tank bioreactor of 11.2 to 12.7 kW m^{-3} compared to 1.4 kW m^{-3} in the plunging jet bioreactor. The maximum shear rate for the plunging jet bioreactor was 85000 s^{-1}, which was greater than the maximum shear rate in the stirred jet bioreactor of 13000 to 13500 s^{-1}. The mode of operation to maintain the DOT above 10 to 20 % for the two bioreactors was different. For the plunging jet bioreactor the k_La increases with the OUR so that the bioreactor is operated with a fixed power per unit volume. Operating the stirred tank bioreactor at a fixed power per unit volume results in a k_La that is fixed whilst the OUR increases. Thus for the stirred tank the power per unit volume was periodically increased resulting in an instantaneous increase in the k_La. For the plunging jet bioreactor the k_La was affected by the position of nozzle with respect to the outlet. For the plunging jet bioreactor operating at a power per unit volume of 1.4 kW m^{-3} with the Fab fermentation at an OUR of 5 mol L^{-1} hr^{-1}; the k_La increased from 0.005 s^{-1} to 0.045 s^{-1} as a result of moving the nozzle angle from vertical (0°) to 5° away from the outlet (-5°).

For both the Wild Type and Fab fermentations there are distinct differences between the resultant performance of these fermentations in the stirred tank bioreactor and in the

plunging jet bioreactor. The Wild Type fermentation was grown as per the protocol in the stirred tank bioreactor whilst in the plunging jet bioreactor lysis occurred within the first 140 minutes of the fermentation. Whilst the Fab fermentation was grown as per the protocol in the both the plunging jet bioreactor and the stirred tank bioreactor, there were significant differences in the resultant performance between the two bioreactors. In the plunging jet bioreactor the Fab fermentation had both a lower maximum OUR and a lower final dry weight. In addition the RQ varied between 0.5 to 1.0, where addition of glycerol resulted in an increase in the RQ. The Fab fermentation is an industrial fermentation that produces a product, a fragmented antibody within the microbial cell, which is then extracted by subsequent downstream processing. In the stirred tank bioreactor the final Fab concentration in the solid and supernatant fractions were 75 mg L^{-1} and 14 to 22 mg L^{-1} respectively. The final Fab concentration in the plunging jet bioreactor was zero in the solid fraction and negligible in the supernatant fraction. A likely explanation for the difference in the final Fab concentration between the two bioreactors is that in the plunging jet bioreactor shear causes the outer polysaccharide layer of the cell to be stripped away. This results in the release of the Fab product, which is then subsequently eroded by the action of shear so that it loses its defined structure. Despite the microbial cell losing its polysaccharide layer it still remains viable and continues to grow (Hewitt et al, 1998).

For the both the Wild Type and Fab fermentations, the most likely explanation for the observed differences in the resultant performance of the fermentations is that the shear rate is higher in the plunging jet bioreactor than the stirred tank bioreactor. Although this requires further investigation as discussed in section 7.5 it is likely that for the plunging jet bioreactor to be a viable disposable microbial bioreactor, the shear rate must be reduced without reducing the k_La. The best potential solution is to use the high turbulence nozzle developed by Kenyeres, which increases the oxygen transfer efficiency of the nozzle by 30 to 60%. Thus for the same k_La the high turbulence nozzle would require a lower power per unit volume and shear rate than the basic nozzle used in this thesis. If using the high turbulence nozzle does not result in the same resultant performance of the Wild Type and Fab fermentations in both the plunging jet bioreactor

and the stirred tank bioreactor, then it is likely that the plunging jet bioreactor is not suitable as a disposable bioreactor. In this scenario the bubble column with a plastic sparger as described in Poulsen and Iversen, (1998) would be the best disposable microbial bioreactor. Whilst the bubble column would provide sufficient k_La unlike the plunging jet bioreactor it would lack an external loop in which both heat exchanger and monitoring and control systems can be located.

For the animal cell bioreactor it was concluded that the airlift was the preferred option. The work presented in chapter 7 shows that the plunging jet reactor is not suitable as a disposable animal cell culture bioreactor. The plunging jet reactor's potential as a disposable animal cell culture was evaluated by measuring the k_La, CO_2 stripping and mixing in an airlift and the plunging jet reactor. The targets for the k_La, CO_2 stripping and mixing were measured in the airlift at superficial velocities of 0.01 and 0.015 ms^{-1}, which define the typical maximum superficial velocity range that a large scale industrial airlift operates at during a biopharmaceutical process. The power per unit volume of the 6 L plunging jet reactor was limited to 0.1 kW m^{-3}, which corresponds to a shear rate and stress of 150000 s^{-1} and 15 N m^2 respectively. Both the upper k_La and mixing targets of 8.9 hr^{-1} and 13 seconds respectively were achieved in the plunging jet reactor at below the maximum power per unit volume. At the maximum power per unit volume of 0.1 kW m^{-3}, the CO_2 stripping was just within range of the lower target of 0.034 hr^{-1}. Whilst the 6 L reactor performance is limited by its CO_2 stripping performance this is not the principle reason for concluding that the plunging jet reactor is not suitable as a disposable animal cell bioreactor. The work suggests that there are problems with increasing the scale of the reactor where increasing the aspect ratio probably requires an increase in the nozzle diameter. For a large scale plunging jet bioreactor it is likely that multiples nozzles would be required so that sufficient mixing and mass transfer occurred without the shear rate in the nozzles exceeding 15000 s^{-1} and creating a foam in the upper part of the reactor.

The chapter concludes that the preferred option for a disposable animal cell bioreactor is the airlift. This is because although the results show that at small scale the airlift and

bubble column have comparable performance, at a large scale the airlift has better mixing and aeration. The only structural difference between the airlift and the bubble column is that the airlift has a divider. For the proposed design in section 7.3, the airlift has a square cross-section so that the divider is inserted diagonally across the airlift. This ensures that the divider is taut and is welded as part of the main seams of the airlift. Thus the airlift's construction is not sufficiently more complex than the bubble column and thus is the preferred option for a disposable animal cell bioreactor. This is because the airlift has better performance at the large scale than the bubble column and thus is more scaleable. Further work is required to determine whether the proposed design will result in a 7 day animal cell culture which is comparable to the same animal culture performed in a conventional airlift or stirred tank bioreactor. This would involve performing the same animal cell culture in both the disposable and conventional bioreactor where the comparison would be based on the viable animal cell concentration and the product concentration. Whilst the conventional animal cell bioreactor would be monitored and controlled by integral probes that measure the pH, DOT and temperature, the disposable animal cell bioreactor would be monitored by taking samples via the sample tube. Thus the comparison between the two bioreactors would include evaluating any differences between the two control systems.

This thesis concerned developing a disposable bioreactor for both microbial fermentation and animal cell culture. As the introduction shows the requirements for microbial and animal cell bioreactors are different. The microbial fermentation is fast growing with a typical growth rate of 1 to 3 hours and is relatively insensitive to shear since it has a rigid cell wall and is smaller in size than an animal cell. Thus the microbial bioreactor requires a considerably higher k_La at about 0.1 s^{-1} compared to 8.9 hr^{-1} for the animal cell bioreactor. The animal cell culture is slow growing with a typical growth rate of 24 hours and is sensitive to shear. Although the oxygen transfer rate is considerably lower in an animal cell bioreactor, the animal cell bioreactor requires good mixing to provide a homogeneous environment. Animal cells are sensitive to shear, where cell damage in suspension culture is almost entirely due to the bursting of bubbles. Despite these distinct differences there was a common problem of providing sufficient mass transfer and

mixing without incurring damage due to shear. In the microbial bioreactor whilst the cells are less sensitive to shear the requirement for mass transfer is greater. The scope of this work was limited to providing mass transfer and mixing for both bioreactors. Whilst future work is required to investigate this further, methods for monitoring and control of both disposable bioreactor also requires development.

9. Appendix

9.1 Appendix 1 : Aeration method for bubble columns and airlifts

Spargers can either be divided into static or dynamic spargers. Static spargers include perforated plates, perforated pipes, porous plates and single hole spargers. Dynamic spargers are ejectors, injectors, venturi slot nozzles and slot injectors. The dynamic spargers are more complex to construct than static spargers and require an external liquid circulation via a pump. Of the static spargers, the perforated plates and pipes are the cheapest to install and operate (Christi and Moo-Young, 1987).

The bubble diameter both at the sparger and some distance from the sparger can be estimated using the following equations.

Bubble diameter at the sparger

For the separate bubble formation regime, the diameter of the bubble at the sparger is dependent on the equilibrium between surface tension and buoyancy forces (Heijnen and Van't Riet, 1984). The bubble diameter can be estimated using the following equation 1.0.

$$db = 1.7\left(\frac{\sigma dh}{\Delta \rho g}\right)^{1/3} \qquad \text{(Equ. 9.0)}$$

(Van Krevelen and Hoftijzer, 1950)

Increasing the gas flow rate so that the chain bubbling regime occurs, the bubble diameter is frequency determined and can be estimated using the following equation 1.1 (Heijnen and Van't Riet, 1984).

$$db = 1.17(Vh^{0.4})(dh^{0.8})(g^{-0.2}) \qquad \text{(Equ. 9.1)}$$

(Wallis, 1969; Davidson and Harrison, 1963)

Where db = Diameter of bubble at sparger (m)

dh = Diameter of sparger hole (m)

σ = Surface tension, assumed 0.0727 N m^{-1}

$\Delta\rho$ = Difference in density between liquid and gas, assumed 1000 kg m^{-3}

g = gravitational acceration, assumed 9.8 m s^{-2}

Vh = Superficial velocity at sparger (m s^{-1})

Bubble diameter at a distance from the sparger

The bubble diameter at a distance from the sparger, ds depends on the coalescing properties of the medium and the gas flow rate of the sparging gas. In coalescing systems the bubble reaches an equilibrium diameter that is determined by the following equation 1.2 and thus is rather insensitive to changes in the superficial gas velocity. Turbulent dispersion acts to reduce bubbles that are produced at the sparger with a greater diameter than the equilibrium bubble's diameter. Coalescence acts to increase bubbles that are produced at the sparger with a smaller diameter than the equilibrium bubble's diameter. The equilibrium bubble diameter, ds is estimated by the following equation 1.2 which gives ds in the units m and is typically about 6 mm in diameter in air water systems. (Heijnen and Van't Riet, 1984)

$$ds = 4 \cdot 15 \left(\frac{\sigma^{0.6}}{\left(P/V\right)^{0.4} \rho^{0.2}} \right) \varepsilon^{0.5} + 9 \times 10^{-4} \qquad \text{(Equ. 9.2)}$$

(Calderbank, 1958; Lee and Meyrick, 1970)

In non-coalescing systems for bubbles that are produced at the sparger with a diameter greater than the equilibrium diameter d*, turbulent dispersion acts to reduce the diameter until it is equal to d* given by 1.3. For bubbles that are produced at the sparger with a diameter less than the equilibrium diameter d*, the bubble diameter remains unchanged. Thus the following equations only applies to bubbles that are produced at the sparger with a larger diameter than given by the equation 1.3. (Heijnen and Van't Riet, 1984) For typical superficial velocities of 0.0037 m s^{-1} to 0.011 m s^{-1}, the equilibrium diameter in water is 24 mm to 15 mm. Thus it can be assumed for non-coalescing systems, the bubble diameter at a distance from the sparger is equal to the bubble diameter at the sparger.

$$d^* = 1 \cdot 93 \left(\frac{\sigma^{0.6}}{\left(P/V\right)^{0.4} \rho^{0.2}} \right) \qquad \text{(Equ. 9.3)}$$

(Lehrer, 1971)

$$P/V = \rho g V s \qquad \text{(Equ. 9.4)}$$

(Roels and Heijnen, 1980)

Where ds = diameter of bubble, some distance from sparger (m)

(P/V) = power per unit volume (W m^{-3})

ρ = density, assumed 1000 kg m^{-3}

σ = surface tension, assumed 0.027 N m^{-1}

ε = gas holdup, where ε = Vs/Vb,

Vs = gas superficial velocity, (m s^{-1})

Vb = rise velocity of bubble relative to liquid. (m s^{-1})

Applying these bubble diameter equations to airlifts and bubble columns used for animal cell culture only produces an estimate of the bubble size. According to Heijnen and Van't Riet (1984) completely non-coalescing media is rarely used. Buchholz et al (1979) used 'coalescence-suppressing' medium which produced a bubble diameter at a distance from the sparger that was between the bubble diameter at a distance of the sparger, ds which is typically 6 mm and db, the diameter at the sparger. According to Varley and Birch (1999) at the low gas flow rates used in animal cell culture, the bubble diameter at a distance from the sparger is likely to be equal to the bubble size at the sparger. Varley and Birch (1999) stated that bubble sizes are likely to be in the region of 4 to 6 mm. According to Merchuk et al (1994) operating a bubble column in the separate bubble regime, the diameter of the bubbles is determined by the size of the sparger holes.

9.2 Appendix 2 : k_La equation

The oxygen transfer rate, OTR can related to the k_La by the following equation.

$$OTR = k_La\ (C^*-C_L) \qquad \text{(Equ 9.5)}$$

The oxygen transfer rate, OTR can also be calculated as follows.

$$OTR = \frac{\partial C_L}{\partial t} \qquad \text{(Equ. 9.6)}$$

Putting equation 8.1 and 8.2 together, the following equation results

$$k_La = \frac{\partial C_L}{\partial t}\left(\frac{1}{(C^*-C_L}\right) \qquad \text{(Equ. 9.7)}$$

$$k_La\partial t = -\frac{\partial C_L}{(C^*-C_L)} \qquad \text{(Equ. 9.8)}$$

Intergrating from 0 to time t results in the following equation

$$k_Lat = -\int_0^t \ln(C^*-C_L) \qquad \text{(Equ. 9.9)}$$

$$k_Lat = -\ln(C^*-C_L) + \ln(C^*-C_L^\circ) \qquad \text{(Equ. 9.10)}$$

$$k_L a = \left(\frac{1}{t}\right) \ln\left(\frac{(C^* - C_L^\circ)}{(C^* - C_L)}\right)$$

(Equ. 9.11)

The oxygen concentration can be replaced by Y_L, where $C_L = 0$

$$Y_L = \frac{(C^* - C_L)}{C^*}$$

(Equ. 9.12)

$$k_L a = \frac{1}{t} \ln\left(\frac{1}{Y_L}\right)$$

(Equ. 9.13)

$$\exp(t k_L a) = \left(\frac{1}{Y_L}\right)$$

(Equ. 9.14)

$Y_L = \exp(-k_L a t)$ (Equ. 9.15)

Define r_2 as the probe response time (s)

$Y_p = 1/r_2$ (Equ. 9.16)

$$Y_P = \left(\frac{C^* - C_L}{C^*}\right)$$

(Equ. 9.17)

Define Yp as a first order process strictly exponential with a lag

$$\frac{\partial Y_p}{\partial t} = Kp(Y_L - Y_p)$$

(Equ. 9.18)

Substituting equation for Y_L from Equ. 8.10

$$\frac{\partial Y_p}{\partial t} = Kpe^{-k_L at} - KpY_p$$

(Equ. 9.19)

Let

$$Y_p = Ae^{-k_L at} + Be^{-k_L at}$$

(Equ. 9.20)

$$\frac{\partial Y_p}{\partial t} = A(-k_L a)e^{-k_L at} + B(-Kp)e^{-kpt}$$

(Equ. 9.21)

$$\left(\frac{\partial Y_P}{\partial t}\right) = Kpe^{-k_L at} - Kp\left[Ae^{-k_L at} + Be^{-kpt}\right]$$

$-Ak_La = Kp - KpA$ (Equ. 9.22)

$-BKp = KpB$ (Equ. 9.23)

$A(Kp-k_La) = Kp$ (Equ. 9.24)

$-BKp = -KpB$

(Equ. 9.25)

$$A = \left(\frac{Kp}{Kp - k_L a}\right)$$

(Equ. 9.25)

$$B = \left(\frac{k_L a}{Kp - k_L a}\right)$$

(Equ. 9.26)

Put A and B into

$$Y_p = Ae^{-k_L at} + Be^{-kpt}$$

(Equ. 9.27)

$$Y_P = \frac{1}{r_1 - r_2}\left[r_1 \exp\left(\frac{-t}{r_1}\right) - r_2 \exp\left(\frac{-t}{r_2}\right)\right]$$

(Equ. 9.28)

9.3 Appendix 3 : Program used for k_La measurement

```
10 REM kLa calculations
20 REM G. Wright 1986, P. Bloomfield 1987, E. Fischer, 1995.
30
40 REM INTRODUCTION
45
50 SCREEN 0
60 CLS : MT$ = "OXYGEN TRANSFER RATE" : CALL TITLE (MT$)
70 CALL CEN("kLa Calculation")
80 PRINT : PRINT "This program uses equation (7) in the lab notes to calculate K
85 PRINT TAB(10); "Yp=C*-CL"
87 PRINT TAB(13); "------- (where C*=100)"
88 PRINT TAB(16); "C*"
89 PRINT "and CL=Concentration at time T"
90 PRINT "This program is provided to reduce the time required to carry out these"
100 CALL SPACE: CALL TITLE(MT$)
110 PRINT : PRINT : PRINT "The program requires the following information;":print
"i)The probe response time." :PRINT "ii) The stirrer speed and airflow rate"
120 PRINT "iii) The measured Yp for each point used, (the ratio H3/H2)."
130 CALL SPACE
140 REM PROGRAM BODY
150 CALL TITLE (MT$)
160 PRINT TAB(4); "ENTER PROBE CONSTANT (T2) – SECS:  ": INPUT A$
180 T2 = VAL(A$)
181 PRINT : PRINT "ENTER STIRRER SPEED – RPM:":  INPUT A$
182 STIR = VAL(A$)
183 PRINT "ENTER AIRFLOW RATE – L/MIN:": INPUT A$
184 AIR = VAL(A$)
```

```
185 PRINT "HOW MANY DATA PAIRS AT THIS FLOWRATE STIRRER SPEED
COMBINATION?": INPUT A$
186 N = VAL(A$)
188 REDIM RUNTIME(N): REDIM YPMEAS(N): REDIM KL(N): REDIM T3 (N)
189 FOR count = 1 TO N STEP 1: IF count = 7500 THEN 370
190 PRINT : PRINT "ENTER TIME – SECS: ":INPUT A$
210 RUNTIME(count) = VAL(A$)
220 PRINT "ENTER MEASURED YP RATIO: ": INPUT A$
240 YPMEAS(count) = VAL(A$)
250 T1=20
260 REM INITIAL ESTIMATE FOR ITERATION
270 T3(count) = (T2 * EXP(-(RUNTIME(count) /T2)))
280 REM CALCULATED OUTSIDE ITERATION LOOP
290 DO: YPCALC(count) = (1/(T1-T2))*((T1*EXP(-(RUNTIME(count) /T1)))-
T3(count)
300 DIFF = ABS(APCALC(count)-YPMEAS(count))
310 PERCEN = DIFF*100/YPMEAS(count)
320 IF PERCEN <=1 THEN 360
330 IF YPCALC(count) > YPMEAS(count) THEN T1=T1-(T1*PERCEN/1000)
340 IF YPCALC(count) < YPMEAS(count) THEN T1 = T1 + (T1*PERCEN/1000)
350 LOOP
360 KL(count) = 1/(T1/60): KL(count) = (INT(KL(count)*100))/100
370 REM 2DP ONLY
375 NEXT count
376 PRINT : PRINT "PROBE CONSTANT (SECS): ";T2
378 PRINT "AIRFLOW (L/MIN): "; AIR; TAB(10); "stirrer (rpm): "; stir
379 PRINT TAB(10); "YP RATIO"; TAB(40); "TIME(SECS)"; TAB(70); "KLA(MIN-
1)";
380 FOR count = 1 TO N STEP 1
385 PRINT TAB(10); "YP RATIO"; TAB(40); RUNTIME(count); TAB(70); KL(count);
386 NEXT count
```

```
390 CALL CEN("ANOTHER TIME/TRACE (Y/N)?"): INPUT A$
400 IF A$ = CHR$(89) OR A$ = CHR$(121) THEN 450
410 IF A$ = CHR$(78) OR A$ = CHR$(110) THEN 420 ELSE GOTO 400
420 CLS
430 CALL TITLE("END OF PROGRAM"):
440 END
450 CLS:CALL TITLE(MT$)
460 PRINT TAB(4); "PROBE CONSTANT"; T2; " SECS";
470 GOTO 181
480
620 REM STANDAD NUMERICAL INPUT
540 SUB CEN (T$) : T%=(80-LEN(T$))/2
550 PRINT TAB(T%); T$
560 END SUB
580 SUB SPACE
590 CALL CEN("PRESS SPACE-BAR TO CONTINUE"): DO: LOOP UNTIL
INKEY$ = CHR$(32) : C
600 END SUB
490 SUB TITLE (T$) : T% = (80 – LEN(T$)) /2
500 PRINT TAB(T%); T$
520 END SUB
```

10 Nomenclature

AR= airlift reactor

BCR = bubble column reactor

C* = oxygen concentration of the liquid when it is in equilibrium with the gas (Mol L^{-1})

C_L = oxygen concentration in the liquid (Mol L^{-1})

C_{L1} = oxygen concentration in the liquid (Mol L^{-1}) at time t = 0

C_{L2} = oxygen concentration in the liquid (Mol L^{-1}) at time t = t

CO_2stripping = CO_2 stripping coefficient (s^{-1})

pCO_2* = partial pressure of CO_2 in the liquid when it is saturated with CO_2 (mm Hg)

$pCO_2°$ = partial pressure of CO_2 in the liquid at time, t = 0 (mm Hg)

pCO_2^t = partial pressure of CO_2 in the liquid at time, t = t (mm Hg)

db = bubble size at the sparger (m)

di = diameter of impeller (m)

do = diameter of nozzle (m)

dh = diameter of sparger hole (m)

dj = diameter of jet (m)

ds = bubble diameter at a distance from the sparger (m)

d* = equilibrium diameter of bubble (m)

DOT = dissolved oxygen tension (%)

e = energy dissipation rate (m^2 s^{-3})

e_i = energy dissipation rate at impeller, maximum (m^2 s^{-3})

Fr = Froude number

G = shear rate (s^{-1})

Gaverage = Average shear rate (s^{-1})

g = gravitation acceleration (m s^{-2})

Hp = bubble penetration depth (m)

Lj = height of fall of jet (m)

Ln = length of nozzle (m)

k_La = oxygen transfer coefficient (s^{-1})

T = temperature (K)

OTR = oxygen transfer rate (mmol L^{-1} hr^{-1})

OUR = oxygen uptake rate (mmol L^{-1} hr^{-1})

N = stirrer speed (rotational speed) (s^{-1})

P = power (W m^{-3})

PJR = plunging jet reactor

P_{str} =power of the stirred tank (W m^{-3})

Pu = pressure of gas at column outlet (Pa)

Pug = ungassed power (W m^{-3})

Po = power (W m^{-3})

Po/V = power per unit volume (W m^{-3})

Q = volumetric flow rate (m^3 s^{-1})

Qa = rate of air entrainment (m^3 s^{-1})

Q_{kLa} = mass transfer factor, (m^3 s^{-1})

R = universal gas constant (J mol^{-1} K^{-1})

r = radius (m)

r_2 = DOT probe response time from 100% to 36.8% (s)

STR = stirred tank reactor

t = time (s)

V = volume (m^{-3})

v = velocity, m s^{-1}

Vo = velocity of the jet (m s^{-1})

Vh = superficial velocity at sparger (m s^{-1})

Vj = velocity of jet (m s^{-1})

Vs = gas superficial velocity (m s^{-1})

Vb = rise velocity of bubble relative to liquid (m s^{-1})

We_A = weber number

Z= ungassed height of liquid in the column (m)

α = angle of jet inclination (°)

ε = gas hold up

θ = temperature

ρ = density (kg m^{-3})

ρ_G = density of gas (kg m^{-3})

σ = surface tension (N m^{-1})

υ = kinematic viscosity (m^2 s^{-1})

$\gamma_{average}$ = Average shear stress (kg m^{-1} s^{-2})

11 References

Abbas, A. K., Lichtman, A. H., Pober, J. S. 1994. Cellular and Molecular Immunology, 2nd edition. W. B. Saunders company **3**: 34.

Abu-Reesh, I., Kargi, F. 1989. Biological responses of hydridoma cells to defined hydrodynamic shear-stress. Journal of Biotechnology **9**: 167.

Agayn, V. I., Walt, D. R. 1993. Fiber-optic sensor for continuous monitoring of fermentation pH. Biotechnology **11:** 726.

Ahmed, A. 1974. Aeration by plunging jet. Ph.D. thesis, Loughborough University of Technology.

Atkinson, B., Mauituna, F. 1991. Biochemical Engineering and Biotechnology Handbook. 2nd edition. Stockton Press.

Aunins, J. G., Henzler, H-J. 1991. Aeration in cell culture. Bioprocessing. Volume 3. Chapter 11. Editors, Rehm, H. J., Reed, G. VCH Press.

Aunins, J. G., Glazomitsky, K., Buckland, B. C. 1991. Aeration in pilot scale vessels for animal cell culture. Presentation, AIChE Annual meeting, Los Angeles, CA. November p17.

Bachinger, T. Martensson, P., Mandenius, C-F. 1998. Estimation of biomass and specific growth rate in a recombinant Escherichia coli batch cultivation process using a chemical multisensor array. Journal of Biotechnology. **60:** 55.

Bambot, S., Holvanahali, R., Lakowicz J. R., Carter, G. M., Rao, G. 1994. Phase Fluorometric sterilizable optical oxygen sensor. Biotechnology and Bioengineering. **43:** 1139.

Basu, P. K., Quaadgras, J., Mack, R.A., Noren, A.R. 1998. Achieve the right balance in pharmaceutical pilot plants. Chemical Engineering Progress. **94:** 67.

Bavarian, F., Fan, L. S., Chalmers, J. J. 1991. Microscopic visualization of insect cell-bubble interactions. I: Rising bubbles, air-medium interface and the foam layer. Biotechnology Progress. **7:** 140.

Bello, R. A., Robinson, C. W., Moo-Young, M. 1984. Liquid Circulation and Mixing Characteristics of Airlift Contactors. Canadian Journal of Chemical Engineering. **62:** 573.

Bin, A. K., Smith, J. M. 1982. Mass transfer in a plunging liquid jet absorber. Chemical Engineering Communication. **15:** 367.

Bin, A. K. 1983. Comments on 'Oxygen transfer in jets mixers' by Tojo, K., Miyanami, K. Chemical Engineering Journal. **26:** 255.

Bin, A. K. 1988. Gas entrainment by plunging jet liquid jets. VDI-Forschungsh. **648/88:** 1.

Bin A. K. 1993. Gas entrainment by plunging liquid jets. Chemical Engineering Science **48:** 3585.

Birch, J. R. 1999. Suspension culture, animal cells. Encyclopaedia of bioprocess technology: fermentation, biocatalysis, and bioseparation. Editors: Flickinger, M. C., Drew, S., W. John Wiley and Sons, Inc. p2509.

Bliem, R., Katinger, H. 1988. Scale up engineering in animal cell technology. Part II: Trends in Biotechnology. **6**: 224.

Bloemkolk, J. W., Gray, M. R., Merchant, F., Mosmann, T. R. 1992. Effect of temperature on hybridoma cell-cycle and MAB production. Biotechnology Bioengineering. **40**: 427.

Bonetto, F., Lahey, R., T. 1993. An experimental study on air carry under due to a plunging liquid jet. International Journal of Multiphase Flow. **19:** 281.

Bonsignore, D., Volpicelli, G., Campanile, A., Santoro, L., Valentino, R. 1985. Mass transfer in plunging jet absorbers. Chemical Engineering Process. **19:** 85.

Borys, M. C., Linzer, D. I. H., Papoutsakis, E. T. 1993. Biotechnology. **11**: 720.

Bowering, L. 2000. Ph.D. Thesis, University College London, London, UK.

Boulton-Stone, J.M., Blake, J.R. 1993. Gas-bubbles bursting at a free-surface. Journal of Fluid Mechanics. **254**: 437.

Boychyn, M., Yim, S.S.S., Ayazi-Shamlou, P., Bulmer, M., Hoare, M. 2001. Charaterization of flow intensity in continuous centrifuges for the development of laboratory mimics. Chemical Engineering Science. **56**: 1.

Buchholz, R., Adler, I., Schugerl, K. 1979. European Journal of Applied Microbiology Biotechnology. **7**: 135.

Bullock, W. B., Dibner, M. D. 1995. The state of the US Biotechnology industry. Trends in Biotechnology **13**: 463.

Butler, M. 1996. Animal cell culture and technology. IRL Press at Oxford University Press.

Cabilly, S. 1989. Growth at sub-optimal temperatures allows the production of functional, antigen-binding Fab fragments in Escherichia coli. Gene. **85:** 553.

Calderbank, P. H. 1958. Trans IChemE. **36:** 443.

Carter, P., Kelley, R. F., Rodrigues, M. L., Snedecor, B., Covarrubias, M., Velligan, M. D., Wong, W. L. T., Rowland, A. M., Kotts, C. E., Carver, M. E., Yang, M., Bourell, J. H., Shepard, H. M., Henner, D. 1992. High level *E. coli* expression and production of a bivalent humanized antibody fragment. Biotechnology. **10:** 163.

Chalmers, J. J., Bavarian, F. 1991. Microscopic visualization of insect cell-bubble interactions. II: The bubble film and bubble rupture. Biotechnology Progress. **7:** 151.

Chang, Q., Randers-Eichhorn, L., Lakowiez, J. R., Rao, G. 1998. Steam sterilizalbe, fluorescence lifetime based sensing film for dissolved carbon dioxide. Biotechnology Progress. **14:** 326.

Chattopadhyay, D., Rathman, J. F., Chalmers, J. J. 1995. The protective effect of specific medium additives with respect to bubble rupture. Biotechnology and Bioengineering. **45**: 473.

Chen, J., Tannahile, A. L., Shuler, M. L. 1985. Design of a system for the control of low dissolved oxygen concentrations: Critical oxygen concentrations for Azobacter vinelandin and Escherichia coli. Biotechnology and Bioengineering. **27**: 151.

Cherry, R.S., Hulle C.T. 1992. Cell-death in the thin-films of bursting bubbles. Biotechnology Progress. **8**: 11.

Chisti, M. Y., Moo-Young, M. 1987. Airlift reactors: characteristics, applications and design considerations. Chemical Engineering Communication. **60**: 195.

Chisti M. Y., Halard B. Moo-Young M. 1988. Liquid circulation in airlift reactors. Chemical Engineering Science. **43**: 451.

Chisti, M.Y. 1989. Airlift bioreactors, Elsevier, London.

Choi, K. H., Chisti, Y., Moo-Young, M. 1996. Comparative evaluation of hydrodynamic and gas-liquid mass transfer characteristics in bubble column and airlift slurry reactors. The Chemical Engineering Journal. **62:** 223.

Corrigan-Handa, A., Nikolay, S., Fletcher, D., Mistry, S., Young, A. Ferguson, C. 1995. Monoclonal antibody production in hollow - fiber bioreactors: Process control and validation strategies for manufacturing industry. Enzyme and Microbial Technology. **17**: 225.

CPMP - Committee for propriety medicinal products. 1999. Development pharmaceuticals for biotechnological and biological products. CPMP/BWP/328/99

Davidson, A. 1998. Investment status of biopharmaceuticals. DDT Volume 3. Number 8. September.

Davidson, J. K., Harrison, D. 1963. Fluidized Particles, Cambridge University Press, London.

Donovan, R. S., Robinson, C. W. Glick, B. R. 1996. Review: Optimizing inducer and culture conditions for expression of foreign proteins under the control of the Lac promoter. Journal of Industrial Microbiology. **16:** 145.

Doran, P. M. 1996. Bioprocess Engineering Principles. Academic Press.

Drapeau D. SIM Annual Meeting, Orlando Florida, August 1990.

Dutta, N. N., Raghavan, K. V. 1987. Mass transfer and hydrodynamic characteristics of loop reactors with down-flow liquid jet ejector. The Chemical Engineering Journal. **36**: 111.

Edwards, N., Beeton, S., Bull, A. T., Merchuk, J. C. 1989. A novel device for the assessment of shear effects on suspended microbial cultures. Applied Microbiology and Biotechnology. **22:** 325.

Evans, G. M. 1990. A study of a plunging jet bubble column. Ph.D. thesis, University of Newcastle, Australia.

Evans, G. M., Jameson, G. J., Atkinson, B. W. 1992. Prediction of bubble size generated by a plunging jet liquid jet bubble column. Chemical Engineering Science. **47:** 3265.

Evans, G. M., Jameson, G. J. 1995. Hydrodynamics of a plunging liquid jet bubble column. Trans IchemE. **73:** 679.

Farrel, J., Rose, A. H. 1967. Temperature effects on micro-organisms. Thermobiology. Editor: Rose, A.H. New York: Academic Press. p147.

Ferguson, J. A., Healey, B. G., Bronk, K. S., Barnard, S. M., Walt, D. R. 1997. Simultaneous monitoring of pH, CO2 and O2 using an optical imaging fiber. Analytica Chimica Acta. **340:** 123.

Fujie, K., Takaine, M., Kubota, H. 1980. Flow and oxygen transfer in cocurrent gas-liquid downflow. Journal of Chemical Engineering of Japan. **13**: 188.

Funatsu, K., Hsu, Y.Ch., Kamogawa, T. 1988a. Gas holdup and gas entrainment of a plunging water jet with a constant entrainment guide. Canadian Journal Chemical Engineering. **66:** 19.

Funatsu, K., Hsu, Y.Ch., Noda, M., Sugawa, S. 1988b. Oxygen transfer in the water-jet vessel. Chemical Engineering Communication. **73**: 121.

Gamerman, G. E., Mackler, B. F. 1994. Winning in today's biopharmaceutical marketplace. ChemTech **24**: 37.

Garcia-Briones, M.A., Brodkey, R.S., Chalmers, J.J. 1994. Computer simulations of the rupture of a gas bubble at a gas liquid interface and its implications in animal cell damage. Chemical Engineering Science. **49:** 2301.

Gardner, A. R., Gainer, J. L., Kirwan, D. J. 1990. Effects of stirring and sparging on cultured hydridoma cells. Biotechnology and Bioengineering. **35**: 940.

Garner, R. H., Ellis, S. C. M., Lacey, J. A. 1954. The size distribution and entrainment of droplets. Trans. IChemE. **32**: 222.

Gasner, L. L. 1974. Development and application of the Thin Channel Rectangular Air Lift Mass Transfer Reactor to Fermentation and Waste-Water Treatment Systems. Biotechnology and Bioengineering. **16:** 1179.

Gavrilescu, M., Tudose, R. Z. 1996. Effects of downcomer to riser cross sectional area ratio on operation behaviour of external loop airlift bioreactors. Bioprocess Engineering **15:** 77.

Glasgow, L. A., Jones, G.T., Erickson, L.E. 1989. Hydrodynamic charterization of airlift bioreactor operation. Two-Phase Flows, Tapie, Tawan.

Glasgow, L.A., Hua, J. Yiin, T.Y., Erickson, L.E. 1992. Experimental studies of interfacial phenomena in sparged reactor. Editors: Tatterson, G.B., Calabrease, R. V. Process mixing chemical biochemical applications. AIChE Syposium Series 286.

Gosse, M. E., Manocchia, M. A 1996. The first biopharmaceuticals approved in the United States: 1980:1994. Drug Information Journal. **30:** 991.

Gray, D. R., Chen, S, Howarth, W., Inlow, D., Maiorella, B., L. 1996. CO2 in large-scale and high-density CHO cell perfusion culture. Cytotechnology. **22:** 65.

Griffiths, J.B. 1988. Overview of cell culture systems and their scale up. Animal cell biotechnology. Editors: Spier, R. E., Griffiths, J.B. Academic Press, London. **3**: 179.

Grima, E. M., Christi, Y., Moo-Young, M. 1997. Characterization of shear rates in airlift bioreactor for animal cell culture. Journal of Biotechnology. **54:** 195.

Hall, J., Mcneil, B., Rollins, M., Draper, I., Thompson, B., Macaloney., G. 1998. Near infrared spectroscopic determination of acetate, ammonium, biomass and glycerol in an industrial Escherichia coli fermentation. Applied Spectroscopy. **50**: 102.

Handa, A., Emery, N. A., Spier, R. E. 1987. On the evaluation of gas-liquid interfacial effects on hydridoma viability in bubble column bioreactors. Developments in Biological Standardization. **66:** 241.

Handa, A., Emery, A. N., Spier, R. E. 1987a. Procedures of the 4th European Congress on Biotechnology. **3:** 601.

Handa-Corrigan, A, Emery, A. N., Spier R. E. 1989. Effect of gas - liquid interfaces on the growth of suspended mammalian cells: mechanisms of cell damage by bubbles. Enzyme and Microbial Technology. **11:** 230.

Hara, H., Shimada, K., Kumagai, M. 1977. The behaviour of gas entrainment by a liquid jet. Kagaku Kagaku Ronbunshu. **3**: 424.

Harmers, M. N. 1993. Multiuse biopharmaceutical manufacturing. Bio/technology. **11**: 561.

Hatch, R. T. 1975. Fermenter design. Single cell protein. Volume II. Editors: Tanenbaum, S.R. and Wang, D.I.C. MIT Press, Cambridge, MA. p46.

Havelka, P., Linek, V., Sinkule, J., Zahradnik, J., Fialova, M. 1997. Effect of the ejector configuration on the gas suction rate and gas hold-up in ejector loop reactors. Chemical Engineering Science. **52:** 1701.

Hebrard, G., Bastoul, D., Roustan, M. 1996. Influence of the gas sparger on the hydrodynamic behaviour of bubble columns. Trans IChemE. **74:** 406.

Heijenen, J. J., Van't Riet, K. 1984. Mass transfer, mixing and heat transfer phenomena in low viscosity bubble column reactors. The Chemical Engineering Journal. **28**: B21.

Heinzle, E., Dunn, I. J. 1991. Methods and instrumentation in fermentation gas analysis. Biotechnology, second, completely revised edition. Editors: Rehm, H-J., Reed, G., in co-operation with Puhler, A., Stadler, P. Volume 4. Measuring, Modelling and Control. VCH Weinheim.

Henzler, H. J., Kauling, J. 1993. Oxygen supply to cell cultures, Bioprocess Engineering. **9**: 61.

Herbrechtsmeier, P., Schafer, H., Steiner, R. 1981. Gas absorption in downflow bubble column reactors as exemplified by ozonation of water. German chemical Engineering. **4**: 239.

Hewitt, C. J., Boon, L. A., McFarlane, C. M., Nienow, A. W. 1998. The use of flow cytometry to study the impact of fluid mechanical stress on Escherichia coli W3110 during continous cultivation in an agitated bioreactor. Biotechnology and Bioengineering. **59**: 612.

Hill, D. Beatrice, M. 1989. Biotechnology facility requirements. Part 2. Operating procedures and validation. Biopharm. **2**: 28.

Hu, W-S., Aunins, J. G. 1997. Large scale mammalian cell culture. Current opinion in Biotechnology. **8**: 148.

Hua, J., Erickson, L.E., Yiin, T.Y., Glasgow, L.A. 1993. Critical Review of Biotechnology. **13**: 305.

Huges, T. 1998. Personal Communication, UCL validation course.

Ingraham, J. L. 1958. Growth of psychrophilic bacteria. Journal of Bacteriology. **76:** 75.

International Critical Tables. 1928. Volume 3. McGraw-Hill, New York. p257.

Jagusch, L., Puschel, S. 1968. Tauchstrahlbeluftung - ein neuartiges. VEB Kombinat "Schwartze Pumpe" erprobtes Beluftungssystem zur biologischen Reinigung hochbelasteter Abwasser. Wasserwirtschaft Wasser Technik. **18**: 160.

Jagusch, L., Schonherr, W. 1972. Das Tauchstrahl - begasungsverfahren - ein neues okonomisches Verfahren mit vielen Einsatzmoglichkeiten. Chemical Technology (DDR). **42:** 68.

Joly, P. 1998. Applications of single use bags in the biopharmaceutical industry. Biopharm Europe - Conference Proceedings - Dusseldorf 12th October.

Joshi, J. B., Elias, C. B., Patole, M. S. 1996. Role of hydrodynamic shear in the cultivation of animal, plant and microbial cells. The Chemical Engineering Journal. **62**: 121.

Karri, S., Farid, S., Novais, J., Titchener-Hooker, N. 2000. A Modelling framework for managing the cost and utilisation of biopharmaceutical pilot plants. Presented at the Spring National Meeting 2000, March 5-9, T7008 Pilot Plants in the 21st Century II.

Kenyeres, S., et al. 1989. Process for contacting gases with liquids. US patent no. 4,840,751.

Kenyeres, S. 1991. Plunging jet aeration technology and equipment, Brochure.

Kimura, R., Miller, W. M. 1997. Glycosylation of CHO-derived recombinant tPA produced under elevated pCO_2. Biotechnology Progress. **52:** 152.

Knaack, C. A., Hawrylechko, A. M. J. 1998. A systematic approach to the validation of monoclonal antibody manufacturing processes. PSTT Volume 1. Number 7.

Knight, P. 1989. Hollow fiber bioreactors for mammalian cell culture. Biotechnology. **7**: 459.

Kumagai, M., Endoh, K. 1982. Effects of kinematic viscosity and surface tension on gas entrainment rate of an impinging liquid jet. Journal of Chemical Engineering of Japan. **15:** 427.

Kumagai, M., Imai, H. 1982. Gas entrainment characteristics of an impinging water jet. Kagaku Kogaku Ronbunshu. **8:** 1.

Kunas, K. T., Papoutsakis, E. T. 1990. Damage mechanisms of suspended animal cells in agitated bioreactors with and without bubble entrainment. Biotechnology and Bioengineering. **36**: 476.

Kundu, G., Mukherjee, D. Mitra, A. 1994. Gas entrainment and depth of penetration in a co-current gas liquid downflow bubble column. Journal of chemical engineering of Japan. **27:** 621.

Kusabiraki, D., Murota, M., Ohno, S., Yamagiwa, K., Yasuda, M., Ohkawa, A. 1990. Gas entrainment rate and flow pattern in a plunging jet liquid jet aeration system using inclined nozzles. Journal of Chemical Engineering of Japan. **23:** 704.

Kusabiraki, D., Niki, H., Yamagiwa, K., Ohkawa, A.K. 1990a. Gas entrainment rate and flow pattern of vertical plunging liquid jets. Canadian Journal Chemical Engineering. **68**: 893.

Kusabiraki, D., Yamagiwa, K., Yasuda, M., Ohkawa, A. 1992. Gas entrainment behavior of vertical plunging liquid jets in terms of changes in jet surface length. Canadian Journal Chemical Engineering. **70**: 181.

Laari, A., Kallas, J. Palosaari, S. 1997. Gas liquid mass transfer in bubble columns with a T-junction nozzle for gas dispersion. Chemical Engineering Technology. **20**: 550.

Lee, J. C., Meyrick, D. L. 1970. Trans. IChemE. **48:** T37.

Lehrer, I. H. 1971. Industrial and Engineering Chemistry. Process Design and Development. **10**: 37.

Lin, T. J., Donnelly, H. G. 1966. Gas bubble entrainment by plunging laminar liquid jets. AIChE Journal. **12**: 563.

Linek, V., Benes, P., Vacek, V. 1989. Dynamic pressure method for k_La measurement in large scale bioreactors. Biotechnology and Bioengineering. **33**: 1406.

Lu, G. Z., Thompson, B. G., Suresh, M. R., Gray, M. R. 1995. Cultivation of hybridoma cells in an inclined bioreactor. Biotechnology and Bioengineering. **45**: 176.

Margaritis, A., Sheppard, J. D. 1981. Mixing time and oxygen-transfer characteristics of a double draft tube airlift fermenter. Biotechnology and Bioengineering. **23**: 2117.

Marshall, A. 1997a. Laying the foundations for personalized medicines. Nature Biotechnology. **15**: 954.

Marshall, A. 1997b. Getting the right drug into the right patient. Nature Biotechnology. **15**: 1249.

Mather, J. P., Tsao, M. 1990. Large-Scale Mammalian Cell Culture Technology. Editors: Lubiniecki, A. S., et al. Marcel Dekker, New York and Basel, p161.

McCarthy, M. J., Kirchner, W. G., Molloy, N. A., Henderson, J. B. 1969. Mechanism of gas bubble entrainment by plunging liquid jets. Transcripts of the Institute of Minerals and Metallurgy. **78**: C239.

McCarthy, M. J., Molloy, N. A. 1974. Review of stability of liquid jets and the influence of nozzle design. The Chemical Engineering Journal. **7**: 1.

McKeogh E. J., Ervine D. A. 1981. Air entrainment rate and diffusion pattern of plunging liquid jets. Chemical Engineering Science. **36**: 1161.

McQueen, A., Bailey, J., E. 1989. Influence of serum level, cell line, flow type and viscosity and flow-induced lysis of suspended mammalian cells. Biotechnology Letters. **11**: 531.

Medicine Control Agency personal communication. UCL validation course 1998.

Merchuk, J. C., Ben-Zvi, S., Niranjan, K. 1994. Why use bubble column bioreactors? Trends in Biotechnology. **12**: 501.

Michaels, J. D., Nowak, J., E., Mallik, A. K., Koczo, K., Wasan, D. T., Papoutsakis, E. T. 1995. Biotechnology and Bioengineering. **47**: 407.

Michel, Miller. 1962. AIChE Journal. **8**: 262.

Mills, A., Chang, Q., McMurray, N. 1992. Equilibrium studies on colorimetric plastic film sensors for carbon dioxide. Analytical Chemistry. **64**: 1383.

Mills, A., Chang, Q. 1993. Fluorescence plastic thin film sensor for carbon dioxide. Anaivst Cambridge. **118**: 839.

Mills, A., Chang, Q. 1994a. Tuning colorimetric and fluorimetric gas sensors for carbon dioxide. Analytical Chim Acta. **285**: 113.

Mills, A., Chang, Q. 1994b. Colorimetric polymer film sensors for dissolved carbon dioxide. Sensors and Actuators B: Chemical. **21**: 83.

Moppett, G. D., Rielly, C. D., Davidson, J. F. 1997. Waste - water treatment using a plunging jet oxygenator issuing into a downflowing liquid. BHR Group Bioreactor/process Fluid Dynamics.

Murhammer D. W., Goochee C. F. 1988. Scale-up of insect cell cultures: Protective effects of Pluronic F68. Bio/Technology. **6**: 1411.

Newitt D. M., Dombrowski, N., Knelman S. H. 1954. 1. The mechanism of drop formation from gas to vapour bubbles. Transcripts of the Institute of Chemical Engineering. **32**: 244.

Editors: Norris, J. R., Ribbons, D. W. 1970. Methods in Microbiology. Volume 2. New York: Academic Press.

Novais, J. L., Titchener-Hooker, N. J., Hoare, M. 2001. Economic Comparison between conventional and disposable based technology for the production of biopharmaceuticals. To be published.

Oh, S. K. W., Nienow, A. W., AL-Rubeal., M., Emery, A. N. 1989. The effects of agitation intensity with and without continuous sparging on the growth and antibody production of hybridoma cells. Journal of Biotechnology **12**: 45.

Ohashi, R., Singh, V., Hamel, J-F. P. 2001. Perfusion Culture in Disposable Bioreactors. Genetic Engineering News. **21**: 40.

Ohkawa, A., Shiokawa, Y., Sakai, N., Endoh, K. 1985a. Gas holdup in downflow bubble columns with gas entrainment by a liquid jet. Journal of Chemical Engineering of Japan. **18**: 172.

Ohkawa, A., Shiokawa, Y., Sakai, N., Imai, H. 1985b. Flow characteristics of downflow bubble columns with gas entrainment by a liquid jet. Journal of Chemical Engineering of Japan. **18**: 466.

Ohkawa, A., Kusabiraki, D., Kawai, Y., Sakai, N. 1986. Some flow characteristics of a vertical liquid jet system having downcomers. Chemical Engineering Science. **41:** 2347.

Ohkawa, A., Kusabiraki, D., Kawai, Y., Sakai, N. 1986a. Flow and oxygen transfer in a plunging jet water system using inclined short nozzles and performance characteristics of its system in aerobic treatment of wastewater. Biotechnology Bioengineering. **28:** 1845.

Ohkawa, A., Kusabiraki, D., Sakai, N. 1987. Effects on nozzle length on gas entrainment characteristics of vertical liquid jet. Journal of Chemical Engineering of Japan. **20**: 295.

Orazem, M. E., Erickson, L. E. 1979. Biotechnology and Bioengineering. **21**: 69.

Orfaniotis, A., Lalane, M., Doubrovine, N., Fonade, C., Mayr, B., Moser, A. 1996. Oxygen transfer and scale-up in bioreactors using hydro ejectors for gas liquid contacting. Bioprocess Engineering. **14**: 211.

Orton D. R., Wang, D. I. C. 1990. Effects of gas interfaces on animal cells in bubble aerated bioreactors. A paper presented at AIChE Annual meeting, Chicago, IL, Nov. 11-16. Authors at M. I. T., Cambridge, MA.

Ozturk, S. S., Palsson, B. O. 1991. Growth, metabolic, and antibody production kinetics of hybridoma cell culture. 2. Effects of serum concentration, dissolved oxygen concentration, and medium pH in a batch reactor. Biotechnology Progress. **7**: 481.

Ozturk, S. S., Thrift, J. C., Blackie, J. D., Naveh, D. 1997. Real-Time monitoring and control of glucose and lactate concentrations in a mammalian cell perfusion reactor. Biotechnology and Bioengineering. **53**: 372.

Perry, R. H., Chilton, C. H. 1973. Chemical Engineers' Handbook, McGraw-Hill, Tokyo, 5th edition. p18.

Petersen J.F., McIntire L. V., Papoutsakis E. T. 1988. Shear sensitivity of cultured hybridoma cells (CRL-8018) depends on mode of growth, culture age and metabolite concentration. Journal of Biotechnology. **7**: 229.

Pluckthun, A. 1991. Biotechnological aspects of antibody production in *E. coli*. Acta Biotechnology. **5**: 449.

Pouliot, K., Thibault, J., Garnier, A., Acuna Leiva, G. 2000. k_La Evaluation during the course of fermentation using data reconciliation techniques. Bioprocess Engineering. **23**: 565.

Poulsen, B. R., Iversen, J. J. L. I. 1998. Characterization of gas transfer and mixing in a bubble column equipped with a rubber membrane diffuser. Biotechnology and Bioengineering. **58**: 633.

Editors: Prave, P., Faust, U., Sitting, W., Sukatsch, D. A.1987. Fundamentals of Biotechnology. VCH Weinheim.

Prokop, A., Janik, P. Sobotka, M., Krumphanzl, V. 1983. Hydrodynamics, mass transfer and yeast culture performance of a column bioreactor with ejector. Biotechnology and Bioengineering. **25:** 1147.

Reardon, K. F., Scheper, T., H. 1991. Determination of cell concentration and characterization of cells. Biotechnology, second, completely revised edition. Editors: Rehm, H-J., Reed, G., in co-operation with Puhler, A., Stadler, P. Volume 4 Measuring, Modelling and Control. VCH Weinheim.

Riley, M. R., Arnold, M. A., Murhammer, D. W., Walls, E. L., DelaCruz, N. 1998. Adaptive calibration scheme for quantification of nutrients and byproducts in insect cell bioreactors by near-infrared spectroscopy. Biotechnology Progress. **14**: 1998.

Robertson, D. G. C., O'Shaughnessy, D. P., Molloy, N. A. 1973. The mechanism of sheath formation by plunging jets. Chemical Engineering Science. **28**: 1635.

Roels, J. A., Heijnen, J. J. 1980. Power dissipation and heat production in bubble columns: Approach based on nonequilibrium thermodynamics. Biotechnology Bioengineering. **22**: 2399.

Rushton, J. H., Costich, E. W., Everett, H. J. 1950. Power characteristics of mixing impellers. Part 1. Chemical Engineering Progress. **46**: 395.

Rushton, J. H., Costich, E. W., Everett, H. J. 1950a. Power characteristics of mixing impellers. Part 2. Chemical Engineering Progress. **46:** 467.

Russell A. B., Thomas C. R., Lilly M. D. 1994. The influence of vessel height and top-section size on the hydrodynamic characteristics of airlift fermentors. Biotechnology and Bioengineering. **43:** 69.

Schlichling, H. 1979. Boundary layer theory. 7th Edition. McGraw-Hill. p101.

Schmidt, S., Kircher, M., Kasala, M., Locaj J. 1998. Near infrared spectroscopy in fermentation and quality control for amino acid production. Bioprocess Engineering. **19**: 67.

Schugerl, K. 1985. Non-mechanically agitated bioreactor systems. Comprehensive Biotechnology. Editor: Moo-Young. M. Series editors: Cooney, C. L., Humphrey, A. E. Volume 2. Oxford: Pergamon. Section 1. **5:** 99.

Schugerl, K. 1991. Common instruments for process analysis and control. Biotechnology. Second, completely revised edition. Editors: Rehm, H-J., Reed, G., in cooperation with Puhler, A., Stadler, P., Volume 4. Measuring, Modelling and Control. VCH Weinheim.

Schurh, U., Kramer, H., Einsele, A., Widmer, F., Eppenberger, H. 1988. Experimental evaluation of laminar shear-stress on the behaviour of hybridoma mass cell-cultures,

producing monoclonal antibodies against mitochrondrial creating kinase. Journal of Biotechnology. **7:** 179.

Sene, K. J. 1988. Air entrainment by plunging jets. Chemical Engineering Science. **43**: 2615.

Siegel, M. H., Merchuk, J. C., Schugerl, K. 1986. Airlift reactor analysis: interrelationships between riser, downcomer, and gas-liquid separator behaviour, including gas recirculating effects. AIChE Journal. **32**: 1585.

Siegel, M. H. Merchuk, J. C. 1988. Mass Transfer in a Rectangular Air-Lift Reactor: Effects of Geometry and Gas Recirculation. Biotechnology and Bioengineering. **32**: 1128.

Singh, V. 1999. Disposable bioreactor for cell culture using wave induced agitation. Cytotechnology. **30**: 149.

Siphior, J., Randers-Eichhorn, L., Lakowicz, J. R., Carter, G. M., Rao, G 1996. Phase fluorometric optical carbon dioxide gas sensor for fermentation off gas monitoring. Biotechnology Progress. **12**: 266.

Struck, M. M. 1994. Biopharmaceutical R&D success rates and development times. Bio/Technology. **12:** 674.

Suciu, G. D., Smigelschi, O. 1976. Gas absorption by turbulent liquid plunging jets. Chemical Engineering Science. **32**: 889.

Tartakovsky, B., Sheintuch, M., Hilmer, J-M., Scheper, T. 1996. Application of scanning fluorometry for monitoring of a fermentation process. Biotechnology Progress. **12**: 126.

Thorpe, R. B., Jemsby, B., Fairhurst, R., Lee, Y. H., Scott, D, M. 1997. Bioreactor/process Fluid Dynamics. BHR Group.

Tojo, K., Miyanami, K. 1982. Oxygen transfer in jet mixers. Chemical Engineering Journal. **24**: 89.

Tojo, K., Naruko, N., Miyanami, K. 1982. Oxygen transfer and liquid mixing characteristics of plunging jet reactors. Chemical Engineering Journal. **25**: 107.

Tramper, J., Williams, J. B., Joustra D., Vlak J. M. 1986. Shear sensitivity of insect cells in suspension. Enzyme and Microbial Technology. **88**: 33.

Tramper, J., Joustra, D., Vlak, J.M. 1987. Bioreactor design for growth of shear-sensitive insect cell. Plant animal cell cultures: process possibilities. Editors: Webb, C, Mavituna, R. Ellis Horwood, England.

Tramper, J., Smit, D., Straatman, J., Vlak, J. M. 1988. Bubble - column design for growth of fragile insect cells. Bioprocess Engineering. **3**: 37.

Tramper, J., Martens, D., Jobses, I. 1991. Lethal Events during Gas sparging in animal cell culture. Biotechnology and Bioengineering. **37**: 484.

Tramper, J., Vlak, J. M., Gooijer, C. D. 1996. Scale up aspects of sparged insect cell bioreactors. Cytotechnogy. **20**: 221.

Van de Donk, J. A. C., van der Lans, R. G. J. M. and Smith, J. M., (1979) The effect of contaminants on the oxygen transfer rate achieved with a plunging jet contactor, in Proceedings of the 3rd European Conference on Mixing, University of York, Paper F1. p289.

Van de Donk, J. A. C. 1981. Water aeration with plunging jets. Ph.D. thesis. Technische Hogeschool Delft.

Van de Sande, E., Smith, J. M. 1973. Surface entrainment of air by high velocity water jets. Chemical Engineering Science. **28**: 1161.

Van de Sande, E. 1974. Air entrainment by plunging water jets. Ph.D. thesis. Technische Hogeschool Delft.

Van de Sande, E., Smith, J. M. 1974. Mass transfer in a pool with plunging liquid jets. Proceedings of the International Chemical Engineering Symposium Multiphase Flow Systems, Glasgow.

Van de Sande, E., Smith, J. M. 1976. Jet break-up and air entrainment by low velocity turbulent water jets. Chemical Engineering Science. **31**: 219.

Van Holden C. 1998. Personal communication, UCL validation course.

Van Krevelen, D. W., Hoftijzer, P. J. 1950. Chemical Engineering Progress. **46**: 29.

Varley, J., Birch, J. 1999. Reactor design for large scale suspension animal cell culture. Cytotechnology. **29**: 177.

Verlaan, P., Tramper, J., Luyben, K., Vant't Riet, K. 1986. A Hydrodynamic Model for an Airlift-Loop Bioreactor with External Loop. The Chemical Engineering Journal. **33:** B43.

Verlaan, P., Vos J. C., Van't Riet, K. 1988. From bubble column to air lift loop reactor: hydrodynamics and axial dispersion of the transition flow regime. Paper F1. BHRA 2nd International Conference of Bioreactor Fluid Dynamics. Editor: King, R. Elsevier Applied Science, Oxford. p259.

Wachsmann, U., Rabiger, N., Vogelpohl, A. 1985. Effect of geometry on hydrodynamics and mass transfer in the compact reactor. German chemical Engineering. **8**: 411.

Wallis, G. B. 1969. One-dimensional Two-phase Flow. McGraw-Hill, New York.

Wayte, J., Boraston, R., Bland, H., Varley, J., Brown, M. 1997. pH: Effects on growth and productivity of cell lines producing monoclonal antibodies: control in large scale fermenters. The Genetic Engineer and Biotechnologist. **17**: 125.

Weigl, B. H., Wolfbets, O. S. 1995. New hydrophobic materials for optical carbon dioxide sensors based on ion pairing. Analytical Chim Acta. **302**: 249.

Weiland, P. 1984. German Chemical Engineering. **7**: 374.

Wood, L. A., Thompson, P.W. 1986. Paper presented at the International Conference on Bioreactor Fluid Dynamics. Cambridge, England. 15-17 April. Paper 11. p157.

Wu, J., Goosen, M. F. A. 1995. Evaluation of the killing volume of gas bubbles in sparged animal cell culture bioreactors. Enzyme and Microbial Technology. **17:** 1036.

Wu, W-T, Jong, J-Z. 1994. Liquid phase dispersion in an airlift reactor with a net draft tube. Bioprocess Engineering. **11**: 43.

Xie, L., Wang, D.I.C. 1996. High cell density and high monoclonal antibody production medium design and rational control in a bioreactor. Biotechnology Bioengineering. **51**: 725.

Yamagiwa, K., Kusabiraki, D., Ohkawa, A. 1990. Gas holdup and gas entrainment rate in downflow bubble column with gas entrainment by a liquid jet operating at high liquid throughput. Journal of Chemical Engineering of Japan. **23:** 343.

Zabriskie, D. W., Arcuri, E. J. 1986. Factors influencing productivity of fermentations employing recombinant microorganisms. Enzyme and Microbial Technology. **8**: 706.

Zaidi, A., Ghosh, P., Schumpe, A., Deckwer, W.D. 1991. Xanthan production in a plunging jet reactor. Applied Microbiology and Biotechnology. **35**: 330.

Zhou, W., Hu, W-S. 1994. On-Line characterization of a hybridoma cell culture process. Biotechnology and Bioengineering. **44**: 170.

Zlokarnik, M. 1980. Eignung und Leistungsfahigkeit von Oberflachenbeluftern fur biologische Abwasserreinigun-gsanlagen. Korrespondenz Abwasser. **27:** 14.

Zlokarnik, M, Judat, H. 1988. Stirring. Ullmann's Encyclopedia of Industrial Chemistry. Editor: Gerhartz, W. Vol B2. VCH, Weinheim. p25.

EP 0343 885, Applicant: P. B. Ind. Plant Biotech Industries Ltd, Inventor: Kalfon, Abraham Rami.

WO 98/13469, Applicant: Metabogal Ltd., Inventor: Shaaltiel, Yoseph.

WO 96/12715, Applicant: Netherlands-Production laboratory blood transfusion, Inventor: Van der Heiden J; Hilbrink, H. E.

BP 215370/20, Applicant: Panacea Solutions Inc., Inventor Vijay Singh.

USP 4,840,751, Applicant: Innofinance Altalanos Innovaios Penzintezet, Inventor: Istvan Kenyeres, Lehel Koch.